Airflow Prediction in Buildings for Natural Ventilation Design: Wind Tunnel
Measurements and Simulation

Panagiota Karava

A Thesis

in

The Department

of

Building, Civil, and Environmental Engineering

Presented in Partial Fulfillment of the Requirements
for the Degree of Doctor of Philosophy (Building Studies) at
Concordia University
Montreal, Quebec, Canada

February 2008

ABSTRACT

Airflow Prediction in Buildings for Natural Ventilation Design: Wind Tunnel Measurements and Simulation

Natural / hybrid ventilation systems with motorized operable windows, designed and controlled to utilize the potential for cross-ventilation, represent an area of significant interest in sustainable building design as they can substantially reduce energy consumption for cooling and ventilation. Presently, there is a need for accurate prediction models that can contribute to the improvement of indoor environmental quality and energy performance of buildings, and the increased use of low energy, naturally driven cooling systems. In this regard, the present research aims to enhance airflow prediction accuracy for natural ventilation design of buildings considering advanced experimental and simulation methods.

The study considers a Boundary Layer Wind Tunnel (BLWT) approach to investigate the wind-induced driving forces and ventilation flow rates in various building models subject to cross-ventilation. The Particle Image Velocimetry (PIV) technique was used for the first time to evaluate accurately the air velocity field for various cross-ventilation configurations. Detailed measurements were performed to determine mean and fluctuating internal pressures since they affect airflow prediction, occupants' thermal comfort, as well as cladding and structural wind load design of buildings with operable windows. PIV data for the inflow velocity were compared with those by using conventional techniques (e.g., hot-film anemometry) and results show differences,

between the two methods, up to a factor of 2.7. This clearly indicates that accuracy can be enhanced with carefully conducted PIV experiments. The study provides guidelines for implementation of cross-ventilation in design practice. These guidelines were developed on the basis of parametric experimental investigations, which quantify the impact of relative inlet-to-outlet size and location on ventilation airflow rates and thermal comfort of building occupants.

The study develops a novel simulation methodology combined with a sensitivity analysis focused on modelling issues, such as the impact of zoning assumptions, to predict the envelope pressures and related air-exchange rates in buildings due to wind, stack, and mechanical system effects. An integrated simulation tool (ESP-r) was used to model the airflow / energy interactions in an existing high-rise residential building, and simulation results agree well with monitoring data.

Acknowledgements

Table of Contents

List of Figures

List of Tables

Nomenclature

Acronyms

BLWT	Boundary Layer Wind Tunnel
CCD	Charge Coupled Device
CFD	Computational Fluid Dynamics
FFT	Fast Fourier Transform
IAQ	Indoor Air Quality
LDV	Laser Doppler Velocimetry
NBCC	National Building Code of Canada
PIV	Particle Image Velocimetry
T.I.	turbulence intensity

Equation Variables

$\dot{m}$	mass flow rate (kg/s)
ΔP	pressure drop across an opening (Pa)
A	area of ventilation opening (m^2)
A_1	inlet opening area (m^2)
A_1/A_2	inlet-to-outlet ratio
A_2	outlet opening area (m^2)
A_c	cross section area of the vena contracta (m^2)
A_{eff}	effective area of ventilation opening (m^2)
A_w	wall porosity
C	flow coefficient
C_c	contraction coefficient

C_D	discharge coefficient
C_{D1}	inlet discharge coefficient
C_{D2}	outlet dischar coefficient
Cp_e	mean external pressure coefficient
Cp_{eak}	peak pressure coefficient
Cp_{in}	internal pressure coefficient
Cp_L	pressure coefficient on leeward façade
Cp_{mean}	mean pressure coefficient
Cp_{rms}	root-mean-square pressure coefficient
Cp_w	pressure coefficient on windward façade
C_v	velocity coefficient
M	object:image scale factor
n	flow exponent
P_e	external pressure (Pa)
P_{in}	internal pressure (Pa)
P_L	leeward wall pressure (Pa)
P_w	windward wall pressure (Pa)
Q	mean airflow rate
Re	Reynolds number
t	time between pulses (μs)
$U_{opening}$	area-averaged mean velocity at the opening (m/s)
U_{ref}	reference wind speed (velocity at building height - m/s)

U_x	velocity component on the centre-line between the inlet and outlet (m/s)
V_c	air velocity in the vena contracta (m/s)
V_g	velocity at boundary layer height (m/s)
V_{th}	theoretical air velocity (m/s)
Z_g	boundary layer height (m)
Z_o	roughness length (m)
Z_{ref}	reference height (building height - m)
α	inlet-to-outlet ratio
ζ	pressure loss coefficient
θ	wind angle (°)
ρ	air density (kg/m^3)

1   INTRODUCTION

1.1   Background and motivation

The 21st century building is evolving to accommodate three interrelated requirements:

- Promote sustainable development through the use of environmentally friendly materials and utilization of renewable energy sources;

- Minimize energy costs for processes such as heating, cooling, ventilating and electric lighting;

- Enhance indoor environmental quality and comfort which will increase productivity.

In this context, growing concerns about building energy efficiency and climate change have led to renewed interest in natural ventilation systems and the development of a hybrid approach to space conditioning. Natural ventilation systems rely on wind and thermal buoyancy as driving forces for the ventilation air flow. Hybrid ventilation systems can be described as two-mode systems using different features of both passive and mechanical systems at different times of the day or season (Heiselberg, 2002). Generally, they take advantage of natural ventilation when it is available and supplement it as necessary with mechanical ventilation. Natural / hybrid ventilation systems with motorized operable windows designed to fully utilize the potential for cross-ventilation are presently considered as a measure for sustainable design of a building. A schematic representation of a cross-ventilation design concept in an office building is shown in Figure 1.1.

In a survey carried out by Canada Mortgage and Housing Corporation (CMHC, 2004) to verify the use and utility of ventilation systems in new Ontario houses, it was found

1 NIGHT SPRAY RADIANT COOLING
2 COOL TOWER
3 SPECTRALLY-SELECTIVE GLAZING + ROOFING
4 SUNSHADES & LIGHTSHELVES
5 EFFICIENT WATER USE
6 HIGH-VOLUME FLY ASH CONCRETE

7 SALVAGED MATERIALS
8 NATIVE LANDSCAPING
9 NATURAL VENTILATION
10 RADIANT SLAB HEATING + COOLING
11 FULLY DAYLIT INTERIOR WITH LIGHTING CONTROLS
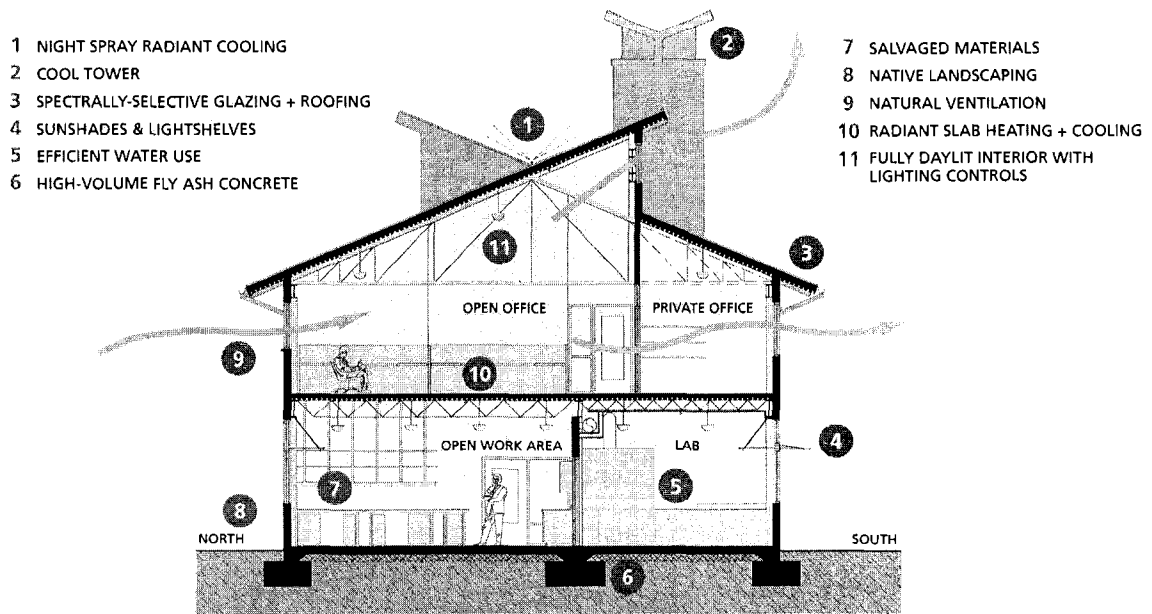
Figure 1.1. Concept of cross-ventilation system (Brager, 2006).

that "over 90% of new homeowners in Ontario do open windows, with over 40% opening windows for periods of the winter. In mid-summer, almost 10% do not open windows at all, which may indicate continuous use of air conditioning systems. These houses would benefit from mid-summer ventilation to provide fresh air". The window opening data collected (CMHC, 2004) are summarized in Figure 1.2. Many complaints reported from the occupants are due to noise and drafts from mechanical systems.

In recent developments in the design of energy efficient houses in Canada such as the EQuilibrium Housing competition launched by Canada Mortgage and Housing Corporation (CMHC) to build 12 low and net-zero energy houses across the country in 2007 (CMHC, 2007), it was shown that integration of natural ventilation with HVAC systems and solar technologies may play an important role in achieving the net-zero

2
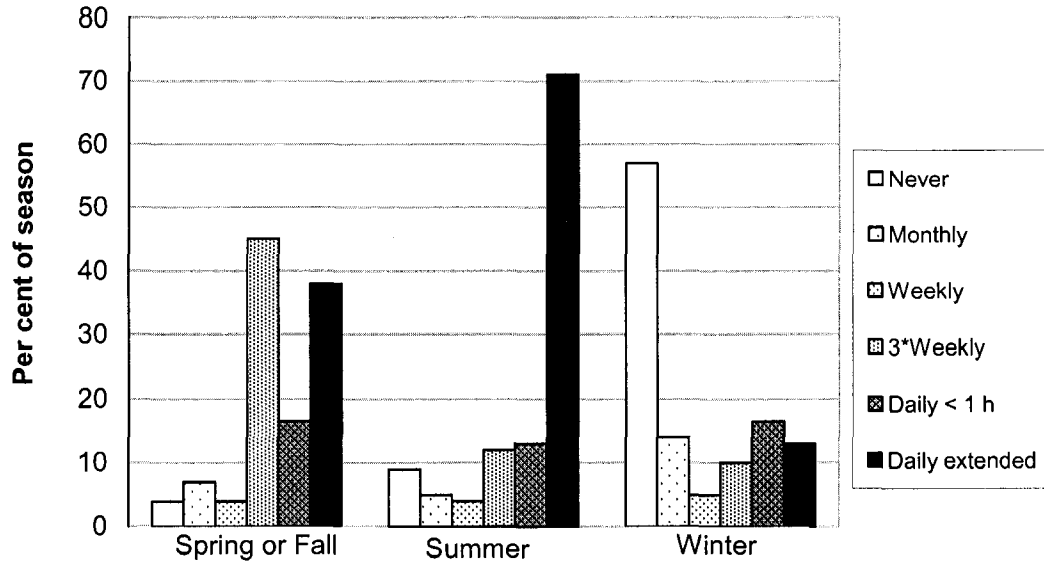
Figure 1.2. Window opening data (after CMHC, 2004).

energy target (e.g. Iolova and Bernier, 2007). Bourgeois et al. (2002) performed a feasibility study and concluded that there are barriers and opportunities to hybrid ventilation in office buildings in Canada. Barriers linked to climate and building regulations may be significant yet solutions are available in most cases. The study showed that hybrid ventilation systems designed in conjunction with other building performance requirements, e.g. integrated with solar technologies, may lead to potential energy savings. For example, the hybrid ventilation system (inlet grilles with motorized dampers at the end of the corridor in the South and North façade of each floor) of the Engineering Building of Concordia University is integrated with an atrium (Tzempelikos et al., 2007).

Past research demonstrated that occupants of naturally ventilated buildings are comfortable in a wider range of temperatures than occupants of buildings with centrally controlled HVAC systems (Brager et al., 2004). As a result, an adaptive comfort was

3

developed and incorporated into the revised ASHRAE Standard 55 (2004) as an alternative compliance method for naturally ventilated buildings. Based on the adaptive comfort zone, thermal comfort can be achieved over a wider range of temperatures and indoor air velocities (up to 0.5 m/s for higher operative temperatures encountered in the summer). Thermal comfort studies in hot and humid climates refer to allowance of even higher indoor velocity values (Santamouris, 2006).

In summary, natural / hybrid ventilation represents an area of significant interest and untapped potential in sustainable building design - both for residential and office buildings. Traditionally these buildings have relied on mechanical ventilation. However, as buildings become more energy efficient and their annual heating period is reduced, during the remainder of the time, natural / hybrid ventilation systems have the potential to significantly reduce energy consumption for cooling and ventilation.

Although natural ventilation is conceptually simple, its design can be a challenge since the ventilation performance involves the building form, its surroundings and climate. Figure 1.3 summarises the influences on the air flow distribution in buildings. Wind-induced cross-ventilation occurs due to static pressure difference across openings in the building envelope and by momentum of the incoming air if the ventilation openings are large. As a number of case studies demonstrate (Chang et al., 2004; Mochida et al., 2005 and 2006), detailed modelling of wind-driven flows in a building when deciding the placement of window openings can substantially enhance the potential for passive cooling.

Modern building systems performance standards create a need for accurate and flexible simulation models that can contribute to better design and increased confidence

4

```
┌─────────────┐      ┌─────────────┐      ┌─────────────┐
│ Wind Velocity│      │ Temperature │      │ Mechanical  │
│ Wind Direction│     │ Differences │      │ Ventilation │
└─────────────┘      └─────────────┘      │ Systems     │
       │                    │             └─────────────┘
       ▼                    ▼                    │
┌─────────────┐      ┌─────────────┐             ▼
│ Surroundings│      │ Vertical Flow│     ┌─────────────┐
└─────────────┘      │ Resistance  │      │ Fan and Duct│
       │             └─────────────┘      │ Characteristics│
       ▼                    │             └─────────────┘
┌─────────────┐             │                    │
│ Shape of the│             │                    │
│ Building    │             │                    │
└─────────────┘             │                    │
       │                    ▼                    ▼
┌─────────────┐      ┌─────────────┐      ┌─────────────┐
│ Wind Pressure│     │ Thermal Buoyancy│  │ Imposed Pressure│
│ Distribution│      └─────────────┘      └─────────────┘
└─────────────┘             │                    │
       │                    ▼                    │
       │             ┌─────────────┐             │
       └────────────▶│  Building   │◀────────────┘
                     └─────────────┘
                            │
┌─────────────┐      ┌─────────────┐
│ Inhabitant  │─────▶│  Leakage    │
│ Behaviour   │      │ Configuration│
└─────────────┘      └─────────────┘
                            │
                            ▼
                     ┌─────────────┐
                     │ Inside Pressure│
                     │ Distribution│
                     └─────────────┘
                            │
                            ▼
                     ┌─────────────┐
                     │  Air Flow   │
                     │ Distribution│
                     └─────────────┘
```
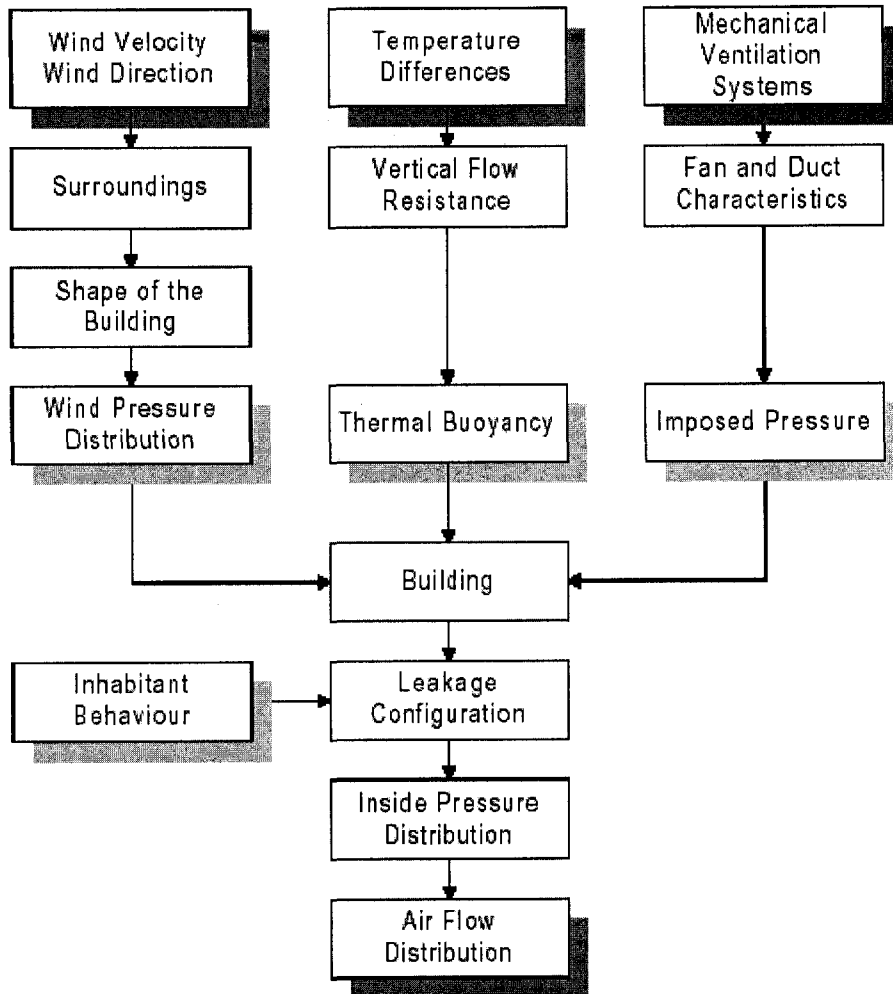
Figure 1.3. Influences on the air flow distribution in buildings (Feustel et al., 1998).

in the end results. Developing improved design tools is particularly critical to increased use of low energy, naturally driven cooling systems, because, in these cases, the cooling power is variable. Development of algorithms for the control of openings, as well as research-based design guidelines in the form of "rules of thumb" that can be used at early design stages is also necessary. A design tool is required so as to predict the pressure drop across the building envelope (driving force) and the airflow rates for various ventilation strategies and opening configurations. Design options, with respect to the

relative inlet and outlet size and location on façade, are evaluated on the basis of their impact on energy, indoor air quality (IAQ) and thermal comfort (e.g. Haves et al., 2004; Carrilho da Graça et al., 2004). To this effect, the present thesis aims to improve the existing knowledge related to a) modelling of the airflow through building openings for wind-driven cross-ventilation and b) use of existing advanced building and airflow simulation software for natural ventilation analysis of buildings with main emphasis on the impact of modelling assumptions.

1.2   Objectives and scope of research

The main objectives of the thesis are:

1. To investigate the wind-induced driving forces and ventilation flow rates in buildings with cross-ventilation.

2. To perform parametric experimental investigations into the effects of relative inlet and outlet size and their location on façade, in order to evaluate the potential for cross-ventilation and develop guidelines for implementation in design practice.

3. To develop a simulation methodology combined with a sensitivity analysis focused on modelling issues and to assess - through a case-study - the capabilities of an integrated energy and airflow simulation tool (ESP-r) to predict the envelope pressures and induced airflow rates in a large building.

The study aims to assist - in the long term - in developing innovative engineering approaches as well as design tools to support the efficient integration of natural / hybrid ventilation systems in sustainable buildings. To this end, the thesis:

1. Extends the existing knowledge regarding the airflow prediction through building envelope openings and resulting internal pressures, particularly for wind-driven cross-ventilation. Outcomes of the study can be applied to typical low-rise buildings. The study follows a Boundary Layer Wind Tunnel (BLWT) approach to investigate the velocity and pressure field in building models with cross-openings. Advanced measurement techniques such as Particle Image Velocimetry (PIV) were employed for the analysis of the flow structure of various cross-ventilation configurations, since wind-driven air flows through buildings are complex and invariably turbulent. The study evaluates mean and fluctuating building internal pressures as they affect airflow prediction, thermal comfort of occupants, and wind load design (peak values). The aim is to focus on relatively simple ventilation systems (i.e. single-zone building with cross-openings), which will increase confidence level and will provide data for validation of Computational Fluid Dynamics (CFD) techniques or airflow network models, which can be extended to more complex systems as well. The study considers a number of parameters such as relative inlet and outlet size, as well as their relative location on façade with respect to each other and the incurring external pressure distribution, e.g. symmetric vs non-symmetric inlets / outlets and configurations with openings located on adjacent or parallel walls. In real buildings, openings should be ideally oriented with respect to the prevailing wind direction in order to enhance the potential for cross-ventilation. Hence, investigations in the present study are mainly focused on configurations with the wind normal to one of the building façades. Although detailed investigations were not performed for other wind directions, some information is provided that can be applied to these cases as well. Results presented in this thesis are limited to upstream open terrain simulation. The study

provides design guidelines, for the size and placement of window openings on façade, developed on the basis of parametric experimental investigations aiming to quantify their impact on ventilation airflow rates and thermal comfort of building occupants. Such guidelines may not apply in cases where a building is in the wake of another building or in presence of vegetation.

2. Develops a simulation methodology combined with a sensitivity analysis focused on modelling issues, such as the impact of zoning assumptions, and predicts the envelope pressures and related air-exchange rates in buildings due to wind, stack, and mechanical system effects. An advanced building simulation tool (ESP-r) was used to model the coupled energy and airflow interactions in a multi-unit high-rise residential building located in Ottawa. Extensive monitoring data were available (Reardon et al., 2003) to be used as inputs in the building simulation model and for validation purposes. The model includes design parameters such as building location and geometry, climatic data (temperature, wind speed / direction), height, leakage area, mechanical supply and exhaust flow rates.

1.3   Thesis plan

Chapter 2 presents a review of natural ventilation studies in buildings, with primary emphasis on wind-driven cross-ventilation. Following this, a brief overview of existing airflow network tools is presented and the current knowledge on modelling studies with main focus on the prediction of building envelope pressures is summarized. Chapter 3 provides the necessary theoretical basis for this research and the justification of the proposed methodology. Chapter 4 presents in detail the experimental set-up for the

application of the PIV technique in a BLWT in order to investigate the air flow field in a building with various cross-ventilation configurations. Results for the mean air velocity field are presented and measured ventilation flow rates are compared with those predicted by using the orifice model. Chapter 5 presents the internal pressure investigation in two building models subject to cross-ventilation. Chapter 6 presents integrated energy and airflow simulations using ESP-r for the prediction of envelope pressures and airflow patterns in buildings where natural - wind and thermal buoyancy - and mechanical driving mechanisms are present. The main conclusions drawn from this research are summarized in Chapter 7, together with the main research contributions and the recommendations for future work.

2   LITERATURE REVIEW

2.1   Introduction

This chapter presents a review of natural ventilation studies in buildings, with primary emphasis on wind-driven cross-ventilation. With the objective of bringing into perspective the significance of the problem as well as past and present research efforts in the area of wind-driven ventilation, data collected from literature has been analyzed to identify points of agreement and areas of concern. Particular emphasis is given on parameters such as the discharge coefficient of openings and the internal pressure coefficient. As part of the analysis, results obtained using different methods (e.g. full-scale, wind tunnel, CFD, and analytical) have been compared to validate the accuracy of the existing work. This further facilitates prioritizing of experimental details and influential parameters for incorporation into the proposed research methodology. Following this, a brief overview of existing airflow network tools is presented. Modelling studies with main focus on prediction of building envelope pressures due to wind, stack, and mechanical system effects are investigated in detail.

2.2   Wind-driven cross-ventilation

For building ventilation to occur, there must be an opening on the envelope and a difference between the internal and external pressures of the building. The mean ventilation flow rate, Q (m^3/s), through any opening - with typical dimensions larger than approximately 10 mm (BSI, 1991) - is a result of this difference in pressure and is described by the following equation:

$$Q = C_D A \sqrt{\frac{2\Delta P}{\rho}}$$ (2.1)

where C_D is the orifice discharge coefficient, A is the opening area (m^2), ΔP (Pa) is the pressure difference across the opening ($P_e - P_{in}$) and ρ (kg/m^3) is the density of air. The external and internal aerodynamic pressures at an opening may be written as a coefficient, Cp_e and Cp_{in} respectively, the ratio of external and internal pressure (with respect to reference pressure, P_{ref}) to the dynamic pressure of the approaching wind ($1/2\rho U_{ref}^2$):

$$Cp_e = \frac{P_e - P_{ref}}{\frac{1}{2}\rho U_{ref}^2}$$ (2.2)

$$Cp_{in} = \frac{P_{in} - P_{ref}}{\frac{1}{2}\rho U_{ref}^2}$$ (2.3)

The opening area generates a wall porosity, defined as:

$$\text{wall porosity} = \frac{A_{opening}}{A_{wall}}$$ (2.4)

Prediction models used for natural ventilation design are discussed in Chapter 3.

2.2.1 Brief overview of previous studies

Research on natural ventilation started in the 50's. Early wind tunnel studies considered scale models and flow visualization experiments to investigate the flow characteristics of window openings and their impact on natural ventilation design of buildings (e.g. Dick, 1950; Caudill et al., 1951; Holleman, 1951; Smith, 1951; White, 1954). Cermak et al.

(1984), Wiren (1984) and Chandra et al. (1986) discuss various airflow prediction methods and quantify typical air-exchange rates in buildings subject to natural ventilation. Over the past two decades, the understanding of cross-ventilation has been significantly advanced and improved by new research considering wind tunnel tests, CFD simulations and field studies. A comprehensive literature review, as well as the analysis methods used are presented in this section.

Vickery and Karakatsanis (1987) carried out a series of tests in a boundary layer wind tunnel to measure external pressure distributions around a sealed model of a simple domestic structure in turbulent shear flow. Internal airflows were then measured for a model of the same dimensions considering a number of different wall porosities. Measured pressure distributions were employed with a theoretical flow model to compute internal flows. It was found that for low airflow rates or porosities less than about 23% and with the wind not strongly inclined to the vented faces (wind angle below 45°), internal flow rates can be predicted with moderate accuracy (about 10%) based on the external pressure distribution on the solid model and commonly accepted values for the discharge coefficients of the openings. At large values of the flow or large porosities and particularly for inclined winds, the prediction based on the previous assumption leads to significant overestimates of the airflow rates. The errors increase with the wall porosity and the wind angle.

The characteristics of cross-ventilation with open windows in buildings were analyzed through wind tunnel measurements and Large Eddy Simulation (LES) by Murakami et al. (1991), Kato et al. (1992), and Kato (2004). It was observed that a "stream tube" forms through the building model and a large part of the dynamic pressure

generated at the opening is preserved within the room while a major part of the preserved energy is directly transferred to the outside. The preservation of energy is reflected as a decrease in the value of the pressure loss coefficient (or increase of C_D). It was found that the approximation of the airflow through small openings is no longer valid in the case of cross ventilation since the use of the orifice equation is based on the assumption that the static pressure difference between the front and the back of the opening is equal to the total pressure difference. A power balance model was proposed as an alternative method. The macroscopic mechanical energy balance is derived from the Reynolds-Averaged Navier-Stokes Equation and it is applied to a simple building with cross-ventilation (Murakami et al., 1991). Axley and Chung (2005) covered the theory of this model and its implementation in a multi-zone approach. It was demonstrated that control volumes involving three or more ports are best modeled with a mechanical power balance while two-port control volumes may be effectively modeled with Bernoulli's equation. The study showed that the orifice equation is a special limited case of the practical application of the power balance model. For the prediction of the airflow rate using the power balance model, the total pressure loss coefficient must be given as an input, as well as the power or static / total pressure at the inflow and outflow boundary of the virtual stream tube. These values can only be determined by means of 3-D wind tunnel tests or 3-D numerical simulation of turbulent flow (Murakami et al., 1991). Also in buildings with more than two openings, where diverging and converging streams exist, it is complicated to determine the control volumes required for the application of the power balance method. In summary, the method may be considered more accurate compared to the conventional method, but it requires detailed input data.

Choiniere et al. (1992) considered a 1:20 scale model of a low-rise structure in wind tunnel tests for the prediction of wind-induced ventilation of livestock housing. External and internal pressure coefficients were measured in various tests performed to:

- Visualize the effect of various structural configurations on the variation of external pressure coefficients around the building and on the variations of internal pressure coefficients;

- Compare the external pressure coefficients for open versus sealed scale models;

- Identify the airflow inlet and outlet zones and the relative magnitude of ΔCp and Q over each opening area;

- Calculate the ventilation rate coefficients.

Measured and calculated values of pressure distributions and ventilation rate coefficients were compared for several cases. Regarding the effect of wind direction on the wind-induced ventilation, it was found that ventilation rates were reduced by approximately 50% when the wind was directed in a plane parallel to that of the openings compared to the wind direction normal to openings. The predicted ventilation rates for the wind normal to the openings was far lower than actually measured. Discrepancy between predicted and measured ventilation rates was found to increase with increasing opening area. This was attributed to larger openings leading to changes in the external pressure distribution that are not considered when predicting ventilation airflow rates using pressures measured on sealed structures.

The variation of discharge coefficient with the pressure difference and the opening area for a side and a bottom-hung window was investigated in a laboratory study by Heiselberg et al. (2001) for isothermal and non-isothermal conditions. The study found

that the discharge coefficient varies at small pressure differences across the opening, while it becomes constant at large pressure differences. This variation was larger in the case of the side hung window and indicates a Re dependency that might be important to consider since natural ventilation systems operate at small pressure differences most of the time. In a subsequent study (Heiselberg et al., 2002b), a bottom hung window positioned close to the ceiling and three different opening configurations were tested. Results showed that besides the opening area, the local geometrical and airflow conditions have a large impact on C_D. Smith (1951) investigated window openings at a model scale building as well as in a full-size building. The study found that details in the design of an opening may cause significant differences in the air flow patterns. More specifically, small errors in scaling of window dimensions, e.g., wall thickness, window placement in wall and sash size may result in considerably different results.

The feasibility of natural ventilation design by means of direct wind tunnel modeling of ventilation rates was investigated by Carey and Etheridge (1999) and Etheridge (2004). The investigation covers the three cases encountered in practice, i.e. wind-driven flow, buoyancy-driven flow, combined wind and buoyancy flow. Attention is focused on the following uses of wind tunnels: direct measurement of time-averaged ventilation rate, measurements of instantaneous flows in stacks, and determination of discharge coefficients for theoretical envelope flow models. From the analysis of theoretical and experimental results, it was concluded that the direct technique is feasible for a wide range of building sizes. It was also found that the direct technique offers more accuracy in the determination of wind effects than the indirect use of wind tunnels where pressure coefficients are measured for use in a mathematical model. The importance of

dimensionless numbers similarity was thoroughly discussed in the study. Results indicate that the discharge coefficient is affected by the external flow. Chiu and Etheridge (2007) carried out wind tunnel tests on two types of openings, namely a sharp-edged orifice (flush to the wall) and a long opening (chimney) using the following method: all the openings are sealed, except the opening of interest and another opening to which a flow meter with a fan is attached. The fan induces a flow through the opening and measurements of the pressure difference and flow rate induced by the fan are made. The key feature of this method is that it can show directly the effect of the external flow for both inflow and outflow for measurements with and without wind. The effects of the wind are considered to comprise three parts, i.e. presence of cross-flow, unsteadiness of the external flow, and non-uniformity of the external surface pressure field around the opening. Using "free streamline" theory and applying simple dimensional analysis it was found that the effect of external flow on the discharge coefficient is primarily determined by the cross-flow ratio, V/u, where V is the reference cross-flow velocity (m/s) and u is the flow velocity, Q/A (m/s). Experimental results obtained with a flush-mounted opening with a low area ratio (0.4% wall porosity) support this argument. The effect of unsteadiness (due to small-and large-scale turbulence) appears to be much smaller than the effect of V/u. These observations were made with the inlet of the opening exposed to the external flow. Only a few results were obtained with the outlet exposed to the wind (outward flow). For the long opening the effects of external flow are smaller. The experimental results agree fairly closely with previous work (Ohba et al., 2004) on similar openings with larger area ratios. The dimensionless parameter P_R^* used in Ohba et al. (2004) also follows from the simple dimensional analysis and is equivalent

to V/u; the latter has a clear meaning and does not tend to infinity for the still-air case. In the context of design methods for natural ventilation systems, the practice of using still-air values of C_D in envelope flow models is unlikely to lead to significant uncertainties, for sharp-orifices wall porosity in the order of 1%.

Straw (2000) and Straw et al. (2000) performed an experimental (field study), as well as theoretical and computational investigations of the wind-driven ventilation through a 6 m cube with openings on opposite faces (wall porosity equal to 2.7%). Full-scale measurements were made of the surface pressures coefficients and mean and total ventilation rates through the cube for the faces with the openings both normal and parallel to the wind. These measurement results were then compared with those from analytical and computational (CFD) methods for the prediction of ventilation rates. Turbulent air exchange can occur through the following physical phenomena:

- Continuous (but variable) airflow (broad banded ventilation) through an opening, which represent fluctuations in the ventilation flow caused by surface pressure fluctuations at the openings across a wide range of frequencies.

- Pulsating flow (resonant ventilation), caused by a body of fluid being driven perpendicular to the opening by the difference between the external and internal pressures; such ventilation flows are significantly affected by the geometry of the enclosure, and by air compressibility.

- Penetration of eddies (shear ventilation), whish is caused by fluid transfer due to eddies in unstable shear layers that exist when the external flow is across the orifice.

For normal wind incidence ($\theta = 0°$), the mean component of ventilation was considerably greater than the fluctuating component, whilst for the parallel configuration ($\theta = 90°$) the

mean component was close to zero, and the ventilation was dominated by the fluctuating component. For the normal configuration the standard discharge coefficient method was shown to under-predict the mean ventilation rate significantly. A CFD calculation using the RNG k-ε model was reasonably accurate. On the contrary, for the parallel configuration the use of the standard discharge coefficient resulted in a small over-prediction of the measured values of ventilation rate. The relative magnitudes of the ventilation produced by the various fluctuating flow mechanisms (broad banded, resonant and shear layer) were established, and methods of calculating the total ventilation rate from the mean and fluctuating components were discussed. Yang (2004) and Yang et al. (2006) performed CFD simulations (using the RNG k-ε model) and full-scale experiments for the same cubic structure to evaluate the coupled external and internal flow field under natural wind and buoyancy forces for a number of wind directions. Wright and Hargreaves (2006) performed unsteady CFD simulations for the same test building (6 m cube structure) using Detached Eddy Simulation (DES) through the use of the SST-DES model in the ANSYS-CFX software. DES employs Reynolds-Averaged Navier-Stokes (RANS) models near the wall and LES in the wake region of a flow where unsteady and chaotic motion of flow is usually found. The RANS model is used away from the wake region of the flow to save computational time compared to the use of LES in the whole computational domain. The main conclusion of this work is that Detached Eddy Simulation is feasible for natural ventilation and that the results are sufficiently accurate to initiate further investigation.

Sandberg (2002), Sandberg et al. (2004), and Jensen et al. (2002a), studied simplified well-defined geometrical shapes in an isothermal free (uniform) flow with a combination

of wind tunnel tests and CFD simulations. The starting point of the analysis was the use of a circular disk placed in a free stream with or without an opening placed in the center of the disk. The analysis was subsequently extended by including openings placed eccentrically in the disk, as well as by expanding the disk to form a cylinder. The purpose of this work was to contribute to the understanding of the parameters affecting the selection procedure of air passing through an opening or going around the building by eliminating some of the complexity involved in the airflow through real building openings. It was found that for perpendicular wind the sealed body assumption is valid for wall porosity up to 30-35%. It was concluded that a better approach might be to regard the flow through openings as a "flow catchment" problem. The flow rate is then expressed as a reference velocity times the catchment area. The basic assumptions behind the orifice equation were scrutinized in Sandberg (2004) and the application of the "catchment" method was investigated. The same geometrical configurations with those of Sandberg et al. (2004) and Jensen et al. (2002a) were investigated through CFD simulation by Jensen et al. (2002b). Two different turbulence models were used in the numerical analysis, the standard k-ε model and a Reynolds Stress Model (RSM). Results using a standard k-ε model did not compare well with experimental data, whereas the same predictions using a Reynolds stress model were almost identical to the measurements. It was also found that the pressure distribution on the windward surface is independent of what is placed downstream, and the pressure distribution from a sealed object can be used for the calculation of the airflow rate through the same object with an opening; however, it may be necessary to include modifications to the orifice equation for large wall porosities. It should be noted that the study considered well-defined

geometrical shapes subject to uniform flow conditions; therefore, results may not be applicable in real buildings.

Sawachi (2002) and Sawachi et al. (2004) conducted measurements in a specially designed wind tunnel that can accommodate full-scale buildings (e.g. 5.7m×5.7m×3.0m). The wind speed range in the working section was between 1 and 5 m/s and its flow distribution was close to uniform. Based on wind pressure and airflow distribution measurements, the inlet and outlet discharge coefficients were calculated for different wind angles. A method for predicting the discharge coefficient as a function of the wind pressure coefficient across an opening was proposed. CFD analysis using the standard k-ε turbulence model was performed for the same building (Nishizawa et al., 2004).

Kurabuchi et al. (2004) and Ohba et al. (2004) proposed the so-called local dynamic similarity model for the evaluation of the discharge coefficient and flow angle at an inflow opening for cross-ventilation. The basic idea is that the total pressure can be considered as a parameter specific to an opening in a manner similar to wind pressure. The proposed dynamic similarity model considers the total pressure in addition to the wind and room pressure, in order to explain the variation of the discharge coefficient. Also the dynamic pressure due to tangent velocity at the wall with the opening, which is important for inclined winds but neglected in the orifice assumption, is considered. The model seems to agree well with BLWT results at least for the range of wall porosities tested and it can be applied for any wind direction and opening location. An appropriate expression of the discharge coefficient as a function of a new parameter, the dimensionless room pressure P_R^* was derived. However, the proposed model is based on the sealed body assumption (the external pressure distribution is not affected by the

presence of openings), which may not be valid for large openings (Vickery and Karakatsanis, 1987; Sandberg, 2002; Jensen et al., 2002). Also the mechanical energy conservation inside the room, which might be considerable, particularly for large openings, is not considered. Numerical simulations were also performed and validated with the experimental results (Kurabuchi et al., 2004; Akamine et al., 2004; and Hu et al., 2005).

Seifert et al. (2006) performed CFD simulations for a simple cubic building with a length of 6 m and different opening configurations (opening size and relative location of inlet and outlet). The wind was modeled as a uniform profile with a speed of 2.5 m/s. The RNG turbulence model was chosen for modeling the effect of turbulence. The study found that the ventilation flow rates are affected by both wind flows around and through the building when the two openings are relatively large. The simplified macroscopic method can provide reasonable engineering accuracy (i.e., less than 10% error) when the porosity of the building envelope does not exceed a critical value; this depends on the degree of alignment between the wind direction and the dominant stream tube associated with the flow through the room. It was also found that when a "flow tube" connecting the inlet and outlet is formed, the conventional macroscopic approach underestimates the flow rate. It should be noted that the uniform wind profile assumed may have an impact on the predicted ventilation flow rates. Also the CFD results have not been validated with measured data for the ventilation flow rates.

Kotani and Yamanaka (2006) presented a simplified method for predicting the inflow direction at the inlet opening and the airflow rate. The method includes the wind velocity parallel to the wall, Cp values as well as the relationship between the inlet wind direction

and the total pressure loss coefficient of the room. Flow visualization experiments were performed using a simple room model subject to uniform flow to investigate the basic flow characteristics at the inlet opening. Tests were also performed in a boundary layer wind tunnel using a three-storey apartment building model. The inflow direction and wind velocity at the inlet openings were measured using a constant temperature hot-film anemometer with a split film probe.

Kobayashi et al. (2006) performed wind tunnel measurements and CFD simulations to investigate the flow and pressure characteristics in buildings with two openings. A house model with dimensions 120 mm (Width) × 120 mm (Height) × 180 mm (Length) provided with rectangular openings of equal size located opposite to each other was considered. The size of the openings expressed as wall porosity was 1.3 %, 5.2 %, 11.6 %, 20.7 %, and 46.5 %. In the wind tunnel, velocity and pressure were measured along the centre line through the openings. In the CFD predictions it was possible to visualize the stream tube by the method of "flying particles". Flow rates predicted by using discharge coefficients from the chamber method and the pressure difference from a sealed building were compared to those recorded. Results showed that this method seemed to be a reasonable approximation for small openings. Regarding the CFD analysis, the Reynolds- Stress Model performed better than the k-ε model in some cases although opposite results found in some other cases.

2.2.2 Comparison of previous studies

Table 2.1 summarizes existing experimental and computational studies on wind-driven cross-ventilation. Different experimental methods have been considered to measure the

airflow through building openings. Although hot-wire anemometry is capable of measuring instantaneous velocities at specific locations with sufficient frequency resolution, it is an intrusive method. Laser Doppler Velocimetry (LDV) is a non-intrusive method, but similar with the hot-wire anemometry it can only measure the velocity at one spatial position at the time. Particle Image Velocimetry (PIV) has the advantages of LDV and can also provide flow mapping over extended areas at the same time. However, the sampling frequency of present PIV systems is still low compared to hot-wire and LDV systems. Tracer gas techniques are complicated when carried out in wind tunnels and involve uncertainties related to the mixing of the tracer gas. With this technique, the use of a mixing fan, alters the internal air motion and could lead to inclusion of turbulent diffusion in the measured flow rate (Chiu and Etheridge, 2007). Birdsall (1993) and Birdsall and Meroney (1995) investigated wind-driven natural ventilation rates of a rectangular single-cell low-rise building considering tracer decay and continuous tracer release tests. The study found that the high volume of the naturally ventilated air is not uniformly mixed with the room air, resulting in a consistent bias on observed ventilation rates; this depends on the tracer gas test method, as well as the location of tracer gas sampling and release equipment in the room. Meroney et al. (1995) proposed a simple method to accommodate the simulated effects of infiltration during fluid modelling. A flow measurement technique, based on the use of suction flow models (i.e., a flow meter with a suction fan is installed at the outlet opening to measure the flow rate) in wind tunnels, was utilized by Kurabuchi et al. (2004) and Etheridge (2004). This method does not completely reproduce the natural conditions, as the internal pressure due to the fan-induced flow is, in general, different from the natural case.

Table 2.1. Computational and experimental methods for cross-ventilation.

Reference	Experimental	CFD	θ (°)	Notes
Vickery and Karakatsanis (1987)	BLWT (flowmeter conduit)	-	0-90	Orifice equation cannot be used for large wall porosities (higher than 23%) and oblique winds
Murakami et al. (1991); Kato et al. (1992); Kato (2004)	BLWT (tracer gas)	LES	0	Virtual stream tube; Power Balance Model produces better results compared to the conventional approach
Choiniere et al. (1992)	BLWT	-	0-90	Changes in the external pressure distribution of buildings with large openings; Cpin variations inside open scale-models
Katayama et al. (1992)	Field (non-directivity thermistor anemometer); wind tunnel (hot wire anemometer)	-	0	Similar trends between field and wind tunnel measurements
Aynsley (1999)	-	-	N/A	Resistance approach
Carey and Etheridge (1999); Etheridge (2004); Chiu and Etheridge (2007)	Wind tunnel (tracer gas, suction flow model)	-	0	Wind effect on discharge coefficient of openings: presence of cross-flow, unsteadiness of the external flow, non-uniformity of the external surface pressure field around the opening
Straw et al. (2000)	Field measurements (tracer gas, 3-D ultrasonic anemometer)	RNG k-ε	0, 90	Ventilation rates are not well predicted by the discharge coefficient method
Ohba et al. (2001) Kurabuchi et al. (2004, 2006); Ohba et al. (2004); Akamine et al. (2004)	BLWT (split-film anemometer, tracer gas, suction flow model)	LES, standard k-ε, Durbin's k-ε	0-75	Dynamic similarity model; C_D and flow angle as a function of a dimensionless parameter (PR*)
Jensen et al. (2002a); Sandberg et al. (2004)	Uniform flow wind tunnel (hotwire anemometer)	Standard k-ε, RSM	0	Flow catchment approach
Jian et al. (2003)	BLWT (LDA)	LES	0	Good agreement between LES and experimental results
Sawachi et al. (2004)	Uniform flow wind tunnel (tracer gas)	-	0-180	Inlet and outlet C_D as a function of ΔCp across the opening
Yang (2004) Yang et al. (2006)	Field measurements (tracer gas, 3-D ultrasonic anemometer)	RNG k-ε	0-180	RANS model predictions are reliable for wind directions near normal to the vent openings; for cases where the fluctuating ventilation rate exceeds the mean flow, RANS models are incapable of predicting the total ventilation rate

24

Table 2.1 ctd. Computational and experimental methods for cross-ventilation.

Reference	Experimental	CFD	θ (°)	Notes
Seifert et al. (2006)	-	Standard k-ε, RNG k-ε, V²f k-ε	0, 45, 67.5	RNG k-ε works better; the conventional macroscopic approach fails to provide acceptable accuracy when the "stream tube" is dominant and parallel to the wind direction
Axley and Chung (2005)	-	DNS	0	Power Balance Model
Hu et al. (2005) Hu et al. (2006)	-	Standard k-ε, RNG k-ε, Standard k-ω, SST k-ω	0-75	Dynamic similarity model; SST k-ω works better
Kobayashi et al. (2006)	Uniform flow wind tunnel (hot-wire anemometer)	Standard k-ε, RSM	0	Airflow rates, predicted using the discharge coefficients from the chamber method and the pressure difference from a sealed building, showed good agreement when compared to measured data, for small openings
Kotani and Yamanaka (2006)	Uniform flow and boundary layer wind tunnel (split-film anemometer)	-	0-90	Simultaneous prediction method of inflow direction and airflow rate
Karava et al. (2006a, 2007a, 2007b)	BLWT (hot-film anemometer, PIV)	-	0 0, 45	Non-uniform Cp_{in} for large wall porosities (i.e. more than 10%); differences between the hot-film and the PIV method up to a factor of 2.7

Hu et al. (2005) compared computational results obtained by using two-equation RANS turbulence models (standard k-ε, RNG k-ε, standard k-ω and SST k-ω) with LES predictions as well as experimental data. Results for the flow field in a building with openings located at the mid-height of the windward and leeward walls for θ = 0°are shown in Figure 2.1. The flow field within the building depicted by the standard k-ε and the RNG k-ε model did not present a "downward" trend at the inlet but an almost straight inflow. This can be attributed to the re-circulating flows (standing vortex) created at the lower portion of the external face of the windward wall that are not resolved adequately by these two models. Calculations by using the standard k-ω model and the SST k-ω model were improved. The SST k-ω model was able to depict the flow features ("downward" inflow characteristics, flow separation on the roof, standing vortex in front of the building) and ventilation flow rate with sufficient accuracy and results were very close to those of LES and to the experimental data. Straw (2000) performed CFD simulations for a cubical structure with openings located in the middle of the windward and leeward walls using the RNG k-ε model and the predicted internal flow field did not present a down-flow at the inlet. In general, since the ventilating flow in the vicinity of the opening is highly turbulent and unsteady, more sophisticated turbulence models may be required. Also selection of the grid size, particularly near the inlet opening, requires attention. The technique that offers a more consistent way of incorporating unsteady flow effects is Large Eddy Simulation. This technique is based on the hypothesis that large eddies are anisotropic and more problem-specific while the smaller ones are more isotropic. Because of the need to select an appropriately small grid size to ensure that the large eddies are captured correctly by the grid, LES has large computer requirements in
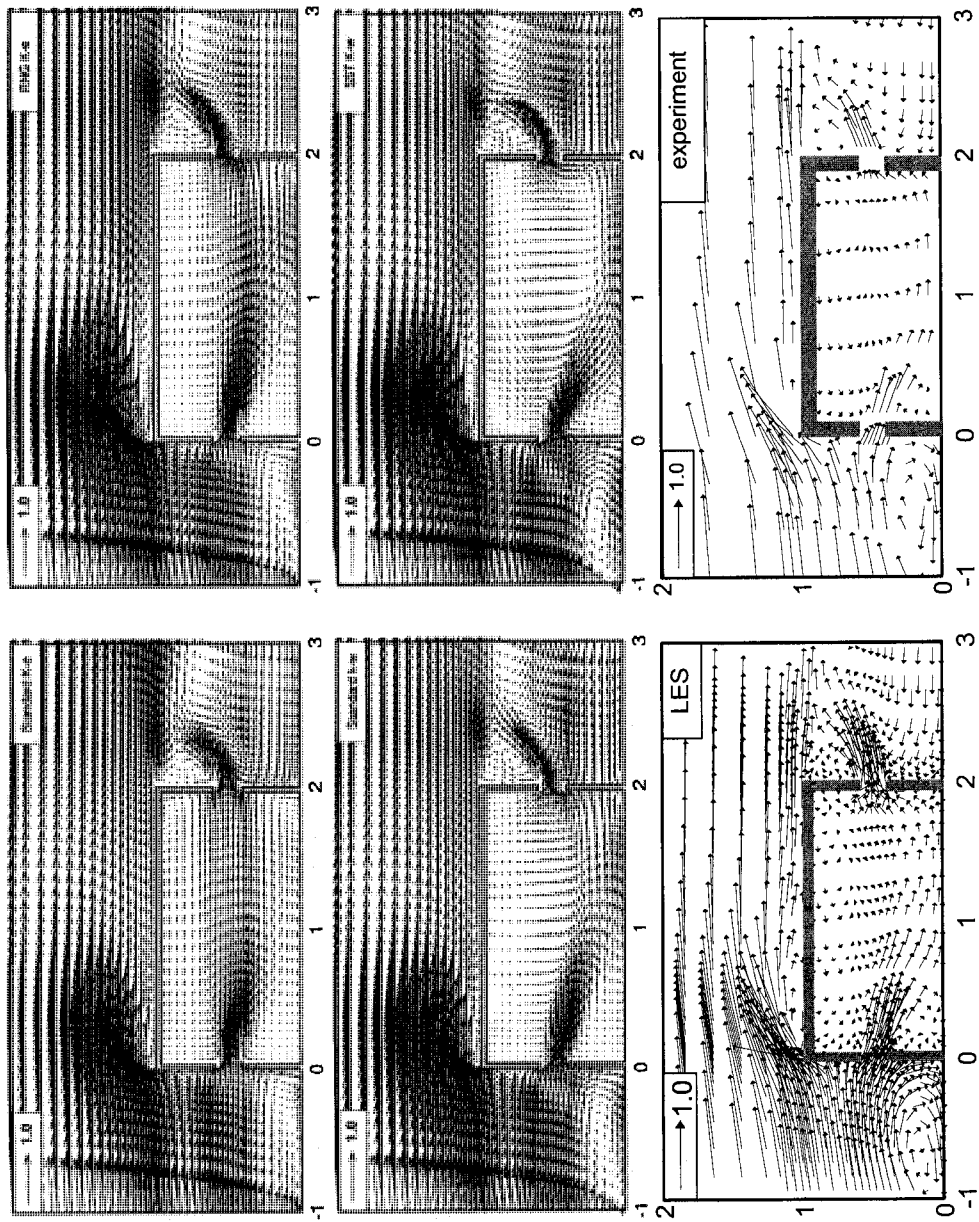
Figure 2.1. Cross sectional view of mean velocity vector field in a building with cross-openings for θ = 0°: wind tunnel and numerical results using RANS models and LES (after Hu et al., 2005).

both memory and processor speed. Also, LES requires the specification of time-dependent boundary conditions (Wright and Hargreaves, 2006).

Figure 2.2 presents mean velocity vectors for cross-ventilation configurations reported in various CFD studies. For openings located in the middle of the wall (4% wall porosity) and $\theta = 0°$, results by Hu et al. (2006) show a downfall of the inflow, while for openings located on the lower part of the wall (Kato et al., 1992, top diagram; Jian et al., 2003) there is a "straight" flow connecting the inlet and outlet. For an inlet opening located on the upper part of the wall and an outlet on the lower part of the wall, Seifert et al. (2004) show the inflow directed upwards.

In general, it can be concluded that the internal flow pattern depends on the opening area (or wall porosity), inlet to outlet ratio, relative location of the openings with respect to each other (aligned vs not aligned openings) or with respect to external pressure distribution and wind direction. It should be noted that these observations are based either on small building models, where the distance between the inlet and outlet is too short for the inflow jet to dissipate or on CFD modeling of buildings without objects inside. However, in field measurements carried out by Straw et al. (2000) similar observations with wind tunnel tests were made. In actual buildings, there are obstacles (e.g. furniture) and the jet may dissipate at a short distance after the inlet. Wind tunnel experiments by Kato et al. (1992) have shown that there is higher dissipation when windbreaks are placed inside the building models (Kato et al., 1992, bottom diagram). On the other hand, even in a building with objects, the flow always follows the easiest path.

In summary, this review shows the large number of variables associated with wind-induced ventilation and the complexity of the mechanisms involved, and stresses the need
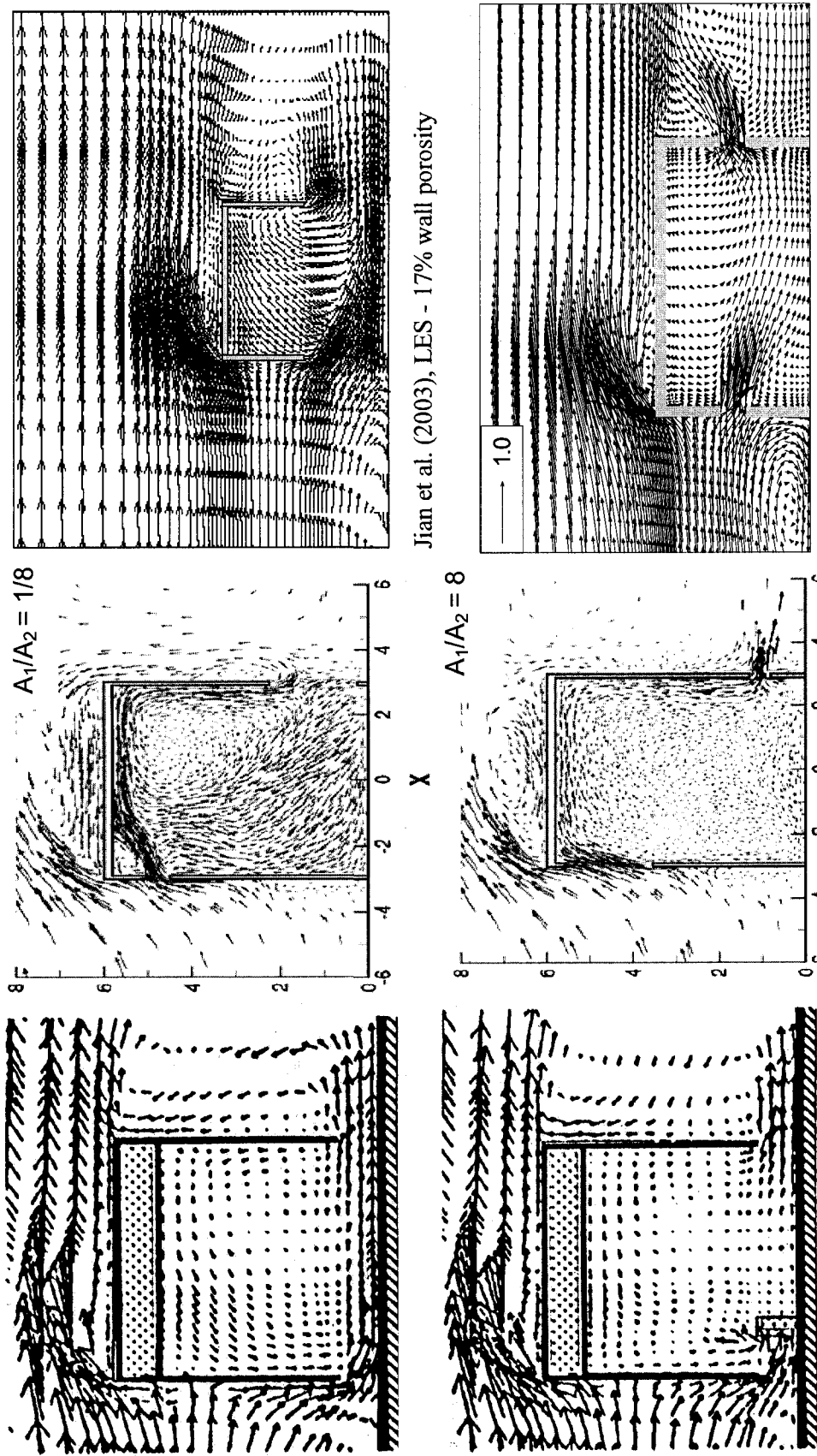
Kato et al. (1992), LES – 4% wall porosity Seifert et al. (2004), RNG k-e Hu et al. (2006), LES - 4% wall porosity

Figure 2.2. Cross sectional view of mean velocity vector field for various cross-ventilation configurations ($\theta = 0°$).

for detailed measurements using advanced experimental methods for the investigation of the velocity and pressure field.

2.2.3 Discharge coefficient

Under the assumption of steady incompressible inviscid flow, Bernoulli equation (derived form the Momentum Equation) can be applied on a horizontal stream line between a point in front of the opening with stagnant air and pressure Po and the vena contracta (minimum cross section area, A_c, of the flow with parallel stream lines, uniform velocity and static pressure equal to the surrounding air pressure). Thus, the following equation is derived for the theoretical air velocity:

$$V_{th} = (\frac{2 \cdot \Delta p}{\rho})^{0.5}$$

(2.5)

The airflow rate through an opening (continuity equation) is:

$$Q = A_c \cdot V_c = C_c \cdot A \cdot C_v \cdot V_{th} = C_D \cdot A \cdot (\frac{2\Delta P}{\rho})^{0.5}$$

(2.6)

The discharge coefficient in Equation (2.6) allows for real flow effects, i.e. includes the influence of contraction and friction, and it is given by the following equation (Andersen, 1996):

$$C_D = C_c \cdot C_v$$

(2.7)

where,

A_c = cross section area of the vena contracta $(A_c = C_c \cdot A)$

V_c = air velocity in the vena contracta $(V_c = C_v \cdot V_{th})$

A = opening area

V_{th} = theoretical air velocity

C_c = contraction coefficient (≤ 1)

C_v = velocity coefficient depending on the friction conditions (≤ 1).

Discharge coefficient is a weak function of Reynolds number and is a strong function of orifice shape and thickness (Straw et al., 2000). For a sharp-edged opening in an infinite plane wall under still air conditions, the discharge coefficient can be taken as a constant that depends only on the opening shape. Basically, the sharp edges fix the points of flow separations and hence lead to a flow pattern that is independent of Re, except at very low Re (creeping flow). A circular sharp-edged opening in a plane wall has a C_D of about 0.61 - 0.65. Even when the opening is placed in a pipe with fully developed turbulent flow, the discharge coefficient is about 0.65 for a wide range of area ratios and Reynolds numbers. Typical C_D values for other opening shapes vary from 0.6 to 0.9 (Etheridge and Sandberg, 1996). For wind-driven cross-ventilation the velocity and pressure fields at the inlet and outlet are unsteady, creating difficulties with the selection of C_D and, more fundamentally, its definition (Etheridge, 2004). In this case, the discharge coefficient depends on the geometry of the opening but also the external and the internal flow field. In fact, for large opening area, there is significant air movement in the room and the flow might no longer be considered as pressure-driven. The total, inlet and outlet discharge coefficients are given by the following equations:

$$C_{D,total} = \frac{Q}{A \cdot \sqrt{\dfrac{2 \cdot | P_w - P_L |}{\rho}}} \qquad (2.8)$$

$$C_{D,inlet} = \frac{Q}{A \cdot \sqrt{\dfrac{2 \cdot | P_w - P_{in} |}{\rho}}} \qquad (2.7) \qquad C_{D,outlet} = \frac{Q}{A \cdot \sqrt{\dfrac{2 \cdot | P_{in} - P_L |}{\rho}}} \qquad (2.9)$$

where

P_w = windward wall pressure (Pa)

P_L = leeward wall pressure (Pa)

P_{in} = internal pressure (Pa)

The so-called total pressure loss coefficient ζ is often used instead of the discharge coefficient (e.g. Murakami et al., 1991; Vickery and Karakatsanis, 1987). The following equation given by Andersen (1996) is used to calculate C_D values based on total pressure loss coefficient values:

$$\zeta = \Delta P_t \cdot \frac{2}{\rho} \cdot \left(\frac{A}{Q}\right)^2 = \frac{1}{C_D{}^2} \qquad (2.10)$$

where

ΔP_t = total pressure drop (Pa)

ρ = air density (kg/m^3).

In this section, data has been gathered from literature sources and are presented in a comparative form. For more information the reader may refer to Karava et al. (2004a; 2004b). The opening configurations (i.e. circular or rectangular openings, inlets or outlets), the parameters considered and the conditions under which the experiments were carried out are different in the various studies. This makes such comparisons a difficult task. It was attempted to compare as "similar" cases as possible by using specific (partial) data from various literature sources. Figure 2.3a illustrates some of the circular openings tested in an isothermal free (uniform) flow (Sandberg, 2002; Jensen et al., 2002a). Figure 2.3b shows the bottom hung window tested by Heiselberg et al. (2002b). Generally, cases with equal inlet and outlet opening area, thin opening walls, and normal wind incidence angle are considered.
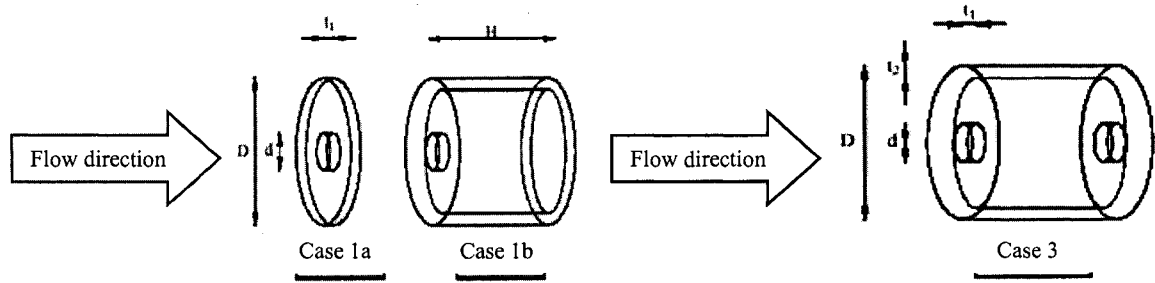
(a) Circular openings (after Sandberg, 2002; Jensen et al., 2002a)
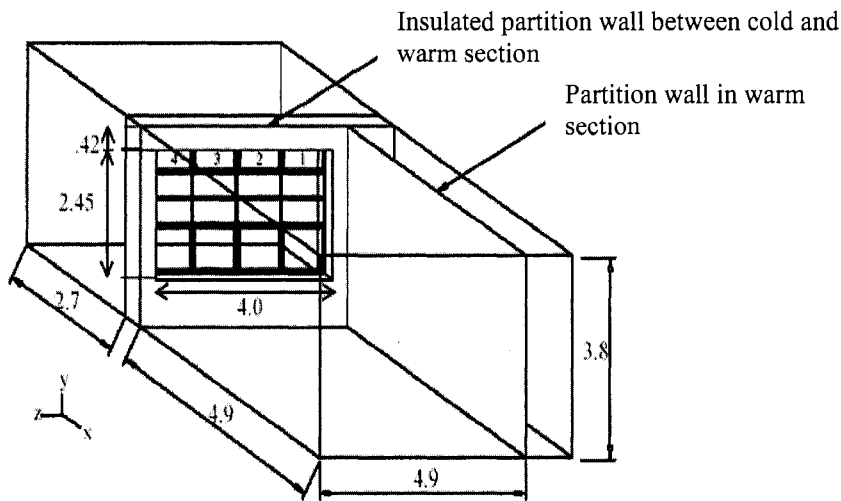
(b) Bottom hung window (after Heiselberg et al., 2002b)

Figure 2.3. Opening configurations used in previous studies.

Figure 2.4 presents discharge coefficients as a function of the wall porosity for circular openings for the configurations shown in Figure 2.3a. Results from wind tunnel measurements are shown in Figure 2.4a while those obtained by CFD simulations are presented in Figure 2.4b. The latter are derived by Jensen et al. (2002a) and Sandberg (2002) who used a Reynolds stress model. Note that the non-linear regression curves for

the respective experimental and CFD data were produced by using reported results of Sandberg (2002) and Jensen et al. (2002a). Analysis of the results presented in Figure 2.4 shows the following:

- There is significant variation of the discharge coefficient with the wall porosity and configuration. This variation is larger for the experimental results compared to those obtained by CFD.

- There is less dependence on the opening configuration for larger porosities (i.e. more than 10%).

Figure 2.5 shows discharge coefficients as a function of the wall porosity for rectangular openings. Note that the regression curves in Figure 2.5 were produced from the results reported by Heiselberg et al. (1999; 2002b). Analysis of Figure 2.5 shows significant variation of C_D with the wall porosity and configuration (C_D changes from about 0.5 to 1) but no clear trend can be established. Aynsley et al. (1977) and Murakami et al. (1991) results show an increase of the discharge coefficient with porosity while studies by Heiselberg et al. (1999; 2002b) found that discharge coefficient might decrease, increase or remain almost constant with the wall porosity for different configurations shown in Figure 2.3b. More specifically, it was found that the discharge coefficient decreases with increase of the porosity for a side hung window or a bottom hung window and configuration W2 (inner window). For configuration W1 (corner window) C_D is almost constant and for configuration W1-4 (window fully open) the discharge coefficient increases with the wall porosity (see also Figure 2.3b). Sawachi (2002) found that there is no variation of the discharge coefficient with wall porosity. The
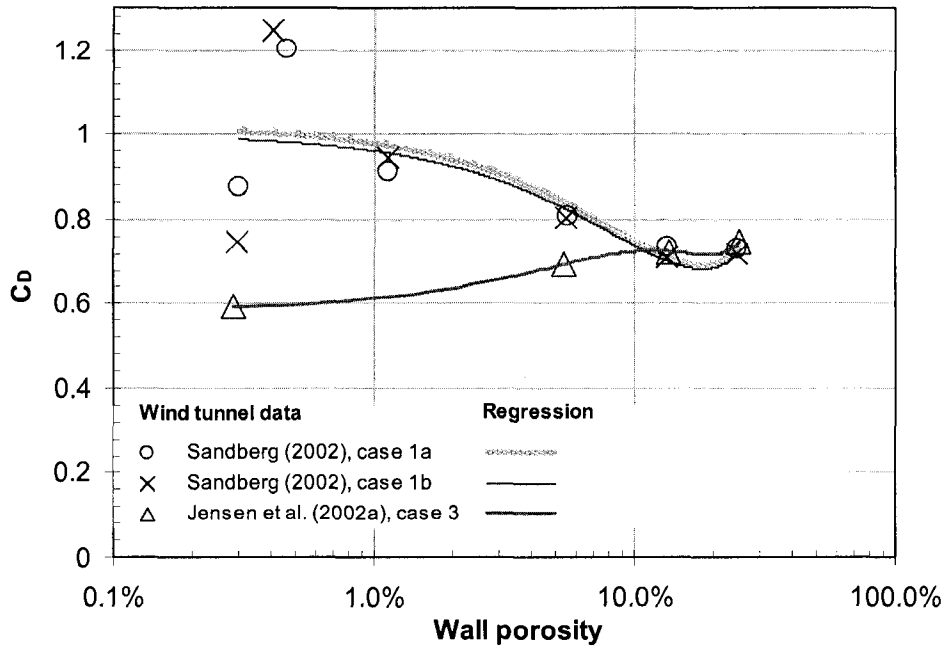
(a) Wind tunnel results
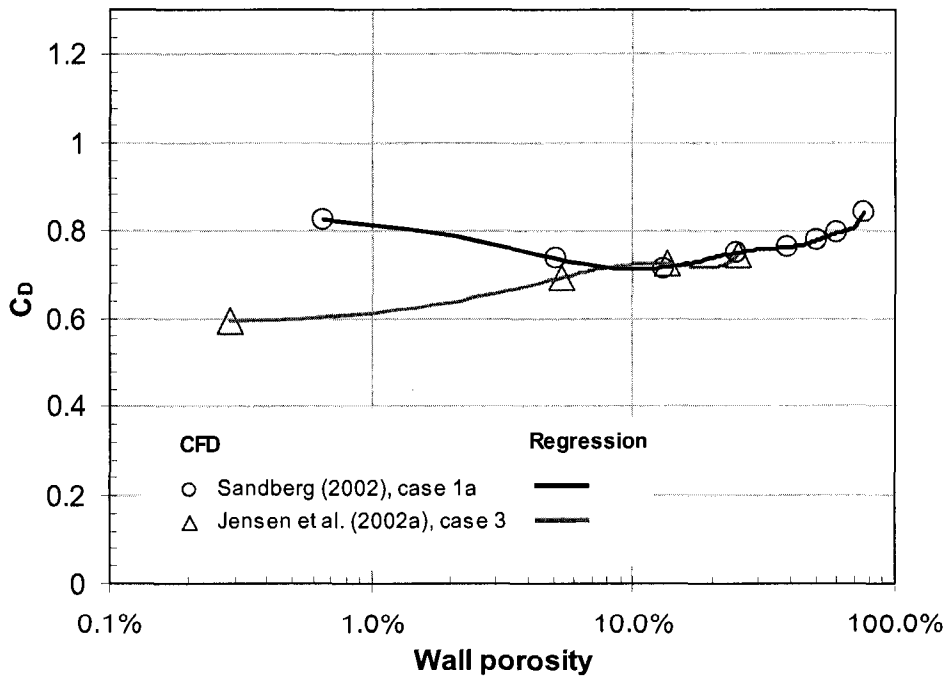
(b) CFD results

Figure 2.4. Discharge coefficients as a function of wall porosity for circular openings.
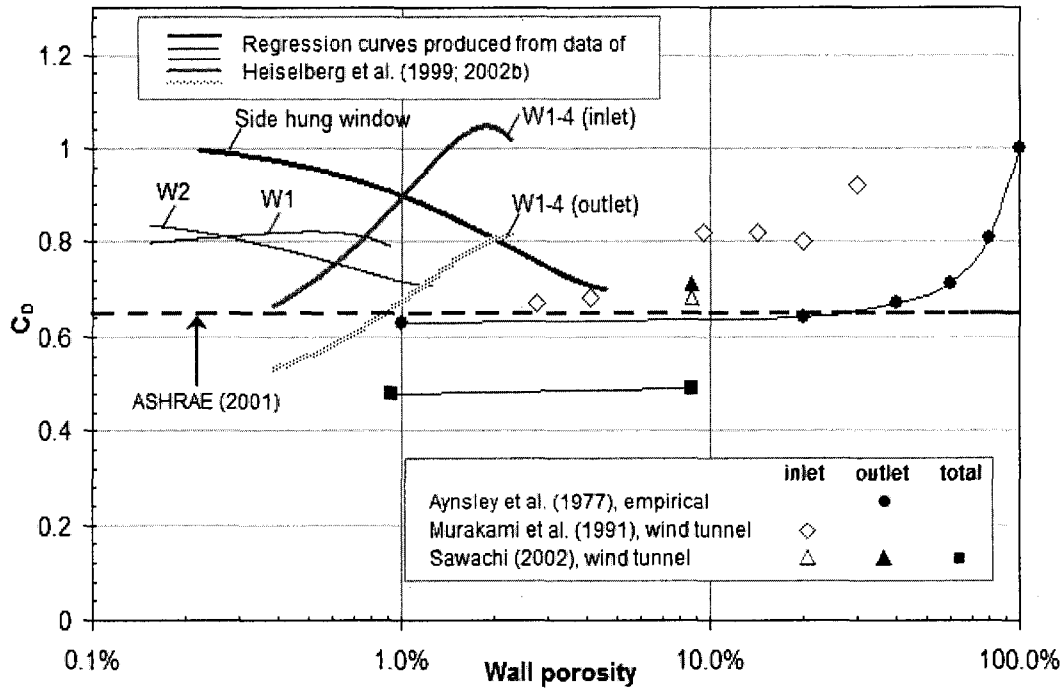
Figure 2.5. Discharge coefficients as a function of wall porosity (rectangular openings, windows).

variation of discharge coefficient with the non-dimensional room pressure for different window openings was investigated by Ohba et al. (2004); discharge coefficient values found are much lower (0.25 - 0.65 for the louver window; 0.25 - 0.6 for the pivoted window) compared to the values found by Heiselberg et al. (2001) (0.65 - 1 for the side hung window; 0.8 - 1 for the bottom hung window). It should be noted that notwithstanding the single window opening in the configurations considered by Heiselberg et al. (1999; 2002b), this was considered as cross-ventilation due to the cross-flow through the opening. Inlet discharge coefficient values for configurations with large wall porosities are higher than typical values, i.e. 0.61 - 0.65 for sharp-edged orifices (Etheridge and Sandberg, 1996).

36

Figure 2.6 illustrates the inlet discharge coefficient variation with the wind incidence angle for rectangular openings. Wind tunnel (for wall porosity 9%) and CFD (for wall porosity 4%) results indicate a decrease of the discharge coefficient with wind angle, as expected.

Figure 2.7 shows the variation of the discharge coefficient with the opening Reynolds number. Discharge coefficient values higher than 1 reported by Vickery and Karakatsanis (1987) for an outlet opening (rectangular) and 46% wall porosity. For the same case, the inlet C_D varies between 0.62 and 0.8. These are results from a series of tests carried out in a boundary layer wind tunnel. Discharge coefficient values reported by Jensen et al. (2002a) from experiments in an isothermal free (uniform) flow wind tunnel vary between 0.6 and 0.9 for a circular opening and wall porosity from 0.3 to 25%. C_D values about
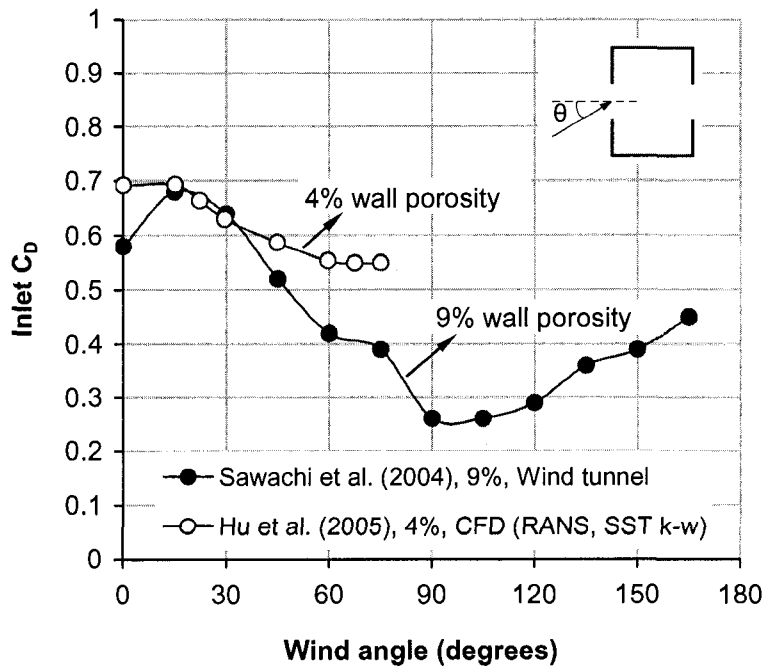
Figure 2.6. Total discharge coefficient for rectangular openings as a function of wind angle.
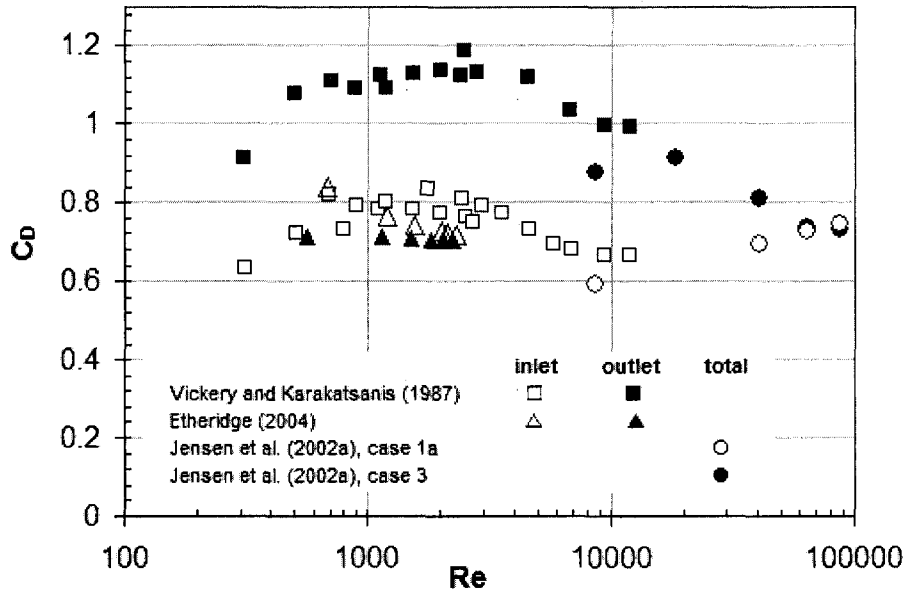
Figure 2.7. Discharge coefficients as a function of Reynolds number of the flow through the opening.

0.7-0.75 that are slightly higher for the inlet opening found by Etheridge (2004) for a circular opening and porosity 0.1%. Chiu and Etheridge (2007) reported little dependence of C_D on Re, except for cases with lower Re (Re < 1000).

In summary, review of the literature shows considerable variation of the discharge coefficient with wall porosity, opening configuration (shape and location on façade), and wind angle; hence, the use of a constant value - based on the assumption of a small opening (e.g. thin orifice) and sufficiently large Reynolds number - such as that used in simplified air flow prediction models (for natural ventilation design) might be an invalid simplification. Different C_D values found in various studies may be due to different opening configurations and external air flow conditions (uniform or boundary layer flow) considered, as well as uncertainties in wind tunnel experiments (e.g. due to scaling,

blockage of the wind tunnel cross-section, lack of consideration of internal partitions) and in airflow measurements.

2.2.4 Internal pressure coefficient

Internal pressure coefficients in buildings with openings in one wall received a lot of attention starting in the 70's mainly for structural applications. Aynsley et al. (1977) investigated the impact of wall porosity on internal pressures. Stathopoulos et al. (1979) carried out BLWT experiments in order to investigate the impact of various opening configurations on internal pressures for different background leakage values, wall openings and exposures. It was reported that the internal pressure is uniform and its value does not depend on the measurement point. Bachlin and Plate (1986) investigated the impact of the building shape on internal pressures in addition to the opening ratio and background leakage. Wu et al. (1998) carried out a comparison among various studies for mean and peak internal pressures for buildings with a dominant opening while a more recent state of the art review was reported by Oh et al. (2007). Several studies have been recently performed on single-sided ventilation (i.e. Jian et al., 2003; Kono et al., 2005) but very few report internal pressure coefficients. The effects of turbulence are dominant for single-sided ventilation, resulting in the classic modes of turbulent air exchange between the building and external flow - pulsating flow and penetration of eddies. More information on unsteady flow effects due to fluctuating wind pressures in natural ventilation design can be found in Haghighat et al. (1991) and Etheridge (2000a; 2000b).

Internal pressure coefficients for buildings subject to cross-ventilation have been reported by Munarin (1978), Holmes (1979), Liu (1991), Choiniere et al. (1992),

Murakami et al. (1991), Womble (1994), Womble et al. (1995), Ginger et al. (1995), Straw et al. (2000), Kurabuchi et al. (2004), Sawachi et al. (2004), and Hu et al. (2005). Generally, studies on internal pressures in buildings with cross-openings are difficult, mainly due to the associated measurement complexities (e.g. scaling of internal volume, sophisticated building models required, etc). In several studies internal pressure is measured only in a single tap.

Munarin (1978) measured the mean internal pressure in a building with symmetric openings located in the middle of the wall using a single floor tap and 19 floor taps and he found similar results. Choiniere et al. (1992) focused on the prediction of wind-induced ventilation for livestock housing and found variations of the mean Cp_{in} value in buildings with large continuous sidewall, ridge or chimney, and end wall openings for different wind directions. It was concluded that detailed studies are needed to evaluate the number of internal pressure taps required and their locations in order to obtain an accurate picture of the Cp_{in} variations. It was pointed out that sufficient data are not available to be able to study the effects of the variation of Cp_{in} on local and total ventilation rates. Murakami et al. (1991) and Straw et al. (2000) measured mean internal pressures using two taps (on the floor or on the inlet / outlet wall respectively) for building with cross-ventilation and large openings (wall porosity 2.5-30% and 2.7% respectively) and reported small differences in Cp_{in} values. Studies by Womble et al. (1995) and Ginger et al. (1995) considered configurations with relatively small openings and reported spatially-uniform mean and peak internal pressures. Comparisons of previous data with more recent findings for internal pressure coefficients in buildings subject to cross-ventilation will be presented in Chapter 5.

2.3 Overview of existing airflow network models

A large number of papers describe multizone airflow network models. A survey of multizone airflow models published in 1992 (Feustel and Dieris, 1992) described 50 different programs with different level of sophistication. Another review on applicable models for air infiltration and ventilation calculations followed by Orme (1999). Models such as AIRNET (Walton, 1989), AIDA (Liddamnet, 1989), AIM (Walker and Wilson, 1990), ESP-r (Hensen, 1991), BREESE (BRE, 1994), AIOLOS (UoA, 1997), CONTAM (Walton, 1997), NATVENT (Svensson and Aggerholm, 1998), COMIS (Feustel, 1999), are only a few of them. COMIS, a simulation tool developed at Lawrence Berkeley Laboratory and CONTAM are the most widely used models. Annex 23, "Multizone Air Infiltration Modeling" focused on the validation of such models (mainly COMIS). A brief summary of the validation exercises can be found in: Haghighat and Megri (1996), Blomsterberg et al. (1999), Borchiellini and Furbringer (1999), Dascalaki et al. (1999), Feustel (1999), Furbringer et al. (1999), Furbringer and Roulet (1999), Upham et al. (2001), Li (2002).

Although significant work during the past 4 decades led to the development of advanced energy simulation tools such as ESP-r (ESRU, 2002), TRNSYS (Beckman et al. 1994), Energy Plus (Crawley et al. 1999) and multizone airflow models, the development of coupled thermal / airflow simulation programs only started in the 90's. In fact, in building energy prediction, it is still common practice to separate the thermal analysis from the estimation of air infiltration and ventilation. This might be a reasonable assumption for many practical problems, where the air flow is predominantly pressure driven; i.e. wind pressure, or pressures imposed by the HVAC system. However, this

simplification is not valid for buoyancy driven airflow where the modeling of thermally induced driving forces is limited since in many applications the room air temperatures are not known. In such cases, coupling of a thermal and an air flow model is needed.

In the case where the thermal model and the airflow model are actually dealt with in programs which run in sequence, the above-mentioned coupling cannot be done on a per time step basis. The so-called sequential coupling, as described by Kendrick (1993) and quantified through a case study by Heidt and Nayak (1994), is applied. In this study, the impact of infiltration on thermal performance of a single-family building was investigated. It was found that infiltration loss with fixed air exchange rate was different from that with an integrated model. For applications involving buoyancy-driven air flow, relative large errors in predicted temperatures and flows may be expected when using inter-model sequential coupling. In cases where the thermal and airflow model are integrated in the same software system, coupling is possible using two different approaches:

1. A de-coupled approach ("ping-pong"), in which the thermal and flow models run in sequence (i.e. each model uses the results of the other model in the previous time step).

2. A coupled approach ("onion"), in which the thermal and flow models iterate within one time step until satisfactory small error estimates are achieved.

Figure 2.8 is a schematic representation of the two approaches. Each of the approaches for integrating heat and air flow calculations has specific consequences in terms of computing resources and accuracy.

The ESP-r's coupled approach has been described by Hensen (1991). The "ping-pong" and "onion" approach were compared by Hensen (1999) assuming a typical case
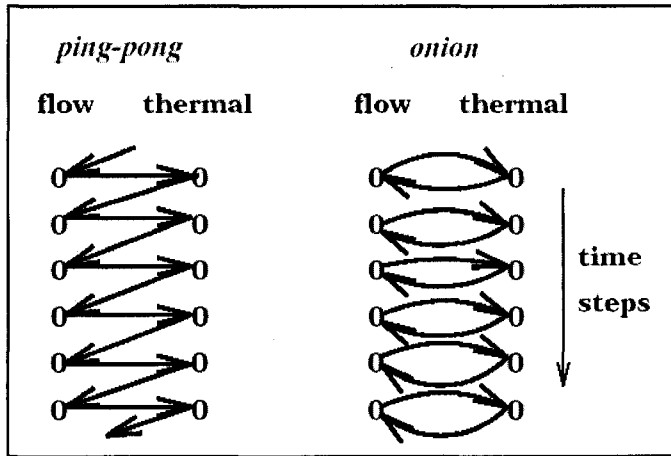
Figure 2.8. Schematic representation of a de-coupled non-iterative (ping-pong) vs a coupled iterative (onion) approach (Hensen, 1996).

study (a free running building), for which the differences in air flow were found larger than the differences in air temperatures. Actually, the temperature differences between the various methods grow with the number of stacked zones. The results indicate that when properly used, each method may give satisfactory results. However, when used improperly in respect to the time step, the onion method will have implications in terms of computing resources, but the ping-pong method may generate substantial errors. In general, it is advisable to be careful with the ping-pong approach in combination with long time steps for problems with strongly coupled heat and air flow.

Dorer and Weber (1999) presented a short description of the concept used for the coupling of the air flow and contaminant transport simulation code of COMIS into the building and systems simulation code TRNSYS. At each time step in the dynamic simulation, a solution is iteratively determined. In each iteration loop, the room air temperature values are passed from the thermal building model to COMV-TRNS, which returns the respective air flow rates to the building model of TRNSYS.

Basic principles of the ESP-r building simulation system are presented in the next section.

2.3.1 ESP-r basic characteristics

ESP-r has been on going development for over three decades. Specifically, ESP-r simulates the thermal state of the building by applying a finite-difference formulation based on a control-volume heat-balance to represent all relevant energy flows. Figure 2.9 illustrates the integrated ESP- r simulator. The multi-zone airflow model network implemented in ESP-r is based on the work of Cockcroft (1979), with extensions and refinements by Hensen (1991). Macroscopic models typically represent large air volumes (e.g. rooms) with uniform conditions, and predict flow through discrete paths (e.g. doors, cracks). Although the method presumes one-dimensional steady-state flow, boundary
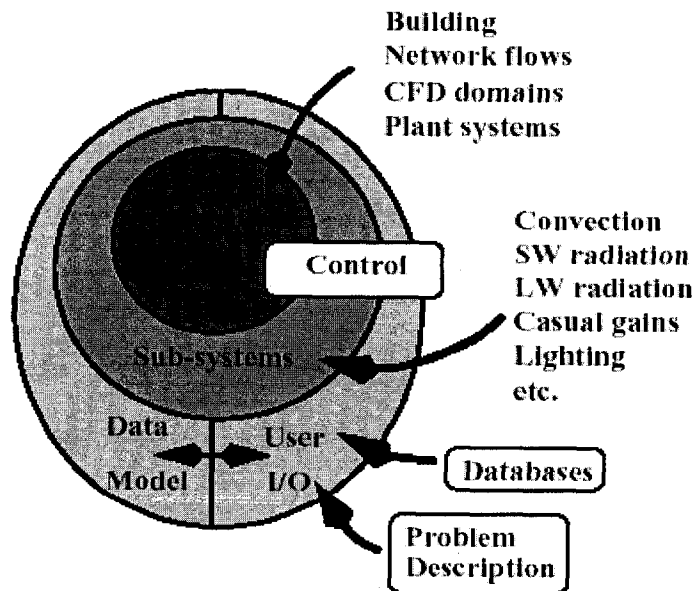
Figure 2.9. The ESP-r integrated simulator (Hensen, 1991).

conditions (wind, temperatures, fan operation, window openings) can vary in time. Stack effect caused by indoor-outdoor and inter-zone temperature difference is also considered. Evaluating the mass balance for each node gives rise to a non-linear set of equations solved by an iterative procedure (Newton-Raphson technique). In order to couple the simulation of heat and air flow, ESP-r overlays its thermal and network airflow models. The two models are coupled by passing information between the solution domains during or at the end of each time-step.

2.3.2 Prediction of envelope pressures and indoor-outdoor air-exchange rate in buildings

Several studies exist related to monitoring and/or development of building simulation models for buildings with natural / hybrid ventilation. Some of them (e.g. Jeong et al., 2003; Wachenfeldt, 2003) were performed within the context of an International Energy Agency program on Energy Conservation in Building Community Service - Annex 35 "Hybrid Ventilation in New and Retrofitted Office Buildings" and main findings are summarized in Heiselberg (2002). A more recent study by Wang and Wong (2007) examined the impact of various ventilation strategies and facade design options on indoor thermal environment for naturally ventilated residential buildings in Singapore. Presenting a detailed review of these studies is out of the scope of the present research work. The review of the literature presented in this section is focusing on studies related to the prediction of building envelope pressures. Most of the work done in this area is related to the monitoring and modelling of the ventilation performance of high-rise residential buildings, which has been mainly driven by the associated high energy costs

(CMHC, 1996; Cooke, 2005; Persily, 1998). Walker et al. (1998) and Li (2002) investigated the issue of superposition of driving mechanisms (mechanical and natural forces) from the fundamental point of view.

The literature on multi-family buildings and especially on high-rise multi-unit buildings is quite extensive. A pioneering study by Tamura and Wilson (1966) measured the pressures across the exterior envelope of a 9-storey building in Ottawa, Canada. An early study on measurements of air leakage in multi-storey apartment buildings was performed by Shaw (1980). A summary of experimental studies for North American multi-family buildings (both high-rise and low-rise) was presented by Diamond et al. (1996). Modelling studies for high-rise residential buildings are very limited (Feustel and Diamond, 1998; Walker, 1999; Liu et al., 2005) due to complexities and lack of detailed experimental data to be used as inputs and for validation. In the previously mentioned studies, the airflow models COMIS (Feustel, 1999) and CONTAM (Walton, 1997) were used for the simulations; therefore, the buoyancy effects have not been taken adequately into account. Methods for controlling stack-driven flows in multi-unit residential buildings are discussed by Lstiburek (2005). Typical leakage areas of multi-unit residential buildings are available in CMHC (1991; 1996) and Cooke et al. (2005). In general, several articles refer to problems in measuring, modeling and designing ventilation systems for high-rise multi-family buildings, but only few offer solutions. Also existing studies mainly focus on ventilation problems in buildings rather than issues related to required modelling detail and validation of airflow network models.

Diamond et al. (1996) and Feustel and Diamond (1998) carried out airflow and air leakage measurements in a 13-storey apartment building located in Chelsea,

Massachusetts. Based on the measured air leakage data from the building, extensive air flow modelling was conducted using the multi-zone air flow model COMIS. Parametric simulations were performed for specific conditions, e.g., height, orientation, outside temperature and wind speed. Over one hundred zones were defined in the model as each floor was divided into four corner zones, one zone describing the hallway and one zone for each of the staircases, the elevators, the supply shaft and the exhaust shafts, with 138 outside pressure points (wind pressure distribution). Results show that ventilation to the individual units varies considerably even with the mechanical ventilation system operating. The study discussed ventilation problems in high-rise buildings associated with the interaction of natural (wind and stack effect) and mechanical forces. However, the level of validation of airflow simulations may not be satisfactory, due to the lack of detailed experimental data.

Edward (1999) carried out a detailed literature search to assemble and interpret the best available data that can be used for performing multi-zone airflow modelling in mid- and high-rise apartment buildings. The purpose of this project was to improve the ability of designers to use multi-zone airflow modelling tools to develop improved building designs. The multi-zone airflow modelling software tool CONTAM was used to provide an analysis of ventilation related energy issues in a newly constructed 10-storey high-rise apartment building located in Mississauga Ontario. Each suite was represented by a single control volume zone as well as the corridor on each floor. The elevator shaft was modelled as a single zone running the height of the building. The stairway shaft was modelled using the Achakji and Tamura (1989) stairway model provided in CONTAM. A total of 177 zones were created to represent independent control volumes linked by

airflow paths. The relative influences of infiltration and ventilation on energy consumption were compared, and other key energy-related questions were looked at as they apply to an actual building modelled within a range of Canadian climatic conditions. With corridor ventilation fans in the building operating as designed, infiltration contributed up to 72% of the total ventilation and infiltration heating load under steady-state weather conditions modelling. Under outdoor conditions representative of typical January weather in the cities of Vancouver, Winnipeg, and Toronto, the average contribution of infiltration to total outdoor airflow heating load (with corridor ventilation fans on) was found to be 33%, 54%, and 42% respectively (with no suite exhaust fans operating). The conclusion drawn from the study is that current ventilation system designs for mid-and high rise apartment buildings do not work well for either ensuring adequate indoor air quality or reducing energy consumption attributable to infiltration airflow.

Richards (2007) performed measurements in a 10-storey multi unit residential building located in Saskatoon, Canada. Monitoring of the building included CO_2 concentration, ventilation effectiveness, and pressure drop across the building envelope, while energy bills indicating electrical and natural gas consumption were also investigated. Building energy simulations using EE4 (2007) and RETScreen (2007) tools were performed to evaluate different retrofit options in order to achieve a factor of 10 reduction of the energy consumption of the building. Over 40 retrofits were presented and the most economically advantageous mechanical system that was added to the building was energy recovery in the outdoor ventilation air. The study presents interesting design concepts but there are some over-simplified assumptions involved in modelling.

3   ISSUES   IN   NATURAL   VENTILATION   DESIGN   OF   BUILDINGS

3.1   Introduction

This chapter discusses unresolved issues related to natural ventilation design of buildings and provides the necessary theoretical basis and justification of the proposed research.

3.2   Natural ventilation in codes and standards

Mechanical ventilation systems have been mandated for office buildings and dwellings in the National Building Code of Canada (NBCC, 2005). Natural ventilation is allowed by NBCC to be used for dwellings. The code specifies the minimum unobstructed operable ventilation area that must be provided in individual rooms for code conformance (e.g. 0.28 m^2 for living rooms, bedrooms, etc.). It is also mentioned that houses with mechanical ventilation can use natural ventilation to control summer overheating. Natural ventilation is referred to in ASHRAE Standard 62.2 (2004), Ventilation for Acceptable Indoor Air Quality (IAQ) for low-rise residential buildings (less than three storeys), as an alternative method to mechanical ventilation. Accordingly, each habitable space shall be provided with ventilation openings with an openable area not less than 4% of the room floor area nor less than 0.5 m^2. According to ASHRAE Standard 62.1 (2007), Ventilation for Acceptable Indoor Air Quality (for any building except low-rise residential), use of natural ventilation systems is permitted in lieu of or in conjunction with mechanical ventilation systems. The Standard regulates a minimum area of operable windows as 4% of the net floor area.

Code or standard specifications with respect to the opening area only are inadequate to provide guidance for natural ventilation design when it is used for passive cooling. Codes should provide specifications for different window types, their location on the façade as well as appropriate methods to calculate the required airflow rates when natural ventilation is used.

3.3   Natural ventilation design

For engineering purposes, a simplified method, the orifice equation is commonly used for ventilation analysis of buildings. A schematic representation of cross-ventilation in a single-zone building with two openings is shown in Figure 3.1. For wind-driven cross-ventilation the mean airflow rate, Q (m^3/s), through two openings (orifices) in series can be calculated by the following equation (Aynsley et al., 1977):

$$Q = (C_{D,total} \cdot A) \cdot U_{ref} \cdot \sqrt{Cp_w - Cp_L} \tag{3.1}$$

where

$$(C_{D,total} \cdot A) = \frac{(C_{D1} \cdot A_1) \cdot (C_{D2} \cdot A_2)}{\sqrt{(C_{D1} \cdot A_1)^2 + (C_{D2} \cdot A_2)^2}} \tag{3.2}$$

A = equivalent opening area (m^2); $C_{D,total}$ = total discharge coefficient; U_{ref} = reference wind speed at building height (m/s); Cp_w = pressure coefficient on windward façade; Cp_L = pressure coefficient on leeward façade; A_1 = inlet opening area (m^2); A_2 = outlet opening area (m^2); C_{D1} = inlet discharge coefficient; C_{D2} = outlet discharge coefficient.

The effects of viscous forces are not explicitly considered in Equation (3.1) but are accounted for in the discharge coefficient that relates pressure losses due to flow
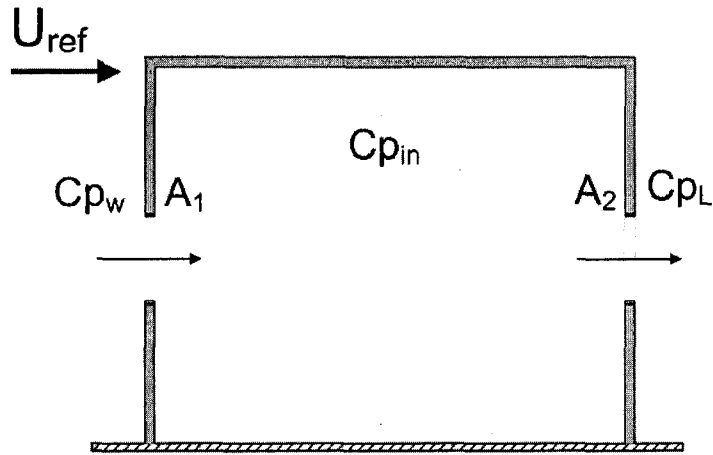
Figure 3.1. Schematic representation of wind-driven cross-ventilation.

resistance in the opening. It is conventional to assign a value to the discharge coefficient as that of a sharp edged orifice. Consequently, the total ventilation area A, becomes the equivalent area associated with that particular opening, i.e. the area of the equivalent sharp-edged orifice which would give the same flow rate as the opening concerned at the same applied pressure. For openings such as open windows (or openings of the same scale), whose depths in the direction of flow is much smaller than the typical lateral dimensions, the equivalent area can be taken as the geometrical area (BSI, 1991). In the case where ventilation is purely wind-induced, the effective equivalent ventilation opening area is found by adding the area of openings in parallel and by summing the reciprocal of the squares (e.g. Equation 3.2) those in series (including interior door openings). For wind-driven cross-ventilation with $A_1/A_2 = 1$ and $C_{D1} = C_{D2} = C_D$, Equation (3.1) becomes:

$$Q = \frac{1}{\sqrt{2}} C_D \cdot A \cdot U_{ref} \cdot \sqrt{Cp_w - Cp_L}$$ (3.3)

51

The mean airflow rate through an inlet opening may be also calculated by the following equation:

$$Q = C_D \cdot A \cdot U_{ref} \cdot \sqrt{Cp_w - Cp_{in}} \qquad (3.4)$$

where, Cp_{in} = internal pressure coefficient.

External pressure distribution, terrain, shape, area and distribution of openings on façade, internal partitions or other restrictions on pressure and airflow within the building, and volume of the internal space are potentially important factors for building internal pressures. In the ideal case of a hermetically sealed building, the internal pressure is not affected by the external wind flow. For a building with uniformly distributed air leakage in all walls, Cp_{in} is about -0.2 (ASHRAE, Fundamentals ch.16, 2007). In a building with two openings, assuming the same leakage characteristics for the inlet and outlet and uniform internal pressure, the following equations can be derived from the mass balance equation (Liu, 1991):

$$Cp_{in} = \frac{Cp_2 + \alpha^2 \cdot Cp_1}{1 + \alpha^2} \quad \text{for large openings (windows, doors – turbulent flow)} \qquad (3.5)$$

$$Cp_{in} = \frac{Cp_2 + \beta \cdot Cp_1}{1 + \beta} \quad \text{for small openings (cracks – laminar flow)} \qquad (3.6)$$

Cp_1 = external pressure coefficient in opening 1

Cp_2 = external pressure coefficient in opening 2

$\alpha = A_1/A_2$; and $\beta = \frac{1}{4}$ for uniform distribution of cracks.

For $A_1/A_2 = 1$, i.e. cross ventilation with equal inlet and outlet area, Equation (3.5) becomes:

$$Cp_{in} = \frac{Cp_w + Cp_L}{2} \qquad (3.7)$$

Application of the simplified orifice model (Eq. 3.1 or 3.3) in the case of wind-driven cross-ventilation is based on several assumptions:

- Unsteady flow effects are assumed to be negligible.

- The velocity and pressure field is uniform in the vicinity of openings.

- The pressure distribution on the building envelope is independent on the presence of openings (sealed body assumption) and wind pressure coefficients for sealed buildings (e.g. Liddament, 1986) are used for predicting the airflow rate through buildings with openings.

- The upwind mean kinetic energy is dissipated downstream of the inlet opening and the pressure drop across the opening is equal to the static pressure difference. Thus, air velocities within buildings are negligible and the internal pressure coefficient is assumed to be uniform inside ventilated space.

- The effect of flow across the openings (i.e. in its plane) is ignored, i.e. the dynamic pressure due to the velocity component parallel to the wall containing the inlet opening, which may be deserving of attention, particularly for oblique winds and large opening area, is insignificant and can be neglected.

The validity of these assumptions has been investigated previously (e.g. Potter, 1979; Bruce, 1975; Cermak, 1984; Vickery and Karakatsanis, 1987; Aynsley, 1988; Ernest et al. 1992; Kato et al., 1992; Jensen et al., 2002a; Karava et al., 2006a; Seifert et al., 2006; Chiu and Etheridge, 2007). Murakami et al. (1991) reported that the approximation of the airflow through small openings (orifice equation) is no longer valid for cross-ventilation with large openings. In that case, the upwind mean kinetic energy is not totally lost when air flows approach these openings. The preservation of kinetic energy of wind-driven air

flows through buildings with large openings is essentially similar to airflow in ducts. This flow was referred to as "virtual stream tube" by Murakami et al. (1991) when the bulk of the airflow is within a distinct stream tube with a diameter of the same scale as that of the ventilation openings in the building. The "stream tube", which is a well-defined concept in fluid dynamics, is less distinct in turbulent flow, but may be defined by a flow regime bounded by mean flow streamlines. The stream tube is shown in Figure 3.2 for the case of wind-driven flow through building openings. Choiniere et al. (1992) reported that use of pressures measured on sealed building surfaces justifies the large discrepancies between measured and predicted airflow rates. Seifert et al. (2006) found that when a "stream tube" connecting the inlet and outlet is formed, the conventional macroscopic approach (orifice equation) underestimates the flow rate. The stream tube phenomenon decreases the resistance to flow and thus, increases the airflow rate, and cannot be modelled by using the orifice equation (Seifert et al., 2006). Recent research into the behavior of flow through openings has highlighted the need to improve the mathematical formulation used for cross-ventilation and different alternative theories have been proposed (e.g. Kato et al., 1992; Sandberg et al., 2004; Axley and Chung, 2005; Kurabuchi et al., 2004). The relative magnitudes of the ventilation produced by the various fluctuating flow mechanisms (broad banded, resonant and shear layer ventilation) were investigated by Straw et al. (2000) and methods of calculating the total ventilation rate from the mean and fluctuating components were discussed. Unsteady envelope flow models including turbulence effects have been proposed by Etheridge and Sandberg (1996).
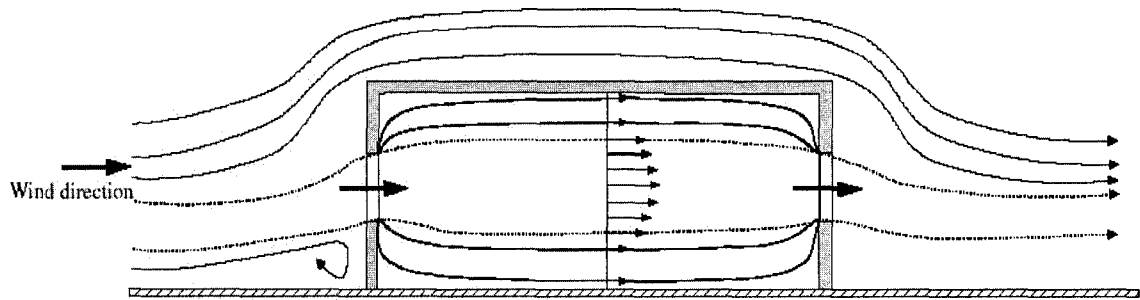
Figure 3.2. Illustration of wind-driven flows around and through a building with two cross-openings (after Seifert et al., 2006).

As interests in low-energy cooling strategies have grown in recent years, large openings such as operable windows are necessarily found in buildings. However, this interest is also coupled with a variety of design challenges. For example, wind-driven natural ventilation is difficult to analyze and control, as airflows around buildings are complex and invariably turbulent. Nevertheless, accuracy in ventilation rate prediction is necessary for development of motorized openings designed and controlled to reduce the need for mechanical cooling and also enhance indoor air quality and occupants' comfort. Therefore, it is reasonable to question if a single equation (orifice model) can represent the flow characteristics of any opening configuration, and, if so, what values are appropriate for C_D and Cp_{in}. This issue has been raised in the past and some interesting suggestions and results were presented. However, further investigations are needed in order to improve the existing knowledge regarding the selection of an appropriate simplified model to predict the ventilation flow rates in buildings with cross-ventilation. Holleman (1951) studied the flow characteristics of standard manufactured windows and developed a set of guidelines that could be used by designers to select the appropriate

window type for natural ventilation. Qualitative results were based on flow visualization experiments in a wind tunnel and a full-scale building. Similar investigations were performed by Smith (1951), Caudill et al. (1951), Caudill and Reed (1952), White (1954). Givoni (1969) attempted to quantify the anticipated airflow rates and develop design guidelines for cross-ventilation. In summary, previous work related to design guidelines for wind-driven ventilation based on quantitative results is rather limited. Presently, there is a need to perform parametric investigations and provide a simple set of guidelines of general application for the design of window openings and their placement on façade. Selection criteria should be based on wind-induced driving forces, ventilation flow rates, airflow distribution, as well as wind load design-related issues.

One of the major factors that becomes evident in this study is the large number of variables associated with wind-induced ventilation and the complexity of the mechanisms involved. The effects of the wind structure within the atmospheric boundary layer, external building aerodynamics as well as the opening configuration are all inextricably linked. Parameters in wind tunnel modelling of cross-ventilation that are important for representing realistic conditions around a building in the atmospheric boundary layer (external flow field) such as approaching airflow and scaling, as well as parameters related to the internal flow field, e.g. blockage of the internal volume and/or internal partitions are often overlooked for simplification purposes. For the evaluation of the ventilation rate, previous wind tunnel research has been limited to velocity measurements by single-point techniques (e.g. hot-film, split-film) or tracer gas methods which may be subject to measurement inaccuracies due to turbulent three-dimensional complex flow field particularly near the inlets and outlets. Particle Image Velocimetry (PIV) can

provide flow mapping over extended areas at the same time. However, the application of the PIV technique for building aerodynamics testing in large boundary layer wind tunnels presents a number of challenges. Internal pressures are insufficiently described in existing building codes and design standards (NBCC, 2005; ASCE 7, 2005) mainly due to complexities involved in their evaluation. Challenges associated with the wind tunnel evaluation of internal pressures include scaling of internal volume for configurations with cross-openings, representation of internal partitions, impact of turbulence, number of measurement points required, and many others. It should be noted that correct assessment of internal pressures in naturally ventilated buildings is essential as it affects airflow prediction, thermal comfort of occupants, and wind load design (peak values). Regarding computational modelling, the field of wind engineering has been shown to be highly complex due to the nature of turbulent flow fields experienced. The degree of uncertainty is even higher in the case of wind-driven cross-ventilation where coupling of the external and internal flow field is required. This highlights the necessity for high quality experimental data to be used for validation of CFD techniques.

For the efficient integration of natural / hybrid ventilation systems in buildings, more accurate simulation of ventilation and infiltration airflows is required. Coupled energy and airflow modelling is the most practical approach to achieve this. Presently, there is a need to assess the predictive capabilities of building simulation programs to model the coupled airflow-energy interactions, particularly in buildings where all the flow driving mechanisms (wind, stack and mechanical system effects) are present. Case studies of real buildings and validation with monitoring data should be considered. Issues such as

required modelling detail, uncertainties due to zoning assumptions, as well as modelling of wind effects need to be resolved.

The present thesis aims to address some of the above-mentioned research needs. The methodology followed and the main findings are presented in Chapters 4, 5 and 6.

4   APPLICATION OF PARTICLE IMAGE VELOCIMETRY FOR CROSS-VENTILATION ANALYSIS

4.1   Introduction

This chapter presents the experimental set-up in a Boundary Layer Wind Tunnel for the evaluation of the airflow field in a building model subject to cross-ventilation, by using the PIV method. Results for the mean air velocity field are presented and the flow structure of various cross-ventilation configurations is investigated. PIV data for the velocity at the inlet are compared with those by using conventional techniques (e.g. hot-film anemometry). The validity of the simplified orifice model to predict the airflow rates in buildings with cross-ventilation is examined through comparisons with measured data.

4.2   PIV Method

The PIV technique has been described by a number of authors. An in depth analysis of PIV principles is presented by Westerweel (1997), Raffel et al. (1998) whilst Stanislas and Monnier (1997) discuss some of the practical issues. Stanislas et al. (2000) presented an overview of PIV applications in large uniform flow wind tunnels, mainly focused on aeronautical applications. Presently, there are very few studies done in which the PIV method was applied in a large boundary layer wind tunnel (e.g. Rasouli et al., 2007). PIV is still considered a new method and there are a number of challenges associated with its application, particularly in large boundary layer wind tunnels for building aerodynamics testing. In the present study, the PIV technique has been applied in a BLWT for wind-driven cross-ventilation analysis, to the author's best knowledge, for the first time. An

innovative way of applying the PIV technique into BLWT testing has been developed and it is presented in detail in Section 4.3.3.

Two-dimensional PIV experiments were performed on a horizontal and a vertical plane of the flow field to obtain the time-averaged velocity field inside and around a cross-ventilated building model with various opening configurations. A PIV system by Dantec Dynamics was used. Measurements were performed on vertical and horizontal planes due to the three-dimensionality of the flow, the complexity of the flow field, as well as challenges associated with the application of PIV method in both planes. Measurements on a vertical plane are essential in order to have a complete picture of the flow field (e.g. velocity distribution inside the building) while measurements on a horizontal plane are required in order to evaluate the velocity along the openings and calculate the airflow rate.

4.2.1 Basic principles of PIV

Particle Image Velocimetry (PIV) is a measurement technique for obtaining instantaneous whole field velocities. A schematic view of its principle of operation is shown in Figure 4.1. Seeding particles, which are good light scatterers, are suspended in the flow of interest, a 2-D plane of the flow is illuminated by a stroboscopic light source (using a pulsed laser), and a CCD (Charge Coupled Device) camera placed perpendicular to the light sheet records scattered light from the seeding particles. A pair of light pulses freezes two consequent position fields, time t apart. The camera images are divided into rectangular regions called interrogation areas (or interrogation regions), and for each of
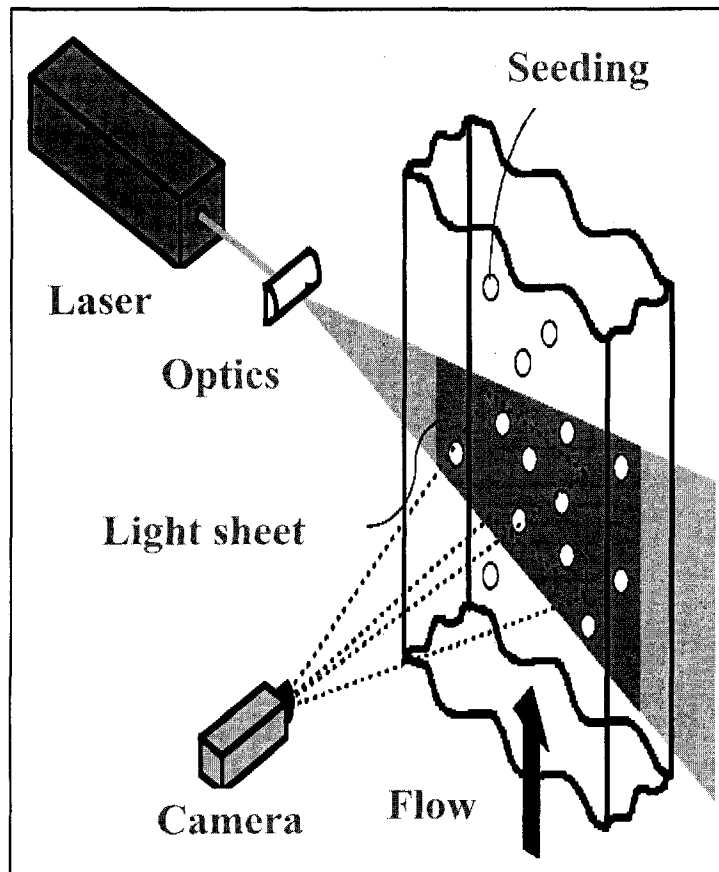
Figure 4.1. Diagrammatic view of principle of operation of PIV technique (Software user's guide; Dantec Dynamics, 2000).

these interrogation areas the image from the first and the second pulse of the light-sheet are spatially correlated (cross-correlation using Fast Fourier Transform) to produce an average particle displacement vector. Doing this for all interrogation regions produces a vector map of average particle displacements. The displacement vector (d) between successive images of the same seeding particle is given by:

$$d = Mvt \qquad (4.1)$$

where

M = object image scale factor

v = local velocity vector

t = time between pulses

Different types of seeding are used depending on the nature of the flow to be investigated. Inherent assumptions in PIV technique are the following:

- The tracer particles are small enough to follow the fluid motion and large enough to scatter sufficient light (Lorenz-Mie light scattering theory applies);

- The tracer particles are distributed homogeneously;

- There is uniform displacement of the tracer particles within the interrogation region.

Ideally, the particles should also be neutrally buoyant in the fluid, i.e. they should have approximately the same density as the fluid itself. Appropriate particles require a compromise between being small enough to have good tracer characteristics and large enough to possess good light scattering characteristics. Proper flow seeding is critical due to the reduced intensity of the laser light sheet as it spreads out from the source. Uniform seeding size reduces the effect of background noise and high intensity light being scattered from larger particles.

The basic parameters influencing measurements are:

- Particle size

- Measurement area size

- Measurement signal to noise ratio

- Particle image density

- In-plane motion

- Out-of-plane motion

- Spatial velocity gradients

- Interrogation region size

- Sample size

The dimensions of the interrogation region, together with the object:image scaling factor, define the spatial resolution or the smallest flow structure that can be measured by PIV. Also for turbulent flows, interrogation region size needs to be a fraction of integral length scale for correct evaluation of turbulent fluctuations and scales. In addition to this, sample size should be large for accurate statistical analysis in order to capture the mean and turbulent characteristics of the flow.

The PIV technique is based on determining the displacement of a group of particles using FFT / correlation techniques. In cross-correlation two sequential image maps are sub-sampled. In the literature, cross-correlation is often normalized to obtain values between 0 and 1, but in PIV only relative correlation levels within the investigated interrogation area are of interest. Within the interrogation area samples, an average spatial shift of seeding particles may be observed from one sample to its counterpart in the second camera image, provided a flow is present in the illuminated plane. A high cross-correlation value is observed, where many particles match up with their corresponding spatially shifted partners, and small cross-correlation peaks may be observed when individual particles match up with other particles. The former is known as true correlations, while the latter is called random correlations. In auto-correlation, only one camera frame is recorded and both initial and final particle positions are recorded on the same camera frame, and the recorded image is then correlated with spatially shifted versions of itself. The above justifies the robustness of the cross-correlation technique. Fast Fourier Transforms (FFT) are used to speed up the cross-correlation process.

Outliers are incorrect vectors resulting from noise peaks in the correlation function and may occur in almost all PIV measurements. It is important to note that by using FFT-processing there will always be an outcome whether the input is meaningful or not.

Huang et al. (1997), Cowen and Monismith (1997), and Prasad et al. (1992) identify three error sources. Interrogation error as a result of the cross-correlation process results in spurious vectors or outliers, which are generally larger than one pixel in size and easy to identify and remove. These usually appear due to poor particle seeding, strong flow velocity gradients or strongly 3-D motion in the flow. Even in a well-seeded flow, outliers can represent 5% of the flow field (Huang et al., 1997). The other two errors are the mean-bias error and the root-mean-square or RMS error. These represent the difference between the actual particle displacement and the mean displacement, as well as the average deviation of the actual displacements from the mean. These errors are generated from a large number of sources including improper particle seeding, strong velocity gradients and three-dimensional flow motion, the camera's dark-current noise, the nonlinear and non-uniform response of the camera, the non-uniformity of the illumination, the non-uniform reflection of particles at different locations and angles, the introduction of noise from the cable (analogue video noise) and digitization error.

4.3 Experimental methodology and set-up

This section presents the wind tunnel, the building and opening configurations considered, as well as the equipment and the experimental set-up for the PIV measurements.

4.3.1 The Boundary Layer Wind Tunnel

The wind tunnel at the Building Aerodynamics Laboratory at Concordia University, Montreal, Canada was used for the experiments. This is an open-circuit, 12 m long wind tunnel facility having a working cross section of 1.8m × 1.8 m. It has an adjustable roof height around 1.8 m, providing negligible pressure gradient of the flow reaching the test section. The geometric model scale of the BLWT of Concordia University is equal to 1/400 ~ 1/500, however, previous work has shown that a scale equal to 1:200 can be safely used for pressures (Stathopoulos and Surry, 1983). More details about this wind tunnel are given by Stathopoulos (1984). The inlet screen was installed with 6 horizontal rods (pipes) of different diameters and four spires. A solid fence and a board mounted with egg boxes were placed adjacent to the inlet screen; this configuration forms the inlet setting. This inlet setting intended to regulate the entrance flow profile and allowed the boundary layer profile to develop as naturally as possible along the floor. Three boards with styrofoam cubes were added upstream while the rest of the wind tunnel was covered with a carpet; this setting was used to simulate Open Country. Figure 4.2 shows the wind tunnel.

The air speed at the test section of the tunnel varies in the range of 4.7 to 13.5 m/s. Experiments are normally performed at the maximum speed for higher measurement accuracy with the building model mounted on the turn table. A reduced speed equal to 8.9 m/s was used in the present experiment to ensure the required seeding quality and to eliminate wind-induced vibrations of the CCD camera for PIV measurements on a horizontal plane (see also Section 4.3.3). The building model was placed downstream the turn table (near the wind tunnel outlet) in small extension of the wind tunnel specially

constructed with a window glass (transparent) in order for the laser sheet to pass through undisturbed (see Figure 4.2). A wind velocity profile over open terrain was simulated with a power-law exponent equal to 0.11 (measured with a hot-film anemometer) and turbulence intensity at building height equal to 11%. The roughness length (Z_o) was about 0.5 cm. These relatively low values were a compromise that had to be made for the present experiment because of the lower wind speed desired. The velocity and turbulence intensity (T.I.) profiles were measured with the hot-film probe placed on the turn table as well as on the actual building model location (near the wind tunnel outlet) with the wind tunnel running at the full and at a reduced speed. Figure 4.3 shows the velocity and turbulence intensity profiles measured in the present study. Repeatability tests for the approaching wind velocity profile were performed and differences in the value of power-law exponent were in the order of 5%. Although experiments were performed close to the outlet of the wind tunnel with additional equipment placed just downwind, it was found that blockage attributed to this equipment was minimal due to its small size. Velocity and turbulence intensity profiles evaluated for cases with and without blockage produced similar results.

4.3.2 The building model and opening configurations

A 10 × 10 × 8 cm building model with a flat roof subject to cross-ventilation was considered. The test model corresponds to a building 20 m × 20 m, 16 m high (assuming a 1:200 scale), i.e., a 4 or 5-storey building. The building model was constructed for the purpose of PIV experiments without any tapping on the walls by using 2 mm-thick clear
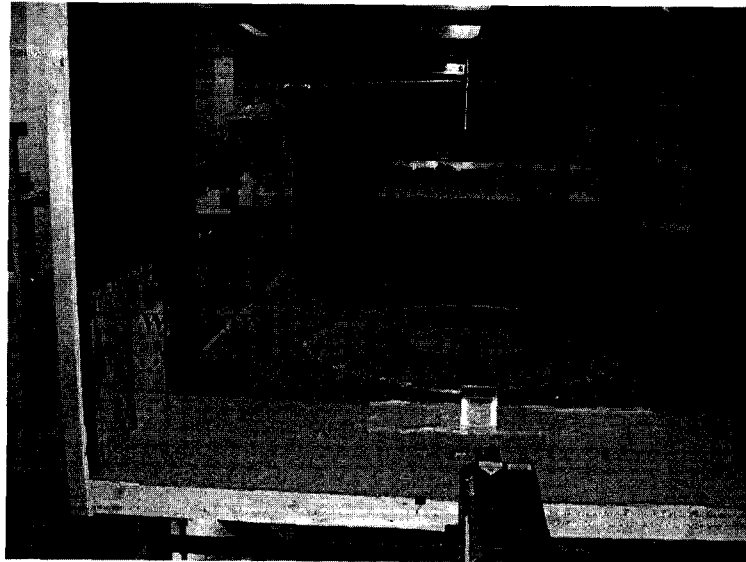
Figure 4.2. The boundary layer wind tunnel.
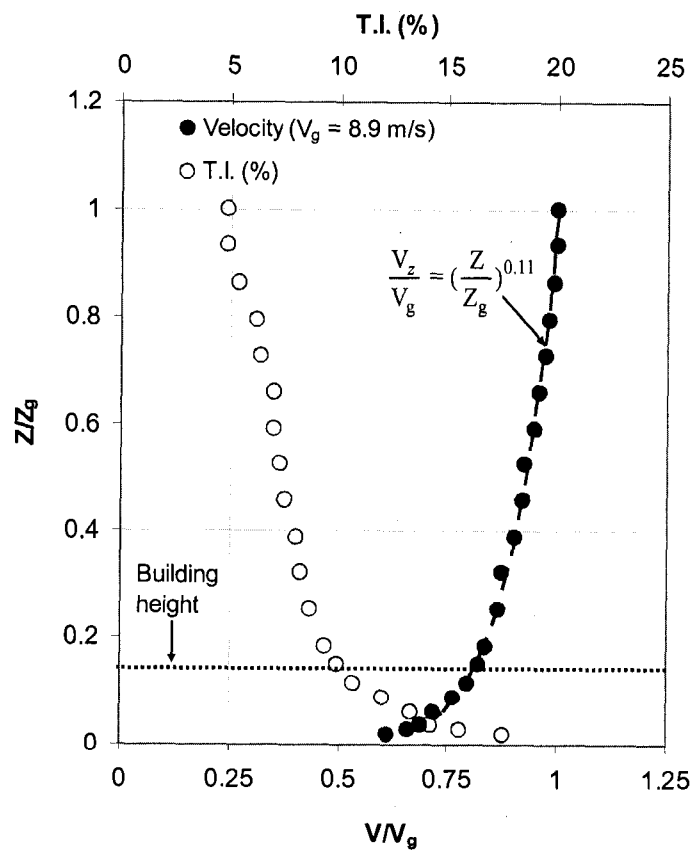
Figure 4.3. Velocity and turbulence intensity profiles considered for the PIV measurements.

cast acrylic (transparent material) in order to allow the laser sheet to pass through, and the camera to see through as well. The model provides variable wall openings (differences in opening areas were induced by different opening widths - sliding windows). The opening area is expressed in terms of wall porosity defined as $A_{opening}/A_{wall}$. Different sets of walls with various porosities were fabricated. The building model and opening configurations considered are illustrated in Figure 4.4 while a schematic is shown in Figure 4.5. The opening configurations are also presented in Table 4.1. Only simple rectangular openings of the same height (18 mm – 3.6 m) were tested. Inlets and outlets are located in the middle (opening mid-height at 40 mm – 8 m from ground), bottom (opening mid-height at 20 mm – 4 m from ground) or top (opening mid-height at 57 mm – 11.4 m from ground) of windward and leeward walls. Configurations with inlets and outlets located at the same height (symmetric openings; configurations A, C, and E) were considered as well as configurations with inlets and outlets located at different heights (non-symmetric

Table 4.1. Opening configurations considered for the PIV measurements.

Wind angle °	Configuration	Opening Location* Inlet mm	Outlet mm	A_1 (%)	A_2 (%)	A_1/A_2
0	A	57	57	5, 10, 20	5, 10, 20	1
0	B	57	20	5, 10, 20	5, 10, 20	1
0	C	20	20	5, 10, 20	5, 10, 20	1
0	D	20	57	5, 10, 20	5, 10, 20	1
0	E	40	40	5, 10, 20	5, 10, 20	1
0	A	57	57	5	20, 10	1/4, 1/2
0	A	57	57	10	20, 5	1/2, 2
0	A	57	57	20	10, 5, 2.5	2, 4, 8
0	C	20	20	5	20, 10	1/4, 1/2
0	C	20	20	10	20, 5	1/2, 2
0	C	20	20	20	10, 5, 2.5	2, 4, 8
0	E	40	40	5	20, 10	1/4, 1/2
0	E	40	40	10	20, 5	1/2, 2
0	E	40	40	20	10, 5, 2.5	2, 4, 8
45	A	57	57	5, 10, 20	5, 10, 20	1
45	C	20	20	5, 10, 20	5, 10, 20	1
45	E	40	40	5, 10, 20	5, 10, 20	1

*Opening location: distance of opening mid-height from the floor
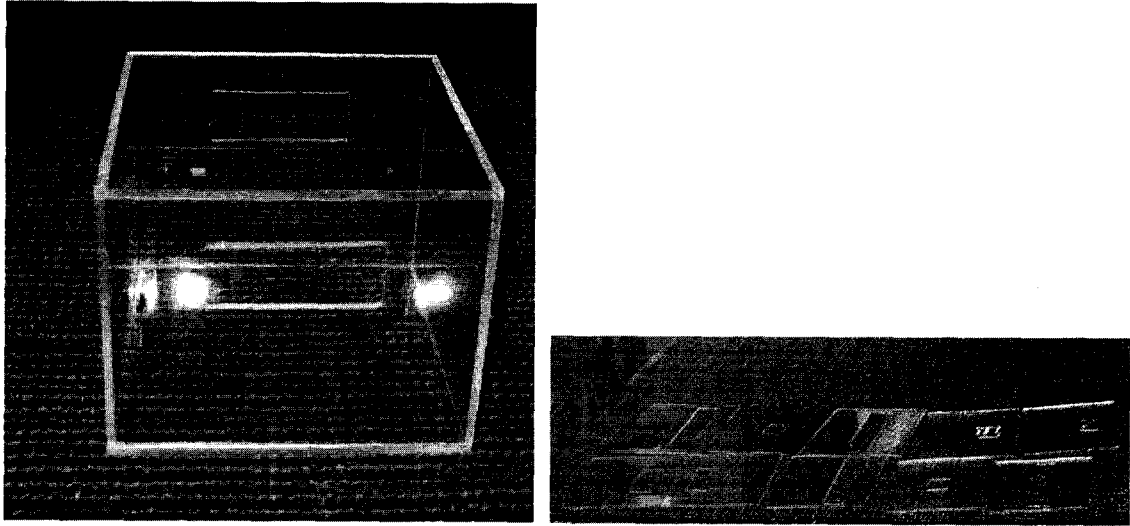
Figure 4.4. The building model (left) and the different opening configurations (right).
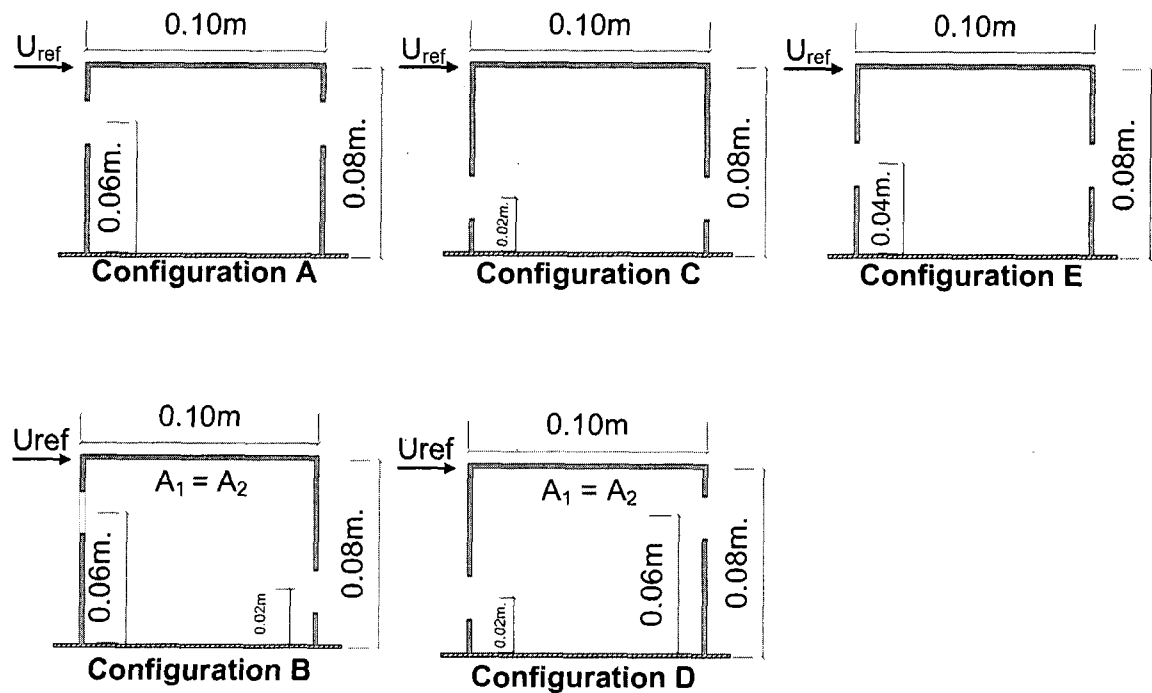
Figure 4.5. The basic opening configurations considered.

openings; configurations B and D). Measurements were performed for configurations with leeward outlets. Configurations with various inlet and outlet opening areas were

tested, with wall porosity ranging from 5 to 20%. The inlet to outlet ratio varies from 0.25 to 4. Inlet-to-outlet ratios different than one were only considered for configurations A, C and E (symmetric openings). Measurements were carried out for a wind angle, θ, equal to 0° and 45°.

4.3.3 PIV set-up

Figures 4.6a and 4.6b show the experimental set-up for PIV measurements on a vertical plane and a schematic of the building model indicating the measurement plane (vertical) for a configuration with 10% wall porosity and openings located in the middle of wall (configuration E). The laser and the camera were mounted on tripods placed near the outlet and on a side wall of the wind tunnel respectively. Measurements were mainly performed for vertical planes in the plane of symmetry. Figures 4.7a and 4.7b show the experimental set-up for PIV measurements on a horizontal plane and a schematic of the building model indicating the measurement plane (horizontal) for the same opening configuration. Measurements were mainly performed on horizontal planes at the mid-height of openings. The laser was mounted on a tripod placed just outside one of the side walls of the wind tunnel. An extension of the wind tunnel was constructed with a window glass in order for the laser sheet to go through. Although low-iron glass has the best transmission characteristics and it is recommended for PIV experiments, in the present study a regular window glass was used and it was found to be sufficiently good. A heavy tripod - equipped with a boom - placed near the wind tunnel outlet was used for the mounting of the camera. Since the camera was practically inside the wind tunnel (see
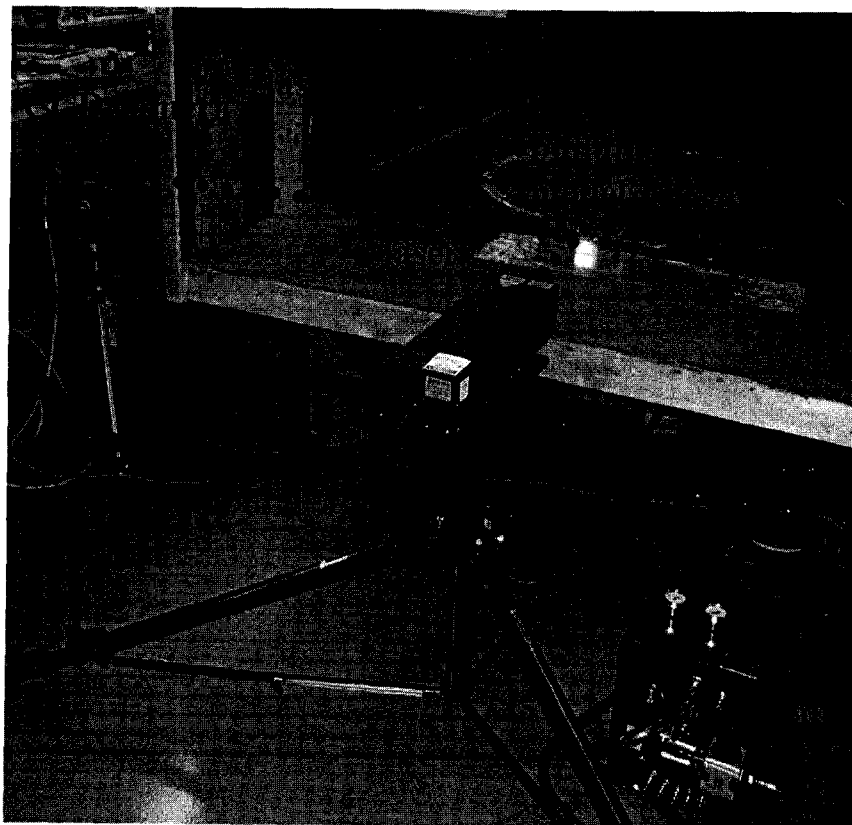
(a) Experimental set-up
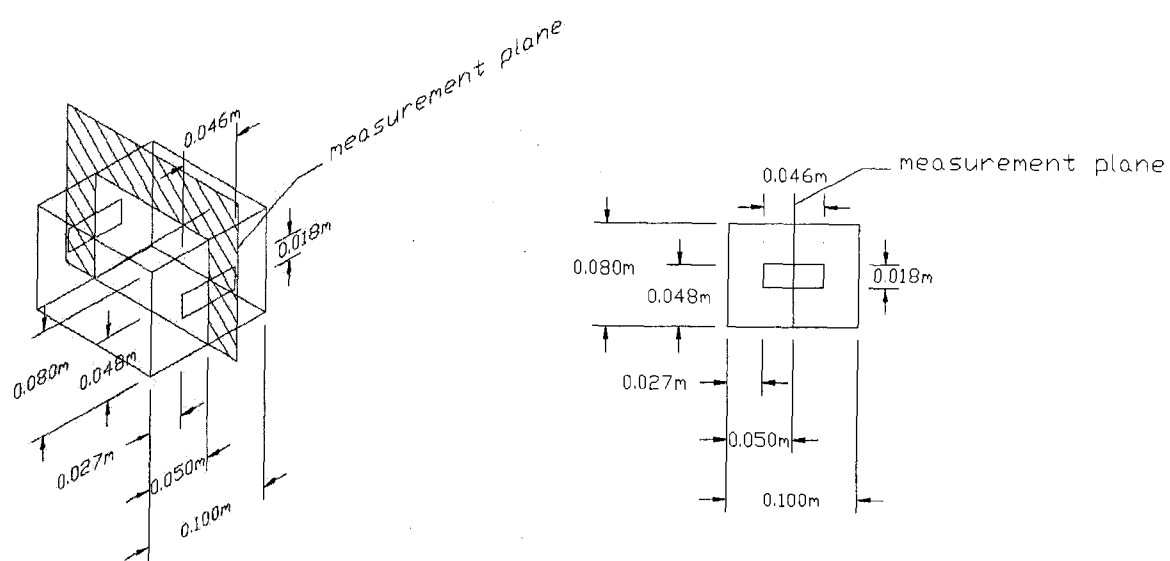
(b) Building model and measurement plane

Figure 4.6. PIV measurements on a vertical plane.
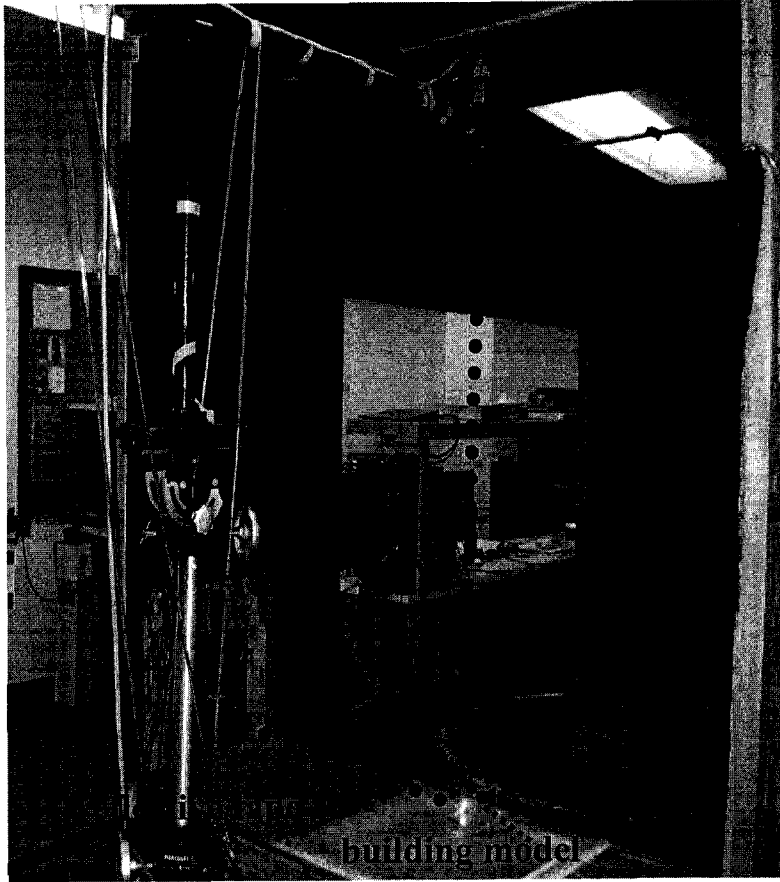
(a) Experimental set-up
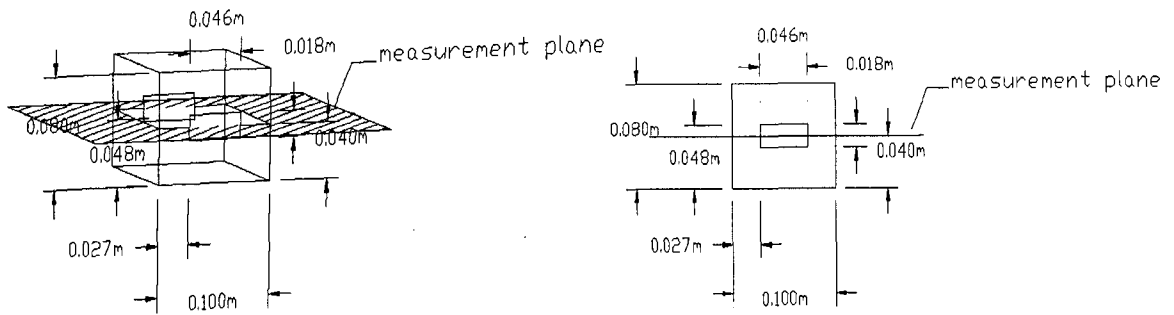
(b) Building model and measurement plane

Figure 4.7. PIV measurements on a horizontal plane.

Figure 4.7a) vibration problems were encountered with the wind tunnel running at high speeds. This problem was resolved by running the wind tunnel at a reduced speed (8.9 m/s). It should be mentioned that although both arrangements for the horizontal and vertical plane worked well, it was tedious to move and align. A motorized arrangement is recommended for future experiments.

Olive oil particles (seeding) generated using Laskin nozzles (atomizer) were used. The generator (PIVPart30 by PIV TEC-GmbH) consists of a closed cylindrical container with two air inlets and one outlet and includes 6 Laskin nozzles, each operating at a pressure of ~ 80psi (551.6 kPa), to generate the oil particles. A schematic view of its principle of operation is shown in Figure 4.8. Compressed air with a pressure difference of 0.5-1 bar with respect to the outlet pressure is supplied to the Laskin nozzles and creates air bubbles within the liquid. Due to the shear stress induced by the tiny jets, small droplets are generated and carried inside the bubbles towards the oil surface and then reach the aerosol outlet. The mean size of the particle depends on the type of the
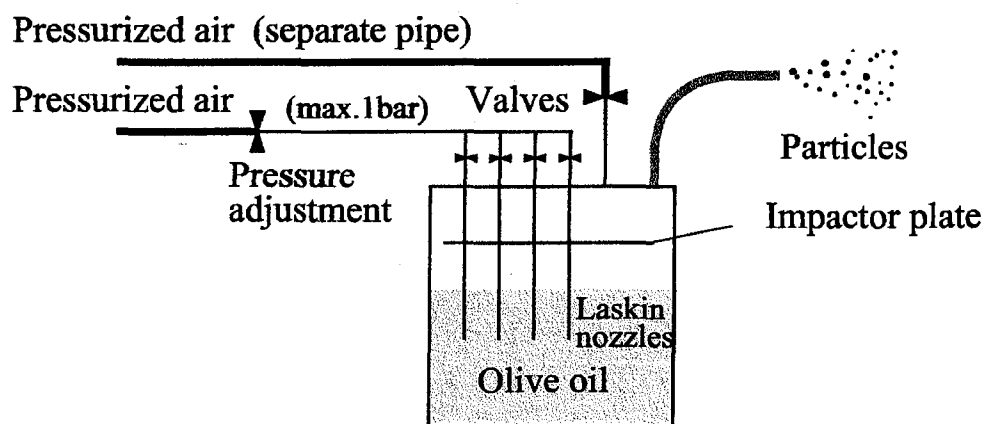
Figure 4.8. Principle of operation of seeding generator (Software user's guide; Dantec Dynamics, 2000).

liquid being atomized. In the present study olive oil droplets of about 1μm diameter were used (probability density function of size has a peak at 1μm).

Since it was not possible to provide uniform seeding in the entire wind tunnel due to its open-circuit type, local seeding supplied at 1 m upstream the building model, through a plastic hose attached to a hole on the wind tunnel floor, was used. Two Laskin nozzles operating at 10 psi (69 kPa) were sufficient to provide uniform seeding in the flow of interest. The use of a mixing box in order to provide uniform seeding has been reported in previous PIV applications in wind tunnels. However, the present study found that the use of a mixing box creates a wake effect and distorts the airflow pattern around the building. This wake effect can be eliminated by having both the front and back wall of the box open; however, seeding uniformity does not improve with this configuration. Consequently, it was decided not to use the mixing box. Water-based fog (smoke) was used as seeding material at an early stage of the study but a number of difficulties were encountered. Smoke is made up of very small particles that are typically much smaller than the resolution of the CCD and tends to disperse and become almost homogeneous throughout the flow field. In regions where there are strong streamlines present, coalescing together of the fine particles results in larger particles that can be detected by the PIV system. However, flow features can not be discerned, in areas of low velocity such as re-circulating regions in the wake of the building or regions inside the building model (internal flow field) where the particles do not coalesce. More specifically, for the same laser intensity, smoke particles were not detected by the PIV system in the vicinity of the outlet, resulting in zero velocity vectors (e.g. zero outflow) while oil particles were successfully detected resulting in valid velocity vectors. Figure 4.9a shows a typical

velocity field measured using water- based fog as seeding material, where the outflow cannot be identified. In contract, the outflow can be clearly seen in the flow field measured using oil particles (Figure 4.9b). In summary, the oil-based particle generator proved to perform very well mainly due to the better scattering characteristics of the oil and the fine size of the droplets (~ 1µm). It should be noted, that water-based fog has been successfully used in applications with streamlined flow; clearly, selection of seeding depends on the nature of the flow to be investigated.

Seeding particles were illuminated with a 532 nm wavelength laser sheet generated using a two-cavity (120 mJ each) Nd:YAG laser (SOLO 120, NewWave Research; Software user's guide; Dantec Dynamics, 2000). The thickness of the laser sheet at the measurement plane was about 1.5 mm and it was created by using a combination of spherical and cylindrical lenses. A pair of light pulses to freeze two consequent position fields at time t apart (t = 50 µs for measurements on a vertical plane and 100 µs for measurements on a horizontal plane) was produced at a frequency of 13 Hz (the pulse frequency can be adjusted in the range between 1 and 15 Hz). The time between pulses was selected in order to achieve the best temporal and spatial resolution. It should be noted that due to low energy (120 mJ at 532 nm) and small pulse duration (9ns), laser-induced thermal effects are insignificant.

A CCD camera (FlowSense10-bit, 1600×1186 pixels) placed perpendicular to the light sheet was equipped with a 60 mm lens (measurements on a horizontal plane) or a 105 mm lens (measurements on a vertical plane) to cover an image of 253 mm (length) ×192 mm (width) and 160 mm (width) ×118 mm (height) respectively. The object-to-image scale factor, which depends on the focal length of the camera lens and the distance

between the camera and the measurement area, was equal to 21.4 and 13.4 for PIV

measurements on a horizontal and vertical plane respectively. A synchronisation board
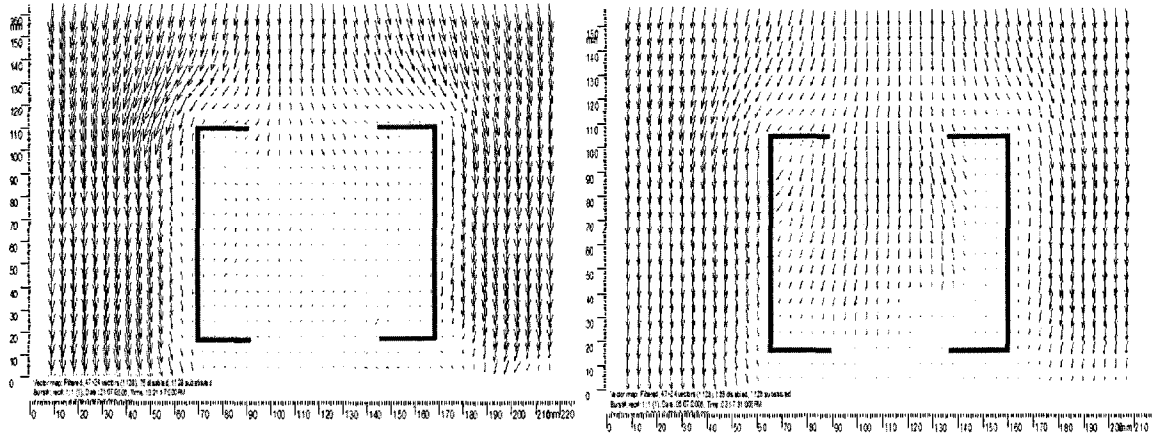
(a) Water-based fog (left: configuration E; right: configuration A)
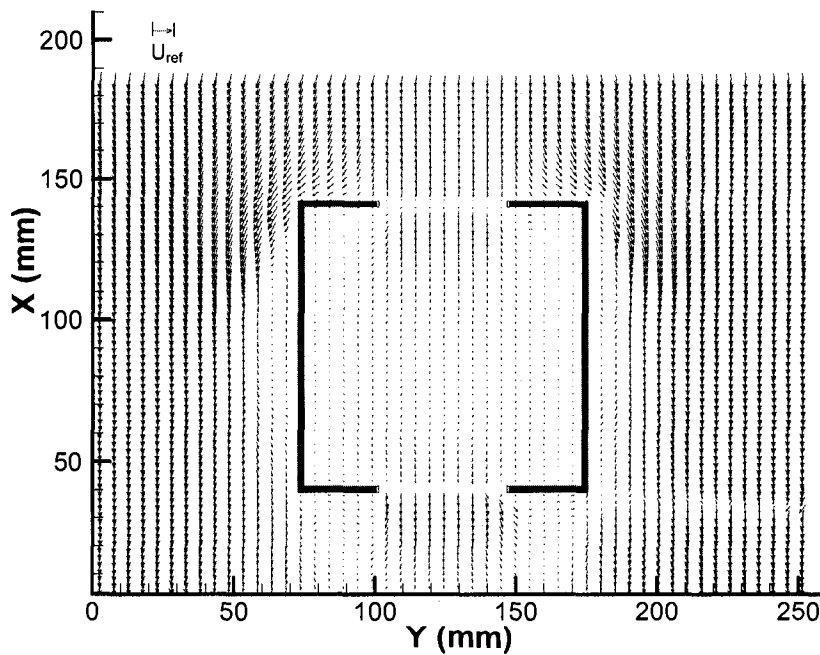
(b) Oil particles (configuration E)

Figure 4.9. Velocity field measured using (a) water-based fog and (b) oil particles as

seeding material (PIV measurements on horizontal planes).

76

was used to control the timing between the laser pulses and the camera shutter open time by using software (Flowmanager, Dantec Dynamics) installed in a PC desktop computer.

For each experiment, 70 pairs of images (sample size) were recorded to capture 5.4 sec of the flow in order to calculate the mean flow field. The duration of the signal (and the sample size) is relatively small, but this option was limited by the version of the software available at the time and the data storage capacity of the system. Measurements were carried out at low repetition rates (e.g. f = 5 Hz) for comparison purposes to capture 15 sec of the flow and similar results were obtained. Additional experiments were performed considering a large number of image pairs (e.g. 500 across 7 non-contiguous experiments to capture 38 sec of flow) and the time-averaged flow fields were consistent with those obtained by using the contiguous method. Hence, it was decided to perform the experiments considering a relatively small but contiguous sample (70 pairs of images to capture 5.4 sec of the flow) as this option appears to be better representing the nature of the wind. It should be noted that very good repeatability was achieved among different tests. The camera images were divided into rectangular regions, i.e. interrogation areas and a 32 × 32 pixels vector field with 50% overlapping was used as it was found to be the best compromise between spatial resolution and velocity dynamic range (maximum displacement within interrogation to result in successful correlations). With this overlapping the resolution of the velocity field was increased to 16 × 16 pixels.

Erroneous vectors produced from random correlations during the image processing (FFT-processing) that do not represent true particle displacements were detected, removed and substituted - when possible - with interpolated values from the adjacent vectors using validation algorithms (e.g. peak height ratio validation, velocity range

validation, etc) available in the Flowmanager Software. These vectors tend to be longer than the true velocity vectors, but random in direction so they can be easily spotted.

In the present study, erroneous vectors are mainly attributed to shadows and surface / edge reflections. Reflections and shadows account for random correlations during image processing and near-zero velocity vectors in the corresponding regions of the vector field. Shadows are produced because the building and opening edges are not transparent and the laser sheet does not pass through. As a result, small sections of the flow field are not illuminated. Sometimes quality of the images can be improved by adjusting the position of the laser to shift the shadow in a less critical region of the flow field. It should be noted that a non-symmetric diverging laser sheet was produced with the present arrangement. Reflections, which appear as saturation in the images, are produced due to the laser light coming off the building model surfaces / edges and the carpet surface (see also Figures 4.6 and 4.7). After several attempts to reduce reflections coming from the carpet, red fluorescent reflective tape was placed on the wind tunnel floor around the building model, and the quality of the images was improved. Initially, a 532nm narrow band filter (±10 nm bandwidth) was mounted on the camera lens to filter out the reflected light coming off the tape-covered surface. Experiments were performed with and without the filter and the quality of images (and vectors) proved to be consistently better without the filter. This occurs because the filter reduces the scattered light reaching the CCD of the camera significantly. Since the camera is not sensitive to the orange light coming from the reflective tape, it was decided to perform the experiments without the filter. Red fluorescent reflective tape was also put over the building edges, where possible. However, it was not possible to completely eliminate reflections as some of the surfaces

and edges have to remain transparent to allow the laser sheet to pass through. Figure 4.10a shows a typical PIV image (instantaneous) for measurements on a vertical plane where the seeding particles as well as the basic flow structures (upstream standing vortex, roof vortex, flow separation at roof edge, wake region) are clearly depicted. The strong edge reflections, near the inlet and outlet openings, are also shown. A typical PIV image for measurements on a horizontal plane is shown in Figure 4.10b. Shadows forming at the building and opening edges can be clearly depicted in Figures 4.10a and 4.10b. For PIV measurements on vertical planes, data near the inlet (within 1.5 cm) and outlet (within 0.5 cm) openings are lost due to reflections; for measurements on horizontal planes data are subject to errors within a 0.5 cm distance from the inlet and outlet due to shadows. These data points have been discarded from the graphs presenting PIV results and they were not considered in the analysis. It should be noted that extraction of erroneous vectors at specific points of the flow field is a typical raw data processing method in various PIV experiments.

Seeding particles entering or leaving the interrogation area between the recording of the first and the second image, will not contribute to the true correlation since either the initial or final particle position is missing. They do however contribute to the random correlations and as such decrease the signal-to-noise ratio. This phenomenon is often referred to as "loss-of-pairs" or "signal drop-out". For measurements on horizontal planes, seeding particles that follow a random motion due to the lateral turbulence result in random correlations. This problem was encountered for small time between pulses (~100 μs) and was not observed for PIV measurements on a vertical plane. A small non-
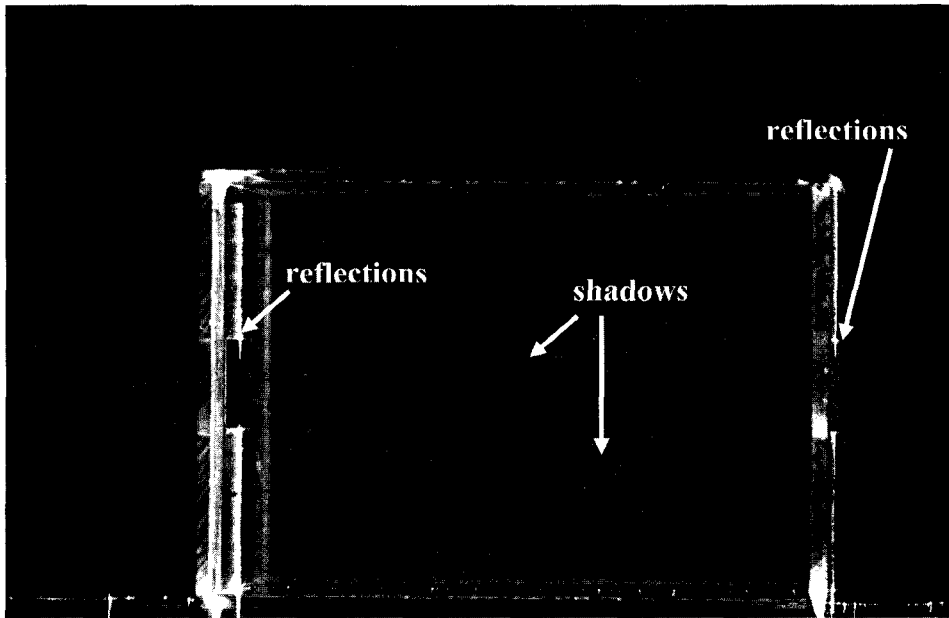
(a) measurements on a vertical plane (side view)
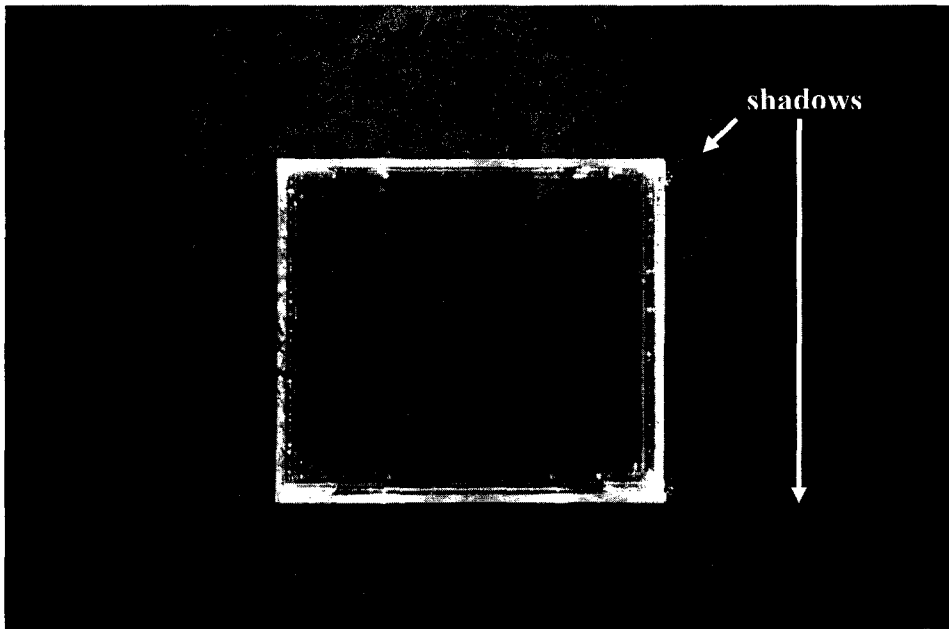
(b) measurements on a horizontal plane (plan view)

Figure 4.10. Typical PIV image (instantaneous) for measurements on a vertical (a) and horizontal plane (b), showing regions affected by shadows and/or reflections.

uniformity of the flow along the wind tunnel cross-section, which was attributed to the reduced speed, may be another reason for bad correlations. For measurements on horizontal planes, filters had to be applied to smoothen the vector field. After resolving all the problems encountered initially, measurements in the present study produced more than 92% and 95% valid vectors on a horizontal and a vertical plane respectively. Valid vectors are subject to errors and/or measurement uncertainties, the detailed estimation of which, is rather complex. Typically, in carefully conducted PIV experiments for turbulence levels up to 30% and sample size equal to 70, the anticipated error in the mean flow field is in the order of 5%.

A typical instantaneous velocity field and the corresponding mean velocity field based on PIV measurements on a vertical plane are shown in Figure 4.11. PIV data near the inlet and outlet openings, subject to measurement errors, were removed from the vector plots. Differences among the two flow fields are expected due to the unsteadiness of the flow. This clearly indicates that selection of sample size, frequency, and time between pulses, significantly affects the quality of PIV experiments.

In summary, application of the PIV technique for building aerodynamics testing in a large boundary layer wind tunnel presents various complexities. These are related, although not limited to, seeding type and quality (particularly for open circuit wind tunnels), camera mounting (e.g. vibrations if placed inside the wind tunnel, restrictions related to the distance from measurement plane), laser mounting, illumination intensity, edge reflections, shadows, size of measurement plane, as well as large sample size and high sampling frequency required if turbulence characteristics are to be resolved.
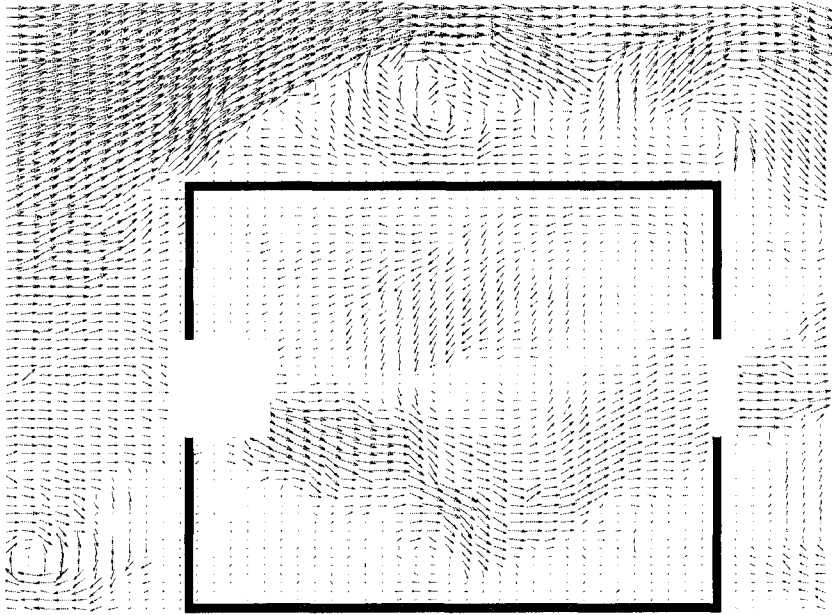
(a) Instantaneous velocity vector field
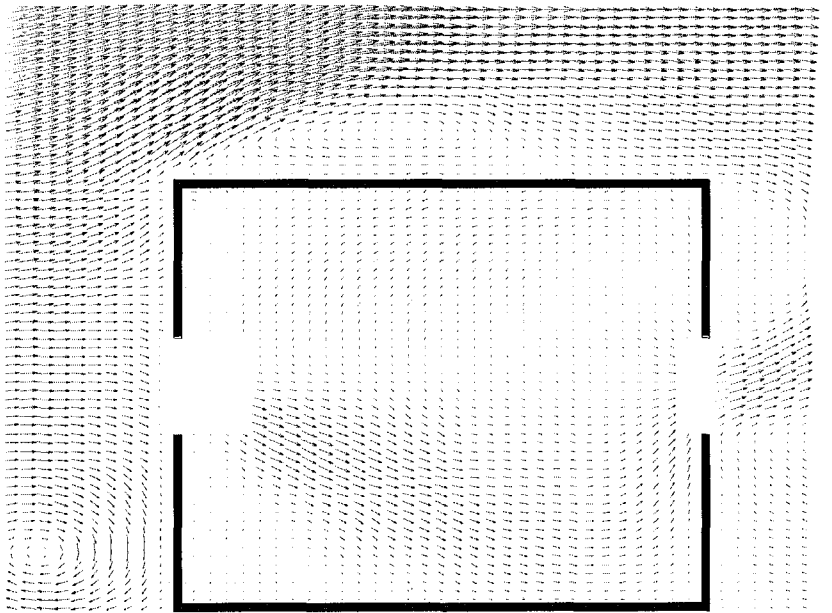
(b) Mean velocity vector field

Figure 4.11. Instantaneous and mean velocity vector field for PIV measurements on a vertical plane.

Although both arrangements worked well in the present study, it was tedious to move and align. In the future, traverse mechanisms can be adapted to move the camera and laser simultaneously so as to accelerate the process of measurement at different locations / planes. Further improvements of the method, to eliminate problems related to edge reflections and shadows, are recommended. Also for PIV measurements in larger areas, improvement of the laser intensity and careful design of a series of nozzles to produce more homogeneously dispersed seeding particles may be necessary.

4.4 Method verification

The velocity profile without any model in the test section measured using a hot-film anemometer was compared with PIV data on a vertical measurement plane for the same location. This comparison was made in order to verify the performance of the PIV method in a large BLWT, as hot-film measurement results for this case have been proved to be accurate. The velocity values were normalized by the velocity (U_{ref} = 6.6 m/s) at building height (Z_{ref}) and results are shown in Figure 4.12. Velocity values are a bit lower with the PIV method near the ground (i.e. for Z/Z_{ref} less than 0.4) which may be attributed to reflections coming from the wind tunnel floor and/or to the high levels of turbulence intensity. Differences between the two sets of data are less than 7%, indicating a good agreement between the two methods. PIV data for the intersection points of the two measurement planes (horizontal and vertical planes without a building model in the test section) have been compared and showed identical values.

A repeatability test is presented in Figure 4.13 for measurements on a vertical plane. Results for the velocity component on the centre-line directly between the inlet and outlet
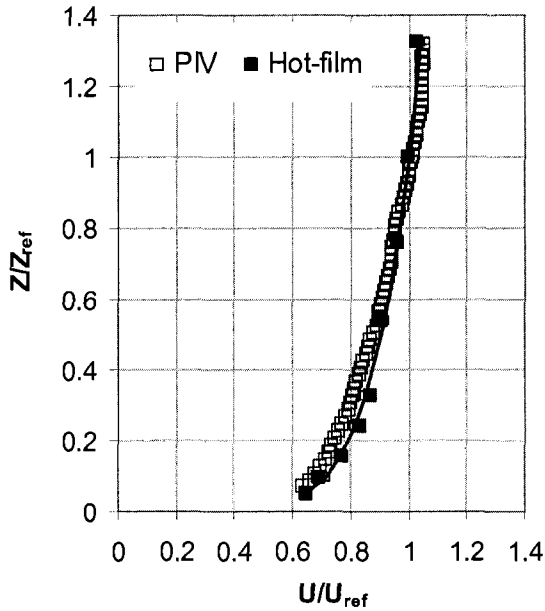
Figure 4.12. Comparison between hot-film and PIV measurements for empty tunnel velocity profiles (reference height = building height = 0.08 m).
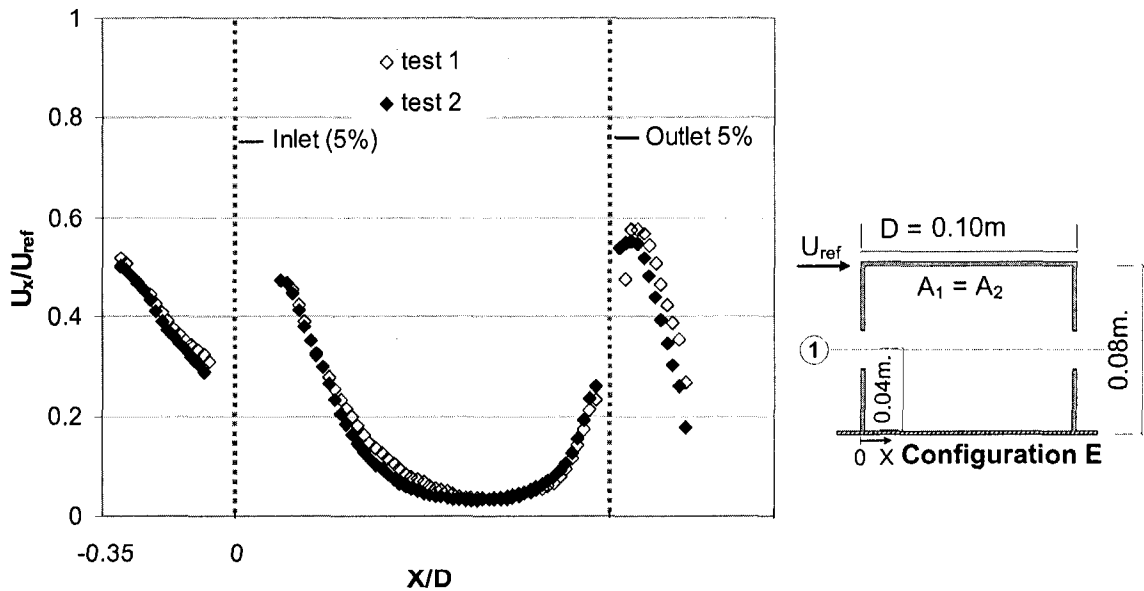
Figure 4.13. Profile of velocity component on the centre-line directly between the inlet and outlet opening (cross-section 1) based on PIV measurements on a vertical plane: Repeatability test for configuration E with 5% wall porosity.

openings (cross-section 1) are shown for configuration E with 5% wall porosity, and θ = 0°. Very good agreement between the results of the two tests is observed. As already mentioned in Section 4.3.3, data near the openings, subject to measurement errors due to reflections, were removed from the profiles shown in Figure 4.13.

Figure 4.14 shows the x-component of the velocity (normalized by the reference velocity) on the center-line directly between the openings (cross-section 1) for the configuration shown. PIV data for measurements on a horizontal and a vertical plane, as well as single point hot-film data have been included. Spurious PIV data, within a distance equal to 1.5 cm at inlet and 0.5 cm at the outlet for measurements on a vertical plane, and within a 0.5 cm distance at both openings for horizontal plane measurements,
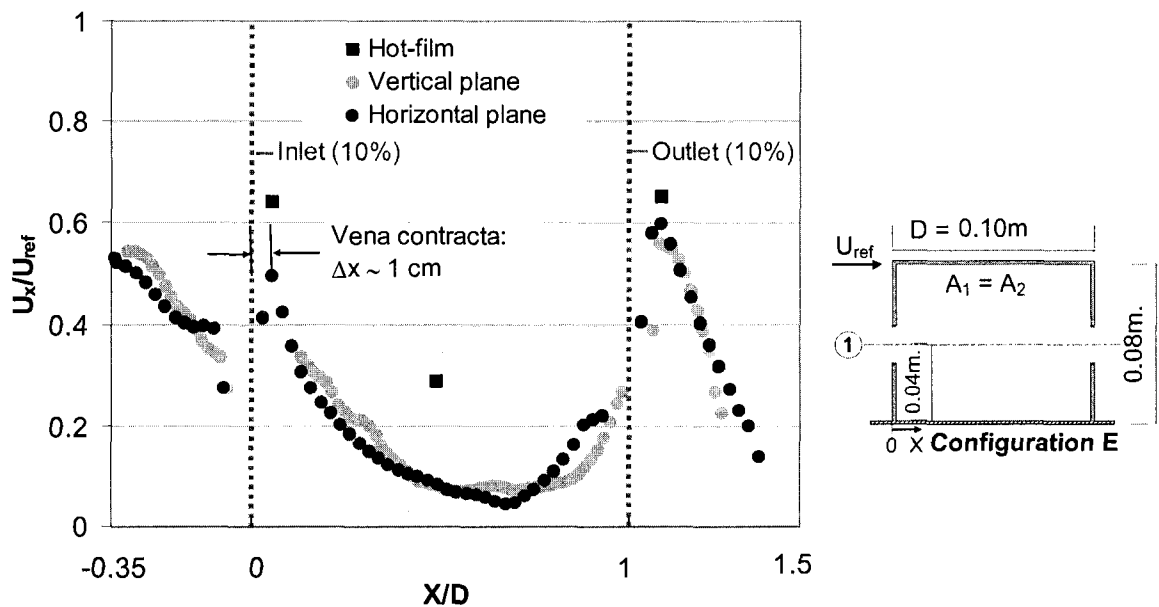
Figure 4.14. Profile of velocity component on the centre-line directly between the inlet and outlet opening (cross-section 1) based on PIV measurements on a horizontal and a vertical plane.

have been removed from the profiles shown in Figure 4.14 (see also Section 4.3.3). Bernouli principle (which can be applied -with some assumptions- on a horizontal stream line between a point in front of the opening and the vena contracta; see also Section 2.2.3) and jet behavior suggest that the entrance jet velocity should initially increase as a vena contracta region forms and then decrease as it entrains surrounding low momentum fluid. Velocity data based on measurements on a horizontal plane show an increase of the velocity up to 1 cm distance downstream the inlet opening (vena contracta), which is equal to 0.55 times the window height (1.8 cm). This value (0.55) is within the range (0.35 - 0.85) suggested by the theory. The ratio of the maximum velocity (velocity in the vena contracta) divided by the velocity at the opening is about 1.29, which is of the order expected due to vena contracta acceleration (~1.67). Overall there is a good agreement between PIV data for measurements on a horizontal and a vertical plane. However, hot-film results at the inlet and in the middle of the building interior overestimate the velocity, while hot-film results at the outlet are closer to the PIV data. Differences between PIV and hot-film data may be attributed to the high turbulence fluctuations and the three-dimensionality of the flow, particularly near the openings. The large velocity gradients near the inlet and outlet indicate that selection of the measurement location when using single-point techniques may introduce significant errors.

4.5 Results

PIV data for the inflow velocity (normalized by the reference velocity) at 1 cm downstream the inlet (vena contracta), averaged along the opening width, are shown in Figure 4.15. PIV data, which correspond to measurements on a horizontal plane at the

mid-height of the opening, are compared with hot-film measurement results on the same plane, as well as with data from the literature. Large differences up to a factor of 2.7 between the hot-film and PIV results are observed and are also confirmed from findings of previous studies notwithstanding a more advanced single point technique through a three dimensional anemometer used by Kato et al. (1992) and Straw et al. (2000). The complicated flow profile through the inlet opening and the large velocity gradients cannot
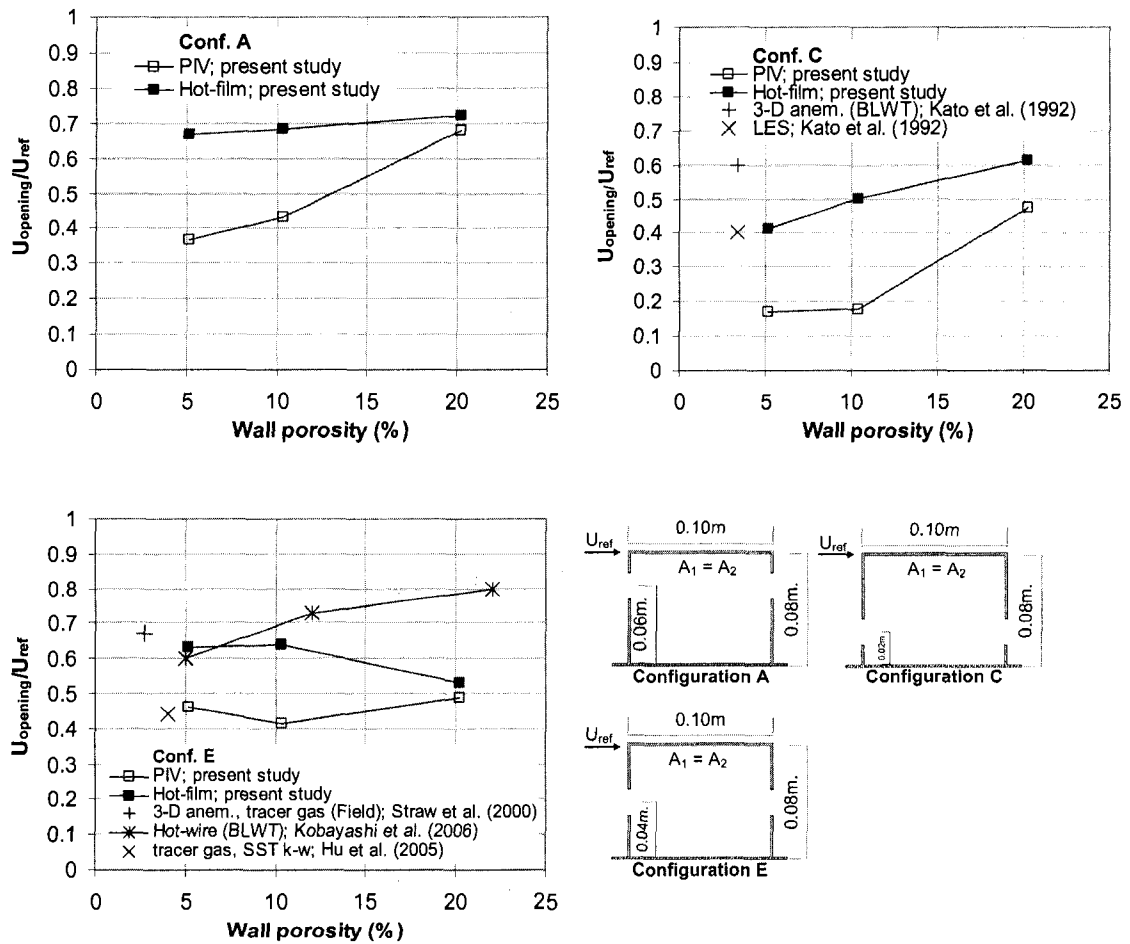
Figure 4.15. Inlet normalized velocity, measured on a horizontal plane for configurations A, B and E by using PIV and hot-film anemometry, compared with previous experimental and computational data.

87

be represented by single point hot-film measurements. Also it is well known that hot-wire anemometry should not be used in regions where instantaneous flow reversals are possible or in regions where the level of turbulence fluctuation is high. Similar observations about the inadequacy of single point measurements using hot-wires at the centre of openings to capture the flow in a cross-ventilated full-scale building have been reported by Yang et al. (2006).

Figures 4.16-4.20 present mean velocity vector fields for different configurations based on PIV measurements on vertical planes. Vectors near the openings subject to measurement errors due to reflections were removed from the plots, as previously described. It should be noted that the original resolution of the velocity vectors computed from the PIV images (100 × 74 vectors) is reduced to 50 × 36 vectors in all plots for better visualization of the vector field.

Figure 4.16 shows a cross sectional view of the mean velocity vector field on a vertical mid-plane for configuration E, $A_1 = A_2$, 10% wall porosity, and $\theta = 0°$. In this plane, the flow through the cube is dominated by a jet passing directly between the ventilation openings while there are slower moving zones above and below the dominant jet region. When the airflow is entering the building, the velocity is accelerated and directed downwards immediately after passing through the opening. This downward inflow is attributed to the location of the opening (mid-height of the building) and to the upstream re-circulating flow (standing vortex) which is clearly depicted in Figure 4.16. The air trapped in the vortex does not enter the inlet, however, air above and in front of the vortex forms a downdraft that flows into the opening. Close to the windward face
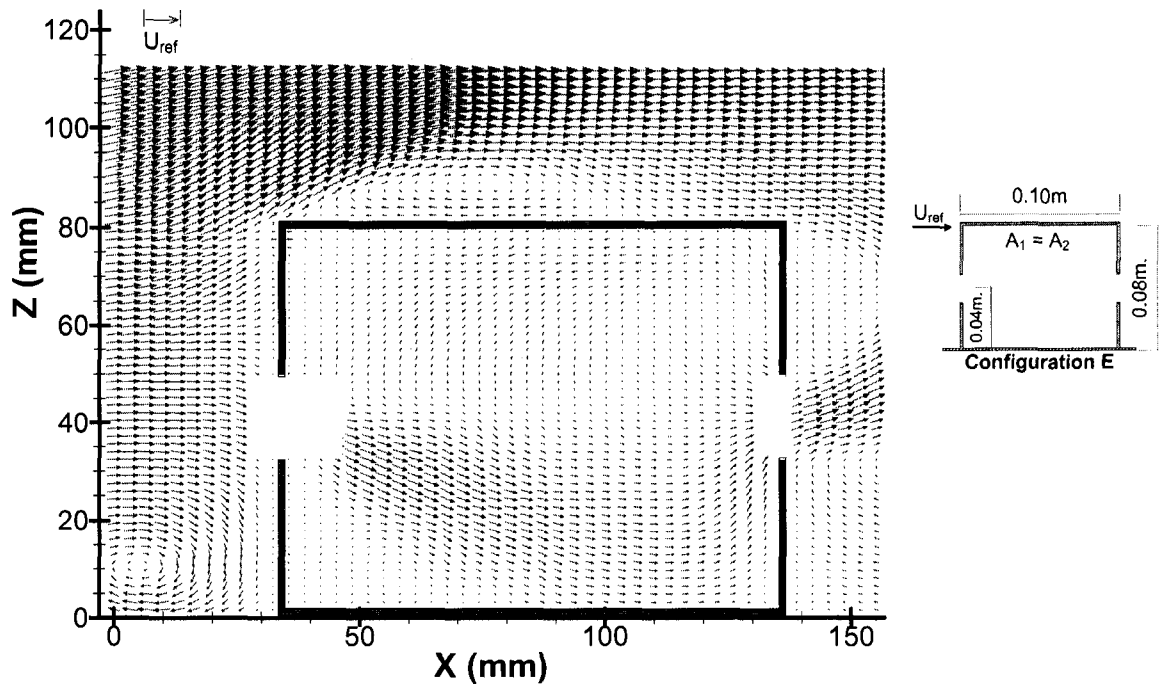
Figure 4.16. Cross sectional view of mean velocity vector field on a vertical mid-plane for configuration E with 10% wall porosity ($\theta = 0°$).

(inlet) there is a small re-circulating zone formed below the jet. The flow decelerates through the central region, with recovery of speed occurring closer to the leeward opening (outlet). At the outlet, the velocity is accelerated immediately after the opening and the discharged jet is induced upward by the presence of the re-circulating flow located in the wake of the building. Some of the jet contracts to exit through the outlet opening; however some of the faster moving flow is directed up the inside of the leeward face above the jet. This flow reaches the top of the leeward face and is directed along the roof where it moves against the direction of the jet until it reaches the windward face where the flow is being drawn towards the jet. Similar flow patterns - shown in Figure 4.17 - are observed for configuration C. However, for this configuration the down-flow at the inlet is more pronounced and occurs at a shorter distance from the opening; then the

flow remains straight and it is directed upwards before the outlet. The effective inlet opening area is smaller than the geometrical area and also smaller compared to configuration E. The effective inlet area can be defined as $A_{eff} = Q_{opening}/U_{opening}$, where $Q_{opening}$ is the actual flow through the opening (considering the losses) and $U_{opening}$ is the mean velocity at the opening. Figure 4.18 shows the mean velocity vectors for configuration A (openings above the mid-height of the building). When the airflow is entering the building, the velocity is accelerated and slightly directed upwards due to upstream upward flow which is clearly depicted in Figure 4.18. At the outlet, the velocity is accelerated and the discharged jet follows a horizontal direction. Generally, almost a straight flow tube connecting the inlet and outlet is observed. The effective area of the inlet opening is almost equal to geometric area and it is larger than that for configurations C and E. In the slow moving region below the dominant jet there is a region close to the leeward face where some of the faster moving flow is directed down. This flow reaches the bottom of the leeward face and is directed along the floor where it moves against the direction of the jet until it reaches the windward face where the flow is being drawn towards the jet.

Figures 4.19 and 4.20 show a cross sectional view of the mean velocity vector field on a vertical mid-plane, for $A_1 = A_2$, 10% wall porosity, $\theta = 0°$ and configurations B and D respectively (non-symmetric openings). The change in flow direction is evident for both configurations; there is almost a vertical (downward and upward for configuration B and D respectively) flow before the outlet. For configuration B, the velocity is accelerated immediately after the outlet and it follows a downward direction. It should be
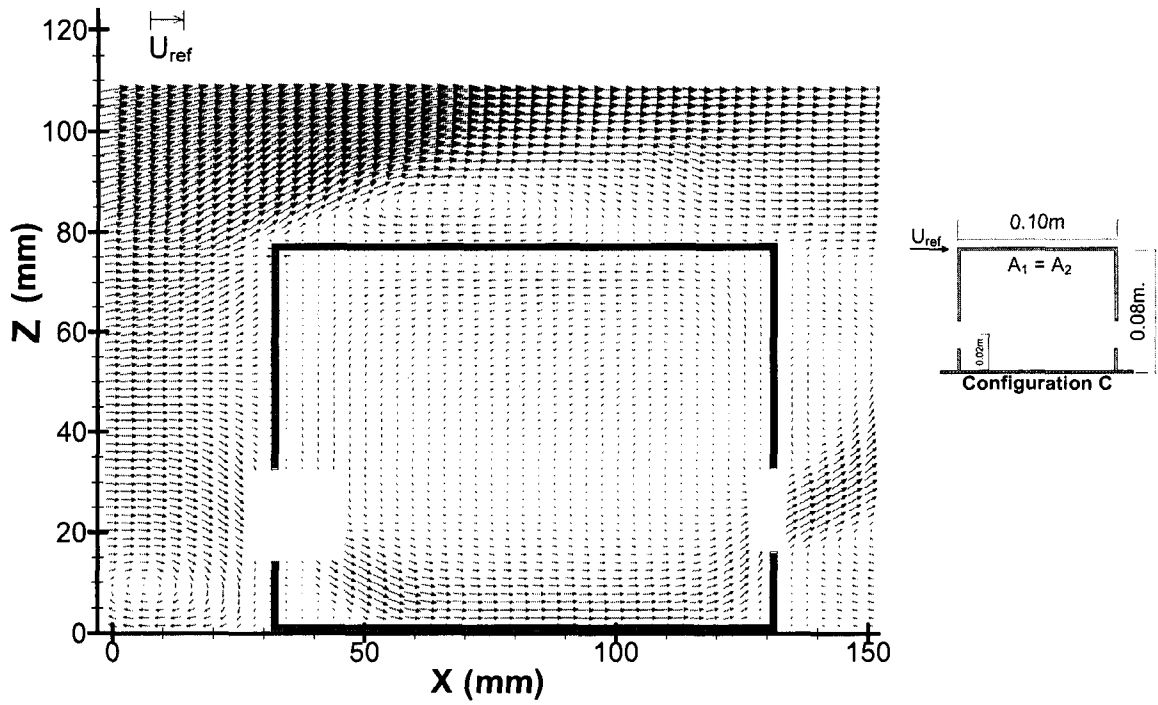
Figure 4.17. Cross sectional view of mean velocity vector field on a vertical mid-plane for configuration C with 10% wall porosity ($\theta = 0°$).
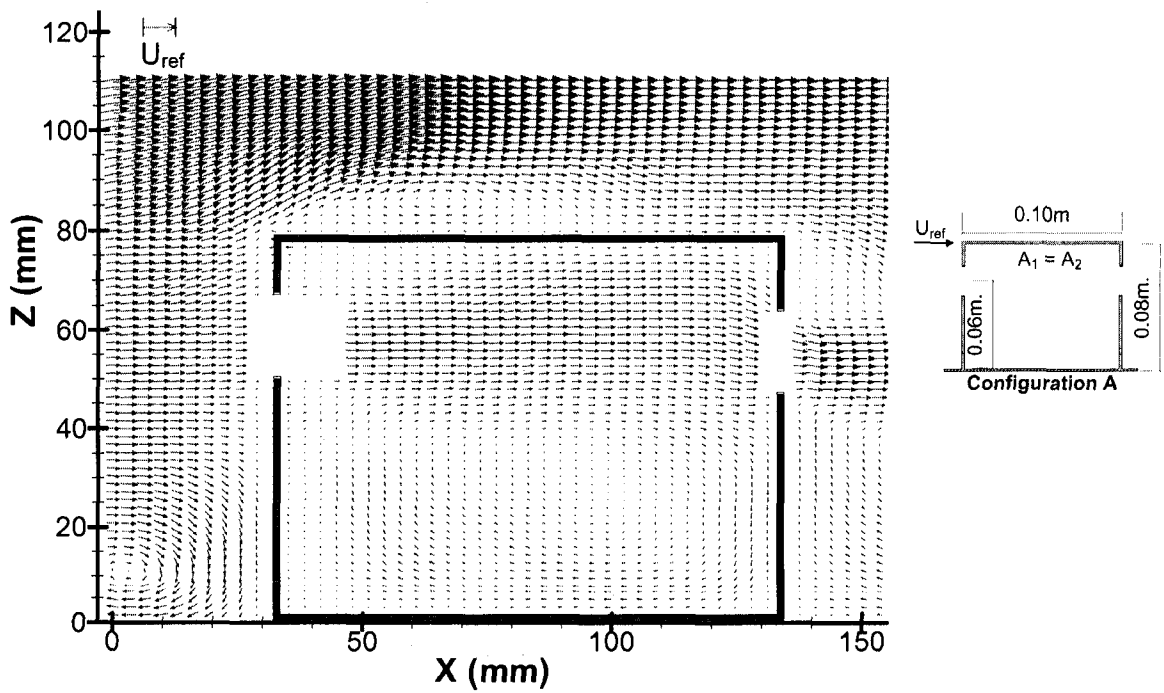
Figure 4.18. Cross sectional view of mean velocity vector field on a vertical mid-plane for configuration A with 10% wall porosity ($\theta = 0°$).
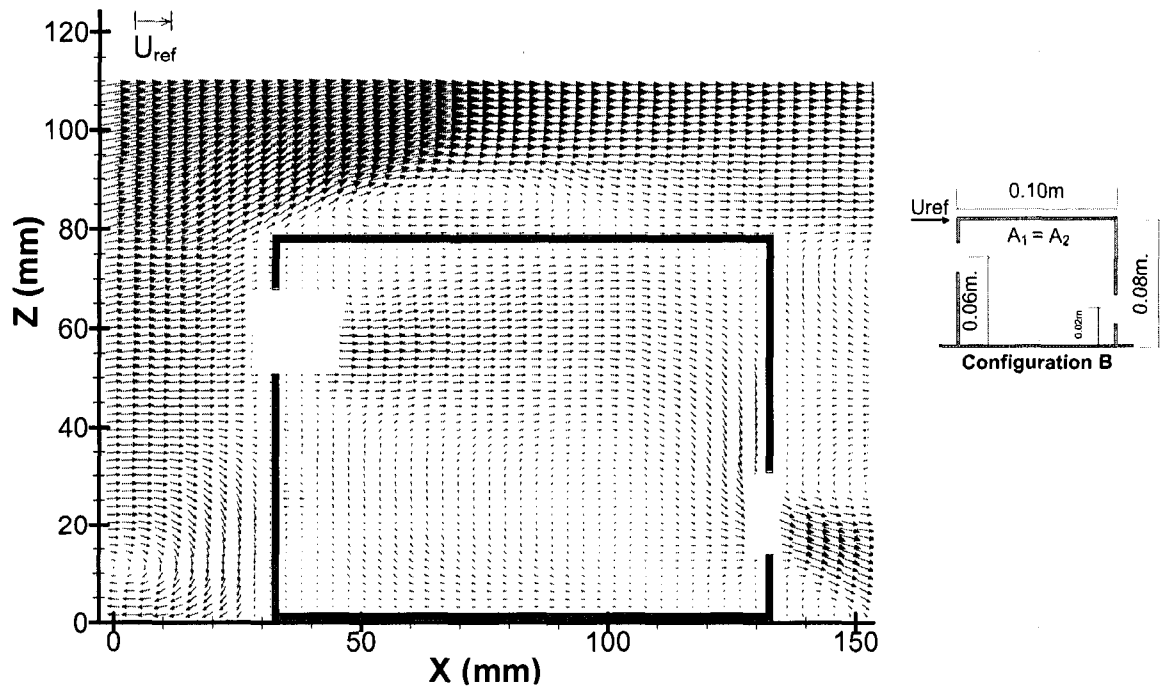
Figure 4.19. Cross sectional view of mean velocity vector field on a vertical mid-plane for configuration B with 10% wall porosity ($\theta = 0°$).
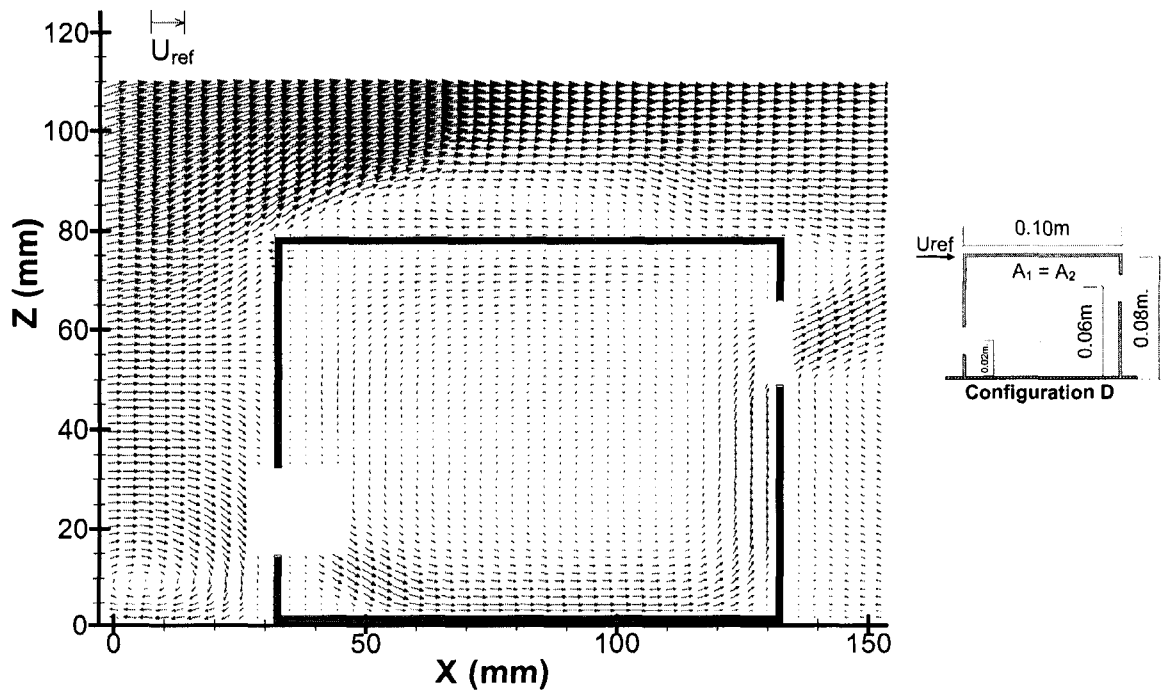
Figure 4.20. Cross sectional view of mean velocity vector field on a vertical mid-plane for configuration D with 10% wall porosity ($\theta = 0°$).

noted that for all other configurations (except for configuration A), the mean flow at the outlet is directed upward due to the re-circulating flow field in the wake region. Thus, it can be concluded that the outflow direction depends on the outlet opening location with respect to the external flow field, as well as the relative location of the inlet and outlet openings (internal flow field).

Examination of Figures 4.16-4.20 shows that the diameter of the flow tube is larger for configurations A, B and E compared to configurations C and D. For configuration A the air speed inside the room is high as the flow tube remains straight while for configuration B the speed is lower since the flow has to change direction before reaching the outlet. For configurations C and D, the effective inlet area is smaller and the flow remains contracted till it reaches the outlet opening resulting in high air speeds. For configuration E the jet is directed downwards immediately after the inlet and also disperses (large flow tube diameter) resulting -for the same inlet area- in lower air speeds compared to the other configurations.

Figure 4.21 shows a plan view of the mean velocity vector field at opening mid-height within and around the building model for configuration E (openings located at the mid-height of the building), A_1 = A_2, 10% wall porosity, and θ = $0°$. Again, the dominating jet flow is obvious. Either side of the jet region are slower moving zones that show circulatory flows driven by the jet. As mentioned earlier, problems were encountered in some regions – see Figure 4.21 - due to shadows. The lateral turbulence (due to its random nature) may be another reason for some bad correlations during the image processing. Similarly, Figure 4.22 presents a plan view of the measured mean
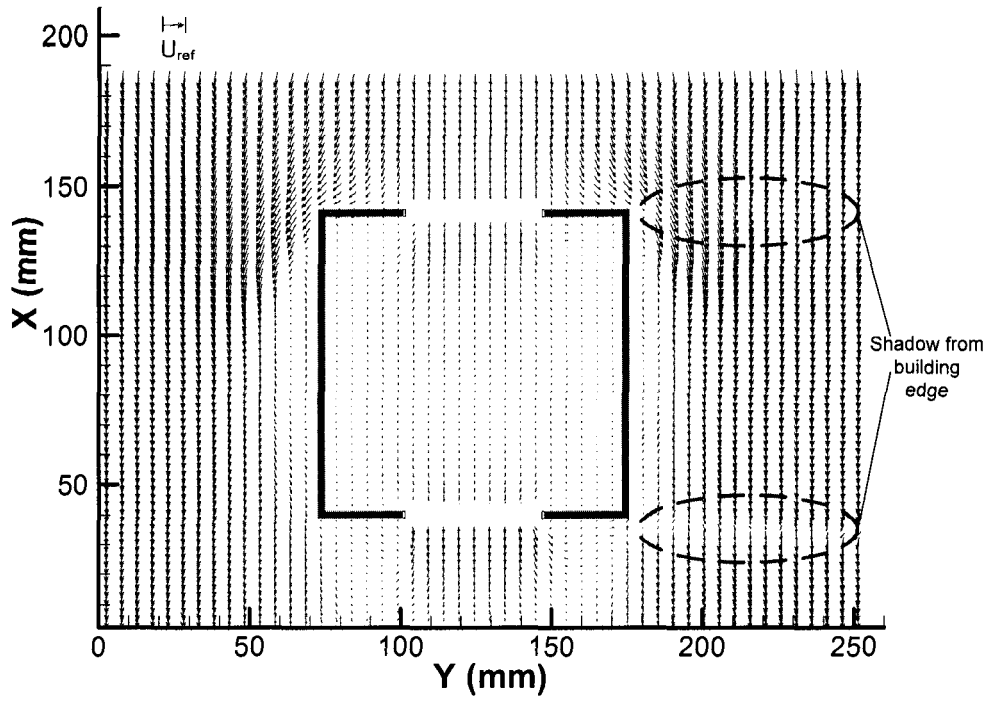
Figure 4.21. Plan view of mean velocity vector field at opening mid-height for configuration E with 10% wall porosity ($\theta = 0°$).
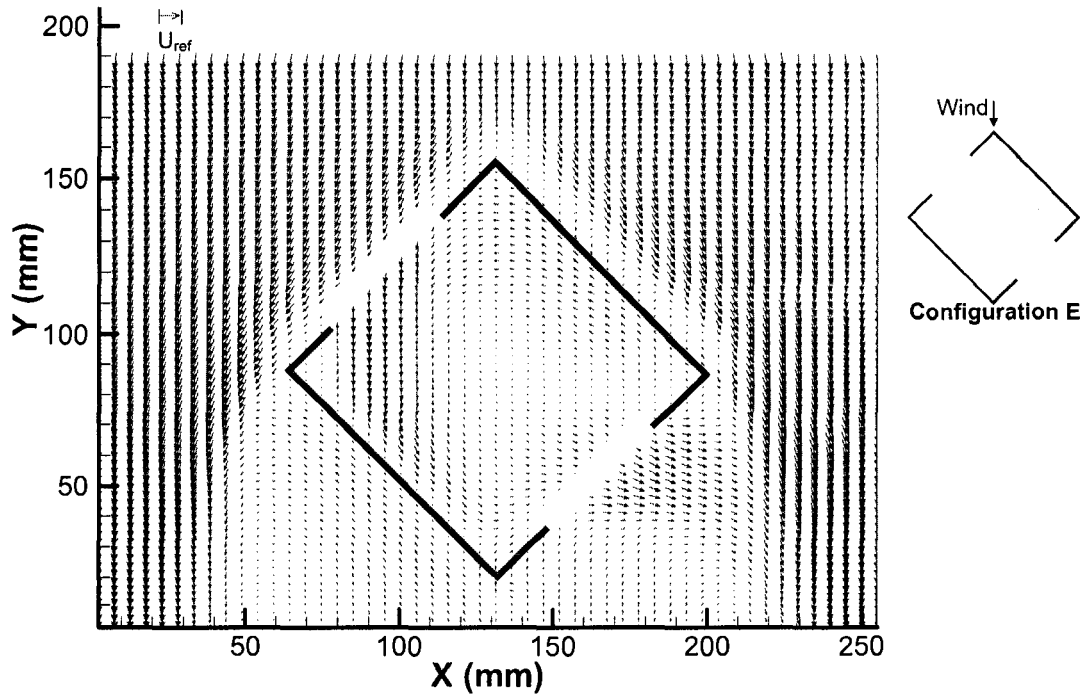
Figure 4.22. Plan view of mean velocity vector field at opening mid-height for configuration E with 10% wall porosity ($\theta = 45°$).

velocity vectors for the same configuration and $\theta = 45°$. In the horizontal plane, the flow enters the building diagonally and the circulated flow is also emitted in a diagonal direction. The shear flows and large vortices around the buildings are clearly shown under this wind direction. Higher velocities are observed for the same configuration and oblique winds ($\theta = 45°$) compared to those for $\theta = 0°$.

Figure 4.23 shows profiles of the x-component of the velocity (normalized by the reference velocity) on the center-line directly between the openings (cross-section 1) for configuration A, C, and E with wall porosity 5, 10, and 20% and $\theta = 0°$. Comparison of data from measurements on horizontal and vertical planes shows good agreement (Section 4.4); consequently, only PIV data for measurements on a horizontal plane are considered here. Results show the flow accelerating from the inlet plane to a peak located approximately 5% (for configurations C and E) to 10% (for configuration A) of the streamwise distance through the building model. Peak inlet velocities are approximately 74% of the free stream reference velocity for configuration A, 56% for configuration C, and 65% for configuration E. This peak corresponds to the narrowest point of the vena contracta region of the jet passing through the inlet. After the peak velocity close to the ventilation inlets, all profiles in Figure 4.23 display a deceleration, while near the exit the flow again accelerates due to the contraction towards the outlet. As mentioned previously, the flow is directed downward after the inlet for configurations C and E and high velocities occur below the centre-line between the two openings. Figure 4.23 presents important information on the impact of wall porosity on the velocity at the inlet, outlet as well as in the interior of the building model for the same configuration. For
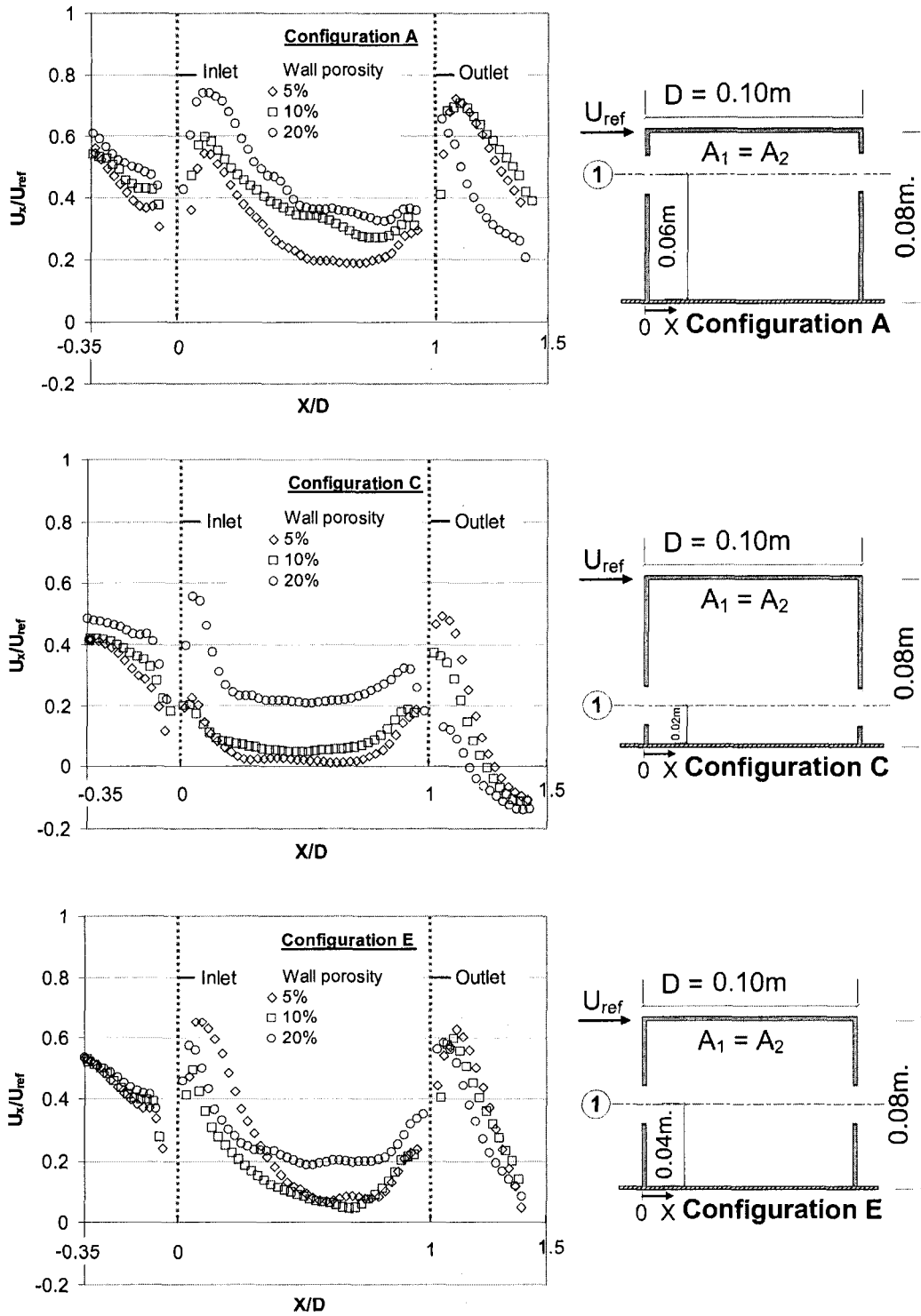
Figure 4.23. Profiles of velocity component on the centre-line directly between the inlet and outlet opening (cross-section 1) for configurations A, C, and E based on PIV measurement on a horizontal plane.

configurations A and C, high velocities at the inlet in the streamwise direction occur for large porosities probably due to the impact of flow tube while high outlet velocities correspond to small porosities. It should be noted that these are observations for specific points on the centre-line through the openings. It is expected that the average velocity at the inlet and outlet openings should be equal for mass conservation. Also for the same configurations (A and C) the approaching velocity (upstream of the inlet) is higher for larger wall porosity (20%) and may also be affected by the flow tube. For configuration E higher inlet and outlet velocities are observed for small porosities.

Figure 4.24 shows the mean airflow rate through the inlet normalized by the reference velocity at the building height ($U_{ref} = 6.6$ m/s) and the opening area for the configurations shown. The airflow (Q) was calculated as $U_{opening} \cdot A$, where $U_{opening}$ = area-averaged velocity downstream (1 cm) the inlet opening and A is the geometric area of the opening.
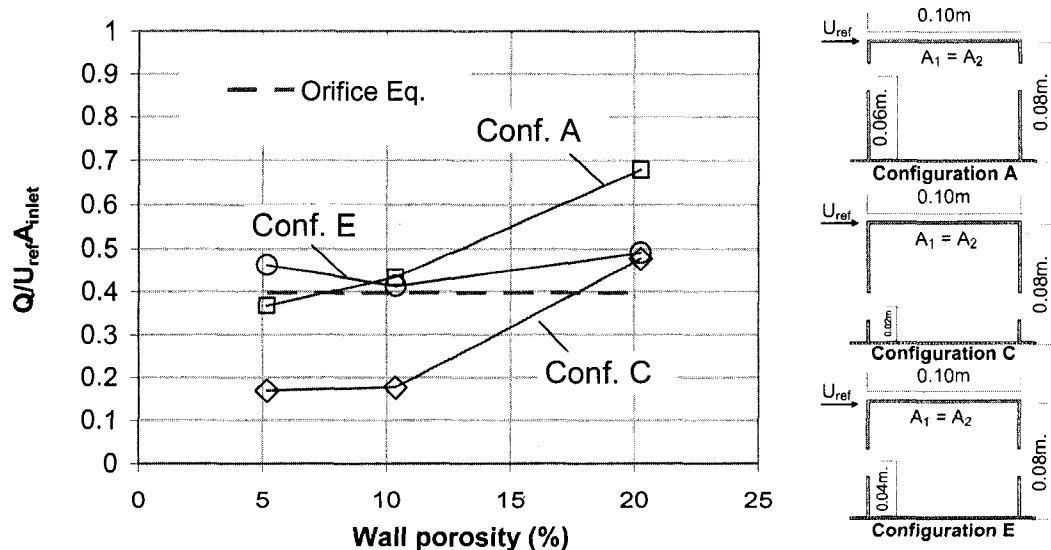
Figure 4.24. Non-dimensional airflow rate at the inlet for configurations A, C, and E ($\theta = 0°$) – results based on PIV measurements on a horizontal plane.

$U_{opening}$ was measured on a horizontal plane (using the PIV technique) located at the mid-height of the opening. Experimental results are compared with the normalized airflow rate evaluated by using Equation (3.3). The windward and leeward wall pressure coefficients were measured in the middle-horizontal-level of the wall for a sealed building and were found equal to 0.7 and -0.15 respectively. These Cp values together with a discharge coefficient value equal to 0.61 (Etheridge and Sandberg, 1996) and a reference velocity equal to 6.6 m/s (measured with a hot-film and PIV) were used for the calculations. It should be noted that previous work (e.g. Karava et al., 2004) has reported significant variations of the discharge coefficient with the wall porosity and the opening configuration. However, for simplification purposes a constant discharge coefficient was used based on the assumption of a small opening (e.g. thin orifice) of sufficiently large Reynolds number. The orifice equation predicts the same normalized ventilation flow rate for the three configurations A, C, and E while measured data show considerable differences (up to a factor of 2.2 for the same wall porosity and different configuration). The orifice model predicts the ventilation flow rate with reasonable accuracy for configurations A and E and wall porosity up to 10%. This finding indicates that the orifice assumption of inlet velocity independent of the wall porosity is only valid for small openings (wall porosity less than 10%). Results for configuration C are overestimated by the theoretical equation except for wall porosity equal to 20%. Differences of this magnitude (factors of 2) may have significant implications on natural ventilation design and control of openings.

Figure 4.25 shows the inlet airflow rate normalized by the reference velocity and the inlet opening area as a function of the inlet to outlet ratio for the configurations shown

with 5, 10, and 20 % inlet area. The normalized airflow rate, evaluated using Equation (3.1) with the same Cp and U_{ref} values used previously and equal inlet and outlet discharge coefficients, is also shown. The ventilation flow rate for configuration C is considerably lower (up to a factor of 2.4 for the same inlet-to-outlet ratio) compared to configurations A and E for all cases considered. This is attributed to the re-circulating approaching flow (standing vortex) that creates a very pronounced down-flow at the inlet and consequently, the effective opening area is reduced. This finding indicates the significance of appropriate boundary layer simulation and accurate evaluation of the approaching flow pattern. Similar airflow rates are observed for configuration A and E for wall porosities up to 10%, while for larger porosities higher airflows are observed for configuration A. This can be probably explained by the straight flow tube connecting the inlet and outlet for configuration A, which is more pronounced for large porosities (see also Figure 4.16and 4.20). The orifice model works well for configuration E with 5% inlet; for 10% and 20% inlet, the orifice model predicts well the ventilation flow rate for $A_1/A_2 \geq 1$. The orifice equation predicts the ventilation flow rate with reasonable accuracy for configurations A and E and wall porosity up to 10%. The orifice equation underestimates the flow rate (up to a factor of 1.7) if any of the inlet or outlet openings covers more than 10% of the wall area; this is more pronounced for configurations with $A_1/A_2 < 1$. For configuration C, the orifice model overestimates the ventilation flow rate (up to a factor of 2.5) except for configurations with large inlets and outlets (20% wall porosity). Therefore, the relative inlet and outlet location and the inlet-to-outlet ratio are very important parameters to be considered, in addition to the wall porosity for evaluating the airflow rate in buildings with cross-ventilation.
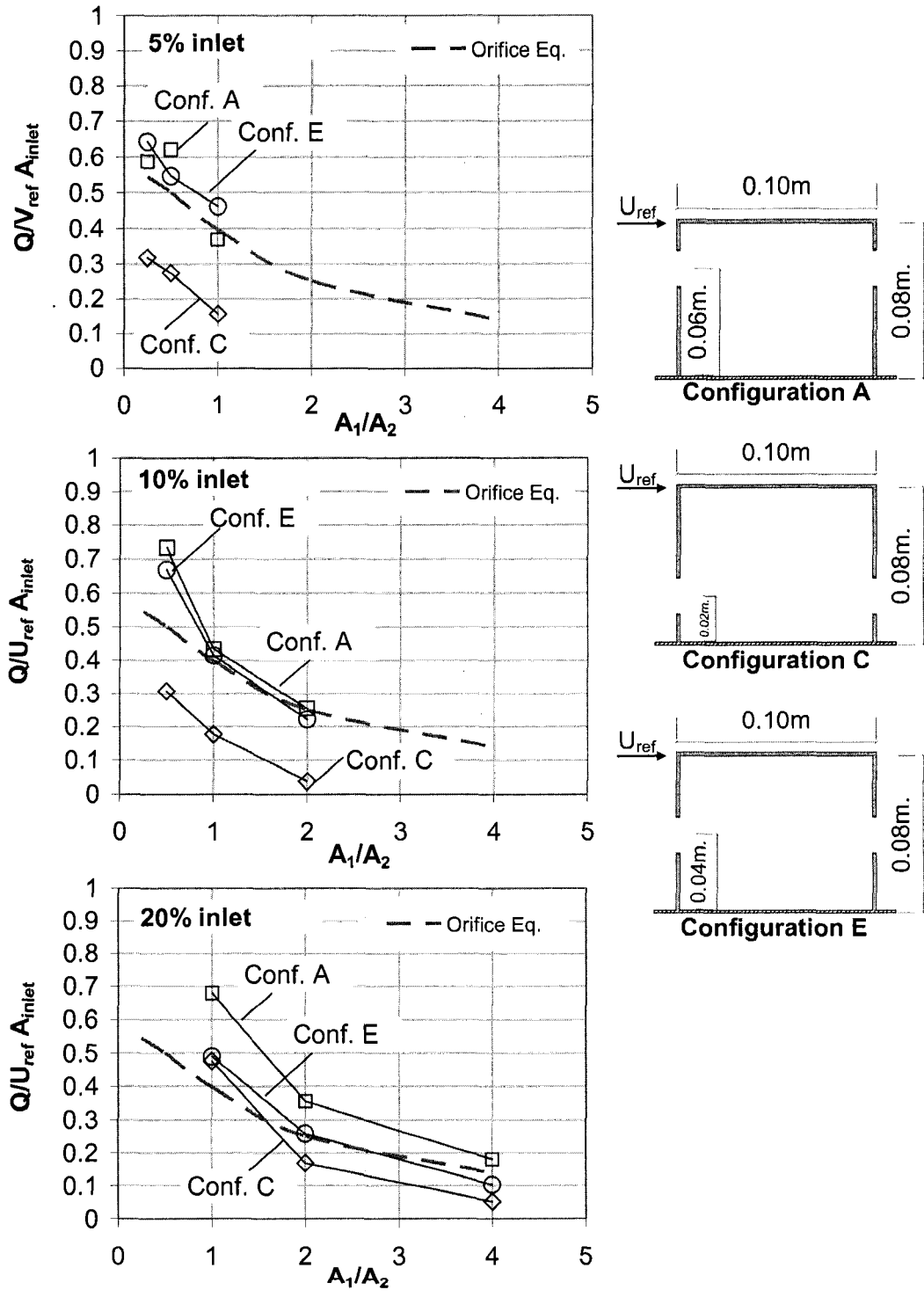
Figure 4.25. Non-dimensional airflow rate at the inlet as a function of inlet to outlet ratio

for configurations A, C, and E with 5, 10, and 20 % windward wall porosity ($\theta = 0°$) -

results based on PIV measurements on a horizontal plane.

Higher airflow rates are observed for configurations with openings located at the mid-height of the building or above, symmetric inlets and outlets, and $A_1/A_2 < 1$. These findings could be considered in the form of design guidelines in the selection of openings and their placement on façade for natural ventilation design of buildings. The positions of the openings would suggest that although a significant volume of air is entering the space, the air flow distribution may also be an important parameter to be considered in the design of passive cooling techniques. Although modelling of the flow phenomena is of importance to this research, indoor airflow distribution and internal pressure coefficients require attention too as they significantly affect occupant thermal comfort.

It is important to mention that impact of furniture and/or internal partitions was not considered in the velocity field measurements mainly because of the challenges involved with the PIV application. However, the impact of blockage of the internal volume was considered in the wind tunnel experiments for the evaluation of internal pressures in buildings subject to cross-ventilation (see Chapter 5). In real buildings, blockage may be created due to furniture and/or internal partitions and in some configurations may affect the flow field.

4.6   Summary

The Particle Image Velocimetry (PIV) method has been applied in a BLWT to investigate the airflow field in a building model subject to cross-ventilation, for the first time. An innovative way of applying the PIV technique into BLWT testing has been developed and presented in detail. Carefully conducted PIV measurements can produce the flow field over extended areas including both horizontal and vertical cross-sections. Results

for the time-averaged flow field have been presented and utilized for the analysis of the flow structure of various cross-ventilation configurations. It was shown that the flow in buildings with cross-ventilation is complex, particularly near the inlets and outlets where sudden acceleration or deceleration (large velocity gradients) occur. This indicates that selection of the measurement location when using single-point techniques may introduce significant errors. PIV data for the inflow velocity have been compared with hot-film measurement results and for the configurations considered here, results show differences between the two methods up to a factor of 2.7. It is well known that hot-wire anemometry should not be used in regions where instantaneous flow reversal is possible or in regions where the level of turbulence fluctuation is high.

Application of the PIV technique for building aerodynamics testing in a large boundary layer wind tunnel presents various challenges. These are related but not limited to seeding type and quality, camera mounting (e.g. vibrations occur if placed inside the wind tunnel), laser mounting, illumination intensity, sample size, etc. With respect to the application of the PIV method for evaluating the airflow field in building models with cross-ventilation, further difficulties are related to shadows and edge reflections. Modifications of the method, which are necessary in order to improve the quality of measurements and to accelerate the process, have been proposed.

The accuracy of the simplified orifice model to predict the ventilation flow rates has been examined. The study found differences up to a factor of 2.5, between the airflow rates measured and predicted using the orifice equation. Such differences may have significant implications on natural ventilation design, the sizing of openings and controls. The orifice model predicts the ventilation flow rate with reasonable accuracy for

configurations A (openings located on top of windward and leeward walls; at 57 mm from the ground) and E (openings located in the middle of windward and leeward walls; at 40 mm from the ground) and wall porosity up to 10%. For the same configurations (A and E), the orifice equation underestimates the flow rate (up to a factor of 1.7) if any of the inlet or outlet openings covers more than 10% of the wall area; this is more pronounced for configurations with $A_1/A_2 < 1$. The ventilation flow rate for configuration C (openings located in the bottom of windward and leeward walls; at 20 mm from the ground) is considerably lower (up to a factor of 2.4 for the same inlet-to-outlet ratio) compared to configurations A and E for all cases considered. For configuration C, the orifice model overestimates the ventilation flow rate (up to a factor of 2.5) except for configurations with large inlets and outlets (20% wall porosity).

The relative inlet and outlet location (with respect to each other and with respect to wind direction) and the inlet-to-outlet ratio are very important parameters to be considered, in addition to the wall porosity for evaluating the airflow rate in buildings with cross-ventilation. In general, higher airflow rates are observed for configurations with openings located at the mid-height of the building or above, symmetric inlets and outlets and $A_1/A_2 < 1$.

5   INTERNAL PRESSURES IN BUILDINGS WITH CROSS-VENTILATION

5.1   Introduction

Internal pressures in buildings with cross-ventilation affect the airflow prediction, occupants' thermal comfort, and wind load design. Although internal pressures play an important role in the design of structures and cladding, they are insufficiently described in existing building codes and design standards (NBCC, 2005; ASCE 7, 2005) mainly due to complexities involved in their evaluation. External pressure distribution, terrain, shape, area and distribution of openings on façade, internal partitions or other restrictions on pressure and airflow within the building, and volume of the internal space are potentially important factors in evaluating building internal pressures. Some of these parameters are investigated in a series of experiments carried out in a boundary later wind tunnel for the evaluation of mean and fluctuating internal pressures in buildings with cross-openings. Experiments with a simple roof-sloped building model were performed at the initial stage of the study to identify the important parameters. A building model with a flat roof was designed and fabricated subsequently to allow testing of configurations with inlets and outlets at various locations. This building model has the same dimensions with the model used for the PIV experiments, results for which were presented in Chapter 4, so as the two sets of data can be correlated.

5.2   Experimental set-up and measurements

This section presents the experimental set-up for the evaluation of internal pressures in

buildings with cross-ventilation. It describes the building models and opening configurations considered, as well as the wind tunnel measurement set-up and instrumentation used.

5.2.1 Building models and opening configurations

A 1:12 gabled roof building model of rectangular plan view 15.3 × 9.8 cm was tested with an eave height of 3 cm. This corresponds to a building 30.5 × 19.6 m and 6 m high assuming a 1:200 geometric scale. The geometric model scale of the BLWT of Concordia University is equal to 1/400 ~ 1/500, however, previous work has shown that a scale equal to 1:200 can be safely used for pressures (Stathopoulos and Surry, 1983). The model provides variable side-wall and windward wall openings and background leakage of 0 and 0.5%. The opening area is expressed in terms of wall porosity ($A_{opening}/A_{wall}$). Figure 5.1 shows a schematic of the building model and the opening configurations while configurations and range of variables considered are summarized in Table 5.1. The openings were located in the middle of the long and short walls. Background leakage was achieved by a series of holes which could be left open or closed. In this study only simple rectangular openings of the same height (1.7 cm) were considered. Differences in opening areas were induced by different opening width (sliding windows). The model building was constructed of acrylic of 3 mm thickness. A single-sided ventilation configuration was considered first for comparison purposes. This was followed by cross-ventilation experiments with 0.5% background leakage and various wall porosities. Configurations with equal inlet and outlet opening areas ($A_1 = A_2$) were tested, as well as
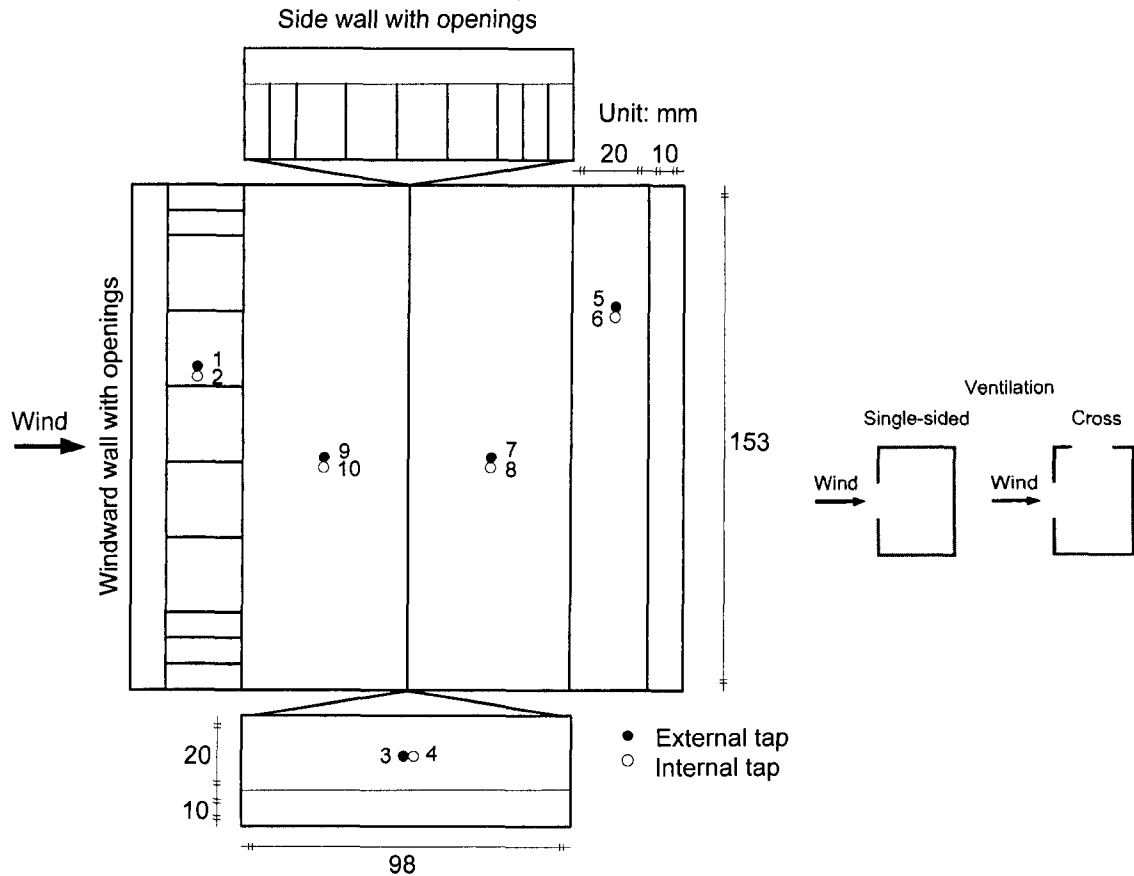
Figure 5.1. Exploded view of roof-sloped building model with pressure tap locations and opening configurations.

Table 5.1. Study considerations and range of variables for the roof-sloped building model.

Ventilation strategy	Cross ventilation with openings located on two adjacent walls
Building dimensions	$30.5 \times 19.6 \times 6$ (eave height) m – $15.3 \times 9.8 \times 3$ (eave height) cm
Roof slope	1:12 (gabled)
Scaling	1:200
Wind direction	0° (perpendicular to long wall)
Window type	Sliding
Windward wall porosity	0 – 22%
Side wall porosity	0 – 33%
A_1/A_2	0 – 8
Building envelope leakage	0.5%

106

configurations with inlet-to-outlet ratio smaller or larger than 1. The two rectangular openings were located in the middle of long wall (windward wall) and short wall (side wall). Five pairs (one for each façade and roof) of closely-located internal and external pressure taps were selected for the measurements, as indicated in Figure 5.1. Measurements were carried out for a wind angle, θ, equal to $0°$.

A $10 \times 10 \times 8$ cm flat roof building model, subject to cross-ventilation, was designed and studied in the atmospheric Boundary Layer Wind Tunnel (BLWT) of Concordia University. The equivalent full-scale dimensions can be considered as 20 m $\times$ 20 m, 16 m high - assuming a 1:200 geometric scale - corresponding to a 4 or 5-storey building. A picture of the building model is shown in Figure 5.2.

Holmes (1979) reported that a building with a single dominant opening behaves like a Helmholtz resonator and internal pressure fluctuations are due to compressibility effects
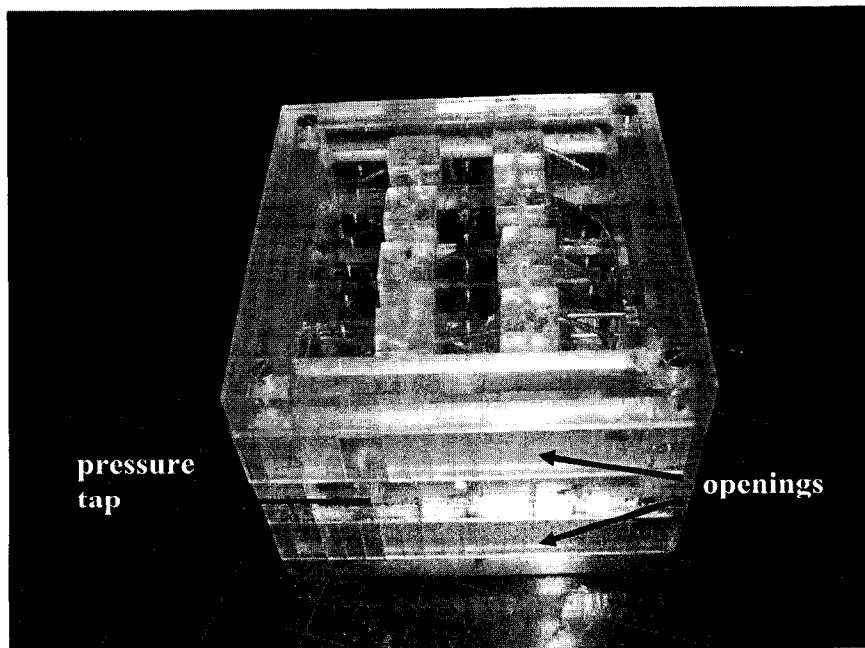
Figure 5.2. The flat roof building model.

of the fluid (i.e., air). This phenomenon can be modelled with an equation of motion for a "slug" of air moving in and out of the opening. Holmes introduced the method of internal volume scaling in wind tunnel experiments to maintain similarity of the dynamic response of the volume at model scale to that in full scale, which is critical for obtaining the correct natural frequency for Helmholtz resonators. This scaling requires that:

$$V_{o,m} = V_{o,f} \frac{(L_m / L_f)^3}{(U_{H,m} / U_{H,f})^2} \qquad (5.1)$$

where L is a characteristic length, V_o is the volume, U_H is the mean roof height wind speed, and the subscripts m and f are for model and full scale, respectively.

A sealed volume chamber is usually installed, fit to the bottom of the model so that the internal volume is increased in order to achieve model to full scale internal volume similarity. The scaling parameter for the internal pressure dynamics has been applied in the experimental studies for the evaluation of internal pressures in buildings with a dominant opening by Liu and Rhee (1986), Womble et al. (1995), Pearce and Sykes (1999), Ho et al. (2004), and Oh et al. (2007). Womble (1994) reported that scaling of internal volume has no effect in the internal pressure fluctuations in buildings with cross-openings. It should be noted that scaling of internal volume has been considered for structural applications where the actual flow patterns inside the building are not significant. However, for the evaluation of ventilation performance, model to full scale airflow patterns similarity is also required. This similarity may be violated if the shape and size of the internal volume is modified. Hence, in the present study, it was decided not to consider scaling of internal volume.

The model provides variable windward, leeward and side wall openings and background leakage of 0.13% and 0.28%. The background leakage was indented to be

almost zero for consistency purposes with the PIV experiments; however, some leakage is expected through the pressure taps that were not in use. This is estimated to be about 0.13%. The wall thickness is equal to 3 mm. In this study, only simple rectangular openings of the same height (18 mm − 3.6 m) were considered. Inlets and outlets are located at the bottom (opening mid-height at 20 mm − 4 m from ground) or top (opening mid-height at 57 mm − 11.4 m from ground) of windward, leeward or side walls. Configurations with inlets and outlets located at the same height (symmetric openings, configurations A1, A2 and C1, C2) were tested as well as configurations with inlets and outlets located at different heights (non-symmetric openings, configurations B1, B2 and D1, D2). The opening configurations (A1, B1, C1, D1 and A2, B2, C2, D2) are shown in Figure 5.3. Configurations with wall porosity ranging from 2.5% to 20% and inlet-to-outlet ratio varying from 0.25 to 8 were tested. Inlet-to-outlet ratios different than one were considered for configurations A1 and C1. Measurements were carried out for a wind angle, θ, equal to 0° and 45°. Configurations and range of variables considered are summarized in Table 5.2. The building model has 20 pairs of closely-located internal and external pressure taps. Figure 5.4 shows an exploded view of the building model and the locations of the pressure taps used in this study (12 external and 20 internal taps). Internal pressures were measured at different locations within the model depending on the blockage ratio of the internal volume and the wind angle. Selected pressure taps for the different cases are presented in Table 5.3. In buildings, blockage of the internal volume may be created due to partition walls, furniture, etc. This effect was modelled using the plastic tubes that connect the pressure taps to the Scanivalve and the different blockage
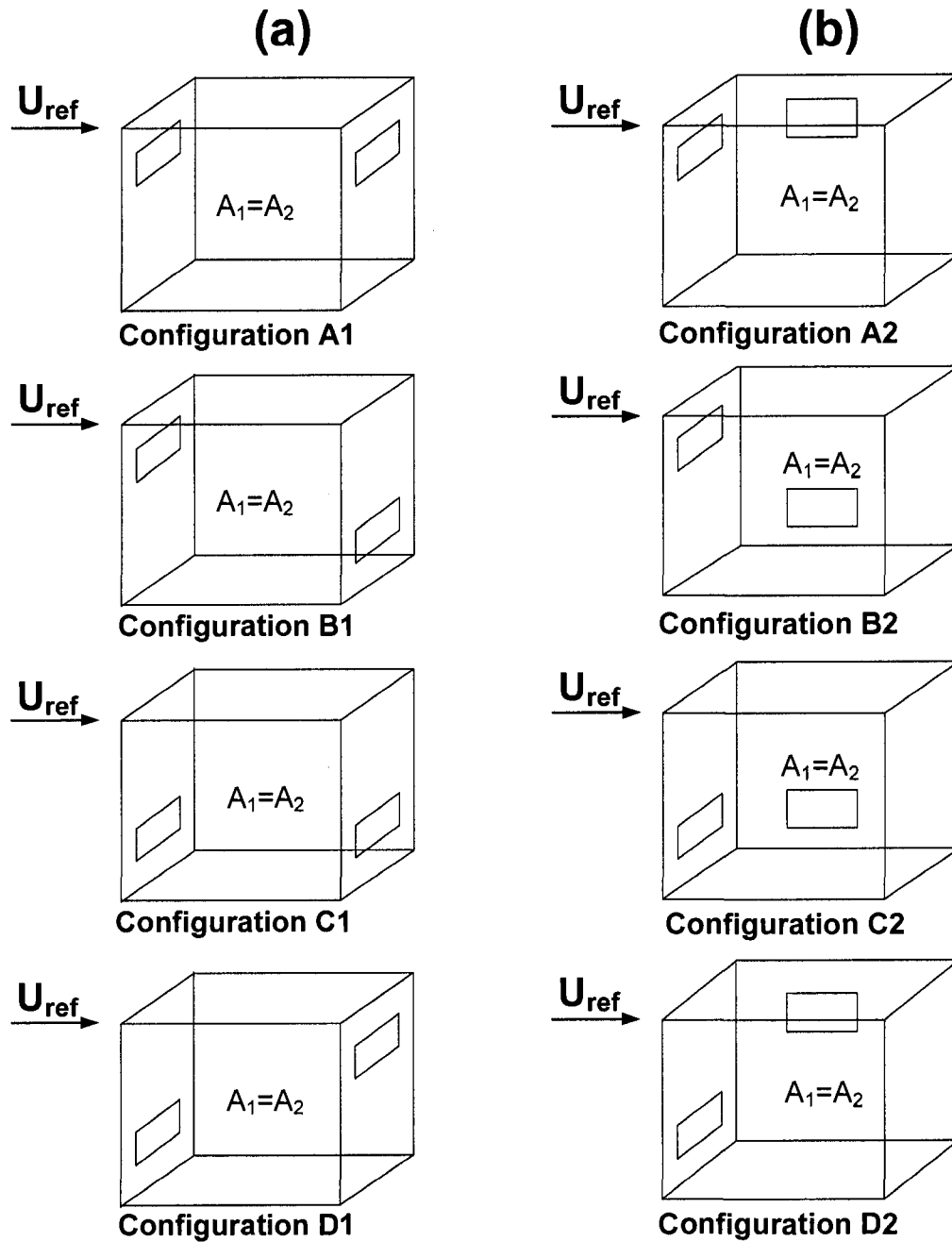
Figure 5.3. Opening configurations considered for studying the effect of wall porosity and opening location on ventilation flow rates; (a) Leeward outlet, configurations A1 and C1: symmetric openings, configurations B1 and D1: non-symmetric openings; (b) Side wall outlet, configurations A2 and C2: symmetric openings, configurations B2 and D2: non-symmetric openings.

Table 5.2. Study considerations and range of variables for the flat roof building model.

Wind angle °	Configuration	Inlet mm	Outlet mm	A_1 (%)	A_2 (%)	A_1/A_2
		Opening Location*				
Leeward outlet						
0	A1	57	57	5, 10, 20	5, 10, 20	1
0	B1	57	20	5, 10, 20	5, 10, 20	1
0	C1	20	20	5, 10, 20	5, 10, 20	1
0	D1	20	57	5, 10, 20	5, 10, 20	1
0	A1	57	57	5	20, 10	1/4, 1/2
0	A1	57	57	10	20, 5	1/2, 2
0	A1	57	57	20	10, 5, 2.5	2, 4, 8
0	C1	20	20	5	20, 10	1/4, 1/2
0	C1	20	20	10	20, 5	1/2, 2
0	C1	20	20	20	10, 5, 2.5	2, 4, 8
45	A1	57	57	5, 10, 20	5, 10, 20	1
45	B1	57	20	5, 10, 20	5, 10, 20	1
Side-wall outlet						
0	A2	57	57	2.5, 5, 10, 20	2.5, 5, 10, 20	1
0	B2	57	20	2.5, 5, 10, 20	2.5, 5, 10, 20	1
0	C2	20	20	2.5, 5, 10, 20	2.5, 5, 10, 20	1
0	D2	20	57	2.5, 5, 10, 20	2.5, 5, 10, 20	1

*Opening location: distance of opening mid-height from the floor
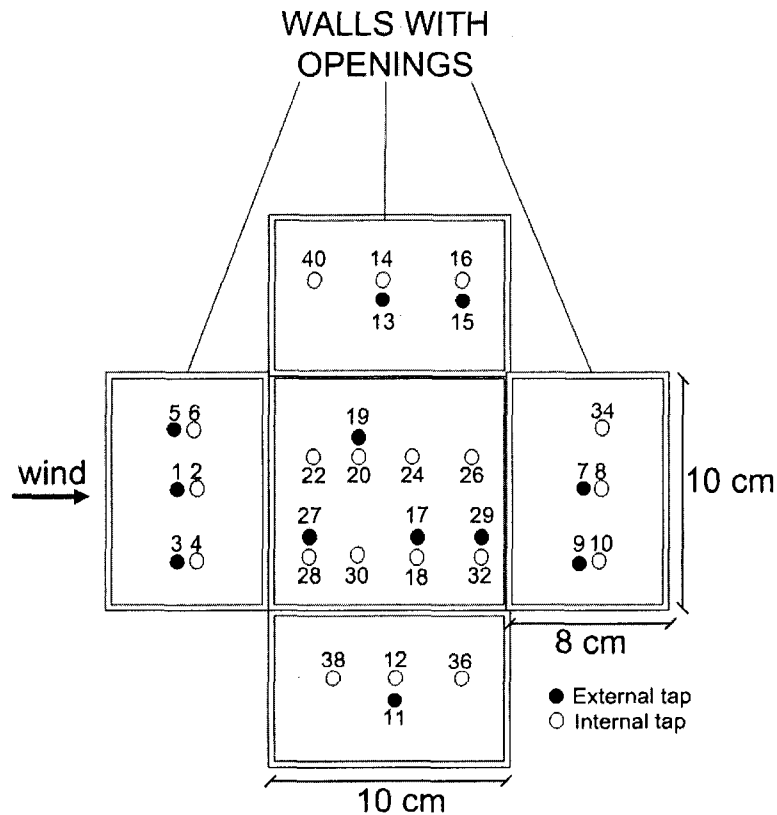
Figure 5.4. Exploded view of flat roof building model with pressure taps locations.

Table 5.3. Internal pressure taps used for different wind angles and blockage ratios.

Wind angle (°)	Blockage ratio (%)	Internal pressure taps
0	5	2, 8, 10, 12, 14*, 16
0	20	2, 4, 6, 8, 10, 12, 14, 16, 18, 20
0	35	2, 4, 6, 8, 10, 12, 14, 16, 18, 20, 22, 23, 24, 25, 26, 28, 30, 31, 32, 33
45	10	2, 8, 10, 12, 14, 16, 26, 34, 36, 40

* Tap 14 was used only for configurations with a side wall outlet

ratios were estimated using the approximate method described below.

A vertical cross-section of the room (flat-roof building model) is considered as shown in Figure 5.5. The cross-sectional area (10 cm width by 8 cm height) is partially covered by the tubing used for the internal pressure measurements. Thus, the tubing creates a blockage ratio in cross-section A that can be calculated by:

$$\text{Blockage ratio of cross-section A} = \frac{\text{area covered by the tubing in cross-section A}}{8 \text{ cm} \times 10 \text{cm}} \quad (5.2)$$

Then a different vertical cross-section of the room (cross-section B) is considered and the blockage ratio of cross-section B is calculated and so on. To calculate an "overall blockage ratio", the blockage ratio of the different cross-sections is averaged. It should be noted that the blockage ratio may have a different value for the various vertical cross-sections depending on the location of the internal pressure taps, i.e. there is a variation of the blockage ratio with the room depth (D). Blockage on a particular cross-section may be non-uniform, which indicates a blockage variation with room height (H) and width (W), resulting in configurations with a particular wall porosity being more sensitive to blockage than others. Blockage ratios from 5% to 35% were estimated in this study.

Figure 5.6 shows a side-view of the building model witn estimated blockage ratio equal to 5%.
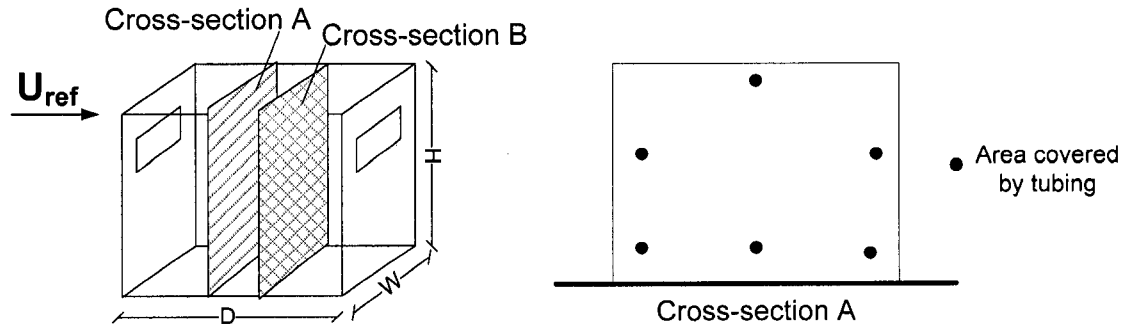
Figure 5.5. Schematic representation of the estimation of blockage ratio.
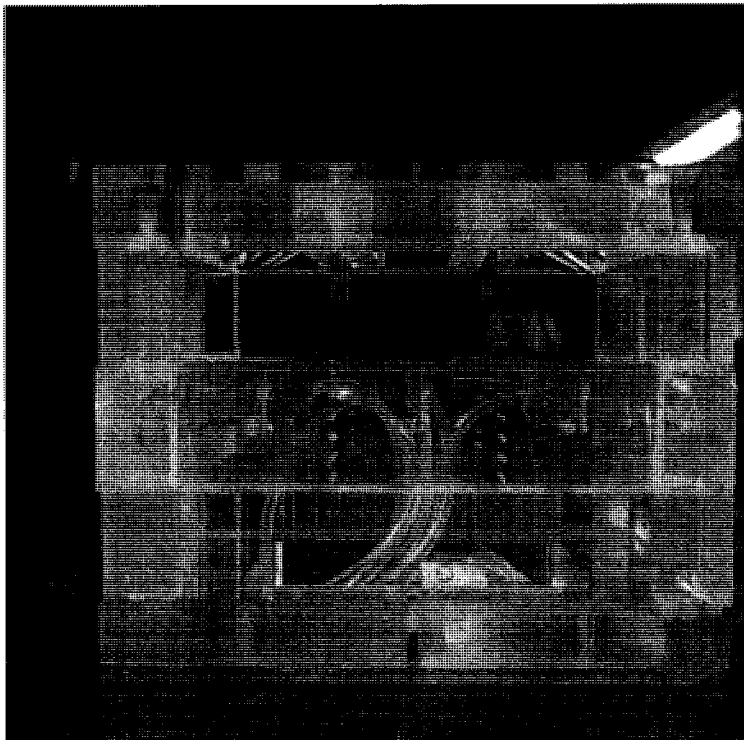
Figure 5.6. Side-view of the building model witn estimated blockage ratio equal to 5%.

5.2.2 Velocity and turbulence intensity profiles

For testing the roof-sloped building model, a standard wind velocity profile over open terrain was simulated with a power-law exponent equal to 0.15 and turbulence intensity at the eave height equal to 22%. The wind tunnel speed was equal to 11.7 m/s at the reference height. For the flat roof building model, a power-law exponent equal to 0.13, turbulence intensity at building height equal to 13% and a reference wind speed equal to 12.4 m/s was considered. The roughness length (Z_o) was about 2.25 cm. Repeatability tests for the approaching wind velocity profile were performed and differences in the value of power-law exponent were in the order of 5%. Velocity (mean and STDEV) was measured with a hot-film anemometer connected to a data acquisition system (DATA 6000). The scan frequency was set at 500 Hz and the record duration was 32 seconds. Figure 5.7 shows the velocity and turbulence intensity profiles considered. The turbulence intensity profiles using the equation T.I. = $1/\ln(Z/Z_o)$ for roughness length equal to 2.25 cm and the ESDU (82026) model are also included in the same figure for comparison purposes. Differences between experimental results and empirical models are smaller at lower heights, where the building openings locate.

5.2.3 Pressure measurements

A honeywell 163 PC differential pressure transducer with range from 0 to 10 in H_2O (2,500 Pa) was used to measure mean and fluctuating pressures. The pressure transducer was calibrated using a TSI DP-Calc micro-manometer of 1% accuracy and the calibration factor is equal to 0.0022 in H_2O/mV. Each pressure tap was connected to a Scanivalve

114
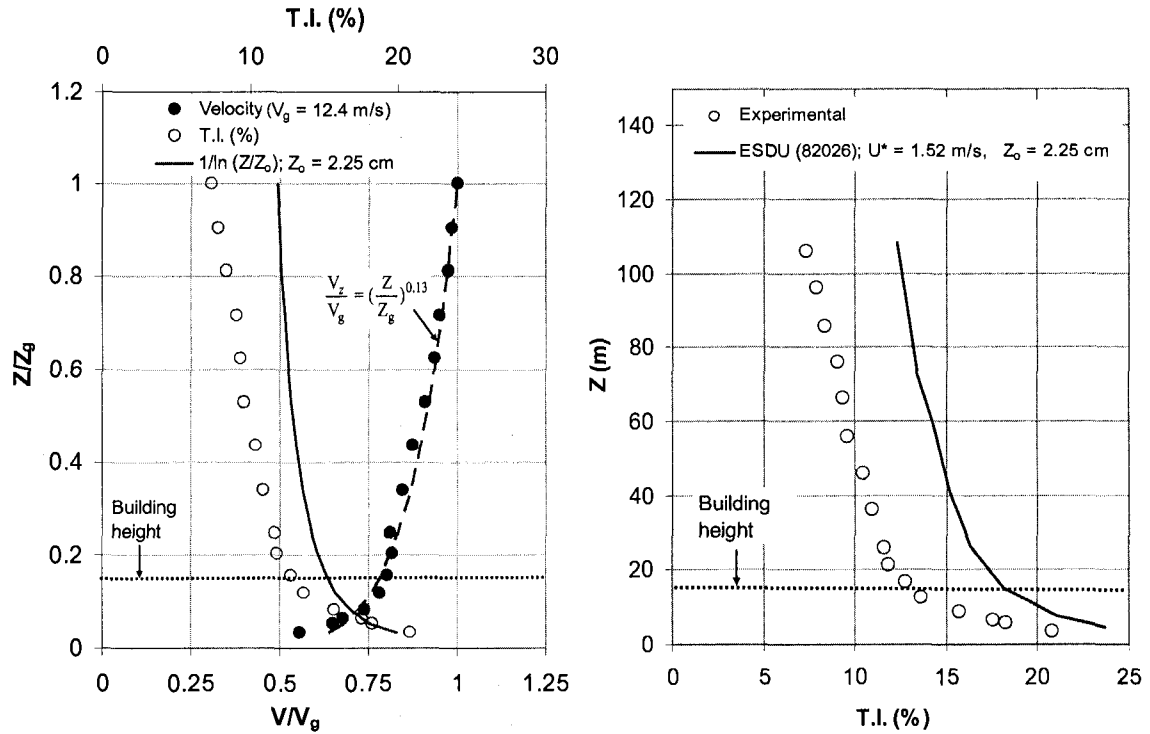
Figure 5.7. Velocity and turbulence intensity profiles considered for the measurements with the flat-roof building model.

system using a 600 mm length of 1.5 mm diameter plastic tube. A restrictor placed at 350 mm tube provided a flat frequency response. The Scanivalve system was in turn connected to the pressure transducer. The pressure signals from each tap were sampled at 500 Hz for 32 s (averaging period used to obtain the mean, STDEV and peak value of the pressure coefficient at each tapping) using a data acquisition system (DATA6000). All measured pressures were referenced to the dynamic pressure at the boundary layer height (~ 600mm) in the wind tunnel measured using a pitot tube. These were then converted to a roof height reference by multiplying them with conversion factors.

5.2.4 Pressure data presentation - Cp definition

The mean pressure coefficient (Cp) is defined as:

$$Cp_{mean} = \frac{\Delta P_{mean}}{\frac{1}{2}\rho U_{ref}^2} \qquad (5.3)$$

where $\Delta P_{mean} = P_{mean} - P_{ref}$, is the mean pressure during a 32 sec record , ρ = air density, U_{ref} = velocity at building height and P_{ref} is the static pressure of the pitot tube. The peak (minimum or maximum) and Cp_{rms} can be defined as follows:

$$Cp_{peak} = \frac{\Delta P_{peak}}{\frac{1}{2}\rho U_{ref}^2} \qquad (5.4)$$

$$Cp_{rms} = \frac{\Delta P_{rms}}{\frac{1}{2}\rho U_{ref}^2} \qquad (5.5)$$

where ΔP_{peak} is the average peak pressure during a 32 sec record (average of 4 readings, one reading every 8 sec) and ΔP_{rms} is the standard deviation during the same period.

5.2.5 Pressure data repeatability

Repeatability tests were performed with the flat roof building model, configuration A1 and 3% blockage. Results for the spatially-averaged mean and peak internal pressure coefficients are shown in Figure 5.8 and they are almost identical for the two tests.

5.3 Results

This section discusses wind-induced mean and peak internal pressures in low-rise buildings with cross-openings. Results of a series of experiments carried out in a BLWT
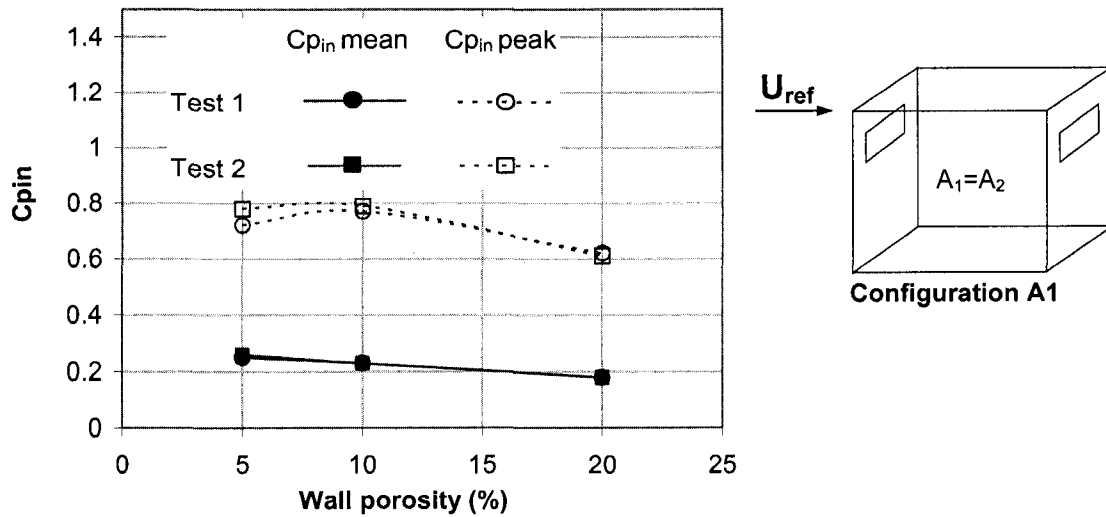
Figure 5.8. Internal pressure coefficients measured during repeatability tests.

for the evaluation of the internal pressures in two building models (with a sloped and a flat roof) with different opening configurations are presented. Experimental results are compared with theoretical values (means) and NBCC provisions (peaks).

5.3.1 Roof-sloped building model

This section presents results for the external and internal pressures measured in a 15.3 × 9.8 × 3 (eave height) cm roof-sloped building model, subject to cross-ventilation. Internal pressures are evaluated for configurations with side wall outlets, different wall porosities and inlet-to-outlet ratios, and for a wind angle, θ, equal to $0°$. The measured mean values of the external pressure coefficients (reference height = building height) are 0.67 for the windward wall, -0.36 for the side wall, -0.25 for the leeward wall and -0.4 and -0.74 on taps 7 and 9 of the roof (see Figure 5.1). The measured mean internal pressure coefficient for 0.5% background leakage (without openings) is -0.36 which is slightly different from

the theoretical value, -0.23, obtained by Equation (3.6) using Cp_1 as the representative of the positive external mean pressure and Cp_2 as the area-averaged pressure on the rest of the building envelope.

Single-sided ventilation

The impact of a windward wall opening (single-sided ventilation) on the internal pressure was investigated for 0 and 0.5% background leakage and results are presented in Figure 5.9. Wind tunnel results by Aynsley et al. (1977) for a building with a windward wall opening and background leakage equal to 0.5% of the windward wall (simulated by a roof opening) as well as results by Stathopoulos et al. (1979) for a building with 0.5% background leakage (uniform distribution) and for an open country exposure are also included. The internal pressure was measured at different internal taps and it was found to be uniform, as also previously reported by Stathopoulos et al. (1979) and Wu et al. (1998). Experimental data are compared with theoretical values obtained by Equation (3.5) for 0% background leakage. For the case of a single opening, Equation (3.5) reduces to $Cp_{in} = Cp_1$, which is equal to 0.67. Figure 5.9 shows good agreement between the experimental results and the theoretical values for 0% leakage. In addition, data obtained for 0.5% background leakage shows a similar trend with that observed in the previous studies. However, Aynsley et al. (1977) reported that there is no significant change in the internal pressure ($Cp_{in} = 0.6$) until the frontal opening is reduced to about 5% while results of the present study show that Cp_{in} becomes almost constant (0.6) for wall porosity larger than 15%. Results by Stathopoulos et al. (1979) show that for 0.5% background leakage the mean Cp_{in} is constant at about 0.3 for any opening area more
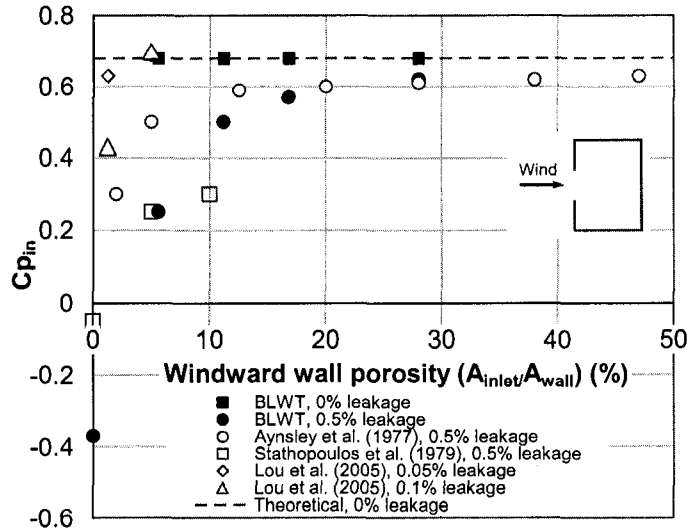
Figure 5.9. Internal pressure coefficients for single-sided ventilation and different windward wall porosity (A_{inlet}/A_{wall}).

than 10% of the wall area. Application of Equation (3.5) for 0.5% background leakage will be arguable due to the undetermined character of the flow.

Cross-ventilation

Wall porosity and inlet-to-outlet-ratio impact

The impact of a windward and a side wall opening of the same area ($A_1 = A_2$) on internal pressure was investigated for 0.5% background leakage and $\theta = 0°$. It should be noted that $A_1 = A_2$ (i.e. equal inlet and outlet opening area) does not correspond to equal windward (A_{inlet}/A_{wall}) and side wall porosity (A_{outlet}/A_{wall}); in fact, for the same opening area, the side wall porosity is higher since the side wall has a smaller façade area compared to the windward wall. The external pressure distribution was monitored and found unaffected by the presence of openings on the façade (sealed body assumption valid) for the range of wall porosities considered here. The internal pressure was

119
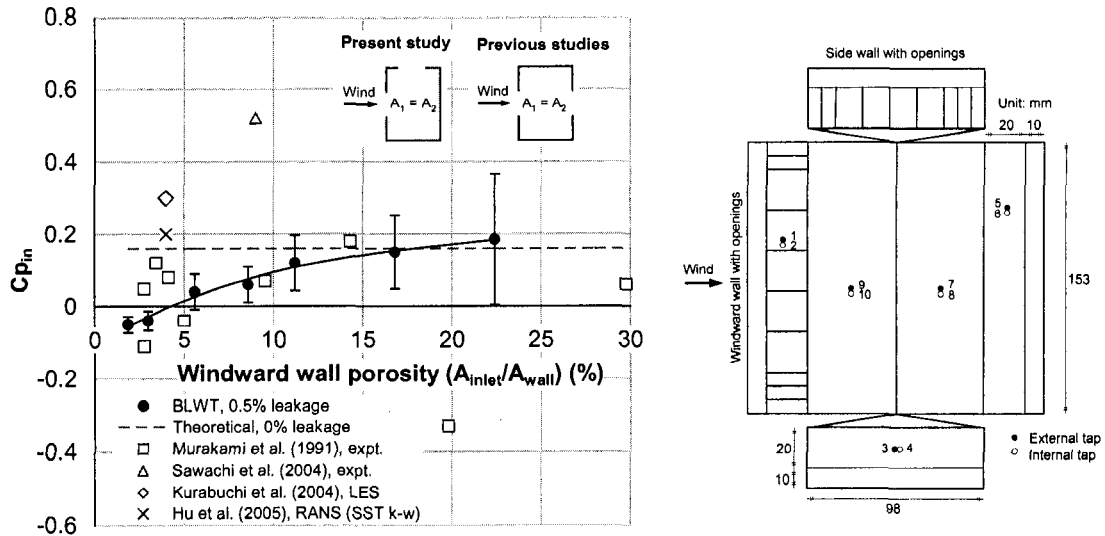
Figure 5.10. Internal pressure coefficients for cross-ventilation with $A_1 = A_2$ and $\theta = 0°$.

measured on taps 2, 4, 6, 8, and 10 as shown in Figure 5.10. All experiments were performed for blockage ratio about 5%. Figure 5.10 presents the spatially-averaged mean value and the standard deviation of the internal pressure coefficient as a function of the windward wall porosity. Wind tunnel results by Murakami et al. (1991) and Sawachi et al. (2004), as well as CFD results by Kurabuchi et al. (2004) and Hu et al. (2005) are also included for comparison purposes. These correspond to configurations with a leeward outlet, since cross-ventilation configurations with a side-wall outlet are only limited to the study by Murakami et al. (1991) for $A_1/A_2 = 2$. Mean internal pressure coefficients in a building with openings can be predicted from the mass balance equation if the external mean pressure coefficient near the openings and the inlet-to-outlet ratio are known (Equation 3.5). The Cp_{in} values obtained by using Equation (3.5) are also shown in Figure 5.10. For $A_1/A_2 = 1$, Equation (3.5) reduces to $Cp_{in} = (Cp_1+Cp_2)/2$ (Eq. 3.7), which does not consider the background leakage. The experimental results show that the

120

average Cp_{in} increases with increasing windward wall porosity, although Equation (3.7) provides a constant value. The internal pressure is not uniform for windward wall porosity higher than 10% resulting in an increase of the standard deviation of the internal pressure coefficient. This non-uniformity of Cp_{in} distribution in the building was not observed in the case of single-sided ventilation and it is not taken into consideration by the theory.

For the building models and configurations considered in Figure 5.10, the windward wall pressure coefficient is in the range of 0.57 to 0.67 and the leeward wall coefficient is ranging from -0.16 to -0.1. Recall that in the present study the external mean pressure coefficients are 0.67 for the windward wall (inlet) and -0.36 for the side wall (outlet). BLWT results are, generally, within the range defined by the other studies; however, substantial differences exist in Cp_{in} values, which may be attributed to the different configurations (leeward vs. side wall outlet) and/or experimental set-up (e.g. scaling, upstream flow conditions) considered in various studies.

The internal pressure coefficient was also investigated for inlet opening area equal to 2.6 cm^2 (5% windward wall porosity), 0.5% background leakage and different inlet to outlet ratios. The experiments were repeated for inlet opening area, A_1, equal to 5.2 cm^2 (10% windward wall porosity). The internal pressure was measured on taps 2, 4, 6, 8, and 10. The mean and standard deviation value of the internal pressure coefficient as a function of inlet-to-outlet ratio (A_1/A_2) for 5% and 10% windward wall porosity is shown in Figure 5.11. The results are compared with wind tunnel data by Murakami et al. (1991) for the case of a side wall outlet and a leeward wall outlet. The Cp_{in} values by using Equation (3.5) are also presented. The experimental results indicate that the average Cp_{in}
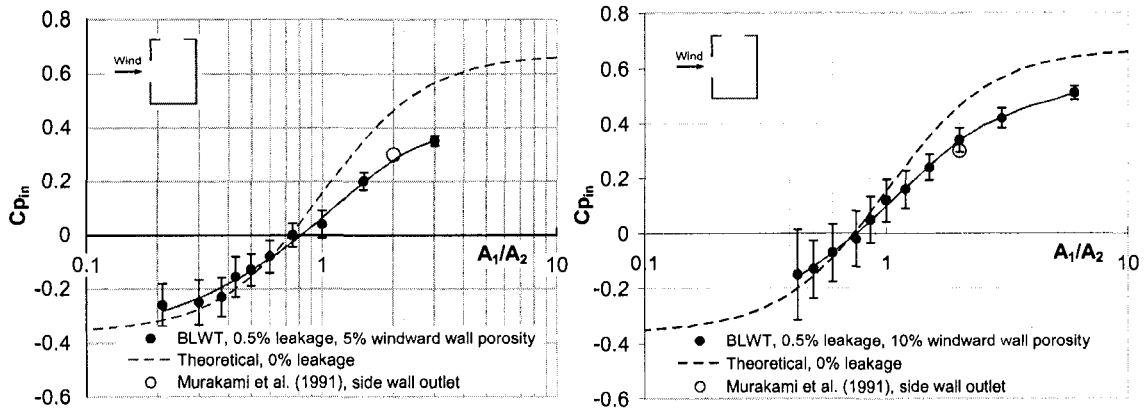
Figure 5.11. Internal pressure coefficients for cross-ventilation with different inlet-to-outlet ratios, 5% and 10% windward wall porosity.

increases with the increase of inlet-to-outlet ratio. The Cp_{in} values predicted by Equation 3.5) are overestimated compared to the experimental data, particularly for higher inlet-to-outlet ratios. This might be due to the impact of the background porosity that is more important for small opening areas and high A_1/A_2 ratios, i.e. $A_1 >> A_2$. There is relatively good agreement between the results of the present study and those by Murakami et al. (1991). In general, the internal pressure coefficient varies considerably (from -0.26 to 0.35) for configurations with $A_1/A_2 > 1$ or $A_1/A_2 < 1$ compared to configurations with $A_1/A_2 = 1$ (from -0.05 to 0.19).

Non-uniform internal pressure

Figures 5.12a and 15.12b show the mean Cp_{in} measured in various internal pressure taps for configurations with $A_1 = A_2$ and $A_1 \neq A_2$ with $A_w = 5\%$ and 10% respectively. Small Cp_{in} values were measured on taps 2 and 10 that may be affected by the stream tube, while high Cp_{in} values were recorded on taps 4, 6 and 8 that are farther from the stream

122
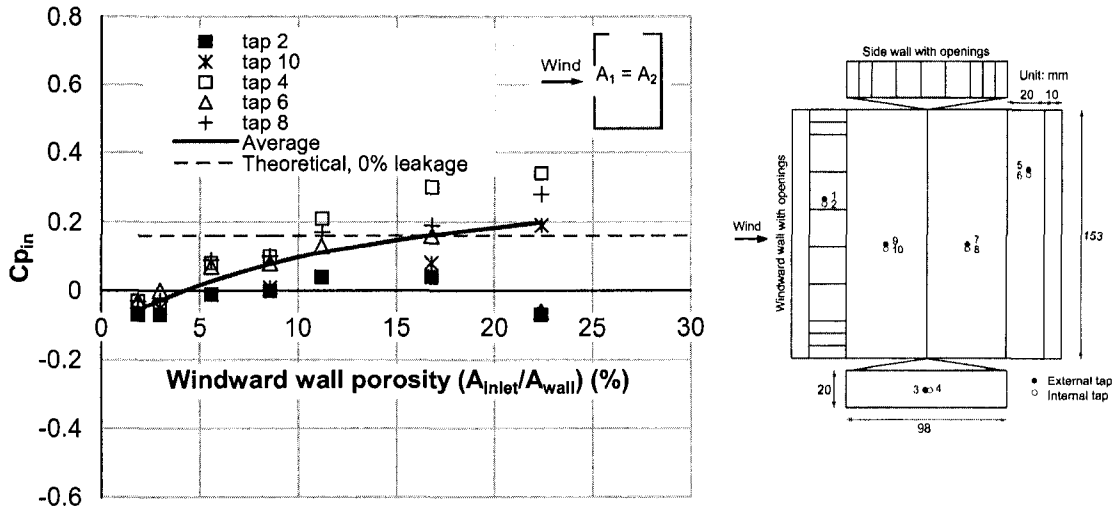
(a) $A_1/A_2 = 1$
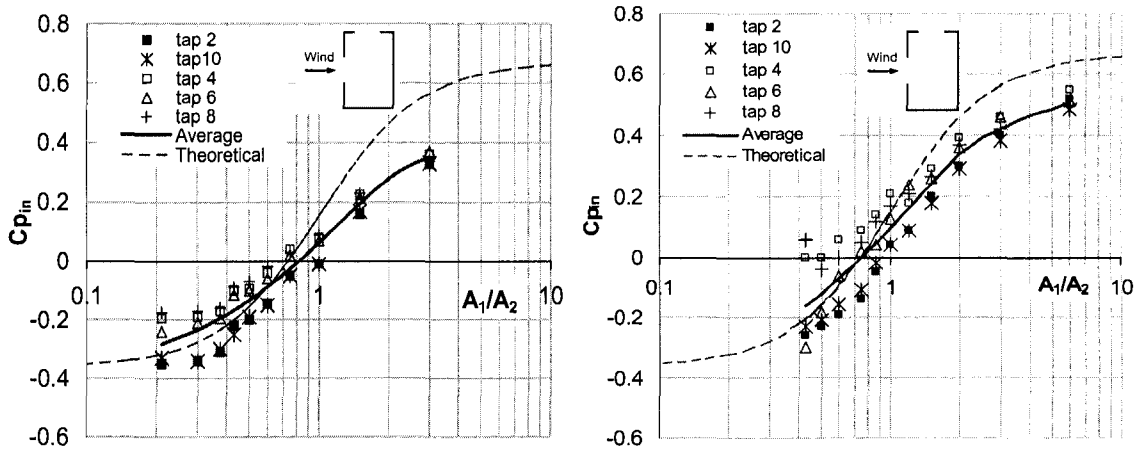
(b) $A_w = 5\%$ (left) and 10% (right)

Figure 5.12. Internal pressure coefficients measured in various pressure taps for cross-ventilation configurations with different inlet-to-outlet ratios and 0.5% background leakage.
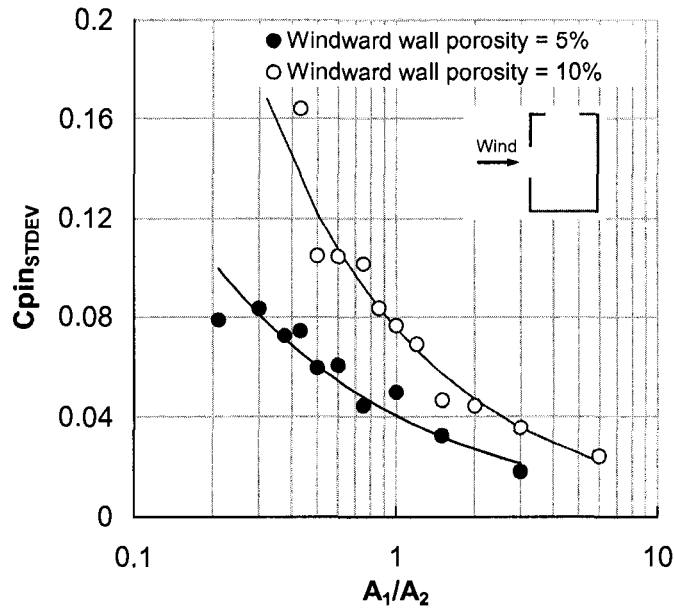
Figure 5.13. Standard deviation of the internal pressure coefficient as a function of A_1/A_2 for 5% and 10% windward wall porosity (A_{inlet}/A_{wall}) and 0.5% background leakage.

tube. Differences among taps can be up to $\Delta Cp = 0.4$ for $A_1 = A_2$ and 0.35 for $A_1/A_2 = 0.4$ and $A_w = 10\%$. These variations should be considered in the selection of measurement points for future experiments. Figure 5.13 shows the variation of the standard deviation of Cp_{in} with the inlet to outlet ratio for 5% and 10% windward wall porosity. For configuration with $A_1/A_2 < 1$ (i.e. large outlet area, A_2) the standard deviation of Cp_{in} is higher. This is more pronounced for configurations with windward wall porosity equal to 10%.

5.3.2 Flat roof building model

This section presents results for the external and internal pressures measured in a $10 \times 10 \times 8$ cm flat roof building model, subject to cross-ventilation. Internal pressures are

evaluated for configurations with different wall porosities, inlet-to-outlet ratios, inlet and outlet location on façade, blockage ratio of the internal volume and for a wind angle, θ, equal to $0°$. Limited results are also presented for $\theta = 45°$ at the end of the section. PIV findings for the air velocity field presented in Chapter 4 are used to justify internal pressure results; hence, the reader should also refer to Section 4.5. The measured mean, rms, max and min values of the external pressure coefficient for a closed building and $\theta = 0°$ are presented in Table 5.4. Internal pressure coefficients for 0.13% and 0.28% background leakage are shown in Table 5.5.

Table 5.4. External pressure coefficients ($\theta = 0°$).

Tap	Cp_{mean}	Cp_{rms}	Cp_{max}	Cp_{min}
1	0.72	0.225	1.55	-
3	0.72	0.225	1.50	
5	0.69	0.225	1.6	
7	-0.15	0.065	-	-0.42
9	-0.16	0.07	-	-0.48
11	-0.51	0.23	-	-1.38
13	-0.565	0.23	-	-1.39
15	-0.3	0.18	-	-0.93
17	-0.48	0.18	-	-1.18
19	-0.79	0.21	-	-1.69
27	-0.94	0.21		-1.81
29	-0.25	0.12		-0.79
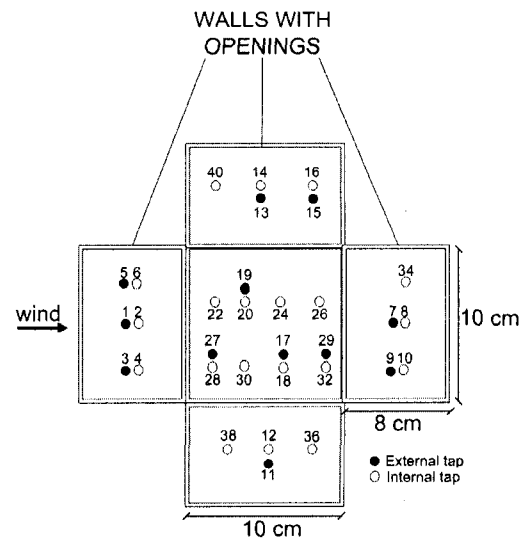
Table 5.5. Internal pressure coefficients for different background leakage ratios ($\theta = 0°$).

Leakage (%)	Cp_{mean}	Cp_{rms}	Cp_{max}	Cp_{min}
0.13	-0.15	0.06	-	-0.39
0.28	-0.19	0.07	-	-0.44
~0.15%*	-0.15	0.06	-	-0.36

* Leakage through the pressure taps that were not in use

125

Configurations with outlets located on the leeward wall of the building

Blockage impact

In real buildings, blockage of the internal volume may be created due to partitions, furniture, etc. Presently, there is limited work done to investigate the effect of internal partitions in buildings with a single opening (e.g. Saathoff and Liu, 1983) while there is hardly any work done for buildings with cross-openings. In the present study, the spatially-averaged mean and peak internal pressure coefficient was the average reading of 5, 10 and 21 internal pressure taps for 5, 20, and 35% estimated blockage respectively (see also Section 5.2.1). The internal pressure coefficients were also calculated by using the same pressure taps for different blockage ratios (i.e. tap 2, 8, 10, 12, and 16) and almost identical results were obtained for all configurations.

Figure 5.14 shows spatially-averaged mean and peak internal pressure coefficients as a function of wall porosity for configurations A1 and D1 (outlets located above the mid-height of the building) with blockage ratios equal to 5%, 20%, and 35% and $A_1 = A_2$. Almost identical mean and peak internal pressure coefficient values were found for all blockage ratios. Results for configurations B1 and C1 (outlets located below the mid-height of the building) are presented in Figure 5.15. For configuration B1, mean and peak Cp_{in} values are not affected by blockage for ratio up to 20%; however, the mean and peak values of the internal pressure coefficient are significantly higher (up to $\Delta Cp = 0.26$ and 0.4 - factor of 1.8 and 1.5 - for the mean and peak values respectively) for 35%blockage. For configuration C1, internal pressure coefficients increase with increasing blockage ratio (up to $\Delta Cp = 0.32$ and 0.46 - factor of 2.7 - for the mean and peak values respectively) due to the increased flow resistance as obstacles mainly cover the lower

126
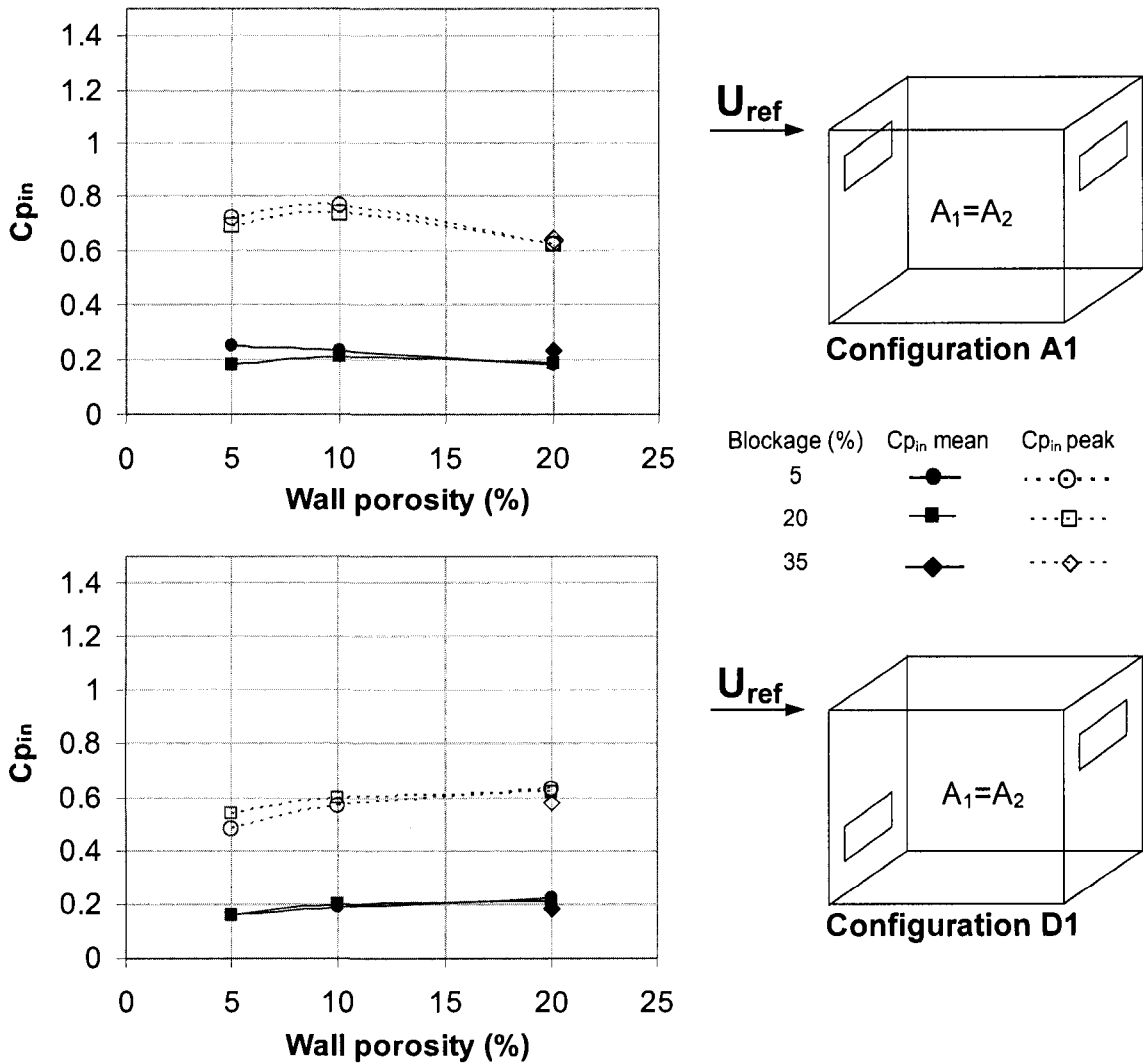
Figure 5.14. Mean and peak internal pressure coefficients for configurations A1 (top) and D1 (bottom) with different blockage ratios.

section of the building model. Results in the following sections are presented for configurations with 5% blockage (almost an empty building) for consistency with the PIV experiments. Although a 20% blockage would be a more realistic approximation, experimental results have shown that for all configurations (except C1), internal pressures
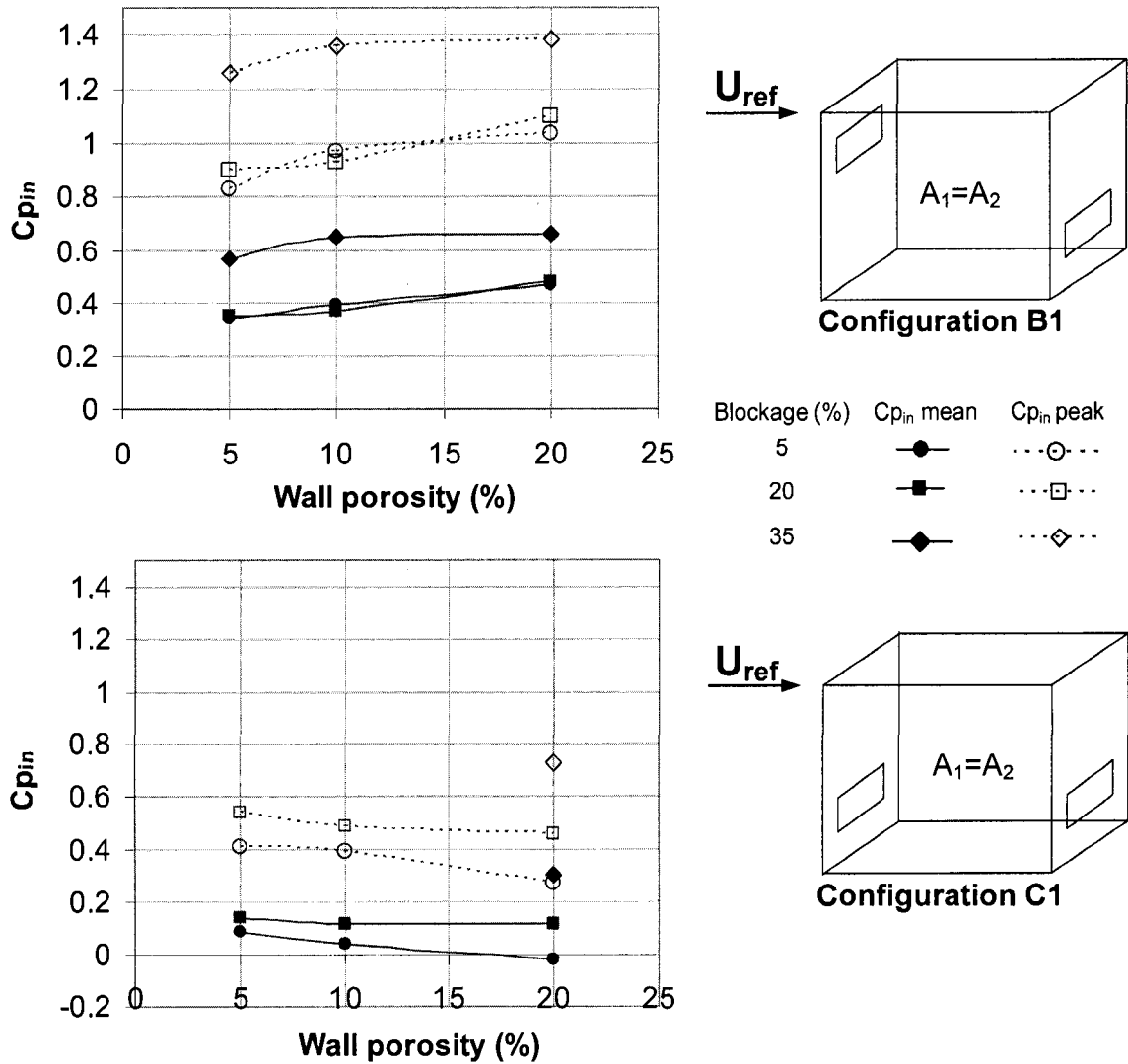
Figure 5.15. Mean and peak internal pressure coefficients for configurations B1 (top) and C1 (bottom) with different blockage ratios.

are identical for blockage ratios ranging from 5% to 20%. Experiments for inlet-to-outlet ratios other than one were carried out for configurations with 20% blockage.

Wall porosity and opening location impact

This section discusses the impact of wall porosity as well as inlet/outlet relative location

on internal pressures in buildings with cross-openings of the same inlet and outlet area

($A_1 = A_2$), for $\theta = 0°$. The internal pressure was measured on taps 2, 8, 10, 12, and 16 (see

also Figure 5.4). Results for the spatially-averaged mean and peak internal pressure

coefficients are shown in Figure 5.16 for configurations A1, B1, C1, and D1 with 5%

blockage. The mean and peak internal pressure coefficients decrease slightly with

porosity for configurations A1 and C1 (symmetric openings). This can be justified by the
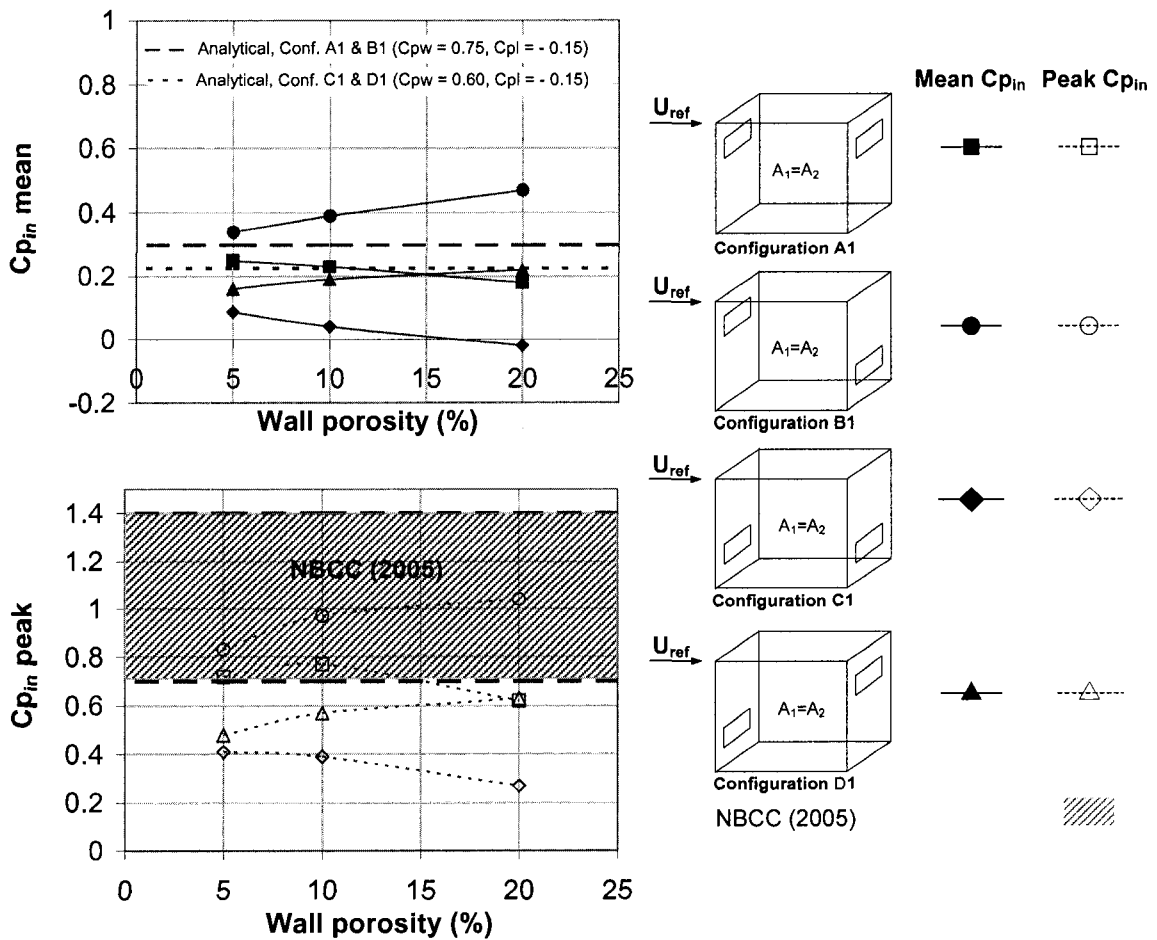
Figure 5.16. Mean and peak internal pressure coefficients for configurations A1, B1, C1,

and D1 with 5% blockage – comparison with theory (mean values) and NBCC (2005)

(peak values).

lower area-averaged external pressure coefficient at the inlet for larger porosities (differences in opening areas were induced by different opening widths - sliding windows); the decrease of internal flow resistance due to a more pronounced flow tube observed for large porosities may be another reason. For configuration B1 (non-symmetric openings) the internal pressure coefficient increases with increasing wall porosity. A slight increase of Cp_{in} with increasing wall porosity was also found for configuration D1.

Cp_{in} values are higher (up to $\Delta Cp = 0.29$ - factor of 2.5 - for the means and 0.41 - factor of 1.65 - for the peaks) for configuration B1 (non-symmetric openings) compared to configuration A1 (symmetric openings) mainly due to the larger curvature of the air stream (higher flow resistance) for configuration B1 (see also section 4.3). Similar results are observed for configurations C1 and D1 (up to $\Delta Cp = 0.2$ for the means and 0.36 - factor of 2.3 - for the peaks). Higher Cp_{in} values (up to $\Delta Cp = 0.45$ for the mean values and 0.77 - factor of 3.85 - for the peak values) were found for configurations A1 and B1 (inlets above the mid-height of the building) compared to C1 and D1 (inlets below the mid-height of the building) due to the higher external pressure coefficient on the windward wall and the different internal flow patterns. These findings indicate the importance of the relative location of inlets and outlets for natural ventilation design.

Experimental results are compared with mean internal coefficients evaluated by using Equation (3.5). The windward and leeward wall mean pressure coefficients were measured along the wall at the horizontal mid-level for a sealed building and were found equal to 0.72 and -0.15 respectively. Since the external mean pressure coefficient on the windward wall varies with the wall height and width (ASHRAE Handbook, 2007), an

area-averaged value equal to 0.75 was used for the calculations for configurations A1 and B1 and equal to 0.6 for configurations C1 and D1. The external mean pressure coefficient is almost uniform on the leeward wall, thus, a value equal to -0.15 was used for the calculations. Equation (3.5) provides a constant value for the mean internal pressure coefficient, equal to 0.3 for configurations A1 and B1 (inlets located above the mid-height of the building) and 0.225 for configurations C1 and D1 (inlets located below the mid-height of the building) for all wall porosities. In other words, variations of the internal pressure coefficient with porosity as well as differences among configurations with symmetric and non-symmetric openings of the same area -mainly attributed to the internal flow patterns- cannot be predicted by this simplified equation. It should be noted that these differences are to be expected as Equation (3.5) is based on a number of assumptions –presented in Section 3.3- which may not be valid for cross-ventilation with large openings.

NBCC (2005) provisions for internal pressure coefficients are summarized in Table 5.6. Measured peak internal pressure coefficients for configurations A1, B1, C1, and D1 with 5% blockage and $A_1/A_2 = 1$ are compared with NBCC (2005) provisions for building category 3 (buildings with large or significant openings) and results are shown in Figure 5.16. Since the code does not specify wall porosities or opening locations for which a gust effect factor (equal to 2 for internal pressures) should be used, the lower (without considering an internal gust effect factor) and upper (considering an internal gust factor equal to 2) boundary of the code provision for the peak Cp_{in} is shown. For configurations C1 and D1 (openings located below the mid-height of the building) with wall porosities up to 20%, measured peak Cp_{in} values are lower than 0.7, therefore, using

a gust effect factor for these configurations may be a conservative approach. For configurations A1 and B1 (openings located above the mid-height of the building) measured peak Cp_{in} values are higher than 0.7 but less than the upper code limit of 1.4, therefore consideration of an gust effect factor (equal to 2 as specified by the code) may be more appropriate. The ratio of the peak to the mean internal pressure coefficient (internal gust effect factor, Cgi) is shown in Figure 5.17 for configurations A1, B1, and

Table 5.6. Internal pressure coefficients, after NBCC (2005).

Category	Cp_{in}	Comments
1	-0.15 to 0	*Buildings without large or significant openings but having small uniformly distributed openings amounting to less than 0.1% of total surface area*
2	-0.45 to 0.3	*Buildings in which significant openings are expected to be closed during a storm but in which background leakage may not be uniformly distributed*
3	0.7 to − 0.7	*Buildings with large or significant openings (through which gusts are transmitted to the interior) which have a high probability of being open during a storm*
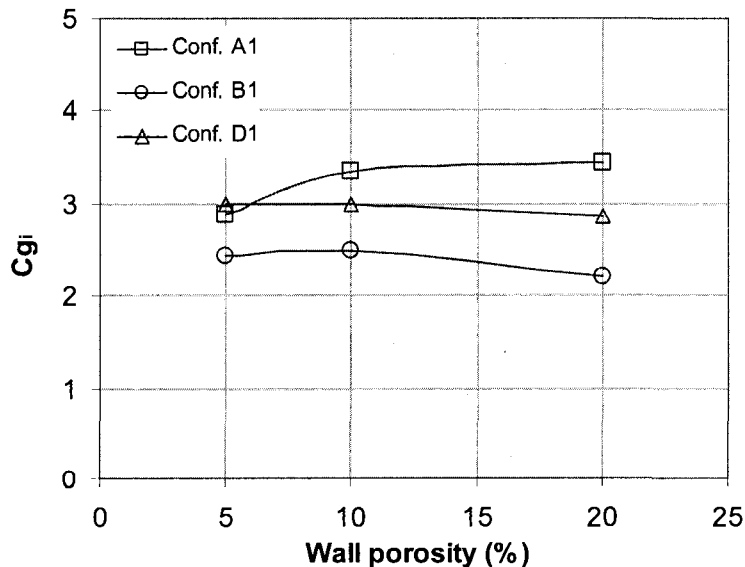
Figure 5.17. Internal gust effect factors as a function of wall porosity for configurations A1, B1, and D1 with 5% blockage.

D1. Results for configuration C1 are not included since the internal gust effect factors are unrealistically high due to the small (near zero) mean Cp_{in} values. Peak internal pressure coefficient values are between 2.2 and 3.4 times higher than the mean values for configurations A1, B1, and D1. The gust effect factor, Cgi, remains almost constant for all configurations with wall porosity larger than 10%.

Spatial distribution of internal pressure

Figure 5.18 shows the mean and peak Cp_{in} values measured in various internal pressure taps for configurations A1, B1, C1, and D1 with 5% blockage and different wall porosities. Results show variations among the different taps, i.e., smaller Cp_{in} values measured on taps 2 and 12 that may be affected by the stream tube and higher Cp_{in} values on taps 8, 10 and 16 that are outside the stream tube. This non-uniformity of the internal pressure is more pronounced for high wall porosities (larger than 10%), non-symmetric configurations (B1 and D1) with inlets located above the mid-height of the building (i.e. configuration B1) and cannot be predicted by the theory. Differences among taps can be up to $\Delta Cp = 0.13$ (factor of 1.3) for the means and $\Delta Cp = 0.3$ (factor of 1.4) for the peaks (configuration B1). This finding should be considered in the selection of measurement points for future experiments. Internal pressure gradients of this magnitude can create discomfort of building occupants and may also have implications on wind load design of buildings.

Murakami et al. (1991) and Straw et al. (2000) measured mean internal pressures on two points inside a building (on the floor and the inlet/outlet wall respectively) with cross-ventilation and large openings and reported small differences in mean Cp_{in} values.
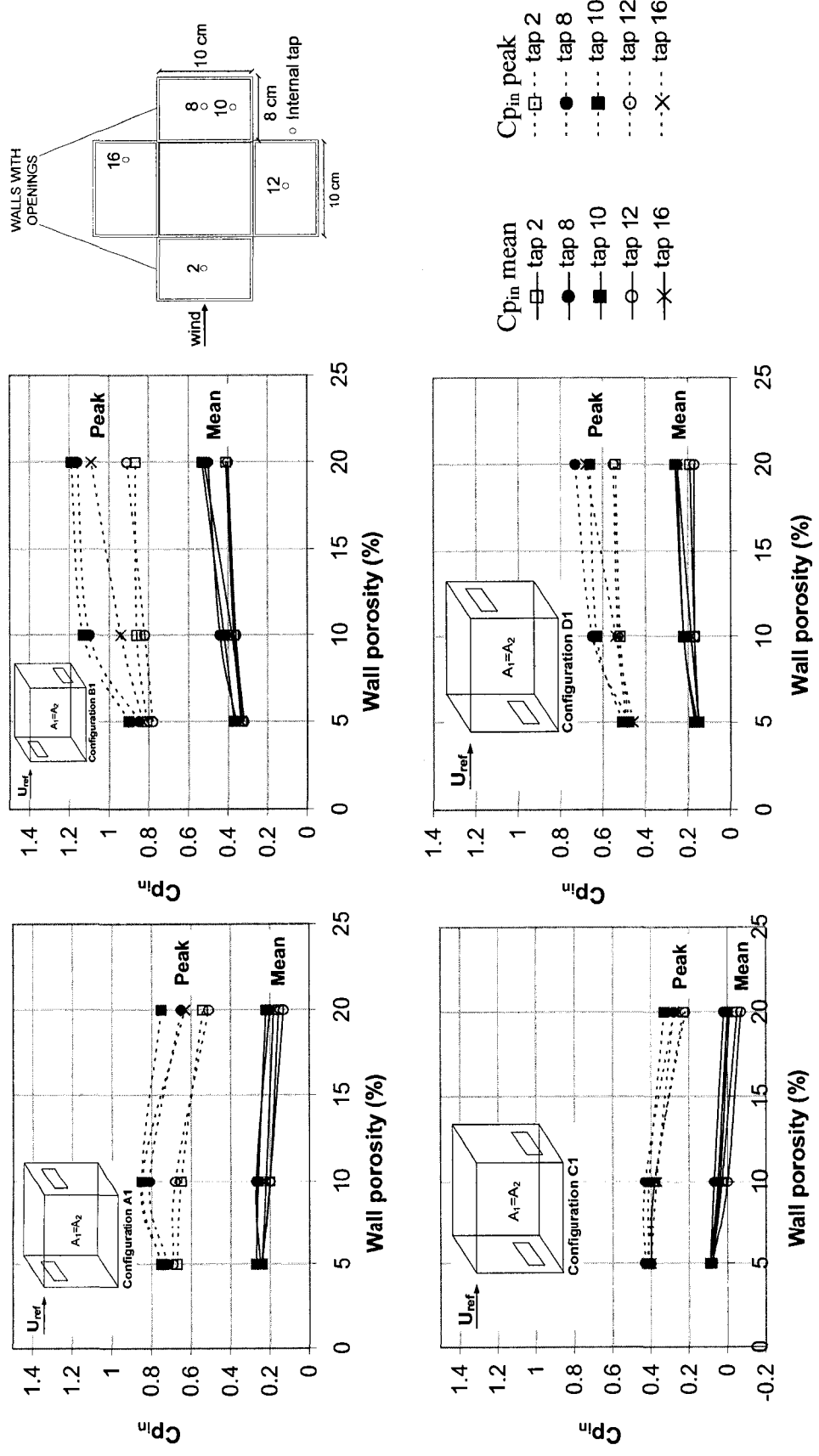
Figure 5.18. Mean and peak internal pressure coefficients measured in different pressure taps for configurations A1, B1, C1, and D1 with 5% blockage.

Choiniere et al. (1992) reported mean Cp_{in} variations in buildings with large continuous sidewall, ridge or chimney, and end wall openings, for different wind directions. Munarin (1978), Womble et al. (1995) and Ginger et al. (1995) reported uniform mean and peak internal pressures. Generally, in studies related to wind load design of buildings (e.g. Womble et al., 1995; Ginger et al., 1995), internal pressure is traditionally measured with a single tap.

Comparison with previous studies

Figure 5.19 compares mean internal pressure coefficients for configurations A1 and C1 with results of previous studies. It should noted that in the studies of Munarin (1978), Straw et al. (2000), Kurabuchi et al. (2004), Sawachi et al. (2004), and Hu et al. (2005) openings are located in the center of the wall while Murakami et al. (1991) considered openings in contact with the ground, in the mid-width of the long or short walls. For the building models and configurations considered in Figure 5.19, the windward wall pressure coefficient is in the range of 0.57 to 0.67 and the leeward wall coefficient is ranging from -0.16 to -0.1. Recall that in the present study the external pressure coefficients are 0.72 and -0.15 as measured in the mid-height of the windward and leeward wall respectively. It should be noted that impact of the relative inlet/outlet location and blockage of the internal volume was not considered in the previous studies. With the exception of the work of Womble (1994), Womble et al. (1995) and Ginger et al. (1995), in which peak values of the internal pressure were evaluated for configurations with inlet-to-outlet ratio other than one, in all other above-mentioned studies only mean
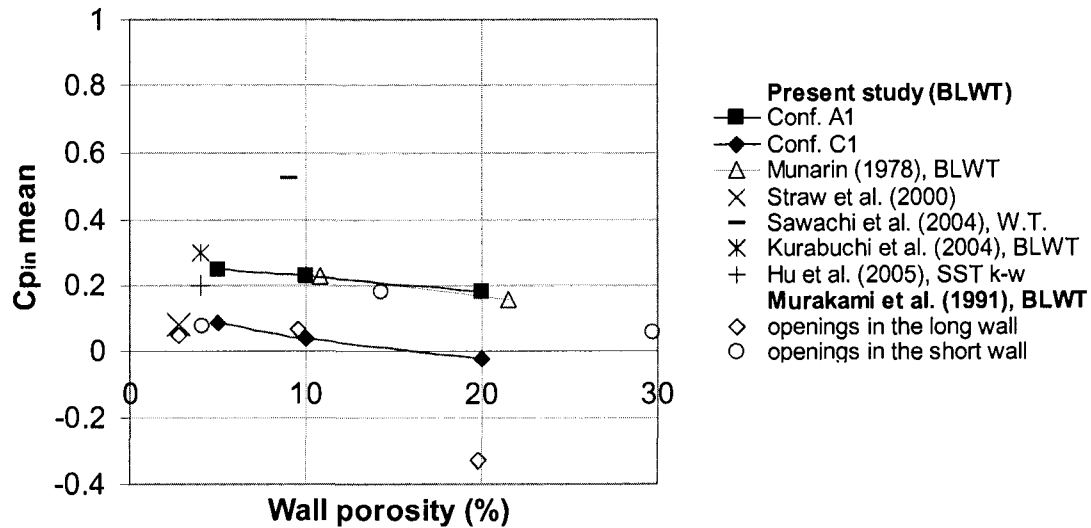
Figure 5.19. Mean internal pressure coefficients as a function of wall porosity for configurations with $A_1/A_2 = 1$ - comparison with previous studies.

internal pressures were evaluated. Results of the present study are within the range defined by the previous studies, although there are differences in the absolute Cp_{in} values. For example, there is good agreement with the results from Murakami et al. (1991) for configuration C1 with porosity less than 10%, while for higher porosities results are quite different. Examination of Figure 5.19 shows that some of the Cp_{in} values given by Sawachi et al. (2004) are outside the range defined by results of other studies, including the field measurements of Straw et al. (2000). Sawachi et al. (2004) placed a full-scale building in a uniform flow wind tunnel and as a result, blockage of the wind tunnel cross-section was about 33%. Holmes (2001) suggests that wind tunnel models should not exceed 5% blockage of the wind tunnel cross section. Comparison of the results by Sawachi with those of other studies that have considered a BLWT approach with smaller blockage (e.g. 0.25% in the present study), indicates the importance of parameters such

as scaling and/or upstream air flow conditions in wind tunnel experiments of cross-ventilation.

Impact of inlet-to-outlet ratio

Figure 5.20 shows the variation of the mean internal pressure coefficient as a function of inlet-to-outlet ratio for configurations A1 and C1 with 20% blockage and 5%, 10%, and 20% windward wall porosity. The internal pressure was measured on taps 2, 4, 6, 8, 10, 12, 14, 16, 18, and 20 (see also Figure 5.4). Results for configuration C1 may be slightly
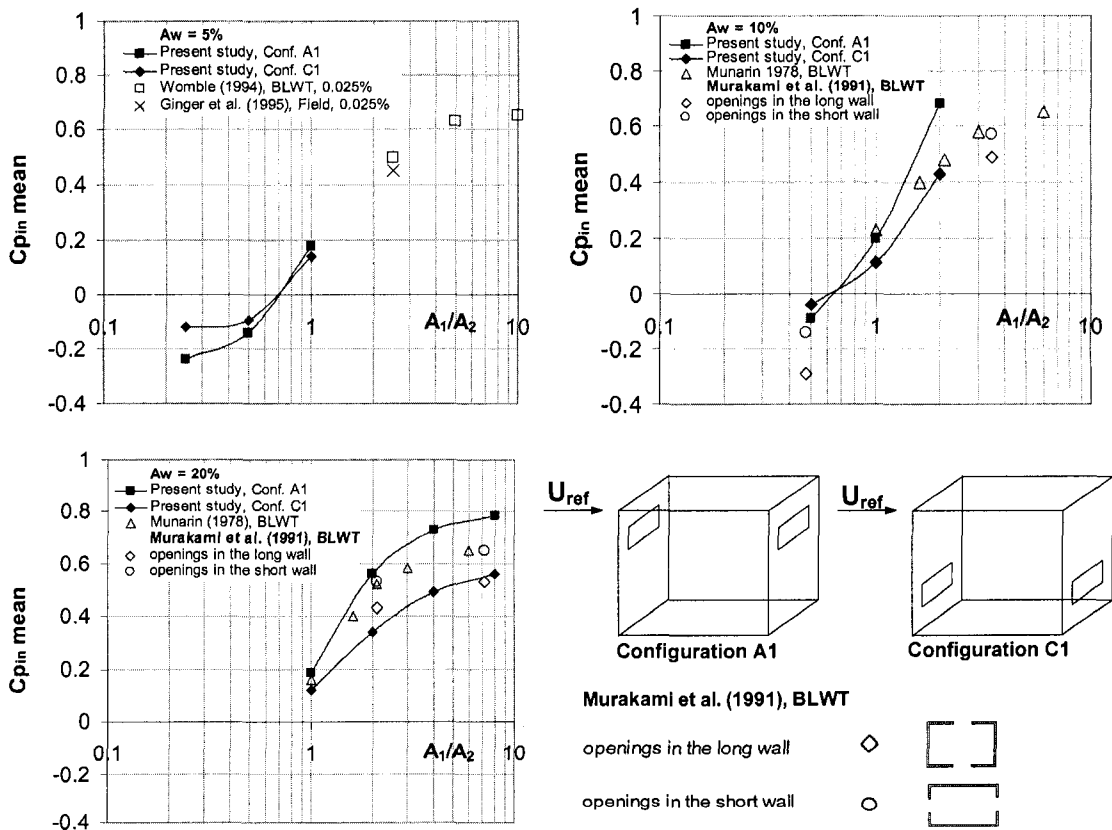
Figure 5.20. Mean internal pressure coefficients for configurations A1 and C1 with A_w = 5%, 10%, and 20%, different inlet-to-outlet ratios, and 20% blockage – comparison with previous studies.

overestimated - ΔCp up 0.1 for means and 0.18 for peaks - due to the high blockage ratio20%) considered. BLWT results from previous studies are also presented. In the study by Womble (1994), Ginger et al. (1995), openings are located at the mid-height of the wall. Mean Cp_{in} values are compared with theoretical predictions using Equation (3.5), as shown in Figure 5.21. The Cp_{in} values evaluated by using Equation (3.5) are in relatively good agreement with the experimental results for configuration A1 with A_1/A_2 > 1 but they are overestimated for configuration A1 with A_1/A_2 < 1 as well as for configuration C1 for all inlet-to-outlet ratios.

Peak internal pressure coefficients for configurations A1 and C1 with A_w = 5%, 10%, and 20%, different inlet-to-outlet ratios and 20% blockage are presented in Figure 5.22. Results of previous studies as well as NBCC provisions for building category 3
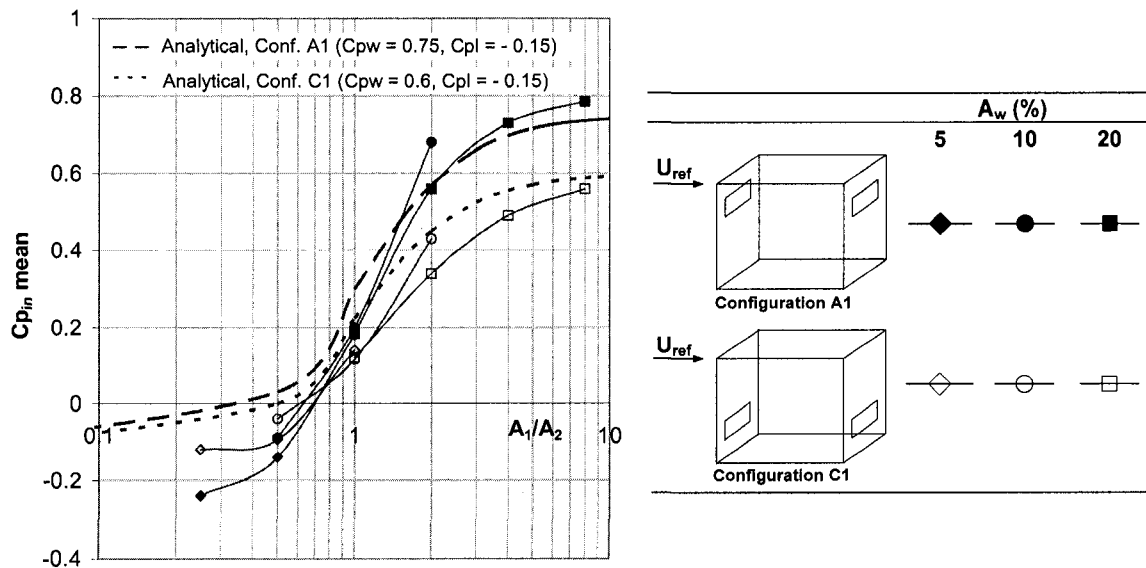
Figure 5.21. Mean internal pressure coefficients for configurations A1 and C1 with A_w = 5%, 10%, and 20%, different inlet-to-outlet ratios, and 20% blockage – comparison with analytical results.
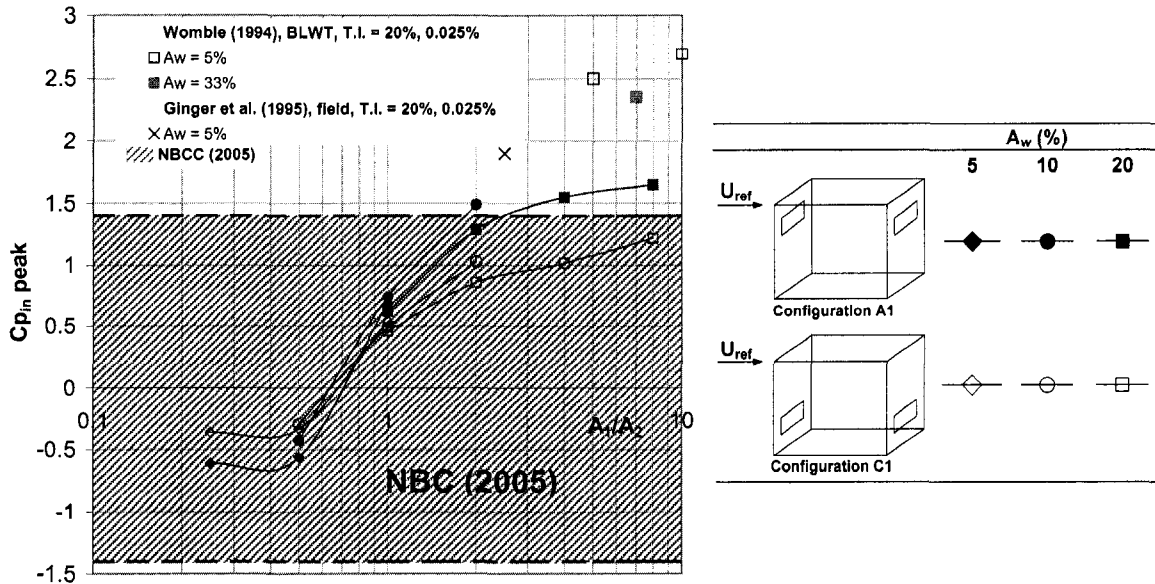
Figure 5.22. Peak internal pressure coefficients for configurations A1 and C1 with A_w = 5%, 10%, and 20%, different inlet-to-outlet ratios, and 20% blockage - comparison with previous studies and NBCC (2005).

considering an internal gust effect factor equal to 2 are also included. Measured peak Cp_{in} values are significantly lower compared to previous studies mainly due to the lower intensity levels at the building height (13% vs. 20%). Previous work of Wu et al. (1998) has shown that peak internal pressure coefficients are significantly affected by the turbulence intensity. Some peak Cp_{in} values were found to exceed the recommended design value, i.e. 1.4 for configurations with $A_1/A_2 \geq 2$ and large openings located above the mid-height of the building (configuration A1). Peak Cp_{in} values for configuration A1 with $A_1/A_2 < 2$ and configuration C1 (for all inlet-to-outlet ratios) are within the limits specified by the code. An internal gust effect factor should be used for configurations A1 and C1 with $A_1/A_2 > 1$, while consideration of a gust effect factor for $A_1/A_2 < 1$ may be too conservative. Figure 5.23 shows the ratio of the peak to the mean internal pressure

coefficient (internal gust effect factor, Cgi) based on wind tunnel measured data for configurations A1 and C1 with 10% and 20% windward wall porosity, $A_1/A_2 > 1$, and 20% blockage.
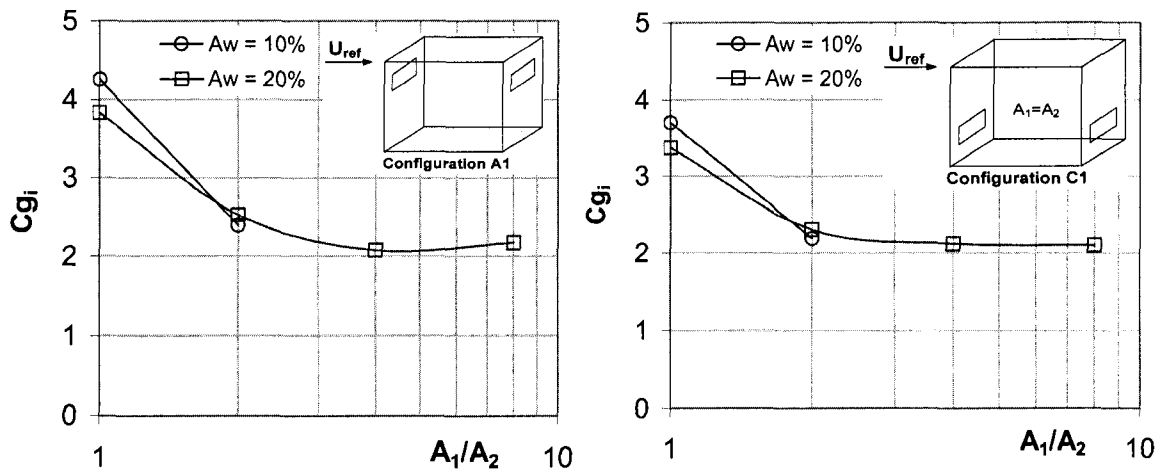
Figure 5.23. Internal gust effect factors for configurations A1 and C1 with $A_w = 10\%$ and 20%, $A_1/A_2 > 1$, and 20% blockage.

Configurations with outlets located on the side wall of the building

Blockage impact

Figure 5.24 presents mean and peak internal pressure coefficients as a function of wall porosity for configurations A2, C2, and D2 with blockage ratio of the internal volume equal to 5%, 20%, and 35% and $A_1 = A_2$. Almost identical mean and peak internal pressure coefficients were found for all blockage ratios, indicating that internal pressure is not affected by blockage for these configurations. Results for configuration B2 are presented in Figure 5.25. Mean and peak internal pressure coefficients increase by 30% and 40% respectively for blockage ratio increasing from 5% to 35%.
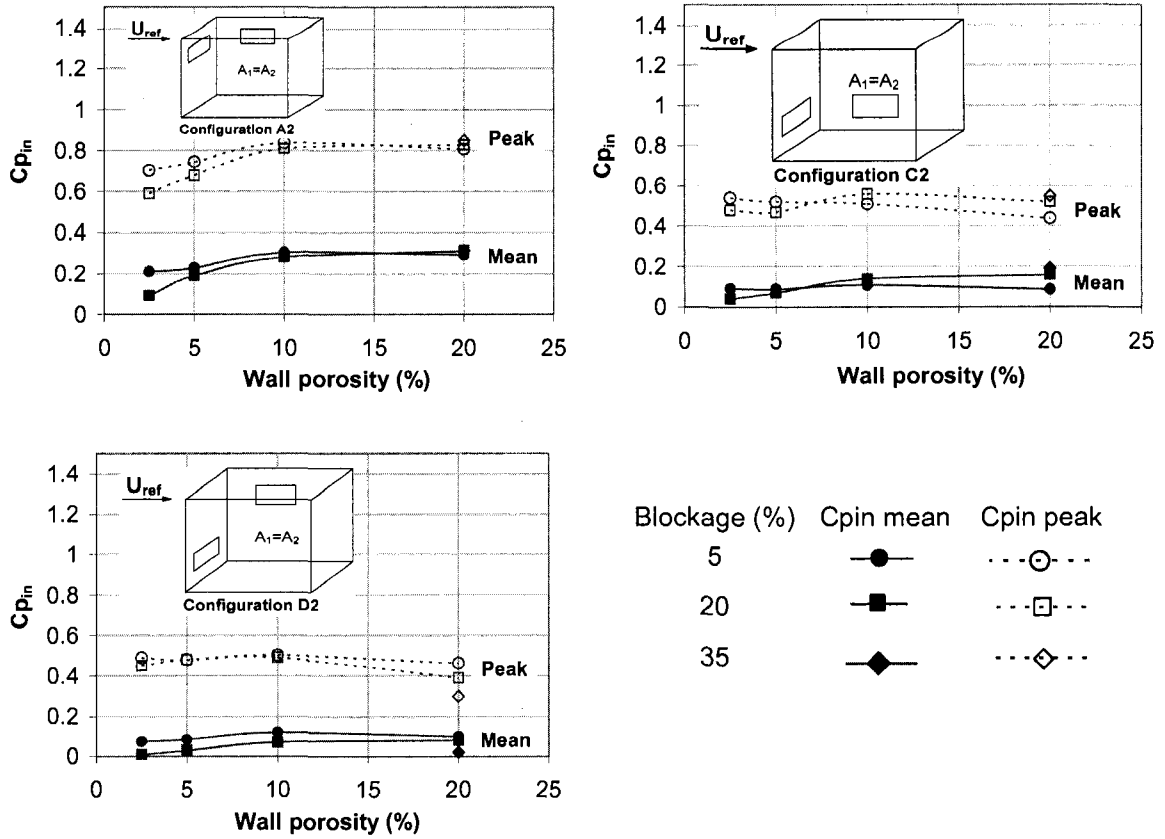
Figure 5.24. Mean and peak internal pressure coefficients for configurations A2, C2, and D2 with different blockage ratios.
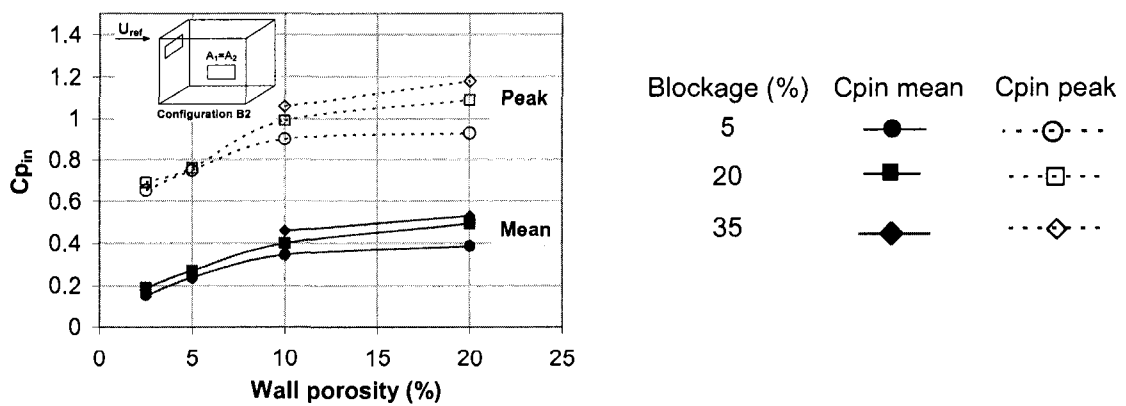
Figure 5.25. Mean and peak internal pressure coefficients for configuration B2 with different blockage ratios.

Wall porosity and opening location impact

The impact of a windward and a side wall opening of the same area ($A_1 = A_2$) on internal pressure was investigated for $\theta = 0°$. The internal pressure was measured on taps 2, 8, 10, 12, 14, and 16 (see also Figure 5.4). Results for the spatially-averaged mean and peak internal pressure coefficients are shown in Figure 5.26 for configurations A2, B2, C2, and D2 with 5% blockage. The internal pressure coefficient (mean and peak value) increases with porosity for configurations A2 and B2 (openings located above the mid-height of the building); mean Cp_{in} may increase by 0.25 (factor of 2.6) and peak Cp_{in} by 0.28 (factor of 1.4) for wall porosity increasing from 2.5% to 20%. The internal pressure coefficient remains constant for configurations C2 and D2 (openings located below the mid-height of the building) with wall porosities ranging from 2.5% to 20%. Slightly higher Cp_{in} values are observed for configuration B2 (non-symmetric openings) compared to configuration A2 (symmetric openings), particularly for wall porosities larger than 10%. Cp_{in} values for configurations A2 and B2 (openings located above the mid-height of the building) are higher (up to $\Delta Cp = 0.29$ - factor of 2 - for the mean values and 0.49 - factor of 2 - for the peak values) compared to configurations C2 and D2 (openings located below the mid-height of the building) due to the higher external pressure coefficient on the windward wall and the different internal flow patterns.

Experimental results are compared with mean internal pressure coefficients calculated using Equation (3.7). The measured area-averaged windward and side-wall wall external mean pressure coefficients at the mid-horizontal-level of the wall for a sealed building are equal to 0.72 and -0.46 respectively. Since the mean pressure coefficient on the
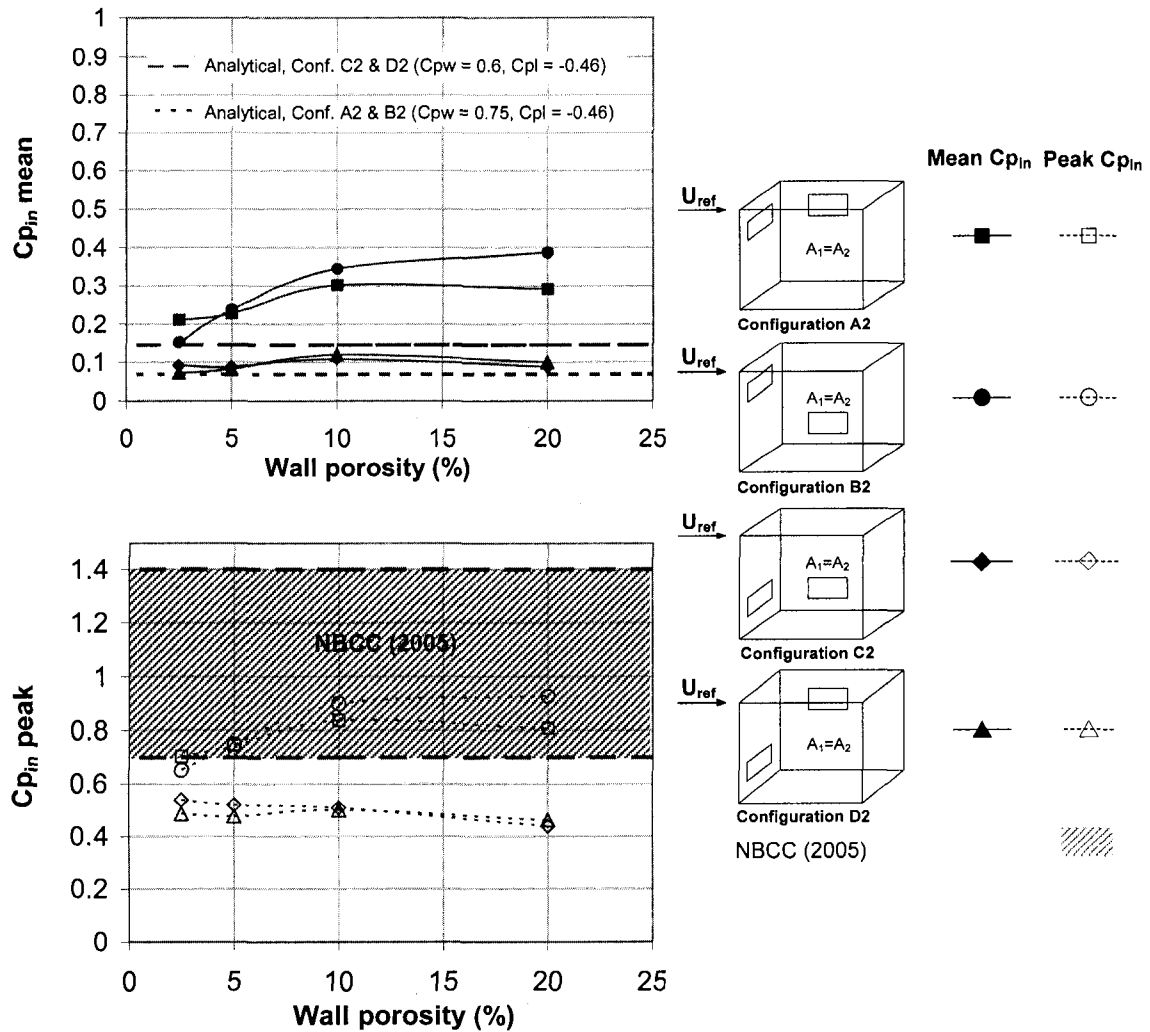
Figure 5.26. Mean and peak internal pressure coefficients for configurations A2, B2, C2, and D2 with 5% blockage.

windward wall varies with the wall height and width (ASHRAE Handbook, 2007), an area-averaged value equal to 0.75 was used for the calculations for configuration A2 and B2 and equal to 0.6 for configurations B2 and D2. The external mean pressure coefficient does not vary with height on the side-wall, thus, a value equal to -0.46 was used for the calculations for all configurations. There is good agreement between the experimental

results and the theory for configuration C2 and D2. However, theoretical values are lower for configurations A2 and B2.

Measured peak internal pressure coefficients for configurations A2, B2, C2, and D2 with 5% blockage are compared with NBCC (2005) provisions for building category 3 as shown in Figure 5.26. The lower (without considering an internal gust effect factor) and upper (considering an internal gust effect factor equal to 2 as specified by the code) boundary of the code provision for the peak Cp_{in} is shown. For configurations C2 and D2 (openings located below the mid-height of the building) with wall porosities up to 20%, Cp_{in} values are lower than 0.7, therefore, using an internal gust effect factor may be a conservative approach. For configurations A2 and B2 (openings located above the mid-height of the building), Cp_{in} values are higher than 0.7 but less than the upper code limit of 1.4, thus consideration of a gust effect factor is more appropriate. The ratio of the peak to the mean internal pressure coefficient (internal gust effect factor, Cgi) is shown in Figure 5.27 for configurations A2 and B2. For both configurations, Cgi decreases for wall porosity up to 10% and it remains almost constant for larger porosities. Gust effect factors for configurations C2 and D2 are not included as they are unrealistically high due to the small (near zero) mean Cp_{in} values.

Considering the same inlet-to-outlet ratio and inlet location, higher Cp_{in} values are expected - based on Equation 3.5 - for configurations with outlets located on the leeward wall compared to side wall outlets due to the lower area-averaged external pressure on the leeward wall (compared to the side wall). Experimental results presented in Figure 5.28 for configurations A1, A2, C1, and C2 with 5% blockage show the opposite effect,
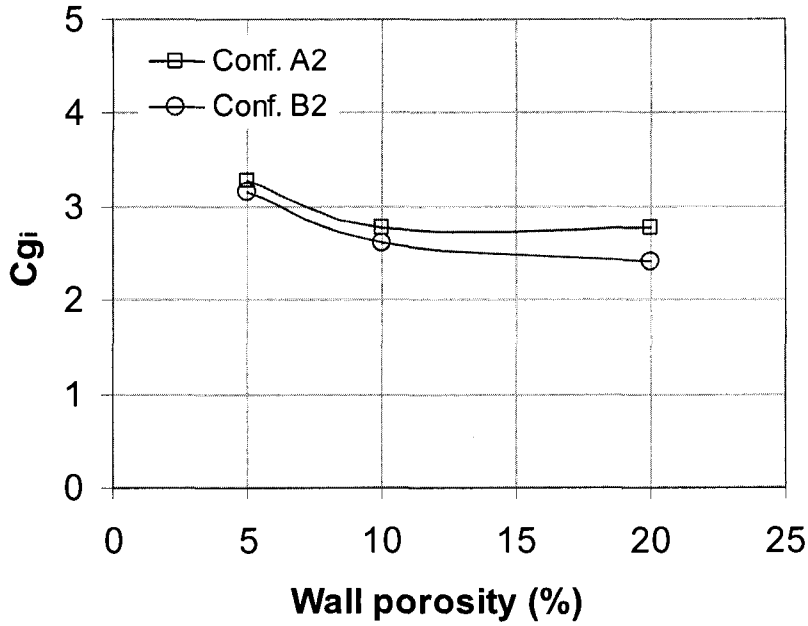
Figure 5.27. Internal gust effect factors as a function of wall porosity for configurations A2 and B2 with 5% blockage.
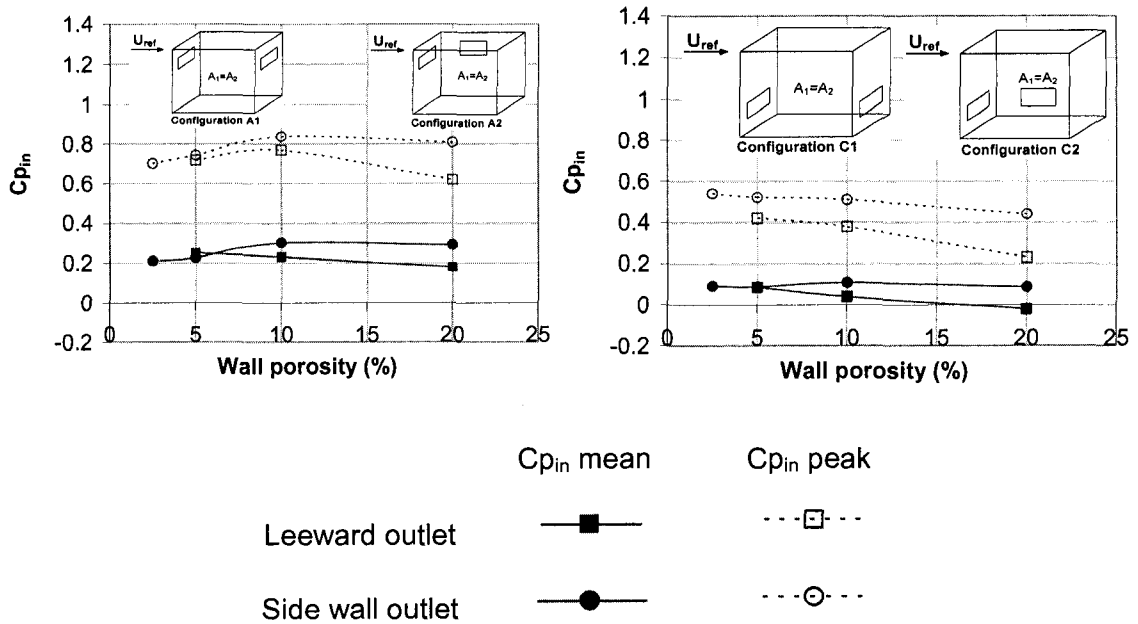
Figure 5.28. Mean and peak internal pressure coefficients for configurations A1 and A2 (left), and C1 and C2 (right) with 5% blockage.

i.e. lower Cp_{in} values for a leeward outlet compared to a side wall outlet for wall porosities larger than 10%. This may be attributed to the straight flow tube (less flow resistance) connecting the inlet and outlet for configurations with outlets on the leeward wall.

Spatial distribution of internal pressure

Figure 5.29 shows the mean and peak Cp_{in} values measured on various internal pressure taps for configurations A2, B2, C2, and D2 with 5% blockage. Results show variations among the different taps, i.e., smaller Cp_{in} values measured on taps 2, 12, 14 that may be affected by the stream tube and higher Cp_{in} values on taps 8, 10 that are outside from the stream tube. Cp_{in} values for tap 16 vary for different configurations. The non-uniformity of the internal pressure is more pronounced for large wall porosities (larger than 10%), configurations with openings located above the mid-height of the wall (i.e. configuration A2 and B2) and cannot be predicted by the theory. Differences among taps can be up to $\Delta Cp = 0.3$ (factor of 3) for the means and $\Delta Cp = 0.43$ (factor of 1.7) for the peaks with configuration A2 and up to $\Delta Cp = 0.3$ (factor of 2.2) for the means and $\Delta Cp = 0.53$ (factor of 1.8) for the peaks with configuration B2. It should be noted that configurations with side-wall outlets have been considered only by Murakami et al. (1991) for $A_1/A_2 = 2$, where the internal pressure was measured on two floor taps. CFD simulations by Seifert et al. (2006) have considered side wall outlets but the study does not report internal pressure coefficient values.

146

Wind angle impact

This section presents results for the impact of wind angle on internal pressures in buildings with cross-openings. The measured mean, rms, max and min values of the external pressure coefficients for a closed building and $\theta = 45°$ are presented in Table 5.7. The internal pressure was measured on taps 2, 8, 10, 12, 14, 16, 26, 34, 36, and 40. The spatially-averaged mean and peak internal pressure coefficients are shown in Figure 5.30 for configurations A1 and B1 with $A_1 = A_2$ and 10% blockage; results by Sawachi et al. (2004) and Hu et al. (2005) are also included. Almost identical internal pressure coefficients were found for both configurations A1 and B1 and wall porosity increasing from 5% to 20%. Cp_{in} values for $\theta = 45°$ are lower compared to the zero wind angle case for all configurations tested; consequently, the effect of oblique wind angles is not significant. Similar results reported by Oh et al. (2007) for the case of a building with a single dominant opening near the centre of the wall and background leakage. Experimental results are compared with the mean internal pressure coefficients evaluated by using Equation (3.7). The measured area-averaged windward and side wall external pressure coefficients at the mid-horizontal-level of the wall for a sealed building are equal to 0.37 and -0.415 respectively. Experimental and theoretical results are in good agreement, for this case.

Experimental results for the minimum peak internal pressure coefficient for configurations A1 and B1 with 10% blockage and porosities up to 20% do not exceed the NBCC (2005) provision (-0.7) for building category 3. Therefore, considering a gust factor of 2 for the internal pressure (NBCC, 2005) may be a conservative approach for oblique winds.

147
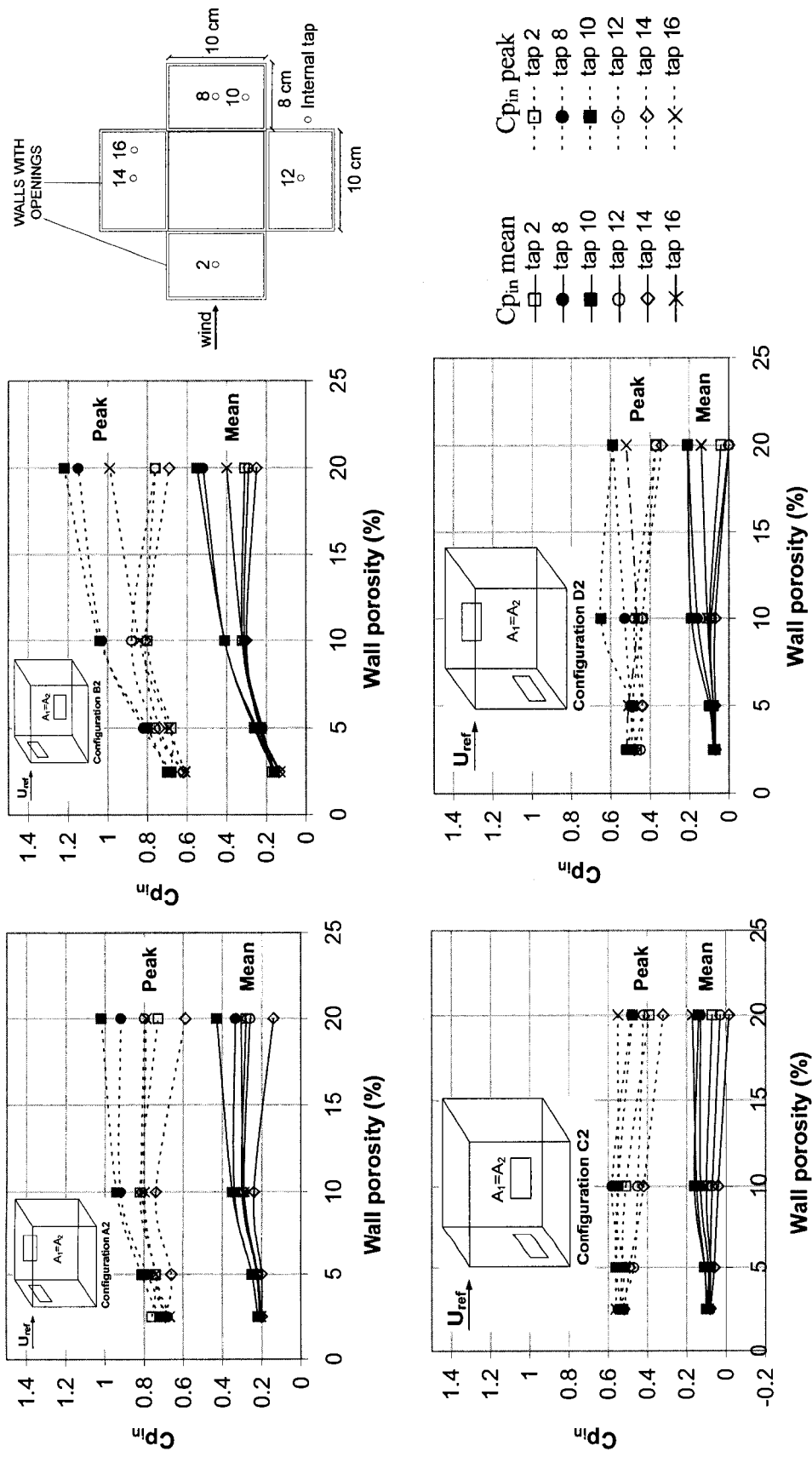
Figure 5.29. Mean and peak internal pressure coefficients measured in various pressure taps for configurations A2, B2, C2, and D2 with 5% blockage.

Table 5.7. External pressure coefficients ($\theta = 45°$).

Tap	Cp_{mean}	Cp_{rms}	Cp_{max}	Cp_{min}
1	0.38	0.16	1.08	-
3	0.48	0.19	1.19	-
5	0.25	0.14	0.84	-
7	-0.43	0.13	-	-0.92
9	-0.4	0.13	-	-0.85
11	0.39	0.16	1.01	-
13	-0.44	0.14	-	-0.96
15	-0.44	0.12	-	-0.96
17	-0.23	0.11	-	-0.94
19	-0.21	0.1	-	-0.85
27	-0.29	0.2	-	-1.4
29	-0.31	0.15	-	-0.97
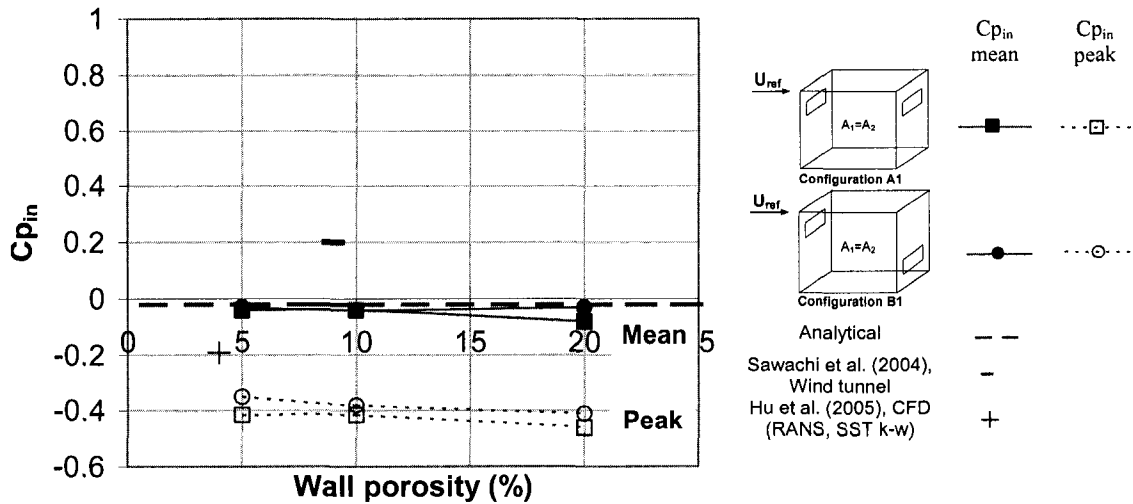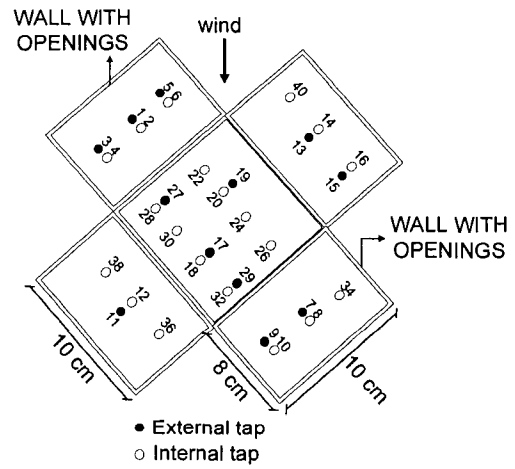
Figure 5.30. Mean and peak internal pressure coefficients for configurations A1 and B1 with 10% blockage and $\theta = 45°$.

5.4 Summary

The main findings of this chapter can be summarized as follows:

149

- Blockage of the internal volume may significantly affect mean and peak internal pressure coefficients, particularly for configurations with blockage ratio higher than 20%, outlets located on leeward wall and/or below the mid-height of the building (e.g. B1 and C1). For all configurations considered (except C1), almost identical Cp_{in} values (means and peaks) are observed for estimated blockage ratios ranging from 5% to 20%. Higher internal pressure coefficients, up to a factor of 1.6, are observed for blockage ratios increasing from 20 to 35%. It is important to note that different blockage ratios were modelled using a rather approximate method; thus, further testing should consider a more realistic approximation of blockage of the internal volume so as results can be generalized to real building conditions.

- Based on internal pressure investigations performed with two different building models (flat and sloped-roof) subject to cross-ventilation, it can be concluded that for cross-ventilation with large porosities (i.e. higher than 10%) the internal flow field has a significant impact on mean and peak values of the internal pressure. For example, for the same inlet-to-outlet-ratio, the mean internal pressure coefficient is higher up to a factor of 2.6 for configurations with non-symmetric openings compared to configurations with symmetric openings. Also for $A_1/A_2 = 1$ the internal pressure coefficients may increase, decrease or remain constant with wall porosity depending on the configuration. It should be noted that these influences cannot be predicted by the existing theory and should be introduced in the theoretical equation.

- The internal pressure is not uniform in buildings with cross-ventilation, particularly for configurations with outlets on the side wall and wall porosity higher than 10%. Differences among taps can be up to $\Delta Cp = 0.3$ for the means and $\Delta Cp = 0.53$ for the

peaks for configurations with side wall outlets, non-symmetric openings and 20% wall porosity (configuration B2). Thus, for a reference velocity at building height equal to 2 m/s there is a gradient of 0.7 and 1.3 Pa in the mean and peak value of the internal pressure inside the building. Internal pressure gradients of this magnitude (in the order of 1 Pa) create discomfort of building occupants. Internal pressure has been traditionally measured on a single tap. For configurations with high spatial variation of internal pressure, selection of the number and location of internal pressure taps is important for evaluating the mean and peak internal pressure coefficients.

- Peak internal pressure coefficients play an important role in the design of structures and cladding. Although the category of the building with a single dominant opening is usually critical for wind load design, the correct assessment of internal pressure behaviour for naturally ventilated buildings with typical opening sizes (wall porosities) is essential. The study found that peak internal pressures in buildings with cross-openings may also be critical, particularly for configurations with large porosities and/or high blockage ratios. Peak values were found to exceed the recommended design value, i.e. 1.4 for buildings category 3 (NBCC, 2005), for configurations with openings located above the mid-height of the building, leeward outlets, and $A_1/A_2 \geq 2$ (configuration A1). A gust factor should be considered for configurations A1 (configurations with openings above the mid-height of the building) and C1 (configurations with openings below the mid-height of the building) with $A_1/A_2 > 1$, while consideration of an internal gust effect factor for $A_1/A_2 < 1$ may be too conservative. Effects of oblique wind angles on internal pressures are not significant, for the configurations considered here. Maximum internal pressures occur for a wind direction normal to the wall having one of the dominant

openings. Findings of this work may be important in advancing our understanding of the flow/pressure mechanisms of cross-ventilation and will be used in the form of design guidelines in wind codes/standards.

Results presented in this chapter are limited to upstream open terrain simulation. However, slightly different approaching wind profiles (within the limits of open terrain) have been considered and results for similar geometries are close to each other. Future work should involve sensitivity analysis tests for other velocity and turbulence intensity profiles.

6 PREDICTING THE ENVELOPE PRESSURE AND INDOOR-OUTDOOR AIR-EXCHANGE RATE IN BUILDINGS – A CASE STUDY

6.1 Introduction

For the improvement of indoor air quality and energy performance as they relate to ventilation, and for developing design guidelines, more accurate simulation of ventilation and infiltration airflows in buildings is required. The efficient integration of natural / hybrid ventilation systems in real buildings requires the use of a design tool for evaluating different design alternatives. This tool could be based on the simulation engine of existing coupled energy and airflow simulation programs (e.g. ESP-r), while the designer uses a more user-friendly interface. Chapters 4 and 5 focus on the airflow prediction through various opening configurations while issues related to modelling and simulation of airflows in real buildings are described here. These are the first necessary steps towards the development of a design tool for natural ventilation analysis of buildings.

This chapter presents the simulation methodology developed combined with a sensitivity analysis, which focuses on modelling issues such as the impact of zoning assumptions. The capabilities of an advanced building simulation tool (ESP-r) to model the energy / airflow interactions and predict the envelope pressures and induced flow rates in buildings, where both natural - wind and thermal buoyancy - and mechanical forces are present and interacting, have been assessed through a case-study. A simulation model was developed for a multi-unit high-rise residential building located in Ottawa, for

which extensive monitoring data (Reardon et al., 2003) were available to be used as inputs and for validation purposes. The building and the basic parameters considered, the modelling assumptions made, the methodology followed as well as the main findings are described in the subsequent sections. It should be noted that numerical modelling of wind-driven cross-ventilation with large openings was not considered in this thesis; however, suggestions for further research are summarized in Section 6.8.

6.2   Description of the building

The building is 41 m long, 16.2 m wide and 59.8 m high. The structure of the building is a combination of steel and concrete construction. There are 250 residential apartment suites on 21 floors of the 22-storey building. The floor numbering scheme omits a 13th floor, thus the topmost storey is the 23rd floor Figure 6.1 is a photo of the actual building. Full height concrete L-shaped shear walls enclose each of the four corner suites and the two stairwells, one at each end of the building. There are two side-by-side elevators that operate over the full height of the building and their combined structural shaft is a three-sided concrete shear wall. This central structural shaft also contains the corridor ventilation supply duct adjacent to the west elevator. A plan of a typical floor is illustrated in Figure 6.2. A typical floor contains 12 residential suites. The two apartments on each floor that wrap around the elevator shaft are bachelor-style suites with no bedroom. All other apartments are one-bedroom style. The corner suites have their windows and balconies on the east and west ends of the building. All the other middle suites have their exterior façade facing North or South. The ventilation system of the building is comprised of a central supply unit providing tempered 100% outdoor air to

each corridor (one diffuser per storey) and exhaust fans in the kitchen and bathroom of each unit. Supply air enters the apartments by the undercut of the entrance door of each unit. Several of the common areas on the ground floor also have separate exhaust fans. The air handling unit (AHU) for the corridor air supply ventilation system is located in the mechanical room (suite 205) on the 2nd floor of the building. The corridor supply system's vertical duct is of concrete block construction and runs from the 2nd to the 23rd floor. A gas-fired boiler provides the heat for tempering the corridor air supply through a coil just downstream of the fan in the corridor supply system's air handling unit. The building is heated with electric baseboard heating in each suite and in common areas on the ground floor (Reardon et al., 2003).
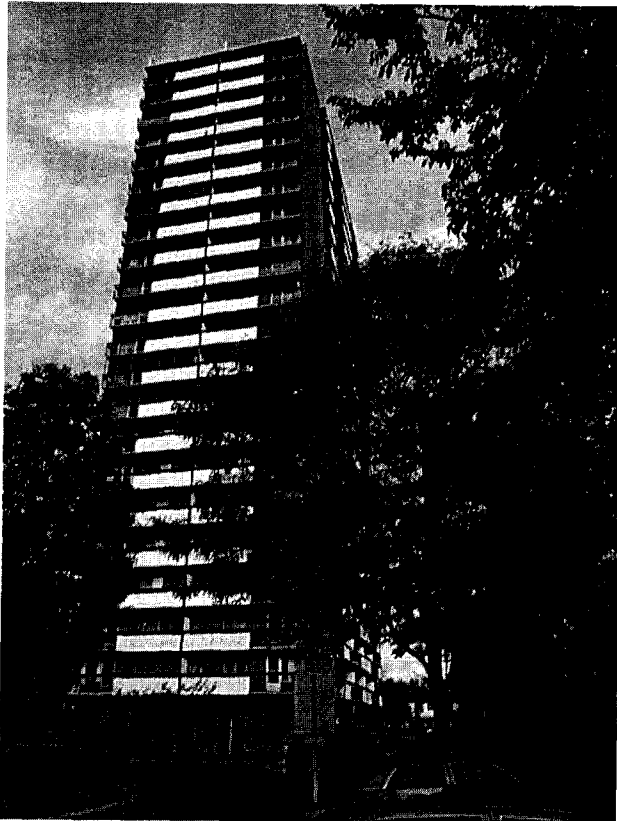
Figure 6.1. The building - West façade view.
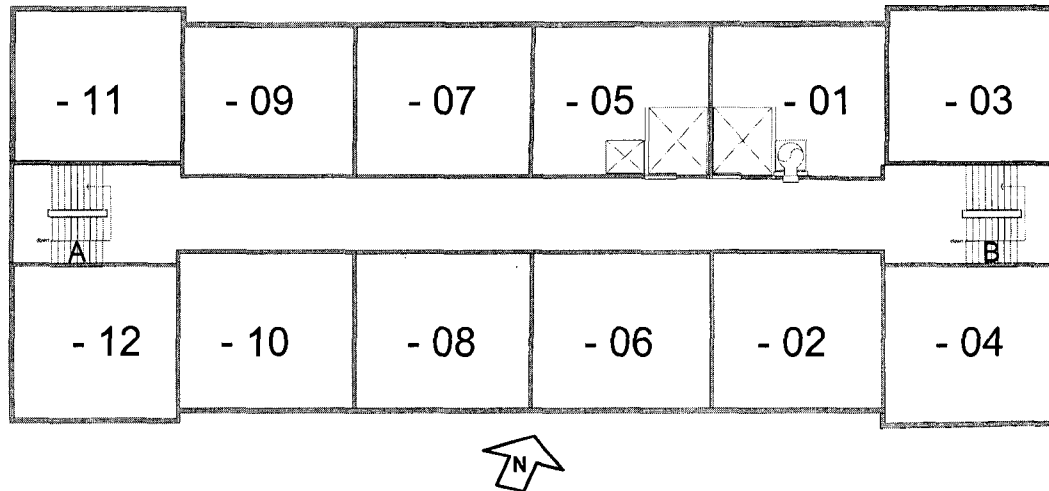
Figure 6.2. Typical floor plan with numbered apartment units.

6.3 Monitoring

In 1999, Canada Mortgage and Housing Corporation (CMHC), in cooperation with the Institute for Research in Construction and the Ottawa Carleton Regional Housing Authority, conducted a testing and monitoring program to determine the leakage characteristics of building envelope openings (fan depressurization and tracer gas tests) and monitor the indoor-outdoor pressure distribution in a high-rise apartment building in Ottawa. The unique feature of this program is the monitoring for almost 15 months (along with the on-site weather conditions) of the indoor-outdoor pressure differences that drive air movement as a result of stack, wind, and mechanical ventilation forces, which presents a significant amount of data that can be used for model validation. However, it should be noted here that these are data from the monitoring of a real building, which presents a number of challenges. As a result experimental data may be subject to uncertainties and/or experimental errors. A significant amount of time was devoted to process the raw data received from IRC (Reardon et al., 2003), to perform

cross-comparison between different sets of data and to apply corrections when required. Particular problems were faced associated with the zero drift of some of the pressure transducers used. During the monitoring period, the zero drift of the differential pressure transducers was checked every two weeks and the transducers were re-calibrated or replaced if required; these data were used to discard invalid data.

The monitoring program includes the following:

1. Air-tightness test of the entire building and three selected suites selected to represent low, mid-height, and top-floor suites (408, 1407, 2303).

2. Tracer gas measurement of ACH in three selected suites for 3 different mechanical ventilation scenarios (phase 1: corridor supply AHU off and local exhaust fans off; phase 2. corridor supply AHU on and local exhaust fans off; phase 3: corridor supply AHU on and local exhaust fans on), during cold and warm conditions.

3. Central corridor's system supply flow rates.

4. Building envelope pressure difference ($\Delta P_{env} = P_{out} - P_{in}$) at 5 elevations along the midline of each of the four façades.

5. Envelope pressure, indoor temperature and relative humidity in the three selected suites.

6. Total energy consumption of electricity and natural gas.

7. Weather data (humidity, outdoor temperature, wind speed and direction).

6.4   Overall methodology

The model includes design parameters such as leakage area, building location and geometry, climate data (temperature, wind speed / direction), height, mechanical supply

and exhaust flow rates. A coupled simulation (thermal and airflow) for the whole building using ESP-r requires a large number of zones (more than 150) and changes in the source code that may induce numerical convergence problems. The ESP-r limitations at the time that the simulations were performed were: 21 thermal zones and 50 airflow nodes. Considering the complexity of the simulation, the large number of zones and input parameters required, as well as the uncertainties involved (leakage characteristics of apartment door undercuts and supply registers, airflow through the stairwells, elevators, operation of exhaust fans, occupants' behavior, window openings) it was decided to initially focus on smaller sections of the building for which experimental data are available for validation purposes. At the second and third stage of the research, transient whole building simulations are performed. The thermal and airflow models were coupled using the "ping-pong" approach in ESP-r (see also Section 2.3), in which the two models run in sequence (i.e. each model uses the results of the other model in the previous time step). In this text, the term ventilation refers to the intended air flow rate while infiltration refers to the air leaking unintentionally into the building. More information on the general methodology followed and results can be found in Karava et al. (2006b; 2006c).

Stage 1

Simplified simulations for small sections of the building for which experimental data are available are carried out first. At this stage, the stack building envelope pressure is fixed to a specific value (boundary condition) for each floor using measured data. The objective is to develop and verify a simplified model in order to extract important information for the whole building transient simulation (second stage of the research) and

identify the most important parameters to consider when simulating air leakage in a high-rise residential building.

Stage 2

At this stage, the whole building is modeled. The ventilation shaft, stairwells, and the supply fan are simulated together with the 21 residential floors. The source code (thermal domain) was modified, i.e. the maximum number of zones and surfaces in the thermal domain. The stack and mechanical pressures are assumed to be the only driving forces (wind-driven leakage was not considered), i.e. the simulation is performed for a winter day with low wind speeds. This was done in order to keep the number of zones as low as possible (consideration of wind-driven flows requires extra zones for the corner suites) and to eliminate uncertainties attributed to wind pressure coefficients. The envelope pressures (stack and mechanical forces) are predicted at different elevations and are compared with experimental data. Results for the corridor supply flow rate, building envelope leakage and related energy consumption are presented.

Stage 3

The whole building is modeled and all the driving mechanisms (stack, wind and mechanical forces) are considered. The envelope pressures are predicted at different elevations and compared with experimental data.

6.5   Simplified one floor simulation

Simplified simulations for small sections of the building for which experimental data are available are carried out in order to extract important information for the whole building transient simulation (second stage of the research).

6.5.1 Model description

Each apartment was modeled as one zone assuming closed windows and internal doors open. Walker (1999) found that open interior doors may result in 6% reduction of envelope flows, for the particular multi-family building tested. Most of the leakage occurs around windows (one crack on each suite near the window area, with leakage area equivalent to that measured for the exterior wall); and there is no leakage between adjacent suites. Walker (1999) reported that the leakage between adjacent suites is less than 5%; Cooke et al. (2005) reported such leakage is insignificant. There are 3 suite types on each floor (1, 2 and 3) with leakage characteristics identical to those of the 3 selected suites tested during the experiments (suite 408 ≡ type 1, suite 2303 ≡ type 2, suite 1409 ≡ type 3; see Figure 6.3). Windows and doors to the exterior and suite access doors, stairway doors, and other doors between zones were kept closed. Stack and mechanical pressures are assumed to be the only driving forces, thus simulation is performed for one winter day with low wind speeds.

Thirteen zones, i.e. one zone for each suite and one zone for the corridor, were considered in the thermal network. Materials for walls and windows as well as different layer dimensions were extracted from the building drawings. In the airflow network, airflow paths between internal zones and between zones and the outside are specified in the input file along with other information related to ventilation system parameters and building envelope pressures. Six additional fictitious nodes (and zones) are considered in the airflow network, i.e. two fictitious zones for each of the two stairwells and the ventilation shaft. Leakage through the elevator shafts was not considered in the airflow network. However, an equivalent leakage area through the stairwell door undercut was

assumed to account for the leakage through the elevators or other unintentional openings in the corridor. There are also four outside nodes (north, south, east and west). A plan of a typical floor and the nodes of the airflow network are illustrated in Figure 6.3. Each fluid flow component relates the fluid mass flow rate, Q, through the component to the pressure drop, ΔP, across it ($\Delta P = P_{out} - P_{in}$). The power law equation was used to express the flow characteristics of cracks:

$$Q = C \cdot (\Delta P)^n \qquad (6.1)$$

For the calculation of the airflow through other openings (i.e. door undercuts, supply registers) the following equation was used:

$$Q = C_D \cdot A \cdot \sqrt{\frac{2 \cdot \Delta P}{\rho}} \qquad (6.2)$$

where C = flow coefficient; n = flow exponent; C_D = discharge coefficient; A = opening area; ρ = air density. Conservation of mass at each internal node is equivalent to the mathematical statement that the sum of the mass flows at such a node is equal to zero:

$$\sum_{k=1}^{k_{i,i}} \dot{m}_k = 0 \qquad (6.3)$$

where $\dot{m}_k$ is the mass flow rate along k^{th} connection to node i and $k_{i,i}$ is the total number of connections linked to node i. A detailed description of the ESP-r airflow network is provided by Hensen (1991). Air is supplied from the ventilation shaft to the corridor on each floor through the corridor registers. In the lower floors, the supply air enters the apartments or the stairwells depending on the pressure drops; there is also leakage flow from outside to the different suites. In the upper floors, in addition to the supply air from the ventilation shaft, there is air delivered to the corridors from the stairwells. Air enters

the apartments via the door undercuts and then it is exhausted to the outside through cracks in the building envelope or through the exhaust fans when operating.

Two sets of experimental data by applying the tracer gas and fan depressurization technique (Reardon et al., 2003) were used to estimate the building envelope leakage of three selected suites. The tracer gas decay tests attempted to measure the air change rate in each of the three suites. Those results cannot distinguish between outdoor air and uncontaminated indoor air from adjacent interior zones, e.g., the corridor and neighbouring suites, in their effect on diluting the tracer gas concentration in the three suites tested. During the tracer gas test (performed on February 12, 2001), the pressure difference between each suite and its corridor was measured to determine the direction of the airflow (i.e. airflow from the corridor into the suite, or from the suite into the corridor). For estimating the impact on energy consumption for space heating the suite, only the air flow between the outdoors and the suite is of interest, since corridor air will likely have a similar temperature as the air in the suite. The fan depressurization tests attempted to measure the airtightness characteristics of the exterior envelope of the suite, by balancing the pressures between the suite and all its adjacent interior zones (corridor and adjacent suites). It should be noted that these two test methods do not measure the same physical quantity, and assumptions are required to relate the results of one type of test to the other. Analysis of the results shows that the fan depressurization leakage data are overestimated compared to the data from the tracer gas test; this might be due to difficulties in balancing the pressures in the fan depressurization technique. By comparing the two sets of data corrected values for the leakage characteristics of the building envelope openings for the 3 suite types were calculated as presented in Table 6.1

and were used as inputs in the ESP-r simulation model. It should be noted that detailed representation of leakage paths in the building envelope might be more important for wind-driven flows.

First, simulations are performed in order to extract necessary inputs such as the discharge coefficient of the door undercut. Only 3 selected suites (and their adjacent corridor), for which experimental data are available, are modeled. The air exchange rate

Table 6.1. The leakage characteristics of the 3 suite types.

| Suite | Leakage characteristics | |
	C (L/s·(Pa)^n)	n
Type 1 (apt -05, -06, -07, -08)	7.92	0.57
Type 2 (apt -03, -04, -11, -12)	3.64	0.74
Type 3 (apt -01, -02, -09, -10)	4.21	0.56
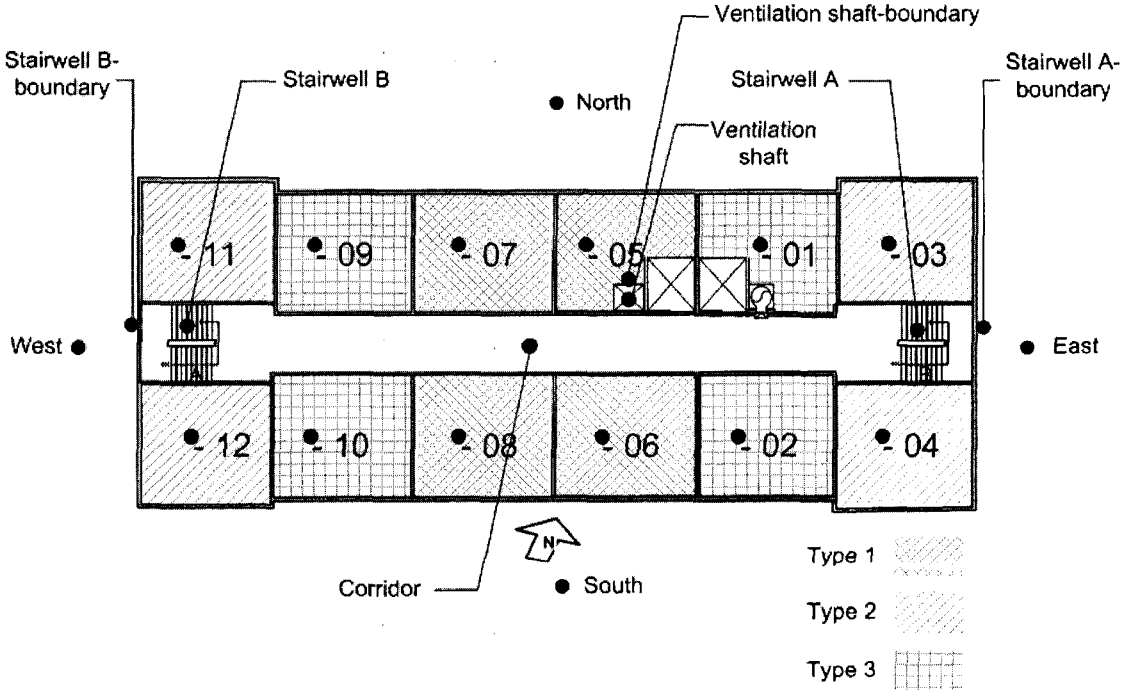
Figure 6.3. The airflow network nodes for a typical floor.

and the pressure drop across the apartment door ($\Delta P_c = P_{in} - P_{corridor}$) is used to calculate the discharge coefficient of the door undercut ($C_D = 0.5$). The opening area of the door undercut is 0.02 m^2 and effective leakage area ($C_D A$) = 0.0095 m^2. Then the 4th (typical floor where infiltration occurs) and the 23rd (typical floor where exfiltration occurs) floor are modeled. The simulation was performed for February 12, 2001 (date that winter tracer gas and corridor flow measurements were carried out) with a 5 min time step for the 4th floor and the 23rd floor. The following cases were investigated:

- Phase 1 (corridor supply AHU OFF and local exhaust fans OFF): there is no supply or exhaust fan operating. Outside air enters the apartments in the lower floors through the building envelope leaks and it is delivered through the ventilation shaft, which acts as a chimney, on the upper floors. For this condition, the ventilation shaft only serves as a multi-connected chimney as stated previously, and helps as a major flow path for indoor air flow patterns driven by stack-effect and wind. The corridor supply ventilation system's AHU had a bank of actuated circular dampers that were supposed to close when the AHU was OFF. This closing of dampers, intended by design, would have removed the outdoor air intake louver from the building's envelope leakage if all dampers were working properly. However, visual inspections revealed that the actuators for several of these dampers were faulty, so that the outdoor air intake louver would have been an infiltration leakage site when the AHU was OFF, although there are no data available to indicate the flow path characteristics of this "leakage site".

- Phase 2 (corridor supply AHU ON and local exhaust fans OFF): The corridor supply AHU is operating. For the simulation of the supply fan, fixed flow rates (available from the experiments) are delivered from the ventilation shaft to the corridor on each floor.

This airflow is distributed to the stairwells or different suites depending on the individual pressure drops available. The corridor flow rate is equal to 85 L/s on the 4th floor and 311 L/s on the 23rd floor.

- Phase 3 (corridor supply AHU ON and local exhaust fans ON in suites 408 and 2303). Supply and exhaust fans ON: the corridor supply AHU is operating at the actual (not design) flow rate and the local exhaust fans (located in the kitchen and washroom of each suite) are also operating continuously in all suites. Studies have shown that when apartment occupants have local control over bathroom and kitchen exhaust, they use them less than one hour per day, if at all (Diamond et al. 1996). Although the exhaust fans are rarely continuously operating, this case is considered for comparison purposes. It was found out that the exhaust fans do not operate at the maximum capacity defined in the mechanical drawings. The exhaust flow rate depends on the actual pressure drop between the exhaust vent and the room. Similar observations have also been reported by Diamond et al. (1996). The actual exhaust fan flow rates were determined via simulations. It was found that in suite 408 the exhaust fans operate at 50% capacity. In suite 2303, the exhaust fans operate at 17% capacity). The same exhaust flow rate was assumed for all suites in one floor since experimental data are available for one unit only.

The leakage flow rate and the pressure drop across the building envelope and between each suite and its respective corridor were calculated and compared with experimental results for two suites (suite 408 and 2303). Actual weather data measured on site were used as boundary conditions (only in the thermal model). The heating load is calculated via thermal simulation for a typical winter design day. Then the baseboard capacities required to maintain the set point temperature are estimated. The required maximum

capacity to maintain the indoor temperature at 23 °C (set-point) is about 2.5 kW in each apartment. This value was selected based on measurement data for the interior air temperature. Proportional controllers were assumed for all the suites and corridors in order to allow for some temperature fluctuation (throttling range = 2 °C) although the actual control of a baseboard heater is most probably closer to a typical ON/OFF control with a dead-band.

The stack building envelope pressure was fixed to a specific value for each floor (boundary condition). Measured values for the envelope pressure with the fans OFF were used. The measured envelope pressure under winter conditions with the supply and exhaust fans OFF is 18.9 Pa, -6.8 Pa and -18.2 Pa across the building envelope of suites 408, 1409, and 2303 respectively. The theoretical value for the stack pressure assuming that the Neutral Pressure Level (NPL) is near the mid-height of the building (confirmed by experimental data for the pressure difference across the envelope at different heights), outdoor temperature equal to -12.4°C and indoor temperature 23°C (monitored values) is equal to 18.9 Pa, -6.8 Pa, and -37 Pa for suites 408, 1409, and 2303 respectively. The measured envelope pressure is very close to the theoretical value (assuming stack-driven flow only) for the 4th and the 14th floor (typical floor near the mid-height of the building). For the 23rd floor the measured value is smaller which is probably due to the impact of the wind since 2303 is a corner suite on the top floor with more pronounced wind impact. For the 4th and the 23rd floor the input stack pressure was 18.9 Pa and -18.2 Pa respectively. A zero wind speed was assumed. However, the monitored average wind speed during the tracer gas test was equal to 3.1 m/s, which corresponds to a 4.6 Pa and – 1.1 Pa pressure on the windward and leeward wall respectively. A pressure coefficient

equal to 0.8 and -0.3 for the windward and leeward wall was assumed (ASHRAE, 2007).

For phases 2 and 3, the same input boundary pressure was used but the "actual" envelope pressure was calculated through simulation by accounting for the mechanical forces as well. The validated one floor-model was used to calculate the air leakage rate and infiltration load for phases 1, 2, and 3 described above. This simulation exercise was carried out mainly for verification purposes. Another case with the corridor supply AHU operating at the design flow rate taken from building's mechanical drawings (354 L/s on each floor through the corridor registers) was considered for comparison purposes.

6.5.2 Results and discussion

Figure 6.4 shows simulation results for the envelope ($\Delta P_e = P_{out} - P_{in}$) and corridor ($\Delta P_c = P_{in} - P_{corridor}$) pressures for suites 408 and 2303. The "sign" of the pressure drop across the doorway of the apartment and the building envelope determines whether the supplied air is entering or leaving the apartments. Tables 6.2 and 6.3 present experimental and simulation results for the two suites (408 and 2303). The infiltration or exfiltration flow rate (Q_{env} in L/s and ach) is shown in addition to the envelope (ΔP_e) and corridor (ΔP_c) pressure drop on each suite. Generally, good agreement between the experimental and simulation results is observed. During phase 1 (building operating without mechanical ventilation system) the air mass flow distribution on the two floors follows a predictable pattern. Suites on the 23rd floor only receive air from the lower floors, which might create IAQ problems in the building, while suites on the 4th floor only receive cold unconditioned air via leakage from outside. The envelope pressures in Phase 2 (corridor supply AHU ON and local exhaust fans OFF) indicate that the corridor supply fan

successfully pressurized the upper floors, which is most clearly indicated by the "sign" and the increase of the pressure drop acting across the entrance door of suite 2303 (ΔP_c). However, due to the strong stack effect, the corridor supply system did not successfully pressurize the lower floors (i.e. 4th floor). The pressure difference across suite 408 and its corridor indicate that the corridor system operation did not reverse the direction of the flow; nevertheless, the corridor pressurization decreases the envelope pressure and the infiltration flow rate. The negative pressure drops across suite's 408 entrance door (ΔP_c) for phases 1 and 2 indicate that air delivered to the corridor system bypasses apartments on the lower floors, exiting the building via stairwells and/or elevator shafts. In phase 3 (corridor supply AHU ON and local exhaust fans ON in suites 408 and 2303), the small pressure difference across the apartment door reveals that the local exhaust fans did not result in interior air in the corridor being drawn into suite 408. Most likely, air flows into the apartments through the building envelope leaks and is exhausted through the fans. For these typical winter conditions, the ventilation rates vary between 0.83 and 1.36 ach. Simulation results indicate that excess air is leaving the corridor through the stairwells (or elevator shafts) on the lower floors, while air is entering the corridor from the shafts on the upper floors. Higher corridor airflows would further increase the leakage from the corridors to the stairwells. This is an expected flow pattern in cold weather due to stack effect, which imposes a significant energy penalty in the building and it should be considered in ventilation system design. The impact of stairwell leakage has also been reported elsewhere (CMHC, 1991; Feustel & Diamond, 1998). The opening area and leakage characteristics of the stairwell door undercut and corridor grilles are important

168

-18.2 Pa 2303 5.9 Pa

Phase 1

Corridor supply OFF

Local exhaust OFF

-9.3 Pa 408 12.8 Pa

-21.8 Pa 2303 -7.5 Pa

Phase 2

Corridor supply ON

Local exhaust OFF

-4.5 Pa 408 -7.1 Pa

-17.3 Pa 2303 -11.7 Pa

Phase 3

Corridor supply ON

Local exhaust ON

0 Pa 408 -13.5 Pa
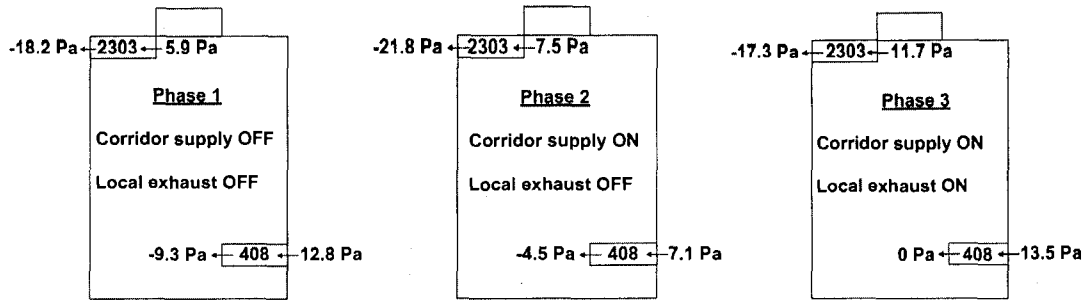
Figure 6.4. Envelope ($\Delta P_{envelope}$) and corridor ($\Delta P_{corridor}$) pressures for suites 408 and 2303.

Table 6.2. Simulation and experimental results for suite 408.

	Q_{env} L/s(ach) sim	Q_{env} L/s(ach) expt	ΔP_e Pa sim	ΔP_e Pa expt	ΔP_c Pa sim	ΔP_c Pa expt
Phase 1	34(1.17)	36(1.24)	12.8	18.9	-9.3	-8.6
Phase 2	24(0.83)	28(0.95)	7.1	9.1	-4.5	-4.8
Phase 3	34(1.17)	41(1.42)	13.5	12.8	0	-1.2

Table 6.3. Simulation and experimental results for suite 2303.

	Q_{env} L/s(ach) sim	Q_{env} L/s(ach) expt	ΔP_e Pa sim	ΔP_e Pa expt	ΔP_c Pa sim	ΔP_c Pa expt
Phase 1	-31(1.05)	-27(0.88)	-18.2	-18.2	5.9	8.2
Phase 2	-35(1.13)	-34(1.12)	-21.8	-21.8	7.5	12.1
Phase 3	-42(1.36)	-36(1.16)	-17.3	-17.8	11.7	13.1

parameters since they affect the airflow patterns inside the building. The present simulation has shown that A = 0.1 m^2 and C_D = 0.6 are suitable values for the corridor grilles and the stairwell door undercut. It should be noted that the opening area of the stairwell door undercut is an equivalent opening area including the leakage area of elevator shafts or other unintentional openings in the corridor.

Figure 6.5 shows simulation results for the total infiltration flow rate on the 4th floor for different ventilation scenarios. The infiltration flow rate can be reduced by 33% with the corridor AHU supply operating compared to that with the supply and exhaust fans OFF. Continuous exhaust ventilation, presents the possibility of over-ventilation and unnecessary use of energy since the infiltration flow is increased by 50% if compared to that with the Supply fan ON. Figure 6.6 shows simulation results for the infiltration load for the 4th floor divided by the total floor area for different ventilation scenarios. The 24 W/m^2 infiltration load with the supply and exhaust fans OFF can be 16 W/m^2 (reduced by 33%) and 3.5 W/m^2 (reduced by 85%) with the corridor AHU supply operating at the actual flow rate (Supply fan ON) or at the design flow rate (Supply fan design). Experimental results by CMHC (1991) are also included in the graph; the infiltration load in the buildings tested varies between 12 and 25 W/m^2. It should be noted that these are data for available buildings and should not be generalized.
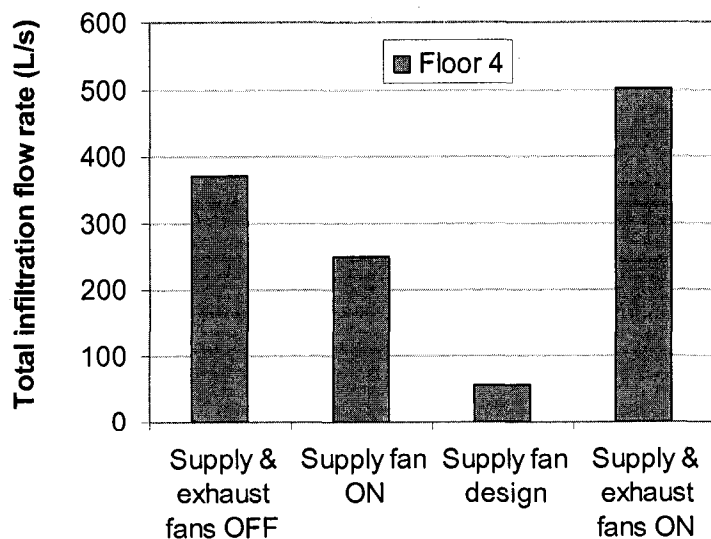
Figure 6.5. Total infiltration flow rate for different ventilation scenarios (floor 4) on a typical winter day (February 12, 2001).
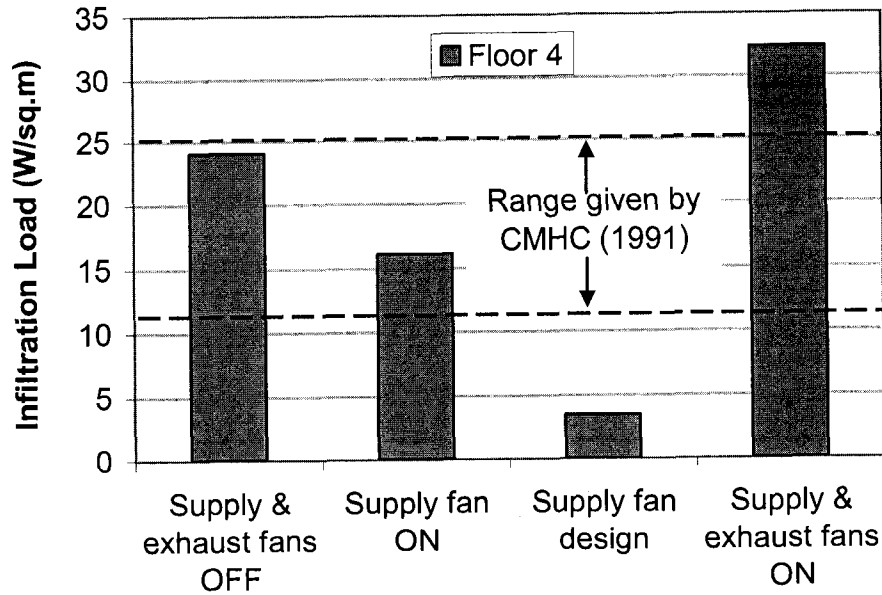
Figure 6.6. Infiltration load per floor area for different ventilation scenarios (floor 4) on a typical winter day (February 12, 2001).

6.6 Whole building simulation – stack and mechanical effect

At this stage the whole building is modeled. The ventilation shaft, stairwells, and the supply fan are simulated together with the 21 residential floors. The stack and mechanical pressures are assumed to be the only driving forces. Envelope pressures predicted at different elevations are compared with experimental data. Results for the corridor supply flow rate, building envelope leakage and related energy consumption are presented. Preliminary guidelines for the design of a simplified tool to predict the indoor-outdoor air exchange in multi-unit high-rise residential buildings are also presented.

6.6.1 Model description

A simplified 35-zone model of the building (including the ventilation shaft, two stairwells, lobby, corridors and the residential suites) was developed. The source code

(thermal domain) was modified, i.e. the maximum number of zones and surfaces in the thermal domain was increased. Several attempts were made to change this number in the ESP-r source code but they were not successful. As a result, zoning assumptions had to be made since the maximum number of airflow nodes in ESP-r is 50. Each floor was divided into one zone describing the apartments on the South façade, one zone describing the apartments on the North façade, one zone for the corridor, one zone for the ventilation shaft and one zone for each of the two stairwells. In order to keep the number of zones as low as possible, adjacent floors were grouped together, i.e. the South or North façade for floors 3 to 7 is one zone, the corridor for floors 3 to 7 is one zone, the ventilation shaft for floors 3 to 7 is one zone and so on. Floors 8 to 12 are also grouped together, as well as 14 to 18 and 19 to 23. This leads to 24 zones. The zoning assumptions are based on results of the first step. The 2nd floor and the lobby are modeled separately (8 and 3 zones respectively). The airflow network consists of 35 internal nodes (described above), 14 external nodes (totally 49 airflow nodes), 14 different airflow components and 57 airflow connections. The ventilation shaft and the two stairwells are divided in different zones assuming fictitious surfaces; these zones are connected in the airflow network through large openings. The opening area of these openings is equal to horizontal cross-sectional area of the shaft or stairwell and the discharge coefficient is equal to 0.65. In the simplified simulation described above, it was found that a suitable value for the (effective) opening area and discharge coefficient of the corridor grilles is 0.1 m^2 and 0.6 respectively (0.5 m^2 for 5 floors grouped together), 0.02 m^2 and 0.5 respectively for the apartment door undercut (0.6 m^2 for 5 floors grouped together) and 0.1 m^2 and 0.6 respectively for the stairwell door undercut (0.5 m^2 for 5 floors grouped together). The

leakage characteristics for the 3 suite types presented in Table 6.1 were used to calculate the total leakage area for each zone. The pressure coefficient values were set equal to zero in one on the existing pressure coefficient databases in ESP-r in order to eliminate the wind effect. A schematic representation (wireframe) of the zoning assumptions is shown in Figure 6.7. Simulations were performed for the same day as the simplified one-floor simulation (February 12, 2001) with the same time step (5 min). It was assumed that the stack and mechanical pressures are the only driving forces (wind-driven leakage was not considered), i.e. the simulation was performed for one winter day with low wind speeds. The average wind speed during that day was equal to 3.3 m/s. Actual weather data measured on site were used as boundary conditions in the thermal and airflow model. The ventilation air is pre-heated to 21 °C. This value is based on approximate corridor supply air temperature measurements on the date for which simulations are performed (February 12, 2001).

The following two cases are considered:

a) Supply and exhaust fans OFF: Outside air enters the apartments in the lower floors through the building envelope leaks and it is delivered through the ventilation shaft, which acts as a chimney, on the upper floors. When the corridor supply system is OFF, the flow rates between the ventilation shaft and the corridor on each floor will have no relation to design-intended flow rates for the system operating.

b) Supply fan ON and exhaust fans OFF: Outside air enters the ventilation system on the 2nd floor and it is delivered from the ventilation shaft to the corridor on each floor; the airflow is distributed to the stairwells or different suites depending on the individual
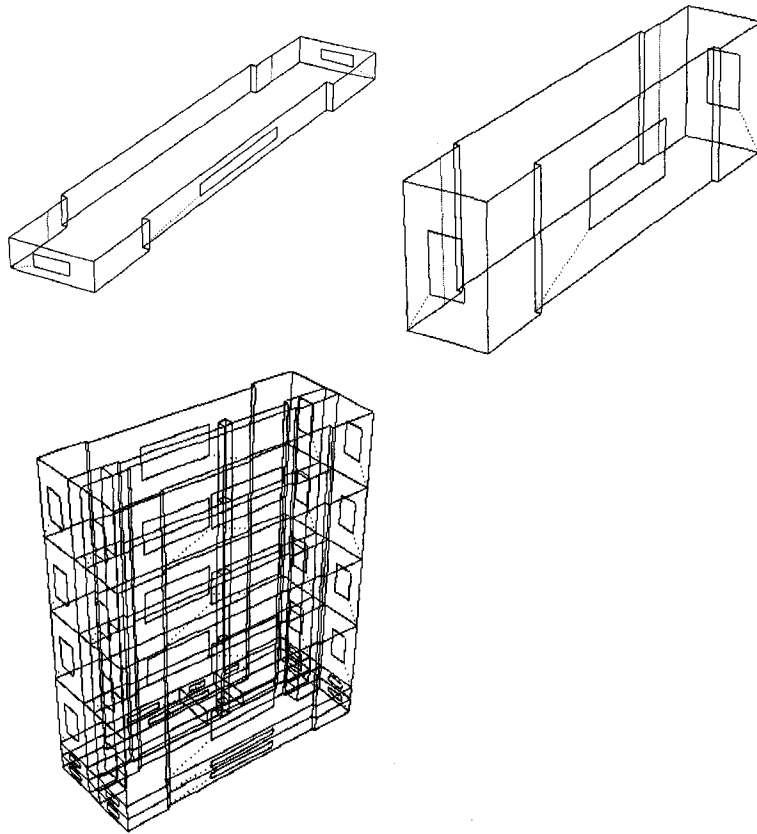
Figure 6.7. Schematic representation (wireframe) of zoning assumptions.

pressure drops available. Experimental data (Reardon et al., 2003) have shown that the supply fan does not operate at the maximum design capacity defined in the mechanical drawings. Both in cold and warm weather the total system flow and the supply flow rates on each floor were typically well below the design specifications (total design flow rate 6800 L/s; design flow rate on each floor = 354 L/s; design flow rate on 2nd floor = 625 L/s). The total measured supply fan flow rate on February 12 is equal to 3800 L/s. In the present study, simulations were performed with supply flow rates equal to 2500 L/s, 3150 L/s, and 3800 L/s (measured flow rate), which correspond to 37, 46, and 56% of the design flow rate (6800 L/s). Simulations were also performed for Q_{supply} equal to design flow rate. Wray et al. (1998) measured the flow rates of corridor ventilation systems in 10

mid and high-rise apartment buildings across Canada (from 6 to 32 stories); corridor flow rates were found to be significantly lower than design airflows, ranging from 34% to 81% of design flows, with an average of 59%.

6.6.2 Results and discussion

Table 6.4 presents simulation results for the flow rate delivered from the AHU air supply ventilation system to the corridor of each floor on February 12 at 13:00 (time that the corridor flow rates were measured). Experimental data are also presented. Since the floors are grouped in the simulation model, the experimental values for the corridor airflow rate were added for every 5 adjacent floors except for the airflow rate on the 2nd floor (see also Section 6.6.1). Results are also presented in Figure 6.8. When the corridor ventilation is shut down (fan OFF), the supply duct (ventilation shaft) behaves like a chimney. Table 6.4 also shows results for the airflow rate delivered through the ventilation shaft on each floor – upper floors (or from the corridor to the shaft – lower floors) with the supply fan OFF. Simulation results for the envelope pressures at different elevations are presented in Table 6.5 and results for the envelope leakage in Table 6.6. Table 6.4 and Figure 6.8 show that the strong stack effect substantially skews the distribution of the corridor ventilation system supply flow rates delivered on each floor, i.e. greater flow rates on the upper floors and lesser flow rates on the lower floors. These differences are more pronounced with the supply fan OFF or with the supply fan ON and low flow rates, i.e. substantial differences in the supply flow rate between upper and lower floors for $Q = 2500$ L/s (37% of Q_{design}) compared to $Q = 3150$ L/s (46% of Q_{design}). For $Q = 3800$ L/s there is almost uniform flow distribution between the different floors.

Table 6.4. Corridor supply flow rate for different floors (February 12, 2001).

| Floor | Node height (m) | Supply Fan ON | | | | | Supply Fan OFF |
| | | Q = 37% | Q = 46% | Q = 56% | Q_{design} | Expt. | - |
		$Q_{corridor}$ (L/s)	$Q_{corridor}$ (L/s)	$Q_{corridor}$ (L/s)	$Q_{corridor}$ (L/s)	$Q_{corridor}$ (L/s)	$Q_{corridor}$ (L/s)
2	3.45	72.1	126.3	175.5	370.7	99	-173.5
3 - 7	10.35	293	578.6	840.1	1892.2	375.6	-814.2
8 - 12	21.85	594.5	740.9	893.8	1567.9	674.5	181.4
14 - 18	33.35	657.8	764.2	881.3	1421.8	1171	883.8
19 - 23	44.85	856.6	938.4	1032	1493.4	1500	1335

Table 6.5. Envelope pressure for different floors (February 12, 2001).

| Floor | Node height (m) | Supply Fan ON | | | | Supply Fan OFF |
| | | Q = 37% | Q = 46% | Q = 56% | Q_{design} | - |
		ΔP_e (Pa)	ΔP_e (Pa)	ΔP_e (Pa)	ΔP_e (Pa)	ΔP_e (Pa)
2	3.45	13.4	11.36	9.31	1.64	18.16
3 - 7	10.35	7.86	5.94	4.05	-2.25	11.73
8 -12	21.85	-2.06	-3.83	-5.67	-12.56	0
14 - 18	33.35	-13.73	-15.31	-16.98	-23.58	-12.265
19 - 23	44.85	-24.24	-25.73	-27.33	-33.68	-23.46

Table 6.6. Envelope leakage for different floors (February 12, 2001).

| Floor | Node height (m) | Supply Fan ON | | | | Supply Fan OFF |
| | | Q = 37% | Q = 46% | Q = 56% | Q_{design} | - |
		Q_{env} (L/s)	Q_{env} (L/s)	Q_{env} (L/s)	Q_{env} (L/s)	Q_{env} (L/s)
2	3.45	282.4	289.1	224.4	75.6	340.9
3 - 7	10.35	1133.6	1082.4	750.6	-520.6	1453.6
8 - 12	21.85	-494.0	-725.6	-925	-1516.4	84.2
14 - 18	33.35	-1602.2	-1714.4	-1828.8	-2242.4	-1494
19 - 23	44.85	-2281.2	-2367.2	-2457.2	-2797.6	-2235
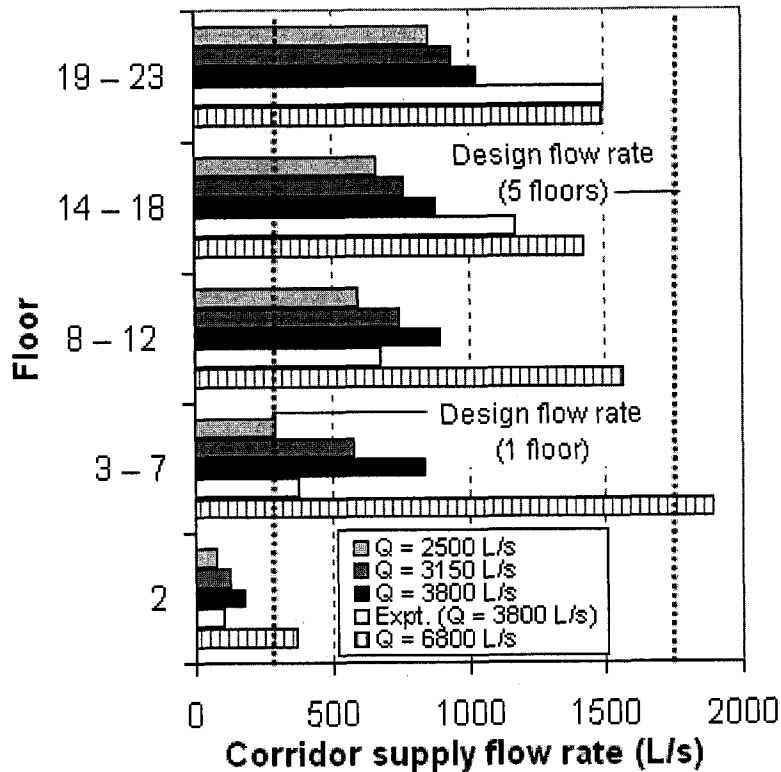
Figure 6.8. Corridor supply flow rate for different floors (February 12, 2001) with the supply fan ON.

However, the experimental results (Q = 3800 L/s or 56% of Q_{design}) show differences in the corridor supply flow rate between the floors (Reardon et al., 2003). This difference between the experimental and simulation results can be explained as follows:

(a) The corridor flow measurements were made using handheld instruments and therefore are subject to large experimental uncertainties. They should, therefore, be used only for observing trends in flow behaviour (Reardon et al., 2003).

(b) The corridor in the upper floors is pressurized due to the airflow from the lower floors through the stairwell. Part of this flow may be directed from the stairwell to the outside through building envelope cracks. However, this effect was not modelled since

177

information for the stairwell leakage is not available. Exploratory simulation results confirm that when the stairwell leakage is modeled the corridor flow to the upper floors is increased.

(c) The baseboard capacities are calculated from the loads. Therefore, this may introduce some uncertainty in the prediction of building thermal behaviour.

(d) Several assumptions made on the zoning of the building (i.e. grouping of floors) in order to simplify the model may have introduced errors in the calculation of corridor flows. However, the good agreement between the experimental and simulation results for the envelope pressures indicate that the actual flow rate was probably close to 3200 L/s and not equal to the measured value, i.e. 3800 L/s.

Table 6.5 shows that the corridor supply system did not successfully pressurize the lower floors due to strong stack effect. Nevertheless, the corridor pressurization decreases the envelope pressure and the infiltration flow rate (compared to the case with the supply fan OFF). The NPL of the building with the supply fan OFF is between 8 to 12 floor (probably close to the 10th floor), as mentioned in the experimental results by Reardon et al. (2003) The NPL with the supply fan ON is between the 6th and 9th floor probably close to 8th floor for Q = 2500 L/s (37% of Q_{design}) and close to 6th or 7th floor for Q = 3150 L/s (46% of Q_{design}) and Q = 3800 L/s (56% of Q_{design}). Experimental results indicate that the NPL was located close to the 7th floor with the mechanical system operating, thus, there is good agreement between the experimental and simulation results with respect to the envelope pressures. If the supply fan operates at its full design capacity the NPL of the building is close to the 2nd floor. Figure 6.9 shows the total infiltration load (kWh) for the building for one cold winter day (February 12) for different ventilation scenarios (supply

fan ON or OFF) and supply fan flow rates. Note that the infiltration load in the lobby is not considered in this calculation. The total infiltration load is reduced by 24% with the corridor AHU supply operating at Q = 2500 L/s (37% of Q_{design}), 35% with Q = 3150 L/s (46% of Q_{design}) and 47% with Q = 3800 L/s (56% of Q_{design}) compared to that with the supply fan OFF.

A sensitivity analysis was performed to explore the importance of different parameters or the uncertainty attributed to the underlying assumptions. Simulations were performed considering the ventilation shaft as one zone. Results for the envelope pressures are reasonable but predictions for the AHU supply flow rate on the lower floors were subject to inaccuracies. The leakage characteristics of the different door undercuts, corridor grilles or intake louver (Fan OFF) affect the airflow patterns inside the building and have a significant impact on the results. It appears that the corridor supply flow rate
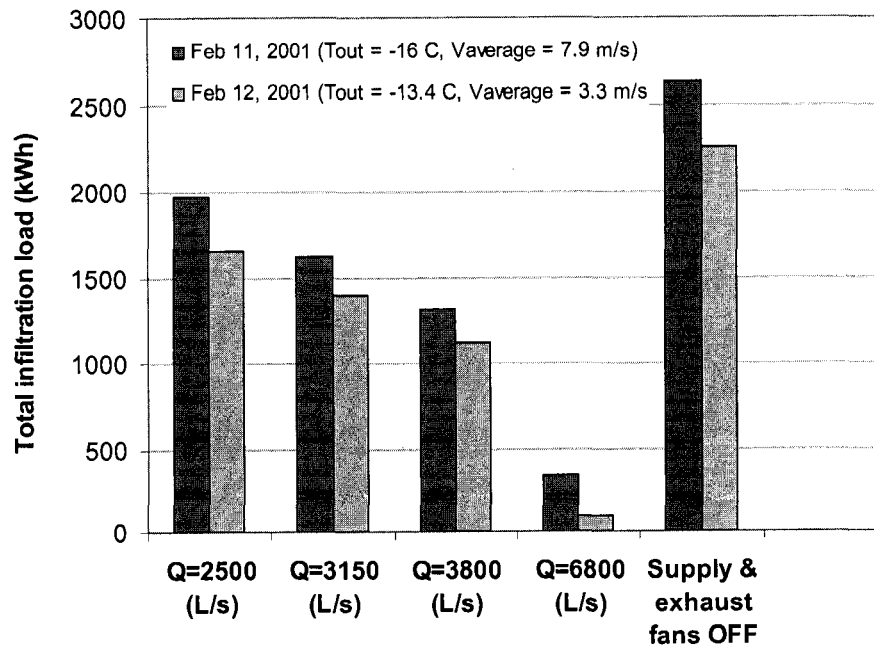
Figure 6.9. Total infiltration load (kWh) for February 12, 2001.

179

is an important parameter when simulating the airflow in a high-rise residential building and probably the most difficult to predict, particularly when the fan does not operate at full design capacity.

6.7 Whole building simulation – stack, mechanical and wind effect

At this stage, the whole building is modeled and all the driving mechanisms (stack, wind and mechanical forces) are considered. Airflow rates through airflow paths in the apartment building are modelled with the corridor ventilation system ON under dynamic weather conditions. The envelope pressures (wind, stack and mechanical forces) are predicted at different elevations and compared with monitoring data.

6.7.1 Model description

Two additional zones (and airflow nodes) per floor should be added to model separately the East and West facing suites (see Figure 6.2) in order to accurate model the wind forces and the impact of the wind direction. This required an increase of the maximum number of airflow nodes in the ESP-r source code but several attempts were not successful. Simulations were limited to dates or periods during a day with winds almost perpendicular to the South or North façade; however, it is anticipated that simulation data may be subject to errors due to the zoning assumptions that had to be made. A set of pressure coefficients, for a flat-roof semi-exposed building, selected from the ESP-r database was used in order to model the wind effect. Other than that, the same model described in Section 6.6.1 was used for the simulations. Hourly wind speed and direction data (along with ambient temperature data) measured on-site were imported in the ESP-r

weather climate file for Ottawa. It should be noted that results presented in the following section may be subject to a number of uncertainties (i.e. zoning assumption, occupant behaviour, pressure coefficient values, etc), therefore, results should be used within the limits of their applicability and within the scope of the study.

6.7.2 Results and discussion

First, simulations were performed for the same day with the simulations described in Sections 6.5.1 and 6.6.1 (February 12, 2001). This date was selected as a typical cold winter day with low wind speeds (average wind speed equal to 3.3 m/s). Figure 6.10 presents simulation and experimental results for the building envelope pressure difference on the 2nd floor (see also Figure 6.3). Wind speed and direction are also shown in the same graph. Simulation results are in relatively good agreement (within 15%) with the monitoring data (floor 2 South-sim. and suite 204-expt.; floor 2 North-sim. and suite 207-expt.) during night time periods (i.e. 2:00-4:00 a.m.) when the wind speeds are low and the impact form the occupants is anticipated to be small. Experimental results show a higher pressure drop across suite 212 as this is located on the windward wall and is affected by the wind (corner suite); correlation between the wind speed and envelope pressure across this suite is remarkable. The discrepancy between experimental and simulation results during the day (e.g. 8-10 a.m.), despite the low wind speeds, clearly indicates the impact of occupants.

Figures 6.11 presents simulation and experimental results for February 11, 2001, a typical cold winter day (average outdoor temperature equal to -16 °C) with high wind
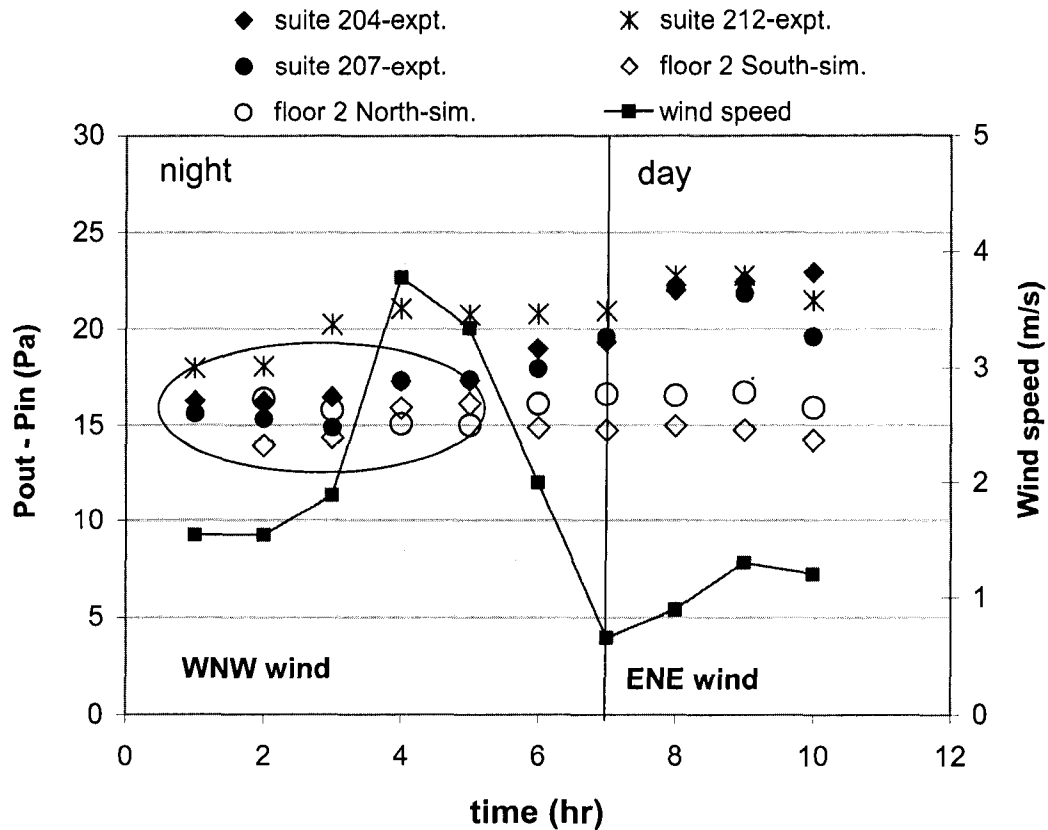
Figure 6.10. Simulation and monitoring data for the building envelope pressure below the NPL height- 2nd floor, South façade- during a cold winter day with low wind speeds (February 12, 2001).

speeds (average wind speed equal to 7.9 m/s). The wind speed and direction are also shown in the same graph. Results are presented for (a) low (below the NPL) and (b) upper floors (above the NPL). Due to the impact of occupants and zoning assumptions (described in Section 6.7.1), comparisons between experimental and simulation results can only be done for periods during the night with winds blowing from North or South (see also Figure 6.3). Examination of Figure 6.11 shows the following:

- Similar trends are observed between simulation and experimental results for NWN winds (i.e. floor 2 South-sim. and suite 204-expt.; floor 19-23 South-sim. and suite 2306-
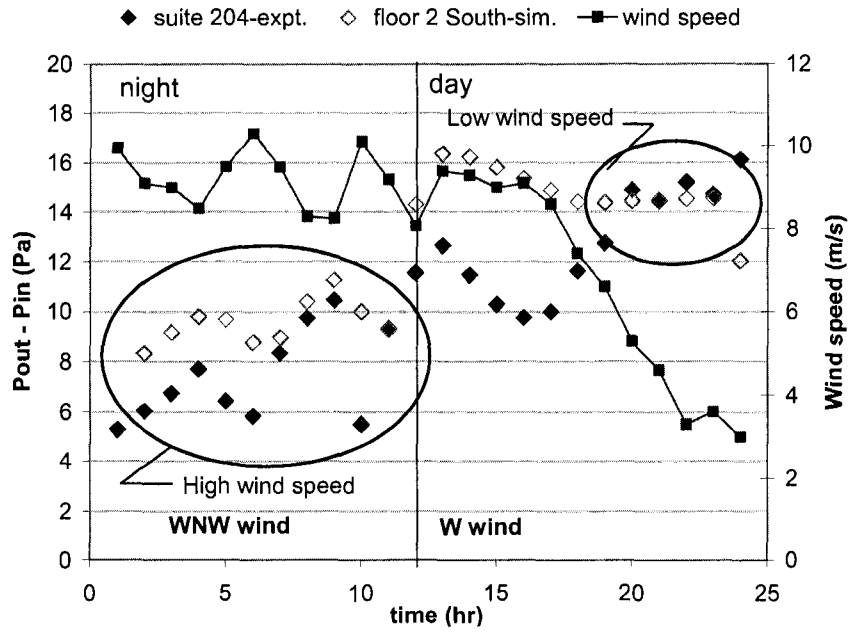
(a) 2nd floor, South façade
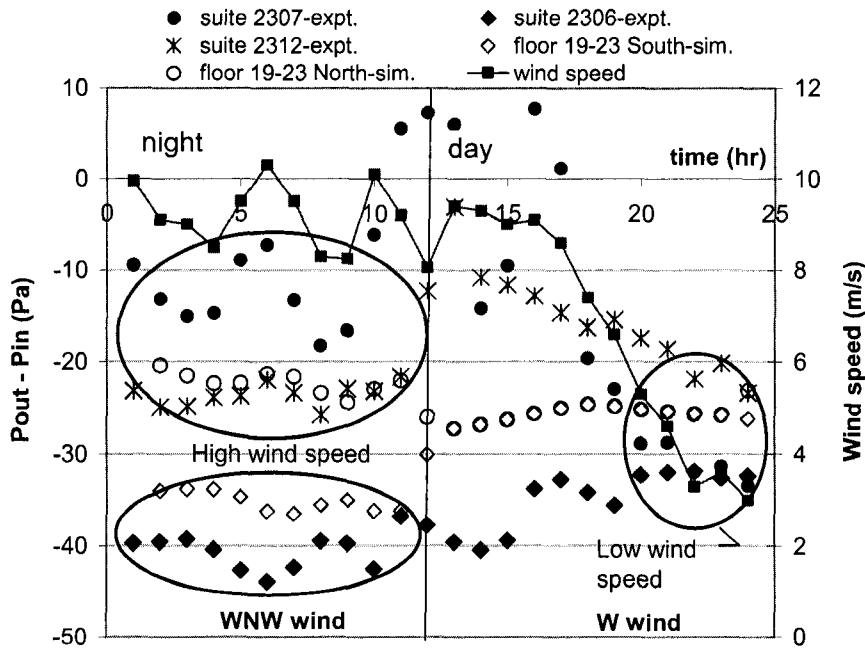
(b) Top floor, North façade

Figure 6.11. Simulation and monitoring data for the envelope pressure during a cold winter day with high wind speeds (February 11, 2001).

expt.; floor 19-23 North-sim. and suite 2307, suite 2312). Correlation between the wind speed data and building envelope pressure variation on walls under positive or negative pressure is remarkable for the period during the night in both experimental and simulation results. Simulation results are underestimated for nodes located on the North façade (windward wall) - floor 19-23 North-sim. and overestimated for nodes located on South façade (leeward wall) - floor 2 South-sim., floor 19-23 South-sim., which can be attributed to the relatively low pressure coefficient (Cp) values used. It should be noted that experimental values for the pressure drop in the building cannot be directly compared with the simulation values since the floors are grouped in the simulation model (e.g. floor 19-23 South-sim. and floor 19-23 North-sim. in Figure 6.11b). Further efforts to quantify the uncertainty attributed to the Cp values considered and to improve the results, were not possible due to time restrictions.

• There is good agreement between simulation and experimental results during periods with low wind speeds (which are specified in the figure) indicating that the model predicts the stack and mechanical effect with reasonable accuracy.

• As expected, large differences between experimental and simulation results are observed for Westerly winds, which are attributed to the zoning assumptions.

Figure 6.12 shows the total infiltration load (kWh) for the building for a typical cold winter day with low (February 12, 2001) and high wind speeds (February 11, 2001). Results are presented for different ventilation scenarios (Supply fan ON or OFF) and various supply fan flow rates. As expected, the infiltration load is higher on February 11 due to the colder temperature and higher wind speed. Figure 6.13 presents the total
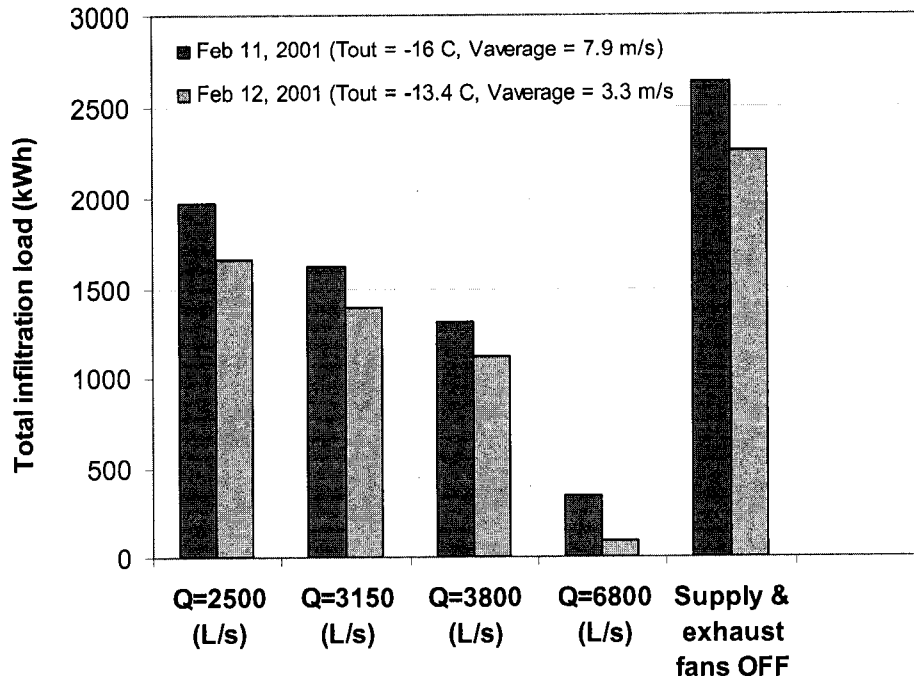
Figure 6.12. Total infiltration load (kWh) for February 11 and 12, 2001 for different ventilation scenarios and supply flow rates.
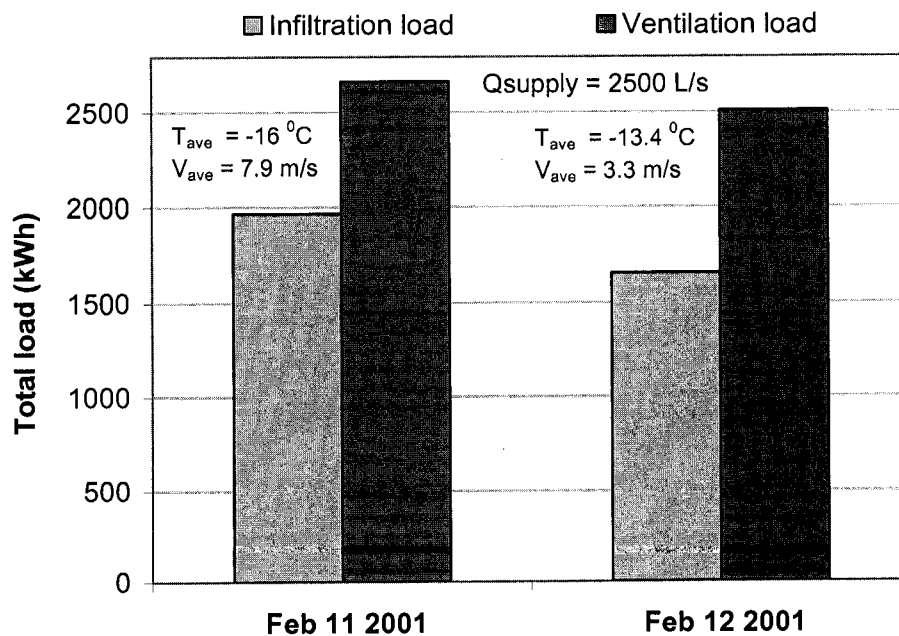
Figure 6.13. Total infiltration load and ventilation (kWh) for February 11 and 12, 2001 for Qsupply = 2500 L/s (37% of the design flow rate).

infiltration and ventilation load (kWh) for the building for a typical cold winter day with low (February 12, 2001) and high wind speeds (February 12, 2001) for Qsupply = 2500 L/S (37% of the design flow rate). Results show that the infiltration load can be up to 42% of the total infiltration and ventilation heating load under cold winter conditions.

6.8 Summary

A simulation methodology combined with a sensitivity analysis focused on modelling issues, such as the impact of zoning assumptions, was developed in order to predict the building envelope pressures and airflow patterns due to natural (wind and thermal buoyancy) and mechanical forces in a large building. An integrated simulation tool (ESP-r) was used to model the airflow / energy interactions in the building, considering a large number of zones, for the first time, and validation with monitoring data. The reasonably good agreement between the simulation and experimental results particularly considering the complexity of the problem, the large number of zones and input parameters required and all uncertainties involved, indicates that airflow modelling of such a large building with different airflow patterns is possible in ESP-r. The study found that the simplified 35-zone model, which exceeds the maximum number of 21 zones allowed in ESP-r, predicts the stack and mechanical effects well. However, simulation data may be subject to errors for inclined winds (Easterly or Westerly winds) due to the underlying zoning assumptions. Two additional zones (and airflow nodes) per floor should be added to have a more realistic representation of the wind impact, however, this was limited by the maximum number of 50 airflow nodes in ESP-r. The work presented in this chapter is the first step towards the development of a simplified tool that can be used by building

designers for energy analysis of buildings, considering the impact of leakage as well as interactions between the natural and mechanical forces.

The stack effect substantially skews the distribution of the corridor ventilation system supply flow rates delivered to each floor, i.e. greater flow rates on the upper floors and lesser flow rates on the lower floors. These differences are more pronounced with the corridor air supply mechanical ventilation system OFF or with the supply fan ON and low supply flow rates. Simplified simulation results show that the infiltration flow rate and the corresponding heating load on the 4th floor can be reduced by 33% with the corridor AHU supply operating compared to that with the supply and exhaust fans OFF. If the supply fan operates at the design rate, the infiltration load can be reduced by 85%. Simulations performed for a typical cold winter day show that the infiltration load can be up to 42% of the total infiltration and ventilation heating load. Note that these are data for the tested building and should not be generalized.

Future work should primarily focus on the increase of the maximum number of airflow nodes and airflow connections in the ESP-r source code. Work should include increase of the number of zones in the simulation model and comparison of results for different zoning assumptions (i.e. grouping of 2 or 3 floors together). The impact of sub-zoning of the living space, building envelope leakage and detailed simulation of air flow paths as well as uncertainties attributed to wind pressure coefficients should be investigated. The importance of integrated thermal and airflow simulation for the prediction of airflow and energy consumption should also be quantified and the impact of different coupling assumptions, i.e. sequential versus onion coupling, should be examined. Simulations should be performed for different buildings in various locations

for which experimental data are available for inputs and validation to produce statistical data that can be of general validity.

Numerical modelling of wind-driven cross-ventilation with large openings was not considered in the present research work. Large openings such as windows can easily be added in the simulation model developed to predict the airflow rates and potential energy savings in evaluating natural ventilation design alternatives, i.e. window openings in parallel and/or adjacent walls. Wind-tunnel data presented in Chapters 4 and 5 in terms of airflow rates and internal pressure coefficients for different opening configurations can be used for validation.

7 CONCLUSIONS AND RECOMMENDATIONS FOR FUTURE WORK

7.1 Summary of findings

Natural / hybrid ventilation systems with motorized operable windows designed and controlled to utilize the potential for cross-ventilation represent an area of significant interest in sustainable building design as they can reduce energy consumption for cooling and ventilation. Modern building systems performance standards create a need for accurate prediction models that can contribute to the improvement of indoor environmental quality and energy performance of buildings, and the increased use of low energy, naturally driven cooling systems. To this effect, the present research is aiming to enhance airflow prediction accuracy for natural ventilation design of buildings considering advanced experimental and building simulation methods.

A Boundary Layer Wind Tunnel (BLWT) approach was considered to investigate the pressure and velocity field in single-zone building models subject to cross-ventilation. Advanced measurement techniques such as Particle Image Velocimetry (PIV) were employed for the analysis of flow structure of various cross-ventilation configurations, since wind-driven air flows through buildings are complex and invariably turbulent. Mean and fluctuating internal pressures were evaluated at various points inside the building model as they affect airflow prediction, occupant thermal comfort, and wind load design (peak values) of buildings.

Novel elements of this work include application of the PIV technique and detailed investigation of mean and peak internal pressures considering measurements on multiple

taps and parameters such as blockage of the internal volume. Consideration of parametric experimental investigations in order to develop guidelines for implementation of cross-ventilation in design practice is another interesting element of this thesis. The main conclusions drawn from this research can be summarized as follows:

Carefully conducted PIV measurements can produce the flow field over extended areas including both horizontal and vertical cross-sections. PIV data for the inflow velocity have been compared with hot-film measurement results and for the configurations considered here, results show differences between the two methods up to a factor of 2.7.

The accuracy of the simplified orifice model to predict the ventilation flow rates in buildings with cross-ventilation has been examined through comparisons with experimental data. The orifice model predicts the ventilation flow rate with reasonable accuracy for openings located on top of windward and leeward walls and openings located in the middle of windward and leeward walls for low wall porosities (up to 10%). For these configurations, the orifice equation underestimates the flow rate up to 42% if any of the inlet or outlet openings covers more than 10% of the wall area. For openings located at the bottom of windward and leeward walls, the orifice model overestimates the ventilation flow rate up to 165% except for configurations with large inlets and outlets (20% wall porosity). Such differences may have significant implications on natural ventilation design, the sizing of openings and controls.

In general, the inlet-to-outlet ratio and the relative inlet and outlet location are very important parameters to be considered, in addition to the wall porosity, for the evaluation of airflow in buildings with cross-ventilation.

Based on internal pressure investigations in two building models subject to cross-ventilation, it can be concluded that for cross-ventilation with large porosities (i.e. higher than 10%) the internal airflow field has a significant impact on mean and peak values of the internal pressure. For example, for the same inlet-to-outlet-ratio, the mean internal pressure coefficient is higher up to a factor of 2.6 for configurations with non-symmetric openings compared to configurations with symmetric openings.

The internal pressure is not uniform in buildings with cross-ventilation for configurations with inlet and outlets located on adjacent walls (i.e. windward and side wall) and wall porosity higher than 10%. Differences among taps can be up to $\Delta Cp = 0.3$ for the means and $\Delta Cp = 0.53$ for the peaks for configurations with side-wall outlets, non-symmetric openings, and 20% wall porosity.

The study found that peak internal pressures in buildings with cross-openings may exceed the recommended design value for buildings category 3 (NBCC, 2005), for configurations with openings located above the mid-height of the building, leeward outlets, and $A_1/A_2 \geq 2$. A gust factor should be considered for configurations with openings above the mid-height of the building and configurations with openings below the mid-height of the building with $A_1/A_2 > 1$.

Regarding natural ventilation design, the following conclusions are drawn:

- Higher airflow rates are observed for configurations with

  - inlets located at the mid-height of the building or above;

  - symmetric inlets and outlets;

  - $A_1/A_2 < 1$.

It should be noted that for configurations with inlets below the mid-height of the building and outlets above the mid-height (non-symmetric openings), buoyancy effects, which are not considered in the present study, may increase the airflow rate.

- Based on this study, it can be suggested that configurations with large openings located on two adjacent walls should be avoided as they may cause internal pressure gradients and consequently, thermal discomfort of building occupants.

- Design recommendations for the relative location and size of openings on façade depend on the building use (residential or office buildings), the cooling strategy considered (i.e. daytime or night cooling), as well as thermal comfort, indoor air quality (IAQ), and security issues. Configurations with symmetric inlets and outlets and $A_1/A_2 <$ 1 result in high indoor air speeds and should be avoided in cases that indoor air speed has to be kept within comfort limits; configurations with $A_1/A_2 > 1$ resulting in lower indoor speeds, may be preferable. However, it should be noted that dependence of thermal comfort conditions on air temperature was not considered in the present study. Recommendations differ considerably when natural ventilation is used for IAQ or cooling purposes. Configurations with non-symmetric inlets and outlets increase the mixing of indoor air and improve IAQ.

The design guidelines described above were developed on the basis of parametric experimental investigations, which quantify the impact of relative inlet / outlet size and location, on ventilation airflow rates and building internal pressures. Detailed results were discussed in Chapters 4 and 5. It should be noted that such guidelines may not apply in cases where a building is in the wake of another building or in presence of vegetation.

Integrated energy and airflow network simulations

Integrated energy and airflow modelling is currently the most practical approach to achieve efficient integration of natural / hybrid ventilation systems in buildings. To this end, the capabilities of an advanced building simulation tool (ESP-r) to model the energy / airflow interactions and predict the envelope pressures and induced flow rates in buildings where both natural - wind and thermal buoyancy - and mechanical forces are present, have been assessed through a case-study.

The reasonably good agreement between the simulation and experimental results particularly considering the complexity of the problem, the large number of zones and input parameters required, as well as the uncertainties involved, indicates that airflow modelling of such a large building with different airflow patterns is possible in ESP-r. The study found that the simplified 35-zone model developed, which exceeds the maximum number of 21 zones allowed in ESP-r, predicts the stack and mechanical effects well. However, simulation data may be subject to errors for inclined winds due to the underlying zoning assumptions.

7.2   Research contributions

The most important contributions of this research are:

(i) Application of Particle Image Velocimetry (PIV) for wind-driven cross-ventilation analysis.

The PIV technique was applied for the investigation of the velocity field of various cross-ventilation configurations, to the author's best knowledge, for the first time. The study developed an innovative approach for application of PIV technique in building

aerodynamics testing in a large BLWT. Comparison of results with those by using conventional single-point techniques (e.g. hot-film anemometry) demonstrated that accuracy can be enhanced with carefully conducted PIV experiments. The study also examined the validity of the simplified orifice model to predict the air flow rates in buildings with cross-ventilation, through comparisons with measured data.

(ii) Systematic method for parametric experimental investigations into the effects of relative inlet and outlet size and their location on façade in order to evaluate the potential for cross-ventilation and develop design guidelines.

Design guidelines for the size and placement of window openings on façade have been provided, based on quantitative results for their impact on ventilation airflow rates and thermal comfort of building occupants.

(iii) Development of a simulation methodology in ESP-r combined with a sensitivity analysis focused on modelling issues to predict the envelope pressures and related air-exchange rates in buildings due to wind, stack, and mechanical system effects.

An integrated simulation tool (ESP-r) was used to model the airflow / energy interactions in a real building, considering a large number of zones and the impact of zoning assumptions, to the author's best knowledge, for the first time, as well as validation with monitoring data.

7.3   Recommendations for future work

Questions arising from research can be as important as the conclusions that are drawn. These questions lead to the development of further work. This section will summarise some of the research needs that were identified within the thesis.

1. Particle Image Velocimetry

The PIV setup for measurements in a large boundary layer wind tunnel presents various complexities. Although both arrangements (horizontal and vertical plane) considered in the present study worked well, it was tedious to move and align. In the future, traverse mechanisms can be adapted to move the camera and laser simultaneously so as to accelerate the process of measurement at different locations / planes. Careful design of a series of nozzles to produce more homogeneously dispersed seeding particles, as well as further improvement of the method to eliminate problems related to reflections and shadows are recommended. Utilization of time-resolved PIV to allow for higher sampling frequencies is also important if turbulence characteristics are to be examined.

2. Internal pressures

- Blockage of the internal volume (due to furniture, partitions, etc.) in internal pressure experiments was modelled considering a rather approximate method in the present study. Further wind tunnel testing should consider a more realistic approximation of the blockage of the internal volume so as results can be generalized to real building conditions. Investigation of the effect of scaling of the internal volume in wind tunnel experiments for the evaluation of the internal pressure in buildings with cross-openings should be also considered.

- Present work is limited to upstream open terrain simulation. Future wind tunnel testing should be extended to suburban or urban terrain and consider sensitivity analysis tests for other approaching wind velocity and turbulence intensity profiles.

- Internal pressure coefficients were compared with NBCC (2005) provisions. Comparisons with wind load provisions of various building codes and/or design standards should be carried out in the future.

- Present research was limited to single-zone generic buildings tested in a BLWT. This work could be extended to include wind tunnel testing of real buildings and full-scale monitoring in order to clarify conversion of the model-scale results to real building conditions.

- Solution of the unsteady-discharge equations can be considered to determine whether mean and fluctuating internal pressure time histories can be accurately predicted based on the external pressures measured on wind tunnel building models when there are two dominant openings present. This method has been applied previously for the prediction of time series of internal pressures in buildings with one dominant opening (Oh et al., 2007).

3. Integrated energy and airflow network simulations

- Numerical modelling of wind-driven cross-ventilation with large openings was not considered in the present research work. Natural ventilation openings such as windows can easily be added in the ESP-r simulation model so as to predict the airflow rates and potential energy savings in evaluating natural ventilation design alternatives (i.e. window openings in parallel and/or adjacent walls). Wind-tunnel data presented in Chapters 4 and 5 in terms of airflow rates and internal pressure coefficients for various opening configurations can be used for validation. As shown in Chapters 4 and 5, for cross-ventilation configurations with large openings, the airflow maintains a significant portion

of its inflow momentum as it moves across the building. In some cases, the existing orifice equation fails to accurately predict the ventilation flow rate (see Section 4.3). A more sophisticated airflow prediction model needs to be developed and implemented in the existing ESP-r source code. A possible solution may be to introduce a momentum conservation term in the orifice equation. Experimental data presented in this thesis can potentially be used for model validation.

- Further work should also focus on the increase of the maximum number of airflow nodes and airflow connections in the ESP-r source code. Work should include increase of the number of zones in the simulation model and comparison of results for different zoning assumptions. The importance of integrated thermal and airflow simulation for the prediction of airflow and energy consumption should be quantified and the impact of different coupling assumptions, i.e. sequential versus onion coupling, should be examined. Simulations should be performed for different buildings in various locations for which experimental data are available for inputs and validation to produce statistical data of general validity.

4. Cross-ventilation design

The present study did not consider temperature effects on ventilation airflow rates (thermal buoyancy-driven ventilation) and internal flow patterns (indoor air mixing). Also, dependence of thermal comfort conditions on air temperature was not addressed. Future research should consider combined wind and buoyancy-driven ventilation, possibly by means of CFD and integrated thermal and airflow simulations, to develop more general design guidelines. Previous work (e.g. Linden, 1999; Carrilho da Graça,

2003) has shown that cross-ventilation systems pose considerable challenges in the calculation of room ventilation heat transfer due to convection, such as defining the relevant characteristics of the airflow pattern, and determining the magnitude of the local heat transfer between the airflow in its different paths, internal surfaces and internal heat sources. These issues should be considered in the future work. Finally, a natural ventilation design optimization tool may ultimately be developed.

REFERENCES

Achakji, G.Y., Tamura, G.T., 1989. Pressure drop characteristics of typical stairshafts in high-rise buildings. ASHRAE Technical Data Bulletin, Smoke Control Technology 5(2), American Society of Heating Refrigerating and Air-Conditioning Engineers.

Akamine, Y., Kurabuchi, T., Ohba, M., 2004. A CFD analysis of the airflow characteristics at inflow openings. International Journal of Ventilation 2 (4), 431-437.

Andersen, K.T., 1996. Inlet and outlet coefficients: a theoretical analysis. In: Murakami S., (Ed.), Proceedings of the 5th International Conference on Air Distribution in Rooms (ROOMVENT 1996) 3, 379-390, Yokohama, Japan, July17-19.

ASCE 7, 2005. Minimum Design Load for Buildings and Structures. American Society of Civil Engineers.

ASHRAE Fundamentals Handbook, 2007. American Society of Heating Refrigeration and Air-conditioning Engineers, Atlanta, GA.

ASHRAE Standard 55, 2004. Thermal environmental conditions for human occupancy. American Society of Heating Refrigeration and Air-conditioning Engineers, Atlanta, GA.

ASHRAE Standard 62.1, 2007. Ventilation for acceptable Indoor Air Quality. American Society of Heating Refrigeration and Air-conditioning Engineers, Atlanta, GA.

ASHRAE Standard 62.2, 2004. Ventilation for acceptable indoor air quality in low-rise residential buildings. American Society of Heating Refrigeration and Air-conditioning Engineers, Atlanta, GA.

Axley, J.W., Chung, H., 2005. POWBAM0 mechanical power balances for multi-zone building airflow analysis. International Journal of Ventilation 4(2), 95-112.

Aynsley, R., 1988. A resistance approach to estimating airflow through buildings with large openings due to wind. ASHRAE Transactions 94, 1661-1669.

Aynsley, R., 1999. Unresolved issues in natural ventilation for thermal comfort. Proceedings of the 1st international forum on natural and hybrid ventilation, Sydney, Australia, September 28. In: Heiselberg, P., (Ed.), International Energy Agency Annex 35 CD, Aalborg University, Denmark, Hybrid Ventilation in New and Retrofitted Office Buildings, IEA Energy Conservation in Buildings and Community Systems Programme.

Aynsley, R.M., Melbourne, W., Vickery, B.J., 1977. Architectural Aerodynamics. Applied Science Publishers LTD, London.

Bachlin, W., Plate, E.J., 1986. Mean internal pressure inside buildings induced by wind - a wind tunnel study. Proceedings of the Specialty Conference Advancements in Aerodynamics, Fluid Mechanics and Hydraulics, 791-798, EM & HY Div/ ASCE, Minneapolis, June.

Beckman, W.A., Broman, L., Fiksel, A., Klein, S.A., Lindberg, E., 1994. TRNSYS-The most complete solar energy simulation software. Proceedings of the 3rd World Renewable Energy Congress, 486-488, Reading, UK, September.

Birdsall, J.B, Meroney, R.N., 1995. Model scale and numerical evaluation of tracer gas distribution due to wind forced natural ventilation. Proceedings of the 9th International Conference on Wind Engineering, 12 pp., CEP94-95-JBB-RaNM-13, New Delhi, India, January.

Birdsall, J.B., 1993. Physical simulation of wind-forced natural ventilation. M.S. Thesis, 139 pp., Civil Engineering, Colorado State University.

Blomsterberg, A., Carlsson, T., Svensson, C., Kronvall, J., 1999. Airflows in dwellings-simulations and measurements. Energy and Buildings 30, 87-95.

Borchiellini, R., Furbringer, J.M., 1999. An evaluation exercise of a multizone air flow model. Energy and Buildings 30, 35-51.

Bourgeois, D., Haghighat, F., Potvin, A., 2002. On the applicability of Hybrid ventilation in Canadian office and educational buildings: Part 1 – Barriers and opportunities stemming from building regulation. Proceedings of the 4th International Forum on Hybrid ventilation, 18-23, Concordia University, Montreal, Canada, May 14-15.

Brager, G.S., 2006. Mixed-mode cooling. ASHRAE Journal 48, 30-37, August.

Brager, G.S., de Dear, R., Paliaga, G., 2004. Operable windows, personal control, and occupant comfort. ASHRAE Transactions 110 (2), 17-35.

BRE, 1994. BREEZE User Manual. Building Research Establishment. UK.

British Standards Institution, BS 5925, 1991. Code of practice for ventilation principles and designing for natural ventilation.

Bruce, J.M., 1978. Natural convection through openings and its application to cattle building ventilation. Journal of Agricultural Engineering and Resources 23, 151-167.

Carey, P.S., Etheridge, D.W., 1999. Direct wind tunnel modeling of natural ventilation for design purposes. Building Service Engineering Research and Technology 20 (3), 131-142.

Carrilho da Graça, G., Linden, P.F., Haves, P., 2004. Design and testing of a control strategy for a large, naturally ventilated office building. Building Service Engineering Research and Technology 25(3), 223-239.

Carrilho da Graça, G., 2003. Simplified models for heat transfer in rooms. Dissertation submitted in partial satisfaction of the requirements of the degree. Ph.D. thesis, Engineering Physics, University of California, San Diego.

Caudill, W.W., Crites, S.E., Smith, E.G., 1951. Some general considerations in the natural ventilation of buildings. Report No. 22, 43 pp., Texas Engineering Experiment Station.

Caudill, W.W., Reed, B.H., 1952. Geometry of classrooms as related to natural lighting and natural ventilation. Report No. 36, 53 pp., Texas Engineering Experiment Station Research.

Cermak, J.E., Poreh, M., Peterka, J.A., Ayed, S.S., 1984. Wind tunnel investigations of natural ventilation. ASCE Journal of Transportation Engineering 110 (1), 67-79.

Chandra, S. Fairey, P.W., Kerestecioglu, A.A., Kamel, A.A., 1986. Wind tunnel and full-scale data on airflow from natural ventilation and ceiling fans. ASHRAE Transactions 92 (2B), 804-814.

Chang, H., Kato, S., Chikamoto, T., 2004. Effects of outdoor air conditions on hybrid air conditioning based on task/ambient strategy with natural and mechanical ventilation in office buildings. Building and environment 39, 153-164.

Chiu, Y-H., Etheridge, D.W., 2007. External flow effects on the discharge coefficients of two types of ventilation opening. Journal of Wind Engineering and Industrial Aerodynamics 95, 225-252.

Choiniere, Y., Tanaka, H., Munroe, J.A., Suchorski-Tremblay, A., 1992. Prediction of wind induced ventilation for livestock housing. Journal of Wind Engineering and Industrial Aerodynamics 41-44, 2563-2574.

CMHC, 1991. Development of design procedures and guidelines for reducing electric demand by air leakage control in high-rise residential buildings. Technical Series 98-107.

CMHC, 2004. Analysis of ventilation system performance in new Ontario houses. Technical Series 04-117, Canada Mortgage and Housing Corporation.

CMHC, 2007. www.cmhc-schl.gc.ca/en/inpr/su/eqho/index.cfm. Canada Mortgage and Housing Corporation.

CMHC, 1996. Energy and water efficiency in multi unit residential buildings. Technical Manual, 63074, Canada Mortgage and Housing Corporation.

Cooke, G., Kokko, J., Greene, T., 2005. Airtightness and ventilation system performance of apartments in new multi-unit residential buildings. Proceedings of the 10th Canadian Conference on Building Science & Technology, Ottawa, May 12-13.

Cowen, E.A., Monismith, S.G., 1997. A hybrid digital particle tracking velocimetry technique. Experiments in Fluids 22, 199-211.

Crawley, D.B., Lawrie, L.K., Predersen, C.O., Liesen, R.J., Fisher, D.E., 1999. Energy Plus-a new generation building energy simulation program. Proceedings of the 6th International IBPSA conference, 81-89, Kyoto, Japan, September 13-15.

Dascalaki, E., Santamouris, M., Buant, M., Balaras, C.A., Bossaer, A., Ducarme, D., Wouters, P., 1999. Modeling large openings with COMIS. Energy and Buildings 30, 105-115.

Diamond, R.C, Feustel, H.E, Dickerhoff, D.J., 1996. Ventilation and infiltration in high-rise apartment buildings. Lawrence Berkeley Laboratory, LBL Report LBL-38103.

Dick, J.B., 1950. The fundamentals of natural ventilation of houses. Journal of the Institute of Heating and Ventilating Engineers 18, 123-134.

Dorer, V., Weber, A., 1999. Air, contaminant and heat transport models: integration and application. Energy and Buildings 30, 97-104.

Edward, C., 1999. Modelling of ventilation and infiltration energy impacts in mid and high-rise apartment buildings. Research Division, Canada Mortgage and Housing Corporation.

EE4, 2007. http://oee.rncan.gc.ca

Engineering Sciences Data Unit ESDU. Data Item 82026. Strong winds in the atmospheric boundary layer. Part 1: hourly-mean wind speeds.

Ernest, D.R., Bauman, F.S., Arens, E.A., 1992. The effects of external wind pressure distributions on wind induced air motion in side buildings. Journal of Wind Engineering and Industrial Aerodynamics 41-44, 2539-2550.

ESRU, 2002. The ESP-r System for Building Energy Simulation. User Guide Version 10 Series, University of Strathclyde, Glasgow UK.

Etheridge, D., Sandberg, M., 1996. Building ventilation: theory and measurement. John Willey & Sons, London.

Etheridge, D.W., 2000a. Unsteady flow effects due to fluctuating wind pressures in natural ventilation design - mean flow rates. Building and Environment 35 (2), 111-133.

Etheridge, D.W., 2000b. Unsteady flow effects due to fluctuating wind pressures in natural ventilation design - instantaneous flow rates. Building and Environment 35 (4), 321-337.

Etheridge, D.W., 2004. Natural ventilation through large openings - measurements at model scale and envelope theory. International Journal of Ventilation 2 (4), 325-342.

Feustel, H.E., Diamond., R.C., 1998. Ventilation in high-rise apartments. In: Mundt, E., Malmstrom, T.G., (Eds.), Proceedings of the 6th International Conference on Air Distribution in Rooms (ROOMVENT 1998), 1, 29-36, Stockholm, Sweden, June 14-17.

Feustel, H.E., 1999. COMIS-an international multi-zone airflow and contaminant transport model. Energy and Buildings 30, 3-18.

Feustel, H.E., Dieris. J., 1992. A survey on airflow models for multi-zone structures. Energy and Buildings 18, 79-100.

FlowManager software and Introduction to PIV Instrumentation, 2000. Software User's guide, Dantec Dynamics.

Furbringer, J.M., Roulet, C.A., 1999. Confidence on simulation results: put a sensitivity analysis module in your model: The IEA-ECBS Annex 23 experience of model evaluation. Energy and Buildings 30, 61-71.

Furbringer, J.M., Roulet, C.A., Borchiellini, R., 1999. An overview of the evaluation activities of IEA ECBCS Annex 23. Energy and Buildings 30, 19-33.

Ginger, J.D., Yeatts, B.B., Mehta, K.C., 1995. Internal pressures in a low-rise full-scale building. Proceedings of the 9th International Conference on Wind Engineering 3, 512-523, New Delhi, India, January 9-13.

Givoni, B., 1969. Man, Climate and Architecture. 2nd ed., Applied Science, Essex, England.

Haghighat, F., Megri, A.C., 1996. A Comprehensive validation of two airflow models - COMIS and CONTAM. Indoor Air Journal 6, 278-288.

Haghighat, F., Rao, J., Fazio, P., 1991. The influence of turbulent wind on air change rates – a modelling approach. Building and Environment 26, 95-109.

Haves, P., Linden, P.F., Carrilho da Graca G., 2004. Use of simulation in the design of a large naturally ventilated commercial office building. Building Service Engineering Research and Technology 25 (3), 211-221.

Heidt, F.D., Nayak, J.K., 1994. Estimation of air infiltration and building thermal performance. Air Infiltration Review15 (3), Air Infiltration and Ventilation Centre, UK.

Heiselberg, P., 2002. Principles of Hybrid Ventilation. In: Heiselberg, P., (Ed.), Annex 35: Hybrid Ventilation in New and Retrofitted Office Buildings, IEA Energy Conservation in Buildings and Community Systems Programme.

Heiselberg, P., Bjorn, E., Jensen, J.T., 2002a. Window openings – air flow and thermal comfort. Proceedings of the 4th International Forum on Hybrid Ventilation, 187-197, Concordia University, Montreal, Canada, May 14-15.

Heiselberg, P., Bjorn, E., Nielsen, P.V., 2002b. Impact of open windows on room air flow and thermal comfort. International Journal of Ventilation, 1 (2), 91-100.

Heiselberg, P., Dam, H., Sorensen, L.C. and Nielsen, P.V., 1999. Characteristics of air flow through window. 1st International Forum on Natural and Hybrid Ventilation, Sydney, Paper no. 103, Australia, September 28. In: Heiselberg P., (Ed.), International Energy Agency Annex 35 CD, Aalborg University, Denmark, Hybrid Ventilation in New and Retrofitted Office Buildings, IEA Energy Conservation in Buildings and Community Systems Programme.

Heiselberg, P., Svidt, K., Nielsen, P.V., 2001. Characteristics of airflow from open windows. Building and Environment 36, 859-869.

Hensen, J.L.M., 1991. On the thermal interaction of building structure and heating and ventilating system. Doctoral dissertation, Eindhoven University of Technology.

Hensen, J.L.M., 1999. A comparison of coupled and de-coupled solutions for temperature and airflow in a building. ASHRAE Transactions 152 (2), American Society of Heating, Refrigerating and Air-Conditioning Engineers.

Ho, T.C.E., Surry, D., Morrish, D., Kopp, G.A., 2004. The UWO contribution to the NIST aerodynamic database for wind loads on low buildings: Part 1. Archiving format and basic aerodynamic data. Journal of Wind Engineering and Industrial Aerodynamics 193, 1-30.

Holleman, T.R., 1951. Air flow through conventional window openings. Report No. 33, 45 pp., Texas Engineering Experiment Station Research.

Holmes, J.D., 1979. Mean and fluctuating internal pressures induced by wind. Proceedings of 5th International Wind Engineering Conference, 435-450, Fort Collins, Colorado, July 8-13.

Holmes, J.D., 2001. Wind Loading of Structures. Spon Press, 128-138 (Chapter 6).

Hu, C-H., Kurabuchi, T., Ohba, M., 2005. Numerical study of cross-ventilation using two-equation RANS turbulence models. International Journal of Ventilation 4 (2), 123-132.

Hu, C-H., Kurabuchi, T., Ohba, M., 2006. CFD modelling of cross ventilation using unsteady methods. Proceedings of the 4th International Symposium on Computational Wind Engineering (CWE2006), 255-258, Yokohama, Japan, July.

Huang, H., Dabiri, D., 1997. On Errors of Digital Particle Image Velocimetry. Measurement Science and Technology 8 (12), 1427-1440.

Iolova, K., Bernier, M., .2007. Simulation of various options for a net zero energy triplex in Montreal. Proceedings of the 2nd Solar Buildings Conference, Calgary, Canada, June 10-14.

Jensen, J.T., Heiselberg, P., Nielsen, P.V., 2002b. Numerical prediction of natural ventilation by means of CFD. In: Melikov, A.K., Nielsen, P.V., (Eds.), Proceedings of the 8th International Conference on Air Distribution in Rooms (ROOMVENT 2002), 537-540, ISBN 87-989117-0-8, Technical University of Denmark, Copenhagen, Denmark, September 8-11.

Jensen, J.T., Sandberg, M., Heiselberg, P., Nielsen, P.V., 2002a. Wind-driven cross-flow analyzed as a catchment problem and as a pressure driven flow. International Journal of Ventilation 1 (HybVent-Hybrid Ventilation Special Edition), 88-101.

Jensen, J.T., Sandberg, M., Heiselberg, P., Nielsen, P.V., 2002a. Wind driven cross-flow analyzed as a catchment problem and as a pressure driven flow. International Journal of Ventilation 1(HybVent-Hybrid Ventilation Special Edition), 88-101.

Jeong, Y., Haghighat, F., 2002. Modelling of a hybrid-ventilated building using ESP-r. International Journal of Ventilation 1, 120-127.

Jian, Y., Alexander, D., Jenkins, H., Arthur, R., Chen, Q., 2003. Natural ventilation in buildings: measurement in a wind tunnel and numerical simulation with Large-Eddy Simulation. Journal of Wind Engineering and Industrial Aerodynamics 91, 331-353.

Karava, P., Stathopoulos, T., Athienitis, A.K., 2006a. Impact of internal pressure coefficients on wind-driven ventilation analysis. International Journal of Ventilation 5(1), 53-66.

Karava, P., Athienitis, A.K., Reardon, J.T., Stathopoulos, T., 2006b. Predicting the pressure regimes and resultant indoor-outdoor air- exchange in a multi-unit residential building. Proceedings of the National Building Simulation Conference (eSim), 65-72 Toronto, Canada, May 4-5.

Karava, P., Athienitis, A.K., Stathopoulos, T., Reardon, J.T., 2006c. Modelling of indoor-outdoor air-exchange in a multi-unit residential building. In: Fazio, P., Ge, H., Rao, J., Desmarais, G., (Eds.), Proceedings of the 3rd International Building Physics Conference, 697-704, ISBN 0-415-41675-2, Concordia University, Montreal, Canada, August 27-31.

Karava, P., Stathopoulos, T., Athienitis, A.K., 2004a. Wind driven flow through openings: Review of discharge coefficients. International Journal of Ventilation 3(3), 255-266.

Karava, P., Stathopoulos, T., Athienitis, A.K., 2004b. Natural ventilation openings: a discussion of discharge coefficients. Proceedings of the World Building Congress (CIB 2004), Paper no. 346, Toronto, Canada, May 2-7.

Karava, P., Stathopoulos, T., Athienitis, A.K., 2007a. Wind-driven natural ventilation analysis. International Journal of the Solar Energy Society 81, 20-30.

Karava, P., Stathopoulos, T., Athienitis, A.K., 2007b. Cross-ventilation building design: Application of Particle Image Velocimetry. Proceedings of the 12th International Conference on Wind Engineering 2, 1407-1414, Cairns, Australia, July.

Katayama, T., Tsutsumi, J., Ishii, A., 1992. Full-scale measurements and wind tunnel tests on cross-ventilation. Journal of Wind Engineering and Industrial Aerodynamics 41-44, 2553-2562.

Kato, S., Murakami, S., Mochida, A., Akabashi, S., Tominaga, Y., 1992. Velocity-pressure field of cross-ventilation with open windows analyzed by wind tunnel and numerical simulation. Journal of Wind Engineering and Industrial Aerodynamics 41-44, 2575-2586.

Kato, S., 2004. Flow network model based on power balance as applied to cross ventilation. International Journal of Ventilation 2 (4), 395-408.

Kendrick, J.F., 1993. An overview of combined modeling of heat transport and air movement. Technical Note AIVC 40, Air Infiltration and Ventilation Centre, UK.

Kobayashi, T., Sagara, K., Yamanaka, T., Kotani, H., Sandberg, M., 2006. Wind-driven flow through openings - analysis of the stream tube. International Journal of Ventilation 4 (4), 323-336.

Kono, R., Kato, S., Ooka, R., Takahashi, T., Hasama, T., 2005. Wind tunnel experiment on characteristics of ventilation with single-sided opening in uniform flow. In: Choi, C.K., Kim, Y.D., Kwak, H.G., (Eds.), Proceedings of the 6th Asian - Pacific Conference on Wind Engineering (APCWE – VI), 427-436, Seoul, Korea, September 12-14.

Kotani, H., Yamanaka, T., 2006. Flow visualization and inflow direction measurement at cross-ventilated large opening. International Journal of Ventilation 5 (1), 79-87.

Kurabuchi, T., Akamine, Y., Ohba, M., Endo, T., Goto, T., Kamata M., 2006. A Study on the effects of porosity on discharge coefficient in cross-ventilated buildings based on wind tunnel experiment. International Journal of Ventilation 5(1), 67-78.

Kurabuchi, T., Ohba, M., Endo, T., Akamine, Y., Nakayama, F., 2004. Local dynamic similarity model of cross ventilation part 1 – theoretical framework. International Journal of Ventilation 2 (4), 371-382.

Li, H., 2002. Validation of three multizone airflow models. MASc Thesis, Concordia University, Montreal, Canada.

Li, Y., 2002. Spurious numerical solutions in coupled natural ventilation and thermal analyses. International Journal of Ventilation 1 (1), 1-12.

Liddament, M.W., 1986. Air infiltration calculation techniques – an application guide. Air Infiltration and Ventilation Centre, UK.

Liddament, M.W., 1989. AIDA. Air Infiltration Review 11(1), Air Infiltration and Ventilation Centre, UK.

Linden, P.F., 1999. The fluid mechanics of natural ventilation. Annual Review of Fluid Mechanics 31, 201-38.

Liu, H., 1991. Wind Engineering – A handbook for structural engineers. Prentice-Hall, New Jersey.

Liu, H., Rhee, K.H., 1986. Helmholtz oscillation in building models. Journal of Wind Engineering and Industrial Aerodynamics 24, 95-115.

Liu, J., Gao, F., Yoshino, H., Li, Z., 2005. Evaluation of the ventilation performance of apartment buildings in winter for a severe cold region of China. International Journal of Ventilation 4(2), 157-166.

Lou, W-J, Yu, S-C, Sun, B-N., 2005. Wind tunnel Research on internal wind effect for roof structure with wall openings. In: Choi, C.K., Kim, Y.D., Kwak, H.G., (Eds.), Proceedings of the 6th Asian - Pacific Conference on Wind Engineering (APCWE – VI), 1606-1620, Seoul, Korea, September 12-14.

Lstiburek, J., 2005. Controlling stack-driven flows. ASHRAE Journal, December.

Meroney, R.N., Birdsall, J.B., Neff, D.E., 1995. Wind-tunnel simulation of infiltration across permeable building envelopes: energy and air pollution exchange rates. Proceedings of the 7th International Symposium on Measurement and Modeling of Environmental Flows, San Francisco, CA, November.

Mochida, A. Yoshimo, H., Miyauchi, S., Mitamura, T., 2006. Total analysis of cooling effects of cross-ventilation affected by microclimate around a building. Journal of Solar energy 80, 371-382.

Mochida, A. Yoshimo, H., Takeda, T., Kakegawa, T., Miyauchi, S., 2005. Methods for controlling airflow in and around a building under cross-ventilation to improve indoor thermal comfort. Journal of Wind Engineering and Industrial Aerodynamics 93, 437-449.

Munarin, J., 1978. Wind tunnel measurements on internal pressures in a two storey house. B.E. thesis, Department of Civil and Systems Engineering, James Cook University.

Murakami, S., Kato, S., Akabashi, S., Mizutani, K., Kim, Y-D., 1991. Wind tunnel test on velocity-pressure field of cross-ventilation with open windows. ASHRAE Transactions 97 (1), 525-538.

NBCC, 2005. National Building Code User's Guide, National Research Council of Canada, Ottawa.

Nishizawa, S., Sawachi, T., Narita, K., Seto, N., Ishikawa, Y., 2004. A wind tunnel full-scale building model comparison between experimental data and CFD results based on standard k-ε turbulence representation. International Journal of Ventilation 2(4), 419-430.

Oh, J.H., Kopp, G.A., Inculet, D.R., 2007. The UWO contribution to the NIST aerodynamic database for wind loads on low buildings: Part 3. Internal pressures. Journal of Wind Engineering and Industrial Aerodynamics 95, 755–779.

Ohba, M., Irie, K., Kurabuchi, T., 2001. Study on airflow characteristics inside and outside a cross-ventilation model, and ventilation flow rates using wind tunnel experiments. Journal of Wind Engineering and Industrial Aerodynamics 89, 1513-1524.

Ohba, M., Kurabuchi, T., Endo, T., Akamine, Y., Kamata, M., Kurahashi, A., 2004. Local dynamic similarity model of cross ventilation part 2: application of Local dynamic similarity model. International Journal of Ventilation 2 (4), 383-393.

Orme, M., 1999. Applicable models for air infiltration and ventilation calculations. Technical Note AIVC 51, Air Infiltration and Ventilation Centre, UK.

Pearce, W., Sykes, D.M., 1999. Wind tunnel measurements of cavity pressure dynamics in a low-rise flexible roofed building. Journal of Wind Engineering and Industrial Aerodynamics 82, 27-48.

Persily, A., 1998. A modelling study of IAQ and energy impacts of residential mechanical ventilation. Building and Fire research laboratory, National Institute for Standards and Technology, NISTIR6162.

Potter, N.J., 1979. Effect of fluctuating wind pressures on natural ventilation. ASHRAE Transactions 85, 445-457.

Prasad, A.K., Adrian, R.J., Landreth, C.C., Offutt, P.W., 1992. Effect of resolution on the speed and accuracy of Particle Image Velocimetry interrogation. Experiments in Fluids 13, 105-116.

Raffel, M., Willert, C., Koupenhans, J., 1998. Particle Image Velocimetry: A practical Guide. Springer, Germany.

Rasouli, A., Hangan, H., Siddiqui, K., 2007. PIV measurements for a complex topographic terrain. Proceedings of the 12th International Conference on Wind Engineering, 1129-1134, Cairns, Australia, July.

Reardon, J.T, Won, D., MacDonald, R.A., 2003. Characterisation of air leakage, pressure regimes and resultant air movement in high-rise residential buildings. Institute for Research in Construction. Indoor Environment Program, National Research Council of Canada.

RETScreen International, 2007. www.retscreen.net

Richards, C., 2007. Retrofitting a high-rise residential building to reduce energy use by a factor of 10. MSc Thesis, Mechanical Engineering, University of Saskatchewan.

Saathoff, P.J., Liu, H., 1983. Internal pressure of multi-room buildings. ASCE Journal of Engineering Mechanics 109 (EM3), 908-919.

Sandberg M., 2002. Airflow through large openings - a catchment problem? In: Melikov, A.K., Nielsen, P.V., (Eds.), Proceedings of the 8th International Conference on Air Distribution in Rooms (ROOMVENT 2002), ISBN 87-989117-0-8, Technical University of Denmark, Copenhagen, Denmark, September 8-11.

Sandberg, M., 2004. An alternative View on Theory of Cross-Ventilation. International Journal of Ventilation 2 (4), 400-418.

Santamouris, M., 2006. Ventilation for comfort and cooling: the state of the art. In: Santamouris, M., Wouters, P., (Eds.), Building Ventilation, James & James, London, UK.

Sawachi, T., 2002. Detailed observation of cross ventilaton and air flow through large openings by full scale building model in wind tunnel. In: Melikov, A.K., Nielsen, P.V., (Eds.), Proceedings of the 8th International Conference on Air Distribution in Rooms (ROOMVENT 2002), 537-540, ISBN 87-989117-0-8, Technical University of Denmark, Copenhagen, Denmark, September 8-11.

Sawachi. T., Narita, K., Kiyota, N., Seto, H., Nishizawa, S., Ishikawa, Y., 2004. Wind pressure and airflow in a full-scale building model under cross ventilation. International Journal of Ventilation 2 (4), 343-357.

Seifert, J., Li, Y., Axley, J., Rosler, M., 2006. Calculation of wind-driven ventilation in Buildings with large openings. Journal of Wind Engineering and Industrial Aerodynamics 94, 925-947.

Shaw, C.Y., 1980. Methods for conducting small-scale pressurization tests and air leakage data of multi-storey apartment buildings. ASHRAE Transactions 86 (1), 241-250.

Smith, E.G., 1951. The feasibility of using models for predetermining natural ventilation. Research Report No. 26, Texas Engineering Experiment Station.

Stanislas, M., Kompenhans, J., Westerweel, J., 2000. Particle Image Velocimetry: progress towards industrial application. Kluwer Academic Publishers, Dordrecht, the Netherlands.

Stanislas, M., Monnier, J. C., 1997. Practical aspects of image recording in particle image velocimetry. Measurement Science and Technology 8(12), 1417-1426.

Stathopoulos, T., 1984. Design and fabrication of a wind tunnel for building aerodynamics. Journal of Wind Engineering and Industrial Aerodynamics 16 (2), 361-376.

Stathopoulos, T., Surry, D., Davenport, A.G., 1979. Internal pressure characteristics of low-rise buildings due to wind action. Proceedings of the 5th International Wind Engineering Conference 1, 541-463, Forth Collins, Colorado USA.

Stathopoulos, T., Surry, D., 1983. Scale effects in wind tunnel testing of low buildings. Journal of Wind Engineering and Industrial Aerodynamics 13 (1-3), 313-326.

Straw, M.P., 2000. Computation and measurement of wind induced ventilation. Ph.D thesis, School of Civil Engineering, University of Nottingham, UK.

Straw, M.P., Baker, C.J., Robertson, A.P., 2000. Experimental measurements and computations of the wind-induced ventilation of a cubic structure. Journal of Wind Engineering Industrial Aerodynamics 88, 213-230.

Svensson, C.S., 1998. The NatVent programme 1.0, Fundamentals. CD Rom.

Tamura, G.T., Wilson, A.G., 1966. Pressure differences for nine-storey building as a result of chimney effect and ventilation system operation. ASHRAE Transactions 72, 180-189.

Tzempelikos, A., Athienitis, A.K., Karava, P., 2007. Simulation of façade and envelope design options for a new university building. International Journal of the Solar Energy Society 81, 1088-1103.

UoA., 1997. AIOLOS: A software for natural ventilation airflow prediction. University of Athens, Greece.

Upham, R.D., Yuill, G.K., Bahnfleth, W.P., 2001. A validation study of multizone airflow and contaminant migration simulation programs as applied to tall buildings. ASHRAE Transactions 107 (2), 619-628.

Vickery, B.J., Karakatsanis, C., 1987. External wind pressure distributions and induced internal ventilation flow in low-rise industrial and domestic structures. ASHRAE Transactions 93(2), 2198-2213.

Wachenfeldt, B.J., 2003. Natural ventilation in buildings - detailed prediction of energy performance. PhD Thesis, Department of Energy and Process Engineering, Norwegian University of Science and Technology, Trondheim, Norway.

Walker, I. S., Wilson, D.J., 1990. AIM 2: The Alberta Air Infiltration Model. Report 71, Department of Mechanical Engineering, University of Alberta.

Walker, I. S., Wilson, D.J., Sherman, M.H., 1998. A comparison of power law to quadratic formulations for air infiltration calculations. Energy and Buildings 27, 293-297.

Walker, I.S., 1999. Distribution system leakage impacts on apartment building ventilation rates. Environmental Energy Technologies Division, Lawrence Berkeley Laboratory, LBL Report LBL-42127.

Walton, G.N., 1997. CONTAM96 User Manual. NIST.

Walton, G.N., 1989. AIRNET. A computer program for building airflow network modeling. National Institute of Standards and Technology.

Wang, L., Wong, N.H., 2007. The impacts of ventilation strategies and facade on indoor thermal environment for naturally ventilated residential buildings in Singapore. Building and Environment 42, 4006-4015.

Westerweel, J., 1997. Fundamentals of Digital Particle Image Velocimetry. Measurement Science and Technology 8 (12), 1379-1392.

White, R.F., 1954. Effects of landscape development on the natural ventilation of buildings and their adjacent areas. Report No. 45, 16 pp., Texas Engineering Experiment Station Research.

Wiren, B.G., 1984. Wind pressure distributions and ventilation losses for a single family house as influenced by surrounding buildings - a wind tunnel study. Proceedings of Wind Pressure Workshop, Air Infiltration Centre Technical Note 13.1, Paper No. 6, 74-101, International Energy Agency, Brussels, Belgium, March 21-22.

Womble, J.A., 1994. Wind-induced internal building pressures. Master's thesis, Department of Civil Engineering, Colorado State University, Fort Collins, Colorado.

Womble, J.A., Yeatts, B.B., Cermak, J.E., Mehta, K.C., 1995. Internal wind pressures in a full and small-scale building. Proceedings of the 9th International Conference on Wind Engineering, 3, 1079-1090, New Delhi, India, January 9-13.

Wright, N.G., Hargreaves, D.M., 2006. Unsteady CFD simulations for natural ventilation. International Journal of Ventilation 5 (1), 13-20.

Wu, H., Stathopoulos, T., Saathoff, P., 1998. Wind-induced internal pressure revisited: low-rise buildings. In: Srivastava, N.K., (Ed.), Proceeding of Structural Engineers World Congress, ISBN: 0-08-042845-2, San Francisco, CA, U.S.A., July 19-23.

Yang T., 2004. CFD and field testing of a naturally ventilated full-scale building. Ph.D thesis, School of Civil Engineering, University of Nottingham, UK.

Yang, T., Wright, N.G., Etheridge, D.W., Quinn, A.D., 2006. Comparison of CFD and full-scale measurements for analysis of natural ventilation. International Journal of Ventilation 4, 337-348.